Property of
Flood Control District of MC Library
Please Return to
2801 W. Durango
Phoenix, AZ 85009

PB86-137171

CHALMERS TEKNISKA HÖGSKOLA

CHALMERS UNIVERSITY OF TECHNOLOGY
GÖTEBORG
SWEDEN

On Urban Runoff Modelling

The Application of Numerical Models Based on the Kinematic Wave Theory

Volume I

by

Sven Lyngfelt

Property of
Flood Control District of MC Library
Please Return to
2801 W. Durango
Phoenix, AZ 85009

REPRODUCED BY
NATIONAL TECHNICAL
INFORMATION SERVICE
U.S. DEPARTMENT OF COMMERCE
SPRINGFIELD, VA. 22161

Report Series A:13
Department of Hydraulics
Chalmers University of Technology
1985

808.002

Property of
Flood Control District of MC Library
Please Return to:
2801 W. Durango
Phoenix, AZ 85009

PB86-137171

CHALMERS TEKNISKA HÖGSKOLA

CHALMERS UNIVERSITY OF TECHNOLOGY
GÖTEBORG
SWEDEN

On Urban Runoff Modelling

The Application of Numerical Models Based on the Kinematic Wave Theory

Volume I

by

Sven Lyngfelt

Property of
Flood Control District of MC Library
Please Return to
2801 W. Durango
Phoenix, AZ 85009

REPRODUCED BY
NATIONAL TECHNICAL
INFORMATION SERVICE
U.S. DEPARTMENT OF COMMERCE
SPRINGFIELD, VA. 22161

Report Series A:13
Department of Hydraulics
Chalmers University of Technology
1985

Institutionen för Vattenbyggnad
Chalmers Tekniska Högskola

Department of Hydraulics
Chalmers University of Technology

On Urban Runoff Modelling

The Application of Numerical Models Based on the Kinematic Wave Theory

Volume I

Sven Lyngfelt

Report
Series A:13
ISSN 0348-1050

Göteborg 1985

Address: Department of Hydraulics
Chalmers University of Technology
S-412 96 Göteborg, Sweden

Telephone: 031/81 01 00

-1-a

ABSTRACT

This study deals with the modelling of stormwater runoff in urban catchments. An analysis of the basic governing equations shows that the kinematic wave equations represent a suitable approximation for urban runoff modelling in general. The Manning formula was found to be a reasonably valid friction relation for the modelling of overland flow. A modified numerical solution algorithm is proposed which reduces the calculation volume in comparison with conventional methods.

Different approaches to discretization of the geometric input data (size of base catchments) were investigated in six small urban catchments (< 1 ha contributing area) and two large ones. From the tests it was concluded that:

- Independent of the model used and the base catchment size, the choice of input parameters in the base catchment model (overland flow parameters) has a significant effect on the attenuation of the outflow hydrograph.
- The kinematic wave model is both simple to use and adequate as a base catchment model.
- With this model, relatively big simplifications can be made in the input data geometry with reasonably well maintained performance, provided the catchment characteristics are properly evaluated.
- The catchment characteristics can be evaluated using relations derived from the kinematic wave theory, assuming constant rain intensity.

In a separate study the ability of the Rational Method to reproduce statistical peak flows was tested. Using a time of concentration based on kinematic wave theory, the method performed well.

PREFACE

The investigations presented in this thesis deal with urban runoff modelling and are mainly concerned with the relevance of basic equations, numerical solution methods and discretization of geometrical input data. The work has been carried out at the Department of Hydraulics, Chalmers University of Technology and is a part of a major research effort by the Urban Geohydrology Research Group at the University.

Other studies in the field of urban runoff modelling carried out by the research group have dealt with selection of storm input for the design of sewer systems, optimization in the design of sewer systems, and storm water quality.

All relations presented in the report are based on SI-units. The SI-unit for rain intensity and discharge per unit area (m/s) is not very practical. Both in figures and when magnitudes of intensities are discussed the unit litres/(second · hectare) 1 l/s·ha = 10^{-7} m/s = 0.36 mm/h) has been used. It is the most commonly used unit among Swedish sanitary engineers. In describing magnitudes of catchment areas, hectares have been used (1 ha = 10^4 m^2).

Göteborg, March 1985

Sven Lyngfelt

ACKNOWLEDGEMENT

This work has been financially supported by the Swedish Council for Building Research (BFR).

I wish to express my gratitude to all colleagues and friends who have contributed to the accomplishment of this study.

My supervisor, Anders Sjöberg, has encouraged me greatly and given valuable advice during all phases of the work.

Parts of the field measurements have been carried out in cooperation with Viktor Arnell who has also given valuable advice in numerous discussions. Several students at the University have also made contributions to the field measurements.

Gösta Lindvall and Steffen Häggström have given valuable advice in the final work involved in this report.

Ann-Marie Holmdahl typed, and patiently retyped the manuscript. Alicja Janiszewska drew the major part of the figures. The language was corrected by Shirley Booth and Appendix I was translated and typed by Ann-Marie Hellgren.

Thank you all!

Sven Lyngfelt

Preceding page blank

LIST OF CONTENTS

Page

VOLUME I

PREFACE		I
ACKNOWLEDGEMENTS		II
CONTENTS		V
SUMMARY		IX
1.	INTRODUCTION	1
1.1	Urban runoff modelling	1
1.2	Scope of the study	3
1.3	Arrangement of the contents	4
2.	URBAN RUNOFF CHARACTERISTISCS	5
2.1	General	5
2.2	Precipitation	5
2.3	Surface runoff	8
2.4	Gutter flow	11
2.5	Flow in conduits	12
3.	BASIC EQUATIONS FOR UNSTEADY GRADUALLY VARIED FREE SURFACE FLOW	15
3.1	General	15
3.2	The shallow water equations	16
3.3	Initial and boundary conditions	17
3.4	Dimensionless shallow water equations - magnitude of the terms	20
3.5	Celerity and attenuation of waves	23
4.	APPROXIMATIONS OF THE SHALLOW WATER EQUATIONS	27
4.1	Simplification of the equation of motion	27
4.2	The kinematic wave approximation	29
4.2.1	The kinematic wave equations	29
4.2.2	Analytical solution of the kinematic equations in case of only lateral inflow	32
4.2.3	Analytical solutions in some special cases	34
4.2.4	The kinematic wave including the lateral momentum term	38
4.2.5	Kinematic shocks	39
4.2.6	Applicability of the kinematic wave equation	42

Preceding page blank

4.3	The diffusive wave approximation	45
4.3.1	Basic equations - the diffusion analogy	45
4.3.2	Applicability of the diffusive wave equations	45
4.4	Summary and discussion	50
5.	THE FRICTION LOSSES OF OVERLAND FLOW	53
5.1	General	53
5.2	Alternative formulations of the friction relation	54
5.3	Investigation of friction losses in surface flow	58
5.3.1	General	58
5.3.2	Flow over a smooth surface	58
5.3.3	Flow over "artificially roughened" surfaces	62
5.3.4	Flow over asphalt and concrete surfaces	66
5.4	Rollwaves	70
5.5	Wind forces	71
5.6	Summary and discussion	72
6.	NUMERICAL SOLUTION METHODS OF THE KINEMATIC WAVE EQUATIONS	77
6.1	General	77
6.2	Finite difference schemes	77
6.3	The weighted box scheme - general properties	80
6.3.1	Finite difference equations	80
6.3.2	Numerical diffusion - consistency	82
6.3.3	Classification of weighted box models	83
6.3.4	'Negative diffusion' ($D_n > 0$)	85
6.3.5	Positive diffusion ($D_n < 0$)	86
6.3.6	Selection of numerical parameters	88
6.4	The weighted box scheme - numerical experiments	89
6.4.1	Aim and scope of the experiments	89
6.4.2	Numerical models and experiments	91
6.4.3	The α-diffusive models (α;0.5)	92
6.4.4	The β-diffusive models (0.5; β)	96
6.4.5	The $\alpha\beta$-diffusive models (α;β)	98
6.5	The Lax-Wendroff scheme	91
6.6	Classification of routing methods	100

6.7	Numerical solution of the diffusive wave equation - a comparison	101
6.7.1	The basic diffusive equation	101
6.7.2	The convective diffusion equation	102
6.8	Summary	103
7.	RESERVOIR AND CASCADE MODELS	106
7.1	General	106
7.2	Reservoir models	107
7.2.1	Linear-nonlinear reservoir models	107
7.2.2	The Time-lag model	108
7.3	Cascade of linear reservoir models	109
7.3.1	Basic equations	109
7.3.2	The time of concentration, t_c, in the Time-Area Method	111
7.3.3	The time area diagram in the Time-Area Method	113
7.4	Summary	118
8.	BASE CATCHMENT MODELS	120
8.1	General considerations	120
8.2	General characterization of the test catchments and measurements	121
8.3	Models and criteria for comparison of runoff hydrographs	124
8.4	Kinematic wave model simulation - comparisons with recorded hydrographs	125
8.4.1	Detailed geometrical description of the catchments	125
8.4.2	Comparison between recorded and simulated runoff	125
8.5	Simulations using simplified geometric input data	130
8.5.1	General	130
8.5.2	Representation of catchments with no sewer net - the KW3, KW4G and KW6G models	131
8.5.3	Representation of catchments with a sewer net - the KW6S, KW6S-S and KW4G-I models	134
8.5.4	Application of simplified geometric models	137
8.5.5	Simulations by simplified geometric models	139
8.6	Simulations by the Time-Area Method	144
8.7	Summary	147

9.	BASE CATCHMENT MODELS APPLIED	150
9.1	General	150
9.2	Kinematic wave model simulation - comparisons with recorded hydrographs	151
9.3	Simulations using different levels of base catchment sizes	152
9.4	Simulation by the Time-Area Method	154
9.5	Summary	156
10.	EVALUATION OF STATISTICAL MAXIMUM FLOWS	158
10.1	General	158
10.2	Basic deterministic relations	158
10.3	The Rational Method	160
10.4	The time of concentration	162
10.5	Evaluation of the maximum flow	163
10.6	Tests - discussion	164
LIST OF SYMBOLS		169
REFERENCES		175
LIST OF FIGURES		189
LIST OF TABLES		195

VOLUME II

PREFACE	I
CONTENTS	III
APPENDIX I - TEST AREAS AND FIELD MEASUREMENTS	1
APPENDIX II - SIMULATED AND RECORDED HYDROGRAPHS	18

SUMMARY

The study deals with modelling of the urban runoff process. The main objectives were to make recommendations for the selection of a basic model and suitable numerical solutions, and also to investigate the importance of discretization of the geometrical input data and develop usable base catchment models. (A base catchment model is the smallest part into which the catchment is subdivided and defines the sewer net modelled.) Runoff from permeable surfaces is not considered in the study.

The runoff process in surfaces, gutters and sewers is described by one continuity and one momentum equation, the shallow water equations. These are not very practical in application and a lot of computation can be saved by simplifying the basic formulation. By neglecting certain terms in the momentum equation, simplified sets of equation systems are obtained. A study of the influence of different terms shows that there are two approaches of interest in urban runoff modelling, the kinematic and the diffusive wave approximations.

The kinematic wave approximation is defined by a very simple set of differential equations and boundary conditions. The momentum equation is reduced to an unique relation between flow and water depth. Despite this, in the general case the equations have to be solved by numerical methods. In the case of constant lateral inflow an analytical solution is obtained. It is then possible to derive relations for the evaluation of the time of concentration based on the kinematic wave model. In the model, the flow waves travel with the kinematic wave velocity which is greater than the mean velocity and varies in both time and space. The kinematic wave model does not take backwater into account and in theory it is not able to reproduce the dynamic attenuation of a flow wave.

In the diffusive wave approximation a downstream boundary condition is needed. Then it is possible to analyse systems significantly influenced by backwater. The model also reproduces the main part of the dynamic attenuation of the wave.

In urban runoff modelling where the geometries usually have to be simplified, it is difficult to formulate the relevant downstream boundary conditions (with the exception of the main sewer line). Flow in lateral inflow reaches, such as surfaces, gutters or sewers with lateral inflow, is exposed to a characteristic (not dynamic attenuation). This "attenuation" is generally more significant than the dynamic attenuation and is properly reproduced by the kinematic wave model. From a theoretical point of view the kinematic wave model appears to be suitably sophisticated for base catchment modelling.

In the kinematic wave approximation the momentum equation is represented by a friction relation. In the study results from reported investigations of friction losses over rough surfaces have been put together. The study gives no base for using differentiated roughness parameters at different types of surfaces in an ordinary urban catchment. Neither could a relation between the friction factor and rain intensity be specified.Several friction relations for instance the Danish L-formula, the quadratic formula and the Manning formula, were compared with the reported friction loss studies. They were found to fit reasonably well to the test data, provided a suitable roughness parameter was used. As a general relation for overland flow, the Manning formula was selected with a roughness coefficient n=0.016 for surface flow and n=0,013 for gutter flow.

The numerical solution method commonly used for the kinematic wave equations gives rise to considerable numerical attenuation of flow waves. In order to keep this to a level close to the dynamic attenuation very

small space steps have to be used ($\Delta x/L < 1/15$). For each space step the solution is evaluated by an iterative technique. By a slight modification of the solution algorithm (the β-diffusive model) greater space steps may be used with retained low numerical attenuation.

By assuming the wave velocity to be constant in space, time or both space and time, simplifications of the solution algorithm can be made. The non linear reservoir model and the Time-Area Method are examples of the first two alternatives; the Rational Method is an example of the third. It was found that the performance of the Time-Area Method in simulating real storm events is as good using a linear time-area diagram as using diagrams of any other shape.

Recorded rainfall and runoff from six small catchments (<1 hectare contributing area) were used to test the kinematic wave model. It was found that the kinematic wave model based on a detailed description of this catchment reproduced the runoff process reasonably well.

The detailed model was used to test the effect of different degrees of simplification of the catchment parameters and to test the Time-Area Method. It was found that the performance of the kinematic wave model is still very good even for quite great simplifications of the catchment geometries such as

- replacement of gutters with increased surface lengths
- assuming only lateral surface inflow to the main sewer line
- using the mean slope of the main sewer line
- excluding minor branches in the sewer system.

The simulations by the Time-Area Method showed that reasonably accurate values of single flow peaks may be obtained. However, the general shape and delay of the

simulated hydrographs were not in level with those of the kinematic wave models.

Independent of which model is used the main difficulty is to choose input data, such as surface length, slope or time of concentration, in order to get properly attenuated hydrographs. In the study the choice was based on the evaluation of representative times of concentration by kinematic wave based relations. As the evaluation is approximate there is a risk of incorrect attenuation. The risk of large errors is greatest for the simplest models (the KW3 model and the Time-Area Method). A closer evaluation of the time of concentration would increase the accuracy of the models. However, a more sophisticated way of estimating this time is not meaningful when the basic idea is to develop a simplified method of creating input data for the models.

The optimal geometric simplification for the kinematic wave model, regarding both the demand for simplicity in input data and accuracy, is described by the KW6S model. The model is built up of a sewer with the length and mean slope of the main sewer line in the catchment. The sewer is lateraly fed by a surface with length and slope corresponding to an estimated time of concentration which is representative for runoff to the main sewer line.

The tested runoff models were also applied as base catchment models in two urban catchments with total areas of 15 and 19 hectares. Three levels of subdivision into base catchments were tested where the finest division corresponds to sizes round 0.5 ha.

The simple KW6S model was applied as base catchment model at the three different levels of subdivision. Using greater base catchment sizes the performance is not quite as good. However, there are no drastic changes and it is obviously possible to obtain a very good performance using quite large base catchments, provided the catchment

characteristics (the representative times of concentration) are properly evaluated. It should here be stressed that as the base catchment area increases the effects of making misjudgements in this evaluation increases. It was also found that when the main sewer system contains several long branches these have to be included in the input data system and should not be replaced by one main sewer line.

The Time-Area Method does not perform quite as well as the kinematic wave model despite the fact that the same amount of catchment data is required. Though the model properly used has a performance which is acceptable in many applications there is no obvious argument for its use.

From the tests with base catchment models it was concluded:

Independent of model and base catchment size, the input parameters in the base catchment model (overland flow parameters) has a significant effect on the attenuation of the outflow hydrograph.

The kinematic wave model (KW6S-model) is both simple to use and adequate as base catchment model.

With this model relatively great simplifications of the input data geometry can be used with reasonably well maintained performance provided the catchment characteristics are properly evaluated.

These catchment characteristics can be evaluated using relations derived from the kinematic wave theory assuming constant rain intensity.

The Rational Method is the traditional method in urban drainage design and is used to evaluate single design flow values. Basically the method relates the distribution functions of rain intensity and runoff in a catch-

ment. The relevance of the method was tested by comparisons with distribution functions evaluated for a number of catchments. The distributions were obtained from simulations of a series of historical storms by a detailed runoff model (the CTH-model). The method was found to perform well when a time of concentration evaluated by relations based on kinematic wave theory was used (also used in base catchment modelling).

Based on the results of the study, the following recommendations are given for use in urban runoff modelling:

- A distributed kinematic wave model is the most suitable model for all parts of the runoff system.

- A numerical solution method with the smallest possible artificial attenuation (preferably the β-diffusive model) should be used. If the conventional solution is used, Δx should be small ($\Delta x/L$ about 1/10).

- The Manning formula is a suitable friction relation which, in the model proposed above and for ordinary applications, should use the roughness coefficient n=0.016 and 0.013 for surface and gutter flow respectively.

- It is advantageous to keep the time step constant beween different applications. For typical Swedish conditions and applications Δt=60s is an appropriate value.

- By using a model as recommended above, quite complex runoff system geometries may be replaced by simple ones. This is true provided that the equivalent parameters in the simplified geometric model are estimated on the basis of equal times

of concentration in the 'real' and simplified geometries (using kinematic wave based relations). One example of a suitable simplified geometric model is the KW6S model.

- The Time Area Method (though not recommended here) should be used with a linear time area diagram and a time of concentration evaluated by kinematic wave based relations.

- The Rational Method is a suitable method for calculating flow rates in the preliminary design stage of a network system, in small or 'simple' systems, and also for checking the input data for more complex models. When this method is used, again, the time of concentration should be evaluated by kinematic wave based relations. Particular care should be taken in estimating t_c when this time is short.

1. INTRODUCTION

1.1 Urban runoff modelling

The analysis and design of urban drainage systems was traditionally, and is still often, executed using the Rational Method. That method, however, has for a long time been regarded as too approximate for many applications. With the introduction of computers into the calculations, several advanced runoff models have been developed and brought into use among consulting engineers. At least five advanced models for the design and analysis of urban network systems are now in commercial use in Sweden. These models use traditional hydraulics in a systematic way giving a very accurate and detailed description of the flow through the drainage system for a prescribed storm input.

Detailed runoff models have been shown to be very useful, especially in the analysis of existing systems and in the design of complex systems (containing detention basins, overflows, constrictions and so on). In the design of "simple" network systems and for estimates and checks, the Rational Method is still an important alternative model.

The user working in the field of urban drainage design must be able to handle models intended for both detailed analysis and making rough estimates. Regardless of the problem to be solved the modelling work should be performed in four main steps

- selection of a suitable model
- transformation of the "real" catchment into the "input data" catchment
- selection of the hydrological design event
- interpretation of the output obtained from the computation step.

Preceding page blank

The second step is very important and may be accomplished at many different levels of precision. Crucial for the success of this step is a thorough knowledge of the properties of the model in use. This is also very important in the last step. An advanced interpretation of the performance of a simple model is always better than a poor interpretation of the performance of an advanced model.

Every detailed runoff model is built up of two main submodels. One treats the collection of stormwater on the surface including the transport to the sewer network system. The other describes the transportation of water within the network system. In available runoff models a wide range of approach is used for overland flow routing from the Time-Area Method to the kinematic wave approximation.

The model user is in practice not able to describe the catchment geometry with every pavement and roof in detail. In generating the model input he has to simplify and this he does by defining a main sewer network. The upstream ends of the network are connection points to what will here be called base catchments. These will normally contain several different runoff surfaces, gutters and small diameter sewers.

The base catchment is represented by a simplified geometry and the runoff from it by a model containing an overland flow routing element. The important geometrical discretization of the catchment in the model input is thus given by the definition of the main network. As the network is usually well specified, the main approximations and difficulties will be in the modelling of runoff from the base catchment. Essential for the effective and precise use of urban runoff models is a balanced geometrical discretization and a sound base catchment modelling.

1.2 Scope of the study

The scope of the study is to

- o discuss various approaches for overland flow models
- o discuss different levels of geometric discretization
- o develop a methodology for base catchment modelling.

The first point includes discussion of both basic equations and numerical methods of solution.

Generally the study is based on theoretical considerations and numerical experiments based on field data. This rather fundamental approach is considered to make the results generally applicable to any runoff model in use today.

In runoff simulation the primary result is a runoff hydrograph. This hydrograph is characterized by its volume and shape. For a given storm the runoff volume is governed only by the prescribed runoff areas and the retention storage and not by the properties of the model (with the exception of systems containing overflows). Comparisons between different models and geometric discretizations will therefore be focused on differences in hydrograph shapes.

All simulations in the report have been executed assuming that there is no influence from permeable urban surfaces. The assumption is applicable to the majority of Swedish urban catchments and runoff cases. It is based on experience from a series of field measurements made over the last ten years in Sweden, see for instance Arnell and Lyngfelt (1975), Falk and Niemczynowicz (1978) and Arnell (1980).

1.3 Arrangement of the contents

The report is made up of three main parts:

The first part deals with the properties of the basic differential equations for free surface flow including the diffusive and kinematic wave equations. Friction relations are also discussed and a literature review of friction loss investigations of surface flow is given.

The second part deals with numerical methods of solution for the kinematic and diffusive wave equations. In connection with these methods, further simplified overland flow models, such as the Time-Area Method and reservoir models, are analysed.

The third part deals with the problem of geometrical discretization and representation in base catchment modelling. The analysis is mainly based on comparative numerical experiments. Simulated hydrographs are given in appendix II.

The basis of the study is a series of field measurements in urban areas and a specially developed runoff model. Details of this work are given in several reports and also in appendix I.

To give a background to the mathematical analysis, an attempt is made in the next chapter to describe the characteristics of urban runoff, such as rain intensity, velocity of rain drops, surface/sewer flow and catchment/network geometry.

2. URBAN RUNOFF CHARACTERISTICS

2.1 General

Storm water runoff in urban areas is a complex process which is governed by many hydrological and geometric variables such as rain intensity and surface slope. The selection and application of urban runoff models requires a thorough knowledge both of the processes involved and of the governing variables. In this chapter these characteristics are described from a rather general point of view. For some variables values which are typical for Swedish conditions are also given.

Some runoff characteristics, such as wave velocity and friction, are discussed in connection with the corresponding mathematical representation in later chapters.

The runoff process is divided into overland flow and flow in the sewer net, where the overland flow is related to all water movement above ground. The overland flow is divided into surface flow and gutter flow, where gutter flow designates all flows that collect surface flow, for instance gutters, rills or roof collectors.

2.2 Precipitation

Precipitation is the origin of runoff and influences overland flow in several ways. The most important variables are rain intensity i, rain drop velocity U_i and the direction of rainfall Ψ.

The rain intensity has a very marked variation with time. A typical pattern for a storm event is given in figure 2.2.1. The averaging time here is one minute. On this scale very high intensities, greater than 150 l/s·ha (54 mm/h), may temporarily occur.

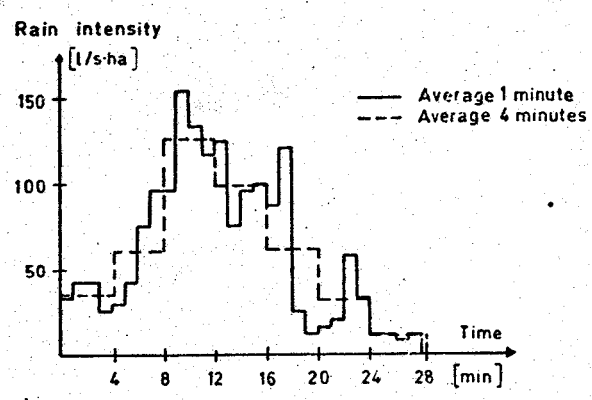

Figure 2.2.1 Typical intensity variations for a storm event

If the averaging time is increased then corresponding intensities will become increasingly attenuated compared with the real storm intensities, figure 2.2.1. The

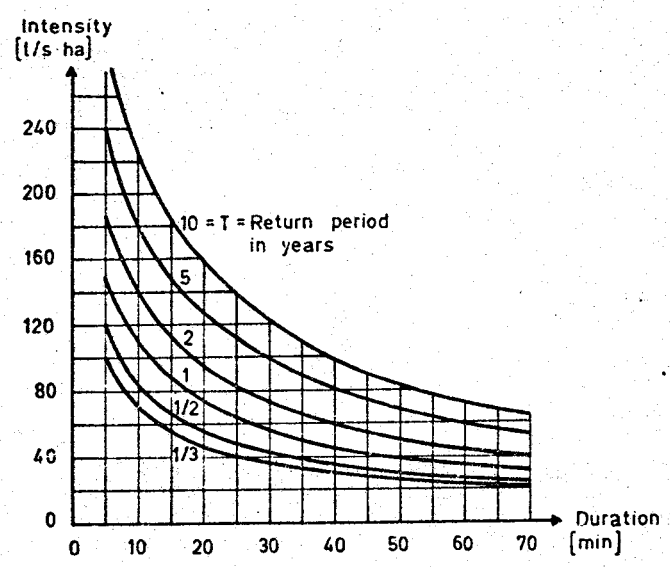

Figure 2.2.2 IDF-diagrams used in Göteborg, after VAV (1976)

intensity duration frequency diagram (IDF-diagram) is based on averaged intensities in a long series of storms using different durations, see figure 2.2.2. The diagram gives an idea of the time scale of rain intensities. Analysis of the characteristics of runoff hydrographs indicates a suitable averaging time of one mirute for typical applications of runoff models. A representative interval for rain intensities used in runoff models is 5 - 150 l/s·ha.

Rain intensities measured by a rain gauge are only valid for the area of the gauge itself. However, in practical applications these point values are used for a catchment surrounding the raingauge. The introduced error will depend on the properties of the storm and the catchment area. As the catchment areas used in this study are quite small (0.04 - 22 ha) the error should not be significant, Niemczynowicz (1984).

Laws et al. (1941) analysed the sizes of raindrops for different types of rain and rain intensities. They found that the drop diameter increased with rain intensity. According to their study the majority of drops have diameters between 1 and 3 mm, in the intensity interval given above. The raindrops have normally reached their terminal velocity when they hit the ground. This velocity

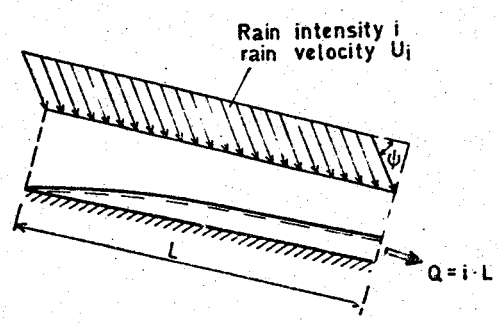

Figure 2.2.3 Water surface at constant rain-intensity and rain velocity vectors

depends on the dropsize and varies between 4 and 9 m/s.

When the raindrops are falling vertically the angle between the surface and velocity vector (see figure 2.2.3) is determined by the slope of the surface. If wind forces are acting on the raindrops they also will be given a horizontal velocity component. A wind velocity of 6 m/s will give a value of Ψ around 45°. The more intense storms are seldom connected with strong winds and 45° is believed to be an extreme value.

2.3 Surface runoff

The surface flow is characterized by the velocity U_s and the water depth Y_s in each flow section. It is governed by the storm variables and the geometric parameters length L_s, slope S_s, and surface roughness.

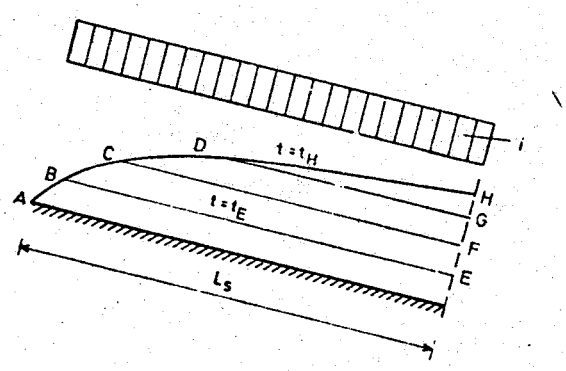

Figure 2.3.1 Water surface profiles when the rain intensity is constant and the time $t < t_c$. (The scaling of water depths is not realistic).

Certain properties of surface runoff are caused by the source of flow being entirely lateral, see figure 2.3.1. From the start of rain, water surface profiles similar to those of figure 2.3.1 (A-B-E → A-C-F → A-D-G) will

develop successively . If the time taken for water particles from the upstream part of the surface to reach the outflow section is denoted by t_c, the profile A-H will be fully developed at time $t=t_c$ after the onset of rain. When $t<t_c$ the part of the surface that has not been reached by water from the upstream end will have uniform water depth (profiles B-E, C-F, D-G).

Typical recession water profiles when the rain has ceased ($t>t_c$) are shown in figure 2.3.2. The water depth is gradually decreasing with time all over the surface (A-D → A-C → A-B).

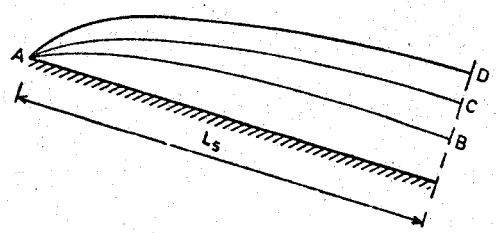

Figure 2.3.2 Water profiles when $i=0$ and $t>t_c$ (The scaling of water depths is not realistic)

This two-dimensional representation of surface flow with constant slope is called sheet flow. The water profiles are valid provided the influence from the downstream boundary is negligible. This is the case for ordinary urban runoff surfaces and the water depth then normally increases downstream ($\partial Y/\partial x>0$). Typical values are 0.5 - 3 millimetres. Corresponding flow velocities are 0.01 - 0.4 m/s.

Evaluation of Reynolds' numbers representative for surface flow indicates laminar flow. This is, however, turned into a turbulent state by the impact of raindrops and by the unevenness of the surface. As the rain recedes, with the decreasing waterdepth, the flow may, however, take on a laminar character.

The main part of the storm water is collected on impermeable surfaces such as roofs, streets and parking areas. Normal flow lengths L_s are 5 to 30 metres. In special cases (for instance at airports) greater lengths are accepted but rarely exceed 70 m. The slope S_s is usually around 0.03 or more and very seldom less than 0.01. The most important reason for using relatively large slopes on surfaces is to avoid the risk of ponding caused by local settings.

When rain starts to fall over the initially dry impermeable surface it first wets the surface and then fills up all the depressions. This part of the rain volume, usually denoted depression storage will evaporate when the rain ceases. The magnitude of depression storage depends basically on the "roughness" of the surface (asphalt, concrete etc.) and the large scale depressions. These are the effects of settlings and the lack of precision in laying the surface. Several investigators have analysed the depression storage, see Pecher (1969, 1970), Arnell and Lyngfelt (1975), Kidd (1978), Falk et al. (1979). For impermeable surfaces most investigators suggest a depression storage ranging from 0.4 to 0.7 mm for surface slopes greater than 0.01.

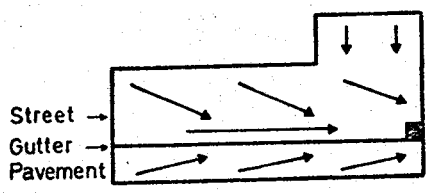

Figure 2.3.3 A part of a street with gutter, pavement and inlet

Very often urban surfaces have a main slope that is not parallel to the boundaries, see for example figure 2.3.3. In this case and others with irregular surfaces, strips along the direction of mean slope have different lengths.

Thus cross-sections perpendicular to this direction will have different water-depths. These differences introduce velocity components perpendicular to the direction of the mean slope. In addition the cross-section is not actually plane which also introduces such components and make the moving water form rills. The water depths are often of the same order as the the irregularities caused by the surface material, for instance asphalt has local differences in level of several millimetres. Furthermore the water is accelerated or retarded because of local differences in slope in the direction of flow.

Surface flow is obviously far more complex and irregular than that described here as sheet flow. In practical modelling it is, however, impossible to get closer to the physical behaviour of surface flow than this assumption.

2.4 Gutter flow

The gutter flow is characterized by the mean flow velocity U_g and the water depth Y_g. It is governed by the surface flow and the geometric parameters length L_g, slope S_g, cross-sectional shape and roughness.

The gutters, in the same way as surfaces, are exposed only to lateral inflow as source. Therefore the development of the water depth in the gutter is, in principle, the same as that described for surfaces.

Normal flow length is 30 to 60 metres but a length up to 100 metres may exist. The slope is generally in the range given for surface flow but sometimes smaller slopes are accepted and a lower limit would be around 0.005. The cross-section of roof drains are well defined, rectangular or circular. The gutters at the side of the pavement or rills on a large surface have usually the same side wall slope as the surface. A standard side wall slope would then be around 0.03. The cross-section for these flows will become relatively wide and have properties

similar to those of the downstream end surface flow.

Considering the geometrical and hydrological factors given above, gutter flow should be mainly turbulent. Laminar flow may occur at the upstream end at low intensities. Typical mean velocities are 0.4 - 0.8 m/s.

The lateral inflow to the gutter will have a velocity vector with a direction angle ϕ as defined in figure 2.4.1. At $\phi = 90^{o}$ the surface flow vector is perpendicular to the gutter flow. This direction angle depends on the slopes of the gutter and surface, S_g and S_s respectively. (S_s is here the surface slope perpendicular to the gutter). For small slopes $\tan \phi \approx S_s/S_g$ which corresponds to values of ϕ in the interval 10° - 85°.

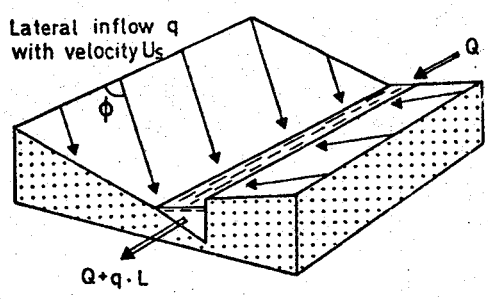

Figure 2.4.1 Gutter flow with lateral inflow

The gutter flow is collected in inlets, which do not always have the required capacity, in which case parts of the flow will pass the inlet. Important properties of the inlet are the grating and the inflow velocity, Eskenazi (1984).

2.5 Flow in conduits

The flow in conduits is characterized by the mean velocity U_p and the water depth Y_p. It is governed by the inflow and the geometric parameters length L_p, slope S_p, diameter D_p and roughness.

The sewers in an urban drainage system are geometrically better defined than the part above ground. This is true in both the analysis of existing systems and the design of new ones. The flow section is also better defined. The sewers are connected by manholes in order to simplify inspection. Between the manholes the sewer is usually straight and has constant slope. The distance between manholes rarely exceeds 100 m. The slope is primarily governed by topography and consequently varies within a wide range of values. In order to avoid sedimentation a minimum slope of 0.001 to 0.005, depending on the diameter, is used, VAV (1976). This limitation of slope and the low friction factor of sewers causes relatively high velocities and often supercritical flow. Typical flow velocities are 0.5 - 1 m/s. Of special interest in this report are sewers connecting gullies or down pipes to the main sewer system. Standard diameters in this part of the network system are 200-400 mm. These sewers are comparatively long and run with small water-depths, both factors which significantly affect the runoff hydrograph.

Despite the use of minimum slopes sedimentation in sewer systems is not unusual. This affects the runoff with respect both to capacity of sewers and attenuation of flow waves, Berg (1983).

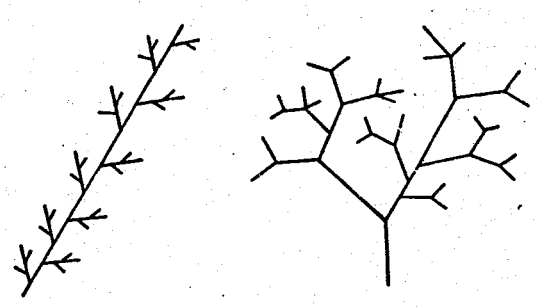

Figure 2.5.1 Network system of the band and the tree type

The network system may be characterized by two basic structures, the tree and the band types, see figure 2.5.1. The two structures may of course be combined to give more irregular types.

3. BASIC EQUATIONS FOR UNSTEADY GRADUALLY VARIED FREE SURFACE FLOW

3.1 General

In application, the modelling of storm water runoff cannot be accomplished in great detail. Simplifying assumptions have to be accepted in the formulation of the differential equations and in their numerical solution, as well as in the geometrical description of the catchment. Despite the fact that the complete basic equations are almost never used in urban runoff modelling, it is necessary to discuss their properties in order to understand the simplified versions.

The movement of water over surfaces, in gutters and in sewers caused by rain can be regarded as unsteady, spatially varied, free surface flow in a prismatic channel. A flow with these characteristics is described by the shallow water equations, which are two partial differential equations derived from the laws of conservation of mass and momentum. The equations are based on several assumptions which appear to limit their application, Yevjevich (1975). However, the equations have been found to be valid for a wide range of unsteady flow cases. The shallow water equations have been verified in natural channels as well as in man made channels, see for instance, Yevjevicn (1975) and Brausert (1971).

The derivation of the shallow water equations can be found in several references, for example, Eagleson (1970), Ligget (1975) and Sjöberg (1976), and is therefore not presented here. In this chapter their basic properties and relevance to urban runoff are discussed.

3.2 The shallow water equations

The equations describe the continuity and dynamic properties of the flow. If the lateral inflow is considered they may be written

$$\frac{\partial Q}{\partial x} + \frac{\partial A}{\partial t} = q \qquad \text{... (3.2.1a)}$$

and

$$\frac{\partial Q}{\partial t} + \frac{\partial}{\partial x}(\beta \cdot \frac{Q^2}{A}) + gA \cdot \frac{\partial Y}{\partial x} - gA(S_o - S_f) - qU\cos\phi = 0 \quad \text{.. (3.2.1b)}$$

where (as also given in chapter 2)

- x = coordinate in flow direction
- t = time
- Y = $Y(x,t)$ = water depth
- A = $A(x,t)$ = cross-sectional area of flow
- Q = $Q(x,t)$ = flow rate
- S_o = $\tan\alpha$ = bottom slope, where α = slope angle
- S_f = friction slope (defined in section 5.1)
- q = $q(t)$ = lateral inflow (flow/unit length)
- i = $i(t)$ = rain intensity (flow/unit area)
- U = mean velocity of lateral inflow
- ϕ = angle between main and lateral flow (figure 2.4.1)
- q = $i \cdot B$ in the surface flow case
- ψ = ϕ in the surface flow case (figure 2.2.3)
- B = width of cross sectional area
- β = correction factor for the cross-sectional velocity distribution
- g = acceleration due to gravity

In the derivation it is assumed that $\sin\alpha \approx \tan\alpha$ and $\cos\alpha \approx 1$, which gives a resulting error less than about 1% for $\tan\alpha < 0.05$. Morris (1979) analysed this approximation for a range of overland flow cases and found no significant effect on depth and velocity profiles.

The terms in the momentum equation are here called

- o local acceleration term $\frac{\partial Q}{\partial t}$
- o convective " " $\frac{\partial}{\partial x}(\beta \cdot Q^2/A)$
- o pressure force " $gA \cdot \frac{\partial Y}{\partial x}$
- o "slope" " $gA \cdot (S_o - S_f)$
- o lateral momentum " $qU\cos\phi$

3.3 Initial and boundary conditions

A solution of the shallow water equations requires initial and boundary conditions to be specified. The basic properties of the equations and their connection to these conditions are best illustrated by applying the method of characteristics.

The basic equations may be transformed to a system of ordinary differential equations, see Sjöberg (1976). Using the formulation from the previous section gives

$$\frac{dQ}{dt} - (V - \sqrt{g\frac{A}{B}})\frac{dA}{dt} - g \cdot A \cdot (S_o - S_f) + q \cdot ((V - \sqrt{g\frac{A}{B}}) - U \cdot \cos\phi) = 0 \qquad \ldots (3.3.1a)$$

which is valid if

$$\frac{dx}{dt} = V + \sqrt{g \cdot \frac{A}{B}} \qquad \ldots (3.3.1b)$$

and

$$\frac{dQ}{dt} - (V + \sqrt{g\frac{A}{B}}) \cdot \frac{dA}{dt} - gA \cdot (S_o - S_f) + q((V + \sqrt{g\frac{A}{B}}) - U\cos\phi) = 0 \qquad \ldots (3.3.1c)$$

which is valid if

$$\frac{dx}{dt} = V - \sqrt{g \cdot \frac{A}{B}} \qquad \ldots (3.3.1d)$$

where $B = B(x,Y)$ is the width of the cross-sectional area at the water table.

Equations (3.3.1b) and (3.3.1d) express two wave velocities of a disturbance emanating from an arbitrary point in the channel. The velocities appear in the x-t plane as two lines or characteristics. The line corresponding to equation (3.3.1b) is here called the p-characteristic, and that corresponding to equation (3.3.1d) is the n-characteristic. Equation (3.3.1a) is satisfied along the p-characteristic and equation (3.3.1d) along the n-characteristic. In each point where two known characteristics meet, the equations may be solved for Q and A. This is what is known as the method of characteristics.

The equations (3.3.1b) and (3.3.1d) may be written

$$\frac{dx}{dt} = \sqrt{g \cdot \frac{A}{B}} \cdot (F_o \pm 1) \qquad \ldots (3.3.2)$$

where the Froude number F_o is given by

$$F_o = \frac{V}{\sqrt{gA/B}} \qquad \ldots (3.3.3)$$

In subcritical flow, where $F_o<1$, the p-characteristic is directed downstream and the n-characteristic upstream, see figure 3.3.1. In supercritical flow both characteristics are directed downstream.

The direction of characteristics clearly demonstrates the required initial and boundary conditions for different flow regimes. The initial conditions

$$A = A(x,0) \quad \text{and} \quad Q = Q(x,0)$$

are always needed, regardless of the flow regime. In <u>subcritical</u> flow the boundary conditions

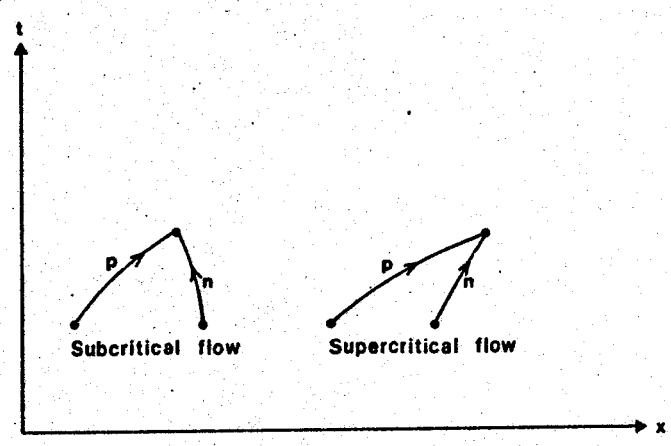

Figure 3.3.1. Characteristic directions in sub- and supercritical flow

$$A = A(0,t) \quad \underline{or} \quad Q = Q(0,t)$$

and

$$Y = Y(L,t) \quad \underline{or} \quad Q = Q(L,t) \quad \underline{or} \quad Q = f(Y)$$

are needed. In <u>super critical</u> flow the boundary conditions

$$A = A(0,t) \quad \underline{and} \quad Q = Q(0,t)$$

are both needed (no downstream condition required).

The requirement of boundary conditions will obviously vary with the flow regime. In sewer routing, the regime will often vary rapidly which will complicate the solution and usually require very small steps in both time and space. The accuracy of the method of characteristics is governed by the distance between the selected calculation points. Using adequate distances the method is very accurate and is often used for comparisons with more approximate numerical schemes. The method is sometimes referred to as the "exact" solution, Sjöberg (1976).

3.4 Dimensionless shallow water equations - magnitude of the terms

There are several reasons both practical and theoretical, for examining the possibility of simplifying the mathematical description given in the shallow water equations. It is thus of interest to analyse the relative magnitudes of terms. One way is to make the equations dimensionless by making the following substitutions

$$A^* = A/A_o$$
$$Q^* = Q/Q_o = Q/(q_o L) \quad (L = \text{length in flow direction})$$
$$Y^* = Y/Y_o$$
$$q^* = q/q_o$$
$$V^* = V/V_o$$
$$U^* = U/U_o$$
$$x^* = x/L$$
$$t^* = tV_o/L$$

which apply to flow elements fed by a lateral source, see Woolhiser (1967). Subscript o refers to a chosen suitable stationary flow, for instance normal flow at a lateral inflow of q_o, and * denotes a dimensionless variable. Here, q_o is used for both lateral inflow (to a gutter) and rain inflow to a surface ($q_o = i \cdot B$ for surface flow).

The continuity equation (3.2.1a) becomes

$$\frac{\partial Q^*}{\partial x^*} + \frac{\partial A^*}{\partial t^*} = q^* \qquad \text{... (3.4.1a)}$$

and the equation of motion (3.2.1b) becomes

$$\frac{\partial Q^*}{\partial t^*} + \beta \cdot \frac{\partial}{\partial x^*}\left(\frac{(Q^*)^2}{A^*}\right) + \frac{Y_o}{V_o^2} \cdot gA^* \cdot \frac{\partial Y^*}{\partial x^*} - \qquad \text{... (3.4.1b)}$$

$$- \frac{L}{V_o^2} \cdot gA^* \cdot S_o \cdot \left(1 - \frac{S_f}{S_o}\right) - \frac{U_o}{V_o} \cdot \cos\phi \cdot q^* \cdot U^* = 0$$

If the kinematic wave number

$$K_o = \frac{L \cdot S_o}{Y_o \cdot F_o^2} \quad \text{or} \quad \frac{L \cdot S_o \cdot g}{V_o^2} \qquad \ldots (3.4.2)$$

is introduced the equation (3.4.1b) may be written

$$\frac{\partial Q^*}{\partial t^*} + \beta \cdot \frac{\partial}{\partial x^*} \left(\frac{(Q^*)^2}{A^*} \right) + \frac{1}{F_o^2} \cdot A^* \cdot \frac{\partial Y^*}{\partial x^*} - \qquad \ldots (3.4.3)$$

$$-K_o \cdot A^* \cdot (1 - \frac{S_f}{S_o}) - \frac{U_o}{V_o} \cdot \cos \phi \cdot q^* U^* = 0$$

The relative importance of different terms in the equation above can be shown by comparing the magnitudes of corresponding dimensionless parameters. This requires estimated representative values of the parameters, which here have been calculated from the characteristic values of rain intensities, slope and lengths of flow reaches etc. given in chapter 2. The following discussion of the relation between terms is based on these values.

In overland flow, the Froude number will not depart very much from unity. The pressure force term is thus of the same order of magnitude as the dynamic terms. Usually, the magnitude of one dynamic term is less than 20% of the pressure force term.

In typical overland flow situations the kinematic wave number exceeds several hundreds. Thus the forth term $K_o A^*$ normally dominates the first three.

If the raindrops have a horizontal velocity component they may give a momentum contribution to the flow as described by the fifth term in equation (3.4.3). However, each drop also create a disturbance when it penetrates the water on the surface. It is questionable if the complex impact of the raindrops could be described as a

pure momentum contribution. Therefore, in surface flow, the lateral momentum term is normally neglected despite the fact that, in theory, it may be significant. The impact of rain drops will be discussed further in the two chapters which follow.

In gutter flow, the lateral term is governed by the relation between surface slope and gutter slope. For the representative values given in chapter 2, the lateral term is not significant in gutter flow.

The slope term appears in typical flow cases to be the most significant. If all other terms are neglected the equation of motion is reduced to

$$K_o \cdot A^* \cdot (1 - \frac{S_f}{S_o}) = 0 \qquad \ldots (3.4.4)$$

or

$$S_f = S_o \qquad \ldots (3.4.5)$$

This considerable simplification of the momentum equation is called the kinematic wave approximation and, together with the continuity equation, forms the kinematic wave equations. The properties and the validity of the kinematic wave approximation are analysed in chapter 4.

The comparison of terms in this section is only valid if upstream and downstream boundary conditions do not significantly influence the flow. This is generally true in overland flow, because of the relatively small water-depth and great slope, see Morris (1979). The discussion presented here is not generally applicable to flow in conduits.

The significance of the different terms in the equation of motion has also been analysed by Jacobsen (1980). He obtained basically the same results including significant shear stresses caused by wind (discussed in section 5.5).

3.5 Celerity and attenuation of waves

The linearized dimensionless basic equations can be solved analytically for certain simplified conditions. An example of such a solution was presented by Ponce and Simons (1977) and is described below. The solution is based on a small amplitude sinusoidal wave superimposed on a steady uniform flow of depth Y_o and involves no lateral inflow and no influence from boundaries (see section 3.4). The dimensionless solution is given by the relations

$$c^* = c^*(F_o, \sigma_o) \qquad \ldots (3.5.1)$$

and

$$\delta = \delta(F_o, \sigma_o) \qquad \ldots (3.5.2)$$

where $c^* = c/V_o$ is the dimensionless wave velocity or celerity and $\delta = \ln(a_2/a_1)$ is the logarithmic decrement (a_1 and a_2 = amplitudes at two sections, 1 and 2, at distance λ along the flow) - a measure of the attenuation of the wave. The wave number σ_o is defined by

$$\sigma_o = \frac{2\pi}{\lambda} \cdot \frac{Y_o}{S_o} \qquad \ldots (3.5.3)$$

where λ is the length of the sinusoidal wave. σ_o characterizes the wave shape. A high value corresponds to a "steep" wave and vice versa. These solutions are shown in figures 3.5.1 and 3.5.2.

Figure 3.5.1 shows the variation in celerity with the Froude number and the wave number. The diagram can be divided into three regions:

- small wave numbers $\sigma_o < 10^0$ and Froude numbers $F_o < 2$ - the celerity is independent of both F_o and σ_o

- intermediate wave numbers $10^0 < \sigma_o < 10^2$ - the celerity is dependent on both F_o and σ_o

- great wave numbers $\sigma_o > 10^2$ - the celerity is dependent on F_o only

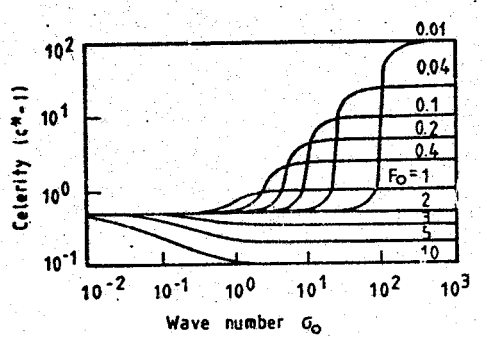

Figure 3.5.1 The relation between the celerity c^*, the wave number σ_o and the Froude number F_o (after Ponce and Simons (1977)).

From the analysis presented by Ponce and Simons it follows that waves in the region of small wave numbers can be described by considering only the slope term in the equation of motion, that is, by means of the kinematic wave equation. As demonstrated in section 3.4, this was the case also for large values of the kinematic wave number K_o. From the relations given in (3.4.2) and (3.5.3) it appears that K_o is proportional to $1/\sigma_o$ if L in K_o is replaced by λ. A large K_o thus corresponds to a relatively slowly varying outflow hydrograph.

According to figure 3.5.1, the kinematic wave velocity is $c = 1.5\ V_o$ where 1.5 is the exponent of the water depth in the Chezy friction relation which was used by Ponce and Simons. In the next chapter the kinematic wave velocity will be derived for an arbitrary friction relation.

Waves in the region of large wave numbers may be described taking only acceleration and pressure force terms

into account - so called gravity waves. Corresponding wave velocity is $c^* = 1+1/F_o$ or

$$c = V_o + \sqrt{gY} \qquad \ldots \quad (3.5.4)$$

which is similar to the characteristic velocity given in equation (3.3.1b).

Waves with intermediate wave numbers are called dynamic waves. They can only be represented by the complete equation of motion.

In figure 3.5.2 the attenuation of the primary wave (associated with the positive characteristic, section 3.3) is given as a function of the Froude and wave numbers (an attenuating wave has a negative logarithmic decrement).

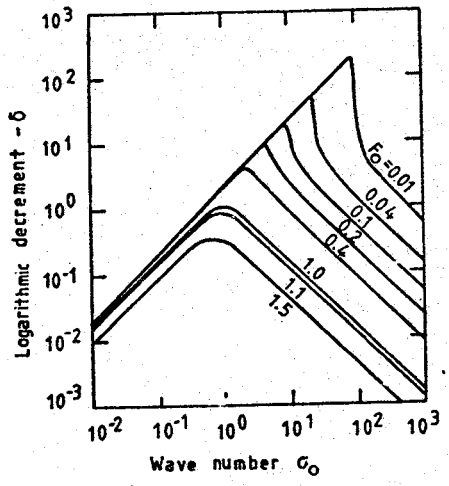

Figure 3.5.2 The relation between the logarithmic decrement $-\delta = \ln(a_1/a_2)$, the wave number σ_o and the Froude number F_o. (After Ponce and Simons (1977)).

The attenuation for $F_o < 2$ is greatest in the dynamic band $10^0 < \sigma_o < 10^2$. With decreasing or increasing wave

number, towards the kinematic or gravity bands, the attenuation decreases.

In the extreme case the gravity and kinematic waves are subject to no attenuation at all. For $F_o > 2$ (see Ponce and Simons (1977)) the waves amplify and at $F_o = 2$ the waves neither amplify nor attenuate. It should be noted that the critical value of the Froude number depends on the friction relation used, and is 2 for Chezy's relation and 1.5 for Manning's.

The analysis made by Ponce and Simons is basically only applicable to waves with small amplitudes (compared to the uniform flow waterdepth) which are not generated by a lateral source. As the storm water waves have great amplitudes compared to the base flow, and as the source in overland flow elements is usually lateral no stronger conclusions may be drawn from the analysis. It illustrates, however, the general properties of flood waves. It is also believed that the results from the kinematic band, namely

- dimensionless celerity, independent of the wave number,
- increasing attenuation with the wave number,

are also largely valid for most storm water waves.

4. APPROXIMATION OF THE SHALLOW WATER EQUATIONS

4.1 Simplification of the equation of motion

Using the basic equations it is possible to obtain an almost complete description of the propagation of an arbitrary wave. From a practical numerical point of view they are, however, difficult to handle and simplifications have to be considered. The difficulties in application may commonly be traced back to the n-characteristic (see figure 3.3.1) which is directed upstream for subcritical flow and downstream for supercritical flow. The boundary conditions required vary with the flow regime, which has to be checked at each time step in the calculation. It is also difficult to ensure numerical stability in the case of steep wave fronts.

In the last chapter, it was shown that several terms in the momentum equation are of lesser importance in urban runoff simulation. By neglecting one or more of these terms new equation systems are created. These systems will have different properties with respect to characteristics, wave velocities, boundary conditions, etc.

In the selection of suitable approximations, systems with one or no positive characteristic direction defined and with only the less important terms neglected are of greatest interest.

The approximations of the momentum equation are named after the main physical characteristics of the associated wave movement. Below, the terms used in the different approximations are indicated.

$$\frac{\partial Q}{\partial t}+\frac{\partial}{\partial x}\left(\beta\cdot\frac{Q^2}{A}\right)+g\cdot A\cdot\frac{\partial Y}{\partial x}-g\cdot A\cdot(S_o-S_f)-q\cdot U\cdot\cos\phi=0 \quad \ldots \quad (3.2.1b)$$

kinematic wave approximation

diffusive " "

steady dynamic " "

dynamic " "

The steady dynamic wave approximation has only one characteristic, which is directed upstream for subcritical flow and downstream for supercritical flow. If the second term is dropped instead of the first, again we have a system with two characteristic directions. As the negative characteristic in this case is always directed upstream this system should be easier to handle than the complete equations.

The two acceleration terms are of the same order of significance and usually very small compared to other terms, as was shown in section 3.4. Furthermore, the two terms are always of opposite sign at the important rising flow stage. Thus cases where the dynamic equations are significantly better than the diffusive equation should be very rare. This leaves only two approximate models of interest; the diffusive wave model and the kinematic wave model. Their properties are the main subject of this chapter.

The significance of the lateral momentum term has been discussed in the previous chapter. It is believed that a significant portion of the momentum of the raindrops is lost due to the disturbances created when the raindrops penetrate the sheet flow and hit the ground. Therefore the effect of falling raindrops on the flow can not be simulated only by means of the momentum term. The impact of raindrops should rather be looked upon as a loss of momentum which could be accounted for by means of an increased friction factor (c.f. chapter 5). The lateral momentum term is therefore neglected in the following. However, in connection with the solution of the kinematic wave equation in the case of constant rain intensity, an example is given where the lateral momentum term is taken into account.

Further approximations can only be made in terms of simplifications of the friction relation, celerity, diffusive coefficients etc., and can always be derived from one of the above mentioned models.

4.2 The kinematic wave approximation

4.2.1 The kinematic wave equations

The kinematic wave is a widely used approximation of the dynamic wave equations. The first thorough analysis of its properties was given by Lighthill and Wittham (1955). In this approximation only the slope term is taken into account. The kinematic wave equations are thus written

$$\frac{\partial Q}{\partial x} + \frac{\partial A}{\partial t} = q \qquad \text{... (4.2.1)}$$

$$S_f - S_o = 0 \qquad \text{... (4.2.2)}$$

If S_f is expressed in terms of Q and A

$$S_f = \left(\frac{Q}{K \cdot A^b}\right)^2 \qquad \text{... (4.2.3)}$$

equation (4.2.2) gives

$$Q = K \cdot S_o^{1/2} \cdot A^b \qquad \text{... (4.2.4)}$$

which is a general expression for a friction relation valid in a prismatic channel. K is mainly a roughness parameter while b is governed by the selected friction relation and channel geometry. For instance, in surface flow, Manning's relation gives b=5/3 and Chezy's gives b=3/2.

The kinematic wave equations may be transformed into a system of ordinary differential equations in the same way as the shallow water equations (see section 3.3)

$$\frac{dx}{dt} = \frac{dQ}{dA} \qquad \text{... (4.2.5a)}$$

$$\frac{dQ}{dt} = \frac{dQ}{dA} \cdot q \qquad \text{... (4.2.5b)}$$

The equation 4.2.5a expresses a wave velocity or a system of positive characteristics in the x-t plane.

Along these characteristics the equation 4.2.5b is satisfied. The kinematic equations evidently only simulate wave propagation in the downstream direction. The necessary initial and boundary conditions are

$Q = Q(x,0)$ (initial condition)

$Q = Q(0,t)$ (upstream boundary condition)

and no downstream boundary condition is needed. This property of the kinematic wave makes it incapable of taking backwater effects into account but simplifies its use. The basic appearance of kinematic characteristics is shown in figure 4.2.1.

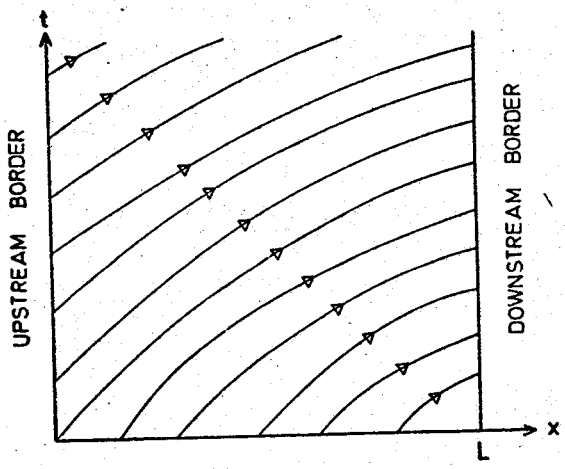

Figure 4.2.1 Kinematic characteristics in the case of lateral and upstream inflow

The equation (4.2.5a) defines the kinematic wave velocity c_k. Using the friction relation, it may be written

$$c_k = \frac{dQ}{dA} = K \cdot S_o^{1/2} \cdot b \cdot A^{(b-1)} \qquad \ldots (4.2.6)$$

or

$$c_k = b \cdot \frac{Q}{A} \qquad \ldots (4.2.7)$$

The kinematic celerity is then always greater than the mean velocity of flow, for instance in surface flow by 67% and in gutterflow by 25% (Manning's formula). It should be noted that the celerity is sensitive to the selection of friction relation.

An alternative way of writing the equation system is

$$\frac{dx}{dt} = b \cdot V \qquad \text{... (4.2.8a)}$$

$$\frac{dA}{dt} = q \qquad \text{... (4.2.8b)}$$

It can also be shown that

$$\frac{dQ}{dx} = \frac{dA}{dt} \qquad \text{... (4.2.9)}$$

Equation (4.2.8b) shows that the kinematic wave is not subject to any attenuation.

If the definition of the kinematic celerity is used, the continuity equation may be written

$$\frac{\partial Q}{\partial x} + \frac{1}{c_k} \cdot \frac{\partial Q}{\partial t} = q \qquad \text{... (4.2.10)}$$

which can be compared to the convective diffusion equation in section 4.3.

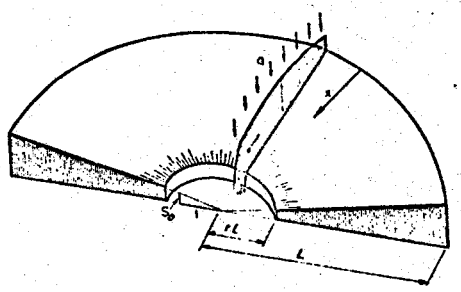

Figure 4.2.2 Converging surface (after Singh (1976))

The equations above assume a plane surface. For comparison, the corresponding equations for a converging surface according to figure 4.2.2 are (Singh 1977)

$$\frac{\partial Q}{\partial x} + \frac{\partial A}{\partial t} = q + \frac{Q}{L-x} \qquad \text{... (4.2.11)}$$

$$S_f - S_o = 0 \qquad \text{... (4.2.12)}$$

4.2.2 Analytical solution of the kinematic equations in the case of lateral inflow only

A typical system of kinematic characteristics of a surface or a gutter flow (in the case of only lateral inflow) is shown in figure 4.2.3. The characteristic starting at x=0, t=0 divides the x-t plane into two zones. The zone Z1 includes all points where the associated characteristics emanate from some point x at t=0 and the zone Z2 includes all points where the characteristics emanate from the upstream end at some time $t=t_o$. The time taken for a wave to travel from the upstream end at t=0 to x=L is the <u>time of concentration</u>, here denoted by t_c.

Every downstream flow value Q(L,t) is associated with a specific characteristic path. By integrating equation (4.2.8b) over this characteristic an expression for the cross-sectional area A is obtained at the downstream end

$$A(L,t) = \int_{t_o}^{t} q(\sigma)d\sigma \qquad \text{... (4.2.13)}$$

as A(0,t)=0 and $t_o=0$, A(x,0) = 0 if $t<t_c$. From equation (4.2.4) and (4.2.13) an expression of downstream outflow is obtained

$$Q(L,t) = KS_o^{1/2} \cdot \left(\int_{t_o}^{t} q(\sigma)d\sigma \right)^b \qquad \text{... (4.2.14)}$$

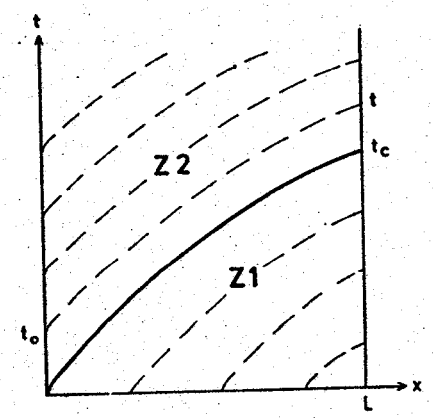

Figure 4.2.3 A system of kinematic characteristics in the case of lateral inflow only

K is assumed independent of x and t and the upstream boundary condition is $Q(0,t) = 0$. Equations (4.2.13) and (4.2.6) inserted in (4.2.5a) yield after integration

$$L = K \cdot S_o^{1/2} \cdot b \int_{t_o}^{t} \left[\int_{t_o}^{\tau} q(\sigma)\, d\sigma \right]^{b-1} d\tau \qquad \ldots (4.2.15)$$

For a given geometry it is possible to determine the outflow at any time by the equations (4.2.14) and (4.2.15). In zone Z1 the flow is directly given by equation (4.2.14) (t_o=0). In zone Z2 the time t_o which is specific for each time t (see figure 4.2.3) must first be determined. This is done by using equation (4.2.15)

If equation (4.2.15) is applied to the characteristic emanating from x=0, t=0 we have

$$L = K \cdot S^{1/2} \cdot b \cdot \int_{0}^{t_c} \left[\int_{0}^{\tau} q(\sigma)\, d\sigma \right]^{b-1} d\tau \qquad \ldots (4.2.16)$$

Analytical solutions are obtained if the lateral inflow is given as an analytical expression which is integrable in equation (4.2.15). Li et al. (1975b) propose an iterative method of solving this equation for an arbitrary analytical function of q based on the Taylor series expansion. The general problem of evaluating the discharge if the lateral inflow is given as a time series must be treated by numerical integration or a finite difference method (see chapter 6). Analytical solutions are therefore not directly used in simulating of runoff.

4.2.3 Analytical solutions in some special cases

Analytical solutions of the kinematic equations are only obtained in special cases. The solutions are based on specific assumptions of the inflow or the friction relation. Below, some cases are discussed in order to illustrate the general properties of the kinematic wave and the limitations of the analytical solution.

Upstream inflow

Integrating equation (4.2.8b) along a characteristic for the case of only upstream inflow ($q=0$, $A(0,t) \neq 0$) shows that the cross-sectional area $A(x,t)$ is constant along this characteristic. Regarding the relation between flow and area (equation 4.2.4) and the definition of wave velocity (equation 4.2.5a), both $Q(x,t)$ and c_k will also be constant along this characteristic. If $A(0,t)$ at the start point of the characteristic is denoted A_{in} we obtain the velocity, see equation (4.2.6)

$$c_k = K \cdot S_o^{1/2} \cdot b \cdot (A_{in})^{b-1} \qquad \ldots (4.2.17)$$

or, if the corresponding flow value Q_{in} is used (see equation (4.2.4)),

$$c_k = b \cdot (K \cdot S_o^{1/2})^{\frac{1}{b}} \cdot (Q_{in})^{\frac{b-1}{b}} \qquad \ldots (4.2.18)$$

The outflow at the downstream end at time t is easily obtained as the upstream inflow at time $(t-L/c_k)$. The solution may, however, give unrealistic outflow hydrographs caused by intersecting characteristics. Such a case is discussed in section 4.2.5.

Constant lateral inflow

For a constant lateral inflow, q_k, stationary flow is obtained at $t=t_c$ and the state of flow is only of interest in zone Z1 (figure 4.2.3). Integration of equation (4.2.14) in this zone gives ($t_o = 0$)

$$Q(L,t) = K \cdot S_o^{1/2} \cdot q_k^b \cdot t^b \qquad (0 \leq t \leq t_c) \quad \ldots \quad (4.2.19)$$

The time of concentration in the case of constant lateral inflow is then

$$t_c = \left[\frac{q_k^{1-b} \cdot L}{K \cdot S_o^{1/2}} \right]^{1/b} \qquad \ldots \quad (4.2.20)$$

(since $Q(L, t_c) = q_K \cdot L$ when $t=t_c$).

Linear friction relation

A linear approximation of the friction relation (b=1 in equation 4.2.4) simplifies the solution procedure considerably. Both the Time-Area Method and the Unit-Hydrograph Method are based on this approximation, Chow (1964).

The equation (4.2.15) may in this case be integrated for an arbitrary lateral inflow, giving

$$L = K \cdot S_o^{1/2} \cdot (t-t_o) \qquad \ldots \quad (4.2.21)$$

All characteristics have, obviously, the same integration time, showing that the wave velocity is constant in time and space (straight line characteristics). It should be noted that representative values for the factor K are very different for different friction relations.

Nonlinear friction in a surface flow case

Analytical solutions may also be obtained for certain time varying lateral inflows when a friction relation with b=2 is used (see chapter 5). An example of such an inflow is given by

$$q = q_o \cdot e^{-t/t_k}(1 - e^{-t/t_k}) \qquad \ldots (4.2.22)$$

where q_o and t_k are constants (see Parlange et al. (1981)). In figure 4.2.4 the function has been plotted to show the principal shape. It is believed to be fairly representative for a storm event and the corresponding inflow to a gutter.

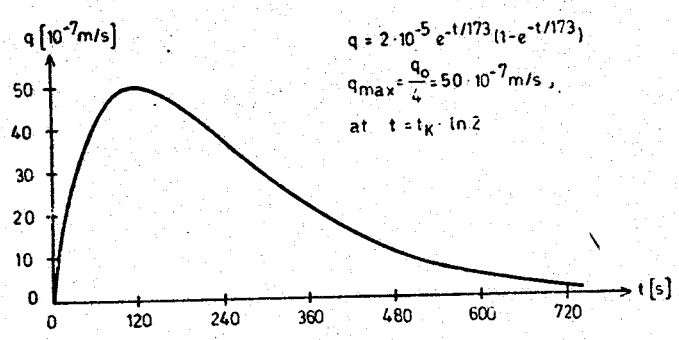

Figure 4.2.4 The lateral inflow

Integrating equation (4.2.14) using this lateral inflow gives the following expression for the outflow at the downstream end

$$Q(L,t) = K \cdot S_o^{1/2} \cdot q_o \cdot t_k^2 \cdot (\tfrac{1}{2} \cdot e^{-2t/t_k} - e^{-t/t_k} + e^{-t_o/t_k} - \tfrac{1}{2} \cdot e^{-2t_o/t_k}) \qquad \ldots (4.2.23)$$

where t_o is first evaluated by equation (4.2.15) when $t > t_c$ (when $t < t_c$ is $t_o = 0$), see figure 4.2.3. Using the above equations, outflow hydrographs have been generated

from a surface of length 40 m (width 20 m) for three different slopes. The hydrographs are shown in figure 4.2.5 together with the lateral inflow hydrograph (from figure 4.2.4) given as the total inflow to the surface. This hydrograph corresponds to an inflow at the upstream end if all the lateral inflow were concentrated to this point.

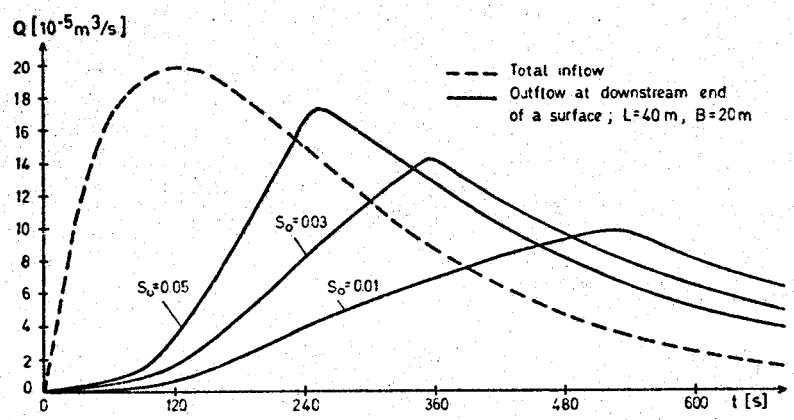

Figure 4.2.5 Outflow hydrographs from an asphalt surface derived by the kinematic equations

It appears that the hydrographs get increasingly attenuated with decreasing slope. According to the equation (4.2.23) an increase in roughness would have attenuated the hydrographs in the same way. This is typical for "flow elements exposed to lateral inflow" such as

surfaces	exposed to rain
gutters	" " inflow from a surface
networks	" " inflow from gutters

Given a lateral inflow with a duration greater than the time of concentration t_c, the outflow will increase until $t=t_c$, see equation (4.2.14). Whether or not the flow maximum is reached at $t=t_c$ depends on the shape of the lateral inflow hydrograph. A steep rising lateral inflow will give an outflow maximum very close to the time of concentration.

The attenuation is generated by the dependence on the outflow of both the time of concentration and the shape and magnitude of lateral inflow. To distinguish it from "dynamic attenuation" of waves the attenuation discussed here will be called "lateral inflow attenuation". This attenuation is as significant as the dynamic attenuation in urban runoff systems.

4.2.4 The kinematic wave including the lateral momentum term

If the lateral term in the momentum equation is taken into account the kinematic wave equations become

$$\frac{\partial Q}{\partial x} + \frac{\partial A}{\partial t} = q \qquad \text{...(4.2.24a)}$$

$$S_f - S_o - \frac{q \cdot U \cdot \cos\phi}{g \cdot A} = 0 \qquad \text{...(4.2.24b)}$$

Using the method of characteristics, see section 3.3, the characteristic equations can be obtained. Although they are expressible analytically, they become very complicated. In the case of constant lateral inflow the rising hydrograph is given by

$$Q(L,t) = K \cdot q_k^b \cdot t^b \sqrt{S_o + \frac{U \cdot \cos\phi}{gt}} \qquad \text{...(4.2.25)}$$

valid for

$$S_o + \frac{U \cdot \cos\phi}{gt} > 0 \text{ and } S_o > 0$$

The corresponding time to equilibrium is

$$t_c^b \sqrt{S_o + \frac{U \cdot \cos\phi}{gt}} = \frac{L}{K \cdot q^{(b-1)}} \qquad \text{...(4.2.26)}$$

As an example, in figure 4.2.6 are plotted the rising hydrographs for a flow case, with and without consideration to lateral inflow momentum. The influence of lateral inflow becomes more stressed for great intensities, short lengths and small slopes, and then i = 150 l/s·ha (54 mm/h)

L_s = 5 m and S_o = 0.01 have been chosen as an extreme case. The rain hits the surface at an angle of Ψ = 135° (ϕ = Ψ

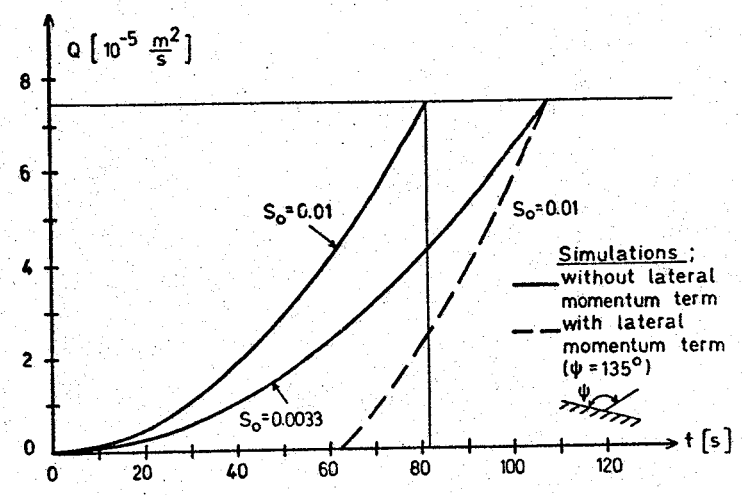

Figure 4.2.6 Comparison between rising hydrographs calculated with and without lateral momentum

in surface flow). As we can see water has to build up before the runoff can start. It is here assumed that the water is not able to pass x=0. The lateral term can be replaced by a correction in slope to give the same time of concentration but, as can be seen in figure 4.2.6, the rising hydrograph is not properly reproduced. However, as discussed in section 4.1 the impact of raindrops on the flow is much more complex than described by the lateral momentum term and the term is neglected in the following analysis.

4.2.5 Kinematic shocks

The analysis in previous sections is only valid as long as no characteristics intersect each other. The condition for two consecutive characteristics (C1 and C2) to meet

can be written, according to Borah and Prasad (1980), as

$$\left[\left(\frac{dx}{dt}\right)_{t_1}\right]_{C1} < \left[\left(\frac{dx}{dt}\right)_{t_1}\right]_{C2} \qquad \ldots (4.2.27)$$

where t_1 is an arbritary time, see figure 4.2.7.

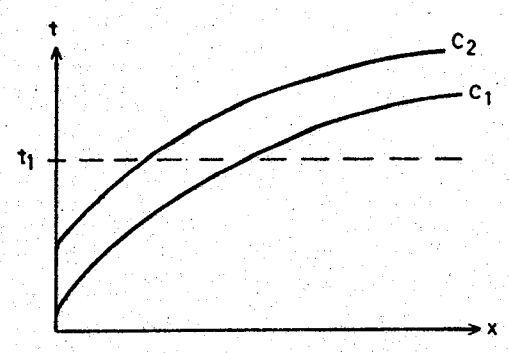

Figure 4.2.7 Two characteristics emanating from the upstream boundary

According to the equations (4.2.4) and (4.2.5a) the celerity may be written

$$\frac{dx}{dt} = (K \cdot S_o^{1/2})^{\frac{1}{b}} \cdot b \cdot Q^{(1-\frac{1}{b})} \qquad \ldots (4.2.28)$$

which inserted in the inequality, gives

$$\left[\left[Q^{1-\frac{1}{b}}\right]_{t_1}\right]_{C1} < \left[\left[Q^{1-\frac{1}{b}}\right]_{t_1}\right]_{C2} \qquad \ldots (4.2.29)$$

In the lateral inflow case we have (equation 4.2.13))

$$\left[\left[\int_{t_o}^{t_1} q(\sigma)d\sigma\right]^{b-1}\right]_{C1} < \left[\left[\int_{t_o}^{t_1} q(\sigma)d\sigma\right]^{b-1}\right]_{C2} \qquad \ldots (4.2.30)$$

When $[t_o]_{C1} = [t_o]_{C2}$ (characteristics in zone Z1 figure 4.2.3) the right and left hand sides are identical and the

inequality is not satisfied. If the characteristics eminate from the upstream boundary $[t_o]_{C2}$ is always greater than $[t_o]_{C1}$. As q is positive the inequality (4.2.30) cannot be satisfied. Thus in the lateral inflow case, no intersecting characteristics are obtained.

The case of only upstream end inflow is characterized by constant wave velocity along each characteristic. As soon as one characteristic leaving the upstream boundary has a velocity greater than the foregoing one they will intersect (provided L is long enough). From the point where two characteristics meet a new one will form with a different celerity. A zone of intersecting characteristics will develop, associated with the rising part of the inflow hydrograph. In this zone what are known as kinematic shocks or bores will form. The movement and shape of these shocks have been analysed by several investigators, Lighthill and Whitham (1955), Kibler and Woolhiser (1970), and an approximate method of routing shocks has been presented by Borah and Prasad (1980).

It is possible to get a pure kinematic solution if the characteristics are allowed to intersect. More than one flow value may then occur at the outflow at each moment, which, of course, is physically unrealistic. In figure 4.2.8 is given an example of the kinematic solution in a case when kinematic shocks form. The lateral inflow from figure 4.2.4 (multiplied by the surface area) is used as the upstream end inflow and routed over the surface (L = 40 m, B = 20 m, S_o = 0.03). Typically, the outflow hydrograph has three flow values at each specific time in the shock forming zone.

In the numerical solution of the kinematic wave equations an artificial attenuation is obtained (see chapter 6). This attenuation smooths out the shock giving, at least, unique flow values at each time step.

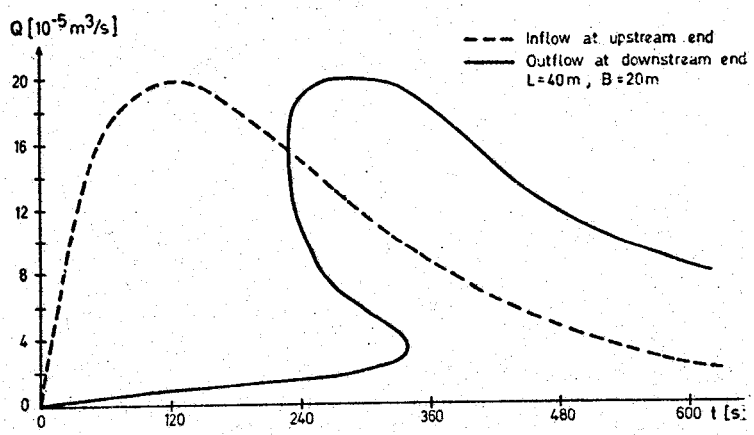

Figure 4.2.8 The kinematic solution in a case of intersecting characteristics (physically unrealistic).

4.2.6 Applicability of the kinematic wave equations

It appears from the dimensionless dynamic equation (3.4.3) and section 3.4 that the kinematic wave number

$$K_o = \frac{L \cdot S_o}{Y_o \cdot F_o^2} \qquad \ldots (3.5.4)$$

is an important parameter in the discussion of the applicability of the kinematic wave model. Generally K_o increases with increasing slope, length and roughness of the surface or gutter. If the flow is generated by a "lateral source", K_o increases with decreasing rate of lateral inflow and increasing length. Several investigators, for instance Woolhiser and Liggett (1967) have discussed limiting values of K_o for the kinematic model.

Woolhiser and Ligget compared dimensionless rising

hydrographs evaluated by the kinematic and dynamic equations for different values of K_o and F_o. They found that the error of the outflow hydrograph using the kinematic equations was less than 10% at $K_o = 10$ (Chezy's friction relation used). The error decreased rapidly with increasing K_o and $K_o = 20$ was then defined as a limiting value below which the kinematic solution does not apply.

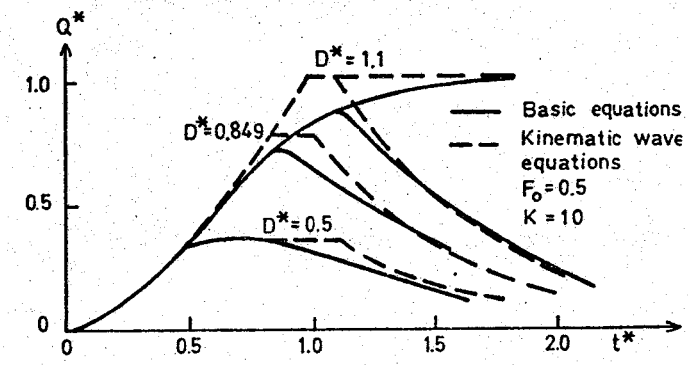

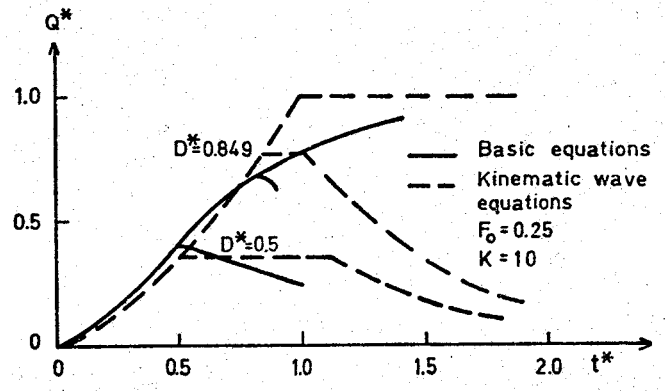

Figure 4.2.9a,b Dimensionless partial equilibrium hydrographs. D^* is the dimensionless time at which the lateral inflow ceases (after Morris and Woolhiser (1980)).

Morris and Woolhiser (1980) analysed in a similar way partial equilibrium hydrographs from a plane, see figure 4.2.9 a,b. They concluded that the condition on K_o must be further restricted in cases of small values of F_o and proposed the general condition:

$$F_o^2 \cdot K_o > 5 \quad \text{when} \quad F_o < 0.5 \qquad \ldots(4.2.31a)$$

$$K_o > 20 \quad \text{when} \quad F_o > 0.5 \qquad \ldots(4.2.31b)$$

Comparing it with Ponce and Simons' analysis referred to in section 3.5, the condition corresponds to the kinematic band $\sigma_o < 1$ in figure 3.5.1, provided the length of flow L is replaced by the wave length λ of Ponce and Simons' sinusoidal wave.

Using the limiting values of surface flow characteristics given in section 2.3, the kinematic wave number $K_o > 38$ and the Froude number $F_o > 0.5$ are obtained. The kinematic wave then applies to surface flow according to the condition given above.

In gutter flow the kinematic wave number may be less than 20 ($F_o > 0.5$) and the use of the kinematic wave approach is in some cases doubtful. For small values of F_o the diffusive wave is a more appropriate approximation, see section 4.3.2. In the great majority of cases the kinematic wave approach, however, applies also to gutter flow.

The condition (4.2.31) also applies to a sewer fed by a lateral source only. Such a flow element is in this report used as an alternative approximation for sewer systems. In this case the kinematic wave number may be less than 20 ($F_o > 0.5$) and the kinematic wave approach is consequently sometimes less appropriate.

The discussion of the applicability of the kinematic wave model in section 4.3 and here is based on the case of constant lateral inflow. It may be regarded as an extreme

type of inflow. According to section 3.5, kinematic waves have long wave periods and gentle slopes of rising and receding parts. If the lateral inflow is increased successively instead of instantaneously, more gentle slopes of the wave will result. The kinematic approximation can in this case be expected to be valid for smaller values of K_o than those given in condition (4.2.31).

Morris (1979) analysed the influence of the choice of downstream boundary conditions on solutions of the shallow water equations. She found no effect on the solution for a range of Froude and kinematic wave numbers covering most overland flow cases. This result is in accordance with the kinematic wave solution which does not take the downstream boundary condition into account.

It should be noted that the analysis so far is purely theoretical and based on assumptions such as sheet flow. However, regarding these limitations the discussions above give a clear indication that the kinematic wave approximation is, despite its simplicity, sufficiently accurate for urban runoff simulation in the great majority of cases.

4.3 The diffusive wave approximation

4.3.1 Basic equations - the diffusion analogy

The diffusive wave equations are obtained by neglecting the local and convective acceleration terms in the basic momentum equation. For prismatic cross-sections ($\partial A/\partial x = B\partial Y/\partial x$) the equations may be written

$$\frac{\partial Q}{\partial x} + \frac{\partial A}{\partial t} = q \qquad \text{... (4.3.1)}$$

$$\frac{1}{B} \cdot \frac{\partial A}{\partial x} + S_f - S_o = 0 \qquad \text{... (4.3.2)}$$

The equations form a system of linear differential

equations which is elliptic, that is, no characteristic can be found. Differentiating the equations (4.3.1) and (4.3.2) with respect to x and t, respectively, and using the friction slope

$$S_f = \frac{Q^2}{K^2 \cdot A^{2b}} \qquad \ldots (4.3.3)$$

(for example Manning's or Chezy's relations, see chapter 5), the kinematic celerity (section 4.2.1)

$$c_k = \frac{dQ}{dA} = \frac{Q}{A} \cdot b \qquad \ldots (4.3.4)$$

gives for surface flow or rectangular channel flow

$$\frac{\partial Q}{\partial t} + c_k \cdot \frac{\partial Q}{\partial x} = D \cdot \frac{\partial^2 Q}{\partial x^2} + c_k \cdot q \qquad \ldots (4.3.5)$$

where

$$D = \frac{Q}{2S_f \cdot B} \qquad \ldots (4.3.6)$$

The second term on the left hand side of equation (4.3.5) represents the convective transport and the first term on the right represents the diffusion of the wave with diffusion coefficient D. The equation will here be called the convective-diffusion equation, Daily-Harleman (1965).

The convective-diffusion equation illustrates the principal ability of the diffusive wave equations to describe an attenuating wave movement. This is not possible using the kinematic wave equations. Comparing the convective-diffusion equation with corresponding expression of the kinematic equations (4.2.10) shows that these are identical if the diffusive term in equation (4.3.5) is omitted.

A solution of the diffusive wave equation requires besides the initial and upstream boundary conditions (compare with the kinematic equations), also a condition at the downstream boundary

$Q = Q(x,0)$ (inital condition)
$Q = Q(0,t)$ (upstream boundary condition)
$Q = Q(L,t)$ (downstream boundary condition)

If the celerity c_k and diffusive coefficient D are assumed constant with respect to independent variables, the equation (4.3.5) can be reduced by the transformation $x_c = x - c_k t$ to

$$\frac{\partial Q}{\partial t} = D \cdot \frac{\partial^2 Q}{\partial x^2} + c_k \cdot q \qquad \ldots (4.3.7)$$

The equation may be further reduced (by manipulating the boundary conditions) to the same form as the classical heat conduction equation or Fick's law in one dimension. This equation has been solved analytically for numerous different applications, mainly regarding molecular diffusion, Crank (1975), and heat conduction Carslaw and Jaeger (1959).

When the above mentioned analytical solutions are applied to channel flow, difficulties in specifying suitable boundary conditions arise. In addition, the analytical solutions will be expressed in terms of integrals that have to be solved by means of numerical integration methods. It is therefore not possible to use analytical solutions to discuss the properties of the diffusive wave equations in the way it was for the kinematic wave equations.

Inserting the friction relation (4.3.3) in the "momentum" equation (4.3.2) and solving for Q gives

$$Q = K \cdot A^b \cdot S_o^{1/2} \cdot \left(1 - \frac{1}{S_o} \cdot \frac{\partial Y}{\partial x}\right)^{1/2} \qquad \ldots (4.3.8)$$

By expanding the square root term as a power series and differentiating with respect to x and t, it is possible to derive the convective-diffusion equation (valid for flow on surfaces or in rectangular channels), see Price (1980a) and Kousis (1982),

$$\frac{\partial Q}{\partial t} + c_k \cdot \frac{\partial Q}{\partial x} = \frac{Q}{2 \cdot S_o \cdot B} \cdot \frac{\partial^2 Q}{\partial x^2} + c_k \cdot q \qquad \ldots (4.3.9)$$

which is identical to equation (4.3.5) if S_f is assumed equal to S_o in the diffusive coefficient D. It should be noted that throughout the derivation of equation (4.3.9) terms containing

$$\frac{\partial^2 Y}{\partial x^2} \quad \text{or} \quad \left(\frac{\partial Y}{\partial x}\right)^2$$

have consistently been dropped. These terms are in dimensionless form, (dimensionless variables denoted by index $*$),

$$\frac{1}{F_o^2 K_o} \cdot \frac{\partial^2 Y_*}{\partial x_*^2} \quad \text{or} \quad \frac{1}{F^2 K_o} \cdot \left(\frac{\partial Y_*}{\partial x_*}\right)^2$$

and are thus of the same order of magnitude as the neglected dynamic terms (see equation 3.4.3), or smaller.

In chapter 6, the diffusive coefficient defined by the equation (4.3.9) will be compared with the diffusion caused by the numerical solution of the kinematic wave equations.

4.3.2 Applicability of the diffusive wave equations

The diffusive wave equation includes the pressure force term as well as the slope term. The dimensionless analysis in chapter 3.4 shows that this term will be more significant for small values of the Froude number. When F_o increases towards unity (K_o less than 20) the acceleration terms become more important and the full dynamic equation should be used.

Morris and Woolhiser (1980) derived partial equilibrium hydrographs from a surface at low Froude numbers, figure 4.3.1. As might be expected, in this region the perform-

ance of the diffusive wave was better than that of the kinematic wave, compare with figure (4.2.9b). It performs less well for the receding part than the rising part. This might be explained by the fact that the sign of the local acceleration term changes at the receding part and the acceleration terms no longer counteract one another.

According to Morris and Woolhiser the diffusive wave approximation should be significantly better than the kinematic wave when $K_o F_o^2 < 5$ and $F_o < 0.5$ (equation (4.2.31a)). The criterion has a simple physical interpretation following directly from the definition of K_o; when the difference in level between upstream and downstream ends is less than 5 times the waterdepth the diffusive wave equations should be used; otherwise the kinematic wave equations apply.

Considering typical slopes and water depths in urban runoff systems the condition is essentially fulfilled only in very flat sewer nets. Runoff simulations in such cases require a downstream boundary condition.

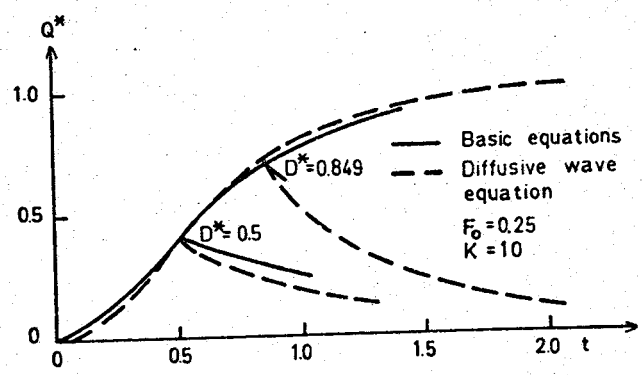

Figure 4.3.1 Dimensionless partial equilibrium hydrograph. D^* is the dimensionless time at which the lateral inflow ceases (after Morris and Woolhiser (1980))

Ponce et al. (1978) developed a similar criterion for

this case based on the analysis discussed in section 3.5 for a single conduit which is fed by an upstream source only. According to this criterion the diffusive wave equations apply to the same cases - flat sewer systems with great water depths.

Again it should be stressed that the discussion is theoretical and the conditions to some extent subjective. Therefore a definite rule for making the choice between the two approximations can not be given. It is, however, evident that in network systems with significant backwater the diffusive wave equations have to be used.

4.4 Summary and discussion

An analysis of the magnitude and sign of the terms in the dimensionless momentum equation shows that there are two simplifying approaches of interest for urban runoff modelling. These are the kinematic wave and the diffusive wave equations.

The kinematic wave approximation is defined by a very simple set of differential equations and boundary conditions (no downstream boundary condition). The equations have in the lateral inflow case no general analytical solution and must be solved by means of numerical methods. Regarding the properties of the equations, the corresponding numerical algorithm can be expected to give comparatively stable solutions.

From a theoretical point of view the kinematic wave approximation is, despite its simplicity, sufficiently accurate for urban runoff simulation in the great majority of cases. This is explained by the rather impressive ability of the equations to reproduce the wave velocity in ordinary urban runoff systems - the kinematic wave velocity.

The kinematic wave equations are not able to reproduce

dynamic attenuation. Provided there is only an upstream source the wave is not subject to any attenuation at all. This is in practice not a serious drawback because in the numerical solution an artificial attenuation is introduced which in most cases is greater than the dynamic attenuation (chapter 6).

The diffusive wave approximation is defined by a system of differential equations which are a bit more complex and also need a downstream boundary condition. The corresponding numerical solutions can also in this case be expected to be "stable" (compared to solutions of the basic equations).

Using the diffusive approximation it is possible to reproduce the main part of the "dynamic" attenuation. It is also possible to take into account the downstream boundary condition which makes analysis of sewer systems with significant backwater possible.

The diffusive wave approximation applies to all cases where the kinematic wave approximation is relevant and also to special cases where backwater is significant. It thus appears to be the most generally valid approximation for urban runoff simulation. It has successfully been used in the analysis of sewer systems, see Sjöberg (1981), Akan and Yen (1981) and Lyngfelt and Svensson (1983).

An important property of urban runoff is that the sources feeding the flows are spread along the "channel" elements. This is, of course, highly relevant for surface and gutter-flow cases but applies in principle also to most sewer network systems. In these kinds of system an attenuation of the wave is obtained that can be related to a characteristic time of concentration for the system. This "lateral inflow attenuation" is believed to be at least as significant in urban runoff systems as the "dynamic" attenuation. Therefore a very important property of a model used

for lateral inflow systems is the wave velocity. As the velocities of kinematic and diffusive waves are equal, the lateral inflow attenuation should be simulated with about the same accuracy by the two approximations.

In this chapter, the properties of urban runoff described by the Froude and kinematic wave numbers and also the properties of the kinematic and diffusive wave approximations have been considered. It is concluded that the former approximation is sufficiently accurate for simulation of overland flow. The approximation is also appropriate in many cases of sewer flow simulations.

The main difference between the two discussed approximations is whether or not they are able to consider downstream conditions. In most practical applications, for instance in designing sewer systems, it is very difficult to take these conditions into account. It is therefore believed that the kinematic wave approximation is more suitable for sewer flow simulations in general than the diffusive wave approximation.

However, in cases of significant effects caused by downstream conditions the diffusive wave approximation must be used. The most flexible model would, of course be one that generally uses the kinematic wave equations but which is capable of changing these for the diffusive wave equations in parts of the system affected by downstream conditions.

As the analysis of systems affected by downstream conditions is beyond the scope of this report, in the discussion to follow only the kinematic wave approximation and "associated" models will be treated.

5. THE FRICTION LOSSES IN OVERLAND FLOW

5.1 General

The friction forces along the wetted perimeter and the water surface (wind) in the momentum equation are summarized in the friction term S_f. The term is defined by

$$S_f = (\tau_{mp} \cdot P + \tau_{ms} \cdot B)/\rho g A \qquad \ldots (5.1.1)$$

where

τ_{mp} = mean shear stress along the wetted perimeter
τ_{ms} = mean shear stress along the water surface
P = wetted perimeter
B = water surface width

The total shear stress is related to the flow velocity, the cross-sectional area, the wetted perimeter and the water surface width. Usually the wetted perimeter is represented by the hydraulic radius $R = A/P$. Using $Q = V A$ and ignoring shear stress at the water surface the standard form of the friction term is obtained

$$S_f = c_1 \cdot Q^{c_2} \cdot A^{c_3} \cdot R^{c_4} \qquad \ldots (5.1.2)$$

where c_1-c_4 are constants or functions related to roughness, rain intensity etc. In stationary uniform flow the friction slope equals the bed slope, $S_f = S_o$. The establishment of a relevant friction relation for this case has long been a fundamental problem in hydraulics. Through numerous investigations several relations that can be regarded as empirical or half empirical have become generally accepted.

In the general case, additional effects caused by non stationarity would be plausible. However, no investigation quantifying such an influence is known (Yevjevich

(1975)). Consequently the friction term in the momentum equation is determined in time and space by traditional friction relations developed for stationary flow.

In this chapter, flow resistance at small water depths (sheet flow) will be discussed. Many investigations of this flow type have been performed and the discussion will be based on some of the best known studies. Friction relations relevant for surface and gutter flow suitable for urban runoff modelling are analysed. Besides the influence of roughness and rain intensity, the effects of wind and rollwaves on the flow are briefly discussed.

5.2 Alternative formulations of the friction relation

The most frequently used friction relation in standard literature is the Darcy-Weissbach equation. For stationary open channel flow (prismatic section) it may be written as a relation between the flow and cross sectional area

$$S_f = S_o = \frac{f}{4R} \cdot \frac{Q^2}{2gA^2} \qquad \ldots (5.2.1)$$

where R is the hydraulic radius and f a dimensionless friction factor. In surface flow, $R \approx Y$ and if Q_b is the flow per unit width the relation is

$$Q_b = Y^{3/2} \sqrt{\frac{8g}{f} \cdot S_o} \qquad \ldots (5.2.2)$$

The relation is derived considering only friction due to shear stresses along the bottom. Raindrop impact and wind shear stress on the surface may, however, be incorporated in f.

The equation covers the laminar flow, the flow in the transition zone and the turbulent flow. In laminar flow over smooth surfaces the friction factor is only dependent

on Reynolds' number R_e

$$f = \frac{24}{R_e} \qquad \text{... (5.2.3)}$$

In surface flow $R_e = Q_b/\nu$ (ν = kinematic viscosity of flow) giving

$$Q_b = Y^3 \cdot \frac{g}{3\nu} \cdot S_o \qquad \text{... (5.2.4)}$$

In turbulent flow over rough surfaces the friction factor depends mainly on the relative roughness and may be represented by

$$f = \frac{8g}{C^2} \qquad \text{... (5.2.5)}$$

where C is the roughness parameter of the surface. Inserting in the Darcy-Weissbach relation gives

$$Q_b = Y^{3/2} \cdot C\sqrt{S_o} \qquad \text{... (5.2.6)}$$

which is the well-known Chezy relation for surface flow. Another relation is the Blasius equation

$$f = \frac{0.223}{R_e^{1/4}} \qquad \text{... (5.2.7)}$$

which is valid for turbulent flow.

Other relations of interest in turbulent flow are:

The Manning formula

$$Q_b = Y^{5/3} \cdot \frac{1}{n}\sqrt{S_o} \qquad \text{... (5.2.8)}$$

the Danish L-formula, Jacobsen (1980)

$$Q_b = Y^{11/6} \cdot K_L\sqrt{S_o} \qquad \text{... (5.2.9)}$$

and

$$Q_b = Y^2 \cdot K_q \sqrt{S_o} \qquad \ldots (5.2.10)$$

here called the quadratic formula (after the exponent of Y). n, K_L and K_q are friction parameters governed by roughness properties of the surface and the impact of the raindrops.

Investigations of the friction properties of the flow are usually presented in a logarithmic f-R_e diagram. A convenient way of making comparisons between suitable friction relations should thus be to express them in terms of f and R_e (by using $R_e = Q_b/\nu$):

The Manning formula

$$f = 8g \cdot \left(\frac{S_o \cdot n^{18}}{\nu^2 \cdot R_e^2}\right)^{1/10} \qquad \ldots (5.2.11)$$

the L-formula

$$f = 8g \cdot \left(\frac{S_o}{K_L^9 \cdot \nu^2 \cdot R_e^2}\right)^{2/11} \qquad \ldots (5.2.12)$$

the quadratic formula

$$f = 8g \cdot \left(\frac{S_o}{K_q^6 \cdot \nu^2 \cdot R_e^2}\right)^{1/4} \qquad \ldots (5.2.13)$$

Using the Manning, L- or quadratic formulas is equivalent to the use of Darcy-Weissbach's equation with a friction factor given by the equations (5.2.11), (5.2.12) or (5.2.13). These relations will appear in the f-R_e-diagram as straight lines, each defined by its "slope" and level. The "slope" is characteristic for each friction relation and is dependent only on the exponent of R_e. In figure 5.2.1 these "slopes" are compared to those of laminar flow given by $f = 24/R_e$ and turbulent flow given by the Blasius equation. The levels of the lines have been chosen arbitrarily.

The quadratic and L-formulas appear as hybrids between the pure laminar and turbulent relations and should fit reasonably in the transition zone and surrounding parts of the laminar and turbulent zones. Manning's formula shows the typical "slope" of a turbulent relation. A relation which gives a "laminar slope" at low Reynolds' numbers and a "turbulent slope" at high ones (illustrated in figure 5.2.1) is

$$\frac{1}{\sqrt{f}} = K_1 \cdot \log R_e \sqrt{f} + K_2 \qquad \ldots (5.2.14)$$

where K_1 and K_2 are constants. This type of relation is, however, inconvenient in a runoff model. If a better

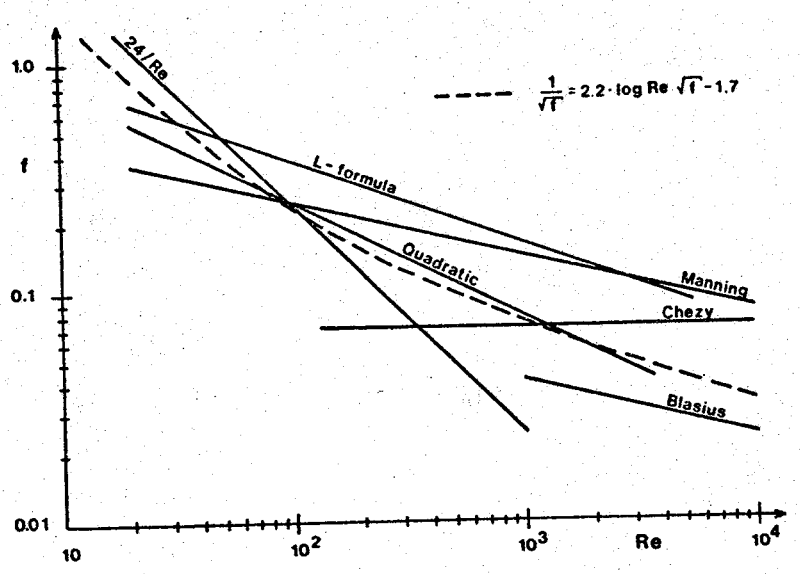

Figure 5.2.1 "Slopes" of the friction factor relation used in different friction formulas

adaption to laminar and turbulent flow is required a combination of a laminar and turbulent relation is preferred. The Manning, Chezy, Blasius, L- and quadratic

relations can all be represented by the more general formulation used in previous chapter, equation (4.2.4)

$$Q = K \cdot S_o^{1/2} \cdot A^b$$

where K is basically a roughness parameter (in surface flow also including the width, and in gutterflow, the slope, of sides).

5.3 Investigation of friction losses in surface flow

5.3.1 General

Generally an empirical friction relation can be established by measuring corresponding flows and water depths at different stationary flow conditions. This requires well controlled measurements and consequently most reported investigations have been carried out "indoors". The used surfaces are very even and the surface lengths are quite small (5-7 m). Rain is generated in simulators of different construction usually covering only a part of the surface. Among the referred tests there are examples of surfaces that are smooth, covered with sand or more realistic textures (asphalt, concrete). However, both the rain and the surface will be different from the real "in situ" situation giving difficulties in generalizing the results. On the other hand the fundamental relations should be best studied under these well controlled indoor conditions, where the effects of different physical phenomena can be separated.

5.3.2 Flow over a smooth surface

The characteristics of flow over a smooth surface have been investigated by Yoon and Wenzel (1971), Yen et al. (1972), Shen and Li (1973), Kisisel et al. (1973), Nittim (1977) and several others. The main objective of these investigations has been to study the effects of raindrop impact on flow.

For flows not exposed to rain, most tests confirm the theoretical laminar relation $f = 24/R_e$. The transition from laminar to turbulent flow is found at a Reynolds' number of about 900 with a transition zone 800-1400. At low slopes (S_o<0.01) laminar flow tends to be maintained at about 1100. For turbulent flow Nittim summarized several investigations and presented a regression equation

$$\frac{1}{\sqrt{f}} = 2 \cdot \log(R_e \sqrt{f}) \qquad \ldots (5.3.1)$$

The relation is plotted together with Nittim's results for flow on glass, in figure (5.3.1). It appears to agree reasonably well with Blasius' solution, see Shen and Li.

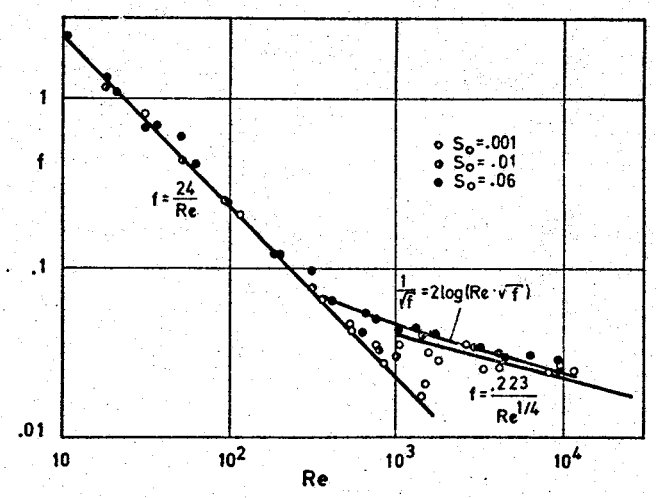

Figure 5.3.1 Values of the friction factor f measured for flow without rain over glass after Nittim (1977)

The influence of rain on the friction factor obtained in investigations by Yoon, Li and Nittim is shown in figures 5.3.2a-d. The tests by Yoon and Li agree quite well and Shen and Li derived from these (and tests by Kisisel) the following regression relation for laminar flow

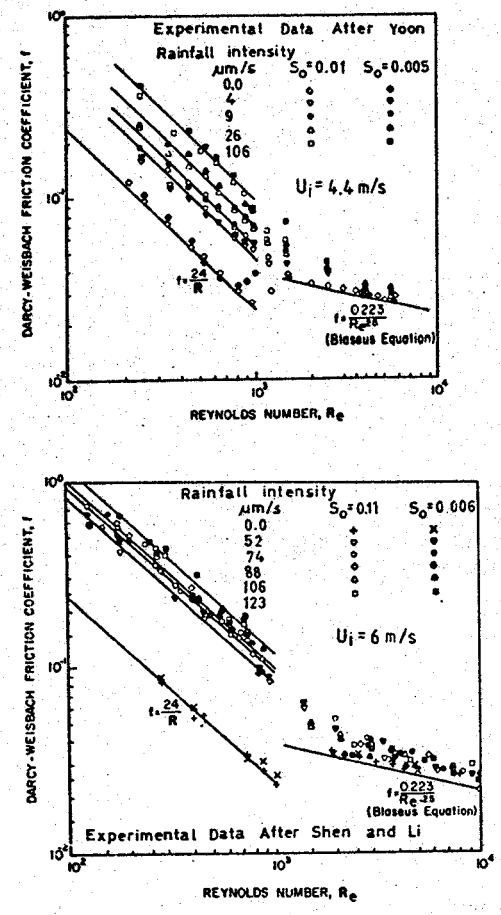

Figure 5.3.2 a,b Tests on the impact of rain on flow over a smooth surface (U_i=raindrop velocity) After Shen and Li (1973) (1 μm/s = 10 l/s·ha)

$$f = \frac{24+3400\cdot i^{0.407}}{R_e} \qquad \ldots (5.3.2)$$

where the rain intensity is given in [m/s]. Nittim was not able to quantify a similar laminar relation. The

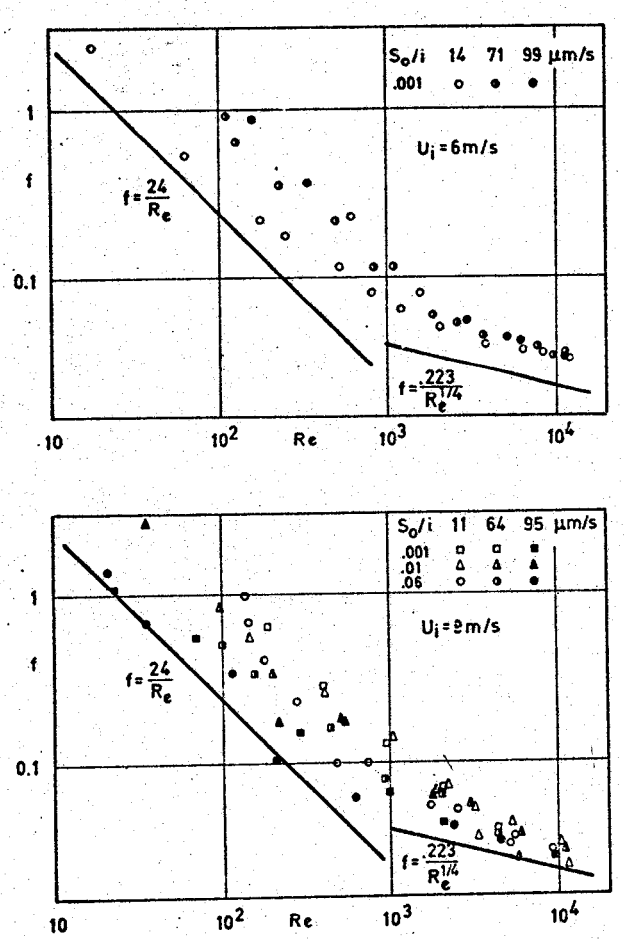

Figure 5.3.2 c,d Tests on the impact of rain on flow over a smooth surface (U_i=raindrop velocity) after Nittim (1977). (1 µm/s = 10 l/s·ha)

series shown in figure 5.3.2c shows the same trend as given by the equation. The second series of measurements by Nittim, figure 5.3.2d, however, shows the opposite trend. The friction factor decreases with increasing rain intensity, but is generally greater than $24/R_e$. A possible explanation for this discrepancy could be the

greater raindrop velocity in this test (figure 5.3.2d). However, Nittim could not show that this velocity had a statistically significant effect.

The interpretation of these contradictory effects on the flow is beyond the subject of this study. However, it serves to indicate that the way raindrops are produced in the laboratory has a significant effect on the flow.

In turbulent flow, Shen and Li found that the Blasius solution can be used if the constant $f \cdot R_e^{1/4} = 0.223$ is increased by 12%. Nittim's tests agree reasonably in the turbulent zone but with a slightly larger value for $f \cdot R_e^{1/4} = 0.260$. It should be noted that the main part of the study discussed above has been carried out using slopes equal to or less than 0.01.

The following conclusions can be drawn from the tests on flow over smooth surfaces:

- Flow without rain agrees well with the laminar relation and reasonably well with the Blasius solution in the turbulent zone (with the value of $f \cdot R_e^{1/4}$ slightly increased)
- The flow is strongly influenced by the raindrop impact in the "laminar" zone resulting in an increased friction factor
- The flow is moderately influenced by the raindrop impact in the "turbulent" zone. The Blasius' solution (with the value of $f \cdot R_e^{1/4}$ increased by about 15%) may be used.

5.3.3 Flow over "artificially" roughened surfaces

On an "artificially" roughened surface (using sand or small spheres) the height and shape of the roughness can be made very uniform. The influence on the flow caused by the surface roughness is thus expected to be best observed

on such surfaces. Investigations of interest in this area have been accomplished by Woo and Brater (1962), Kisisel (1973), Phelps (1975) and Nittim (1977).

Phelps investigated flow without rain over a surface covered by glass spheres with a roughness height k=1.2 mm. His tests show a clear laminar zone for Reynolds' numbers less than 400, figure 5.3.3. In both the laminar zones and transition zone an overall effect of increased friction factor compared to the smooth surface flow can be observed. There is also a tendency for the friction factor to increase with increasing relative roughness k/Y_o. If, however, only tests with a slope greater than 0.008 are considered (marked by squares in figure 5.3.3) the pattern is changed. The laminar zone vanishes and the transition zone moves towards lower values of R_e.

Nittim investigated also flow without rain over a surface covered by spheres (k=2.33 mm). The tests show rather different friction relations compared to those found by Phelps (figure 5.3.4). Generally, considerably smaller

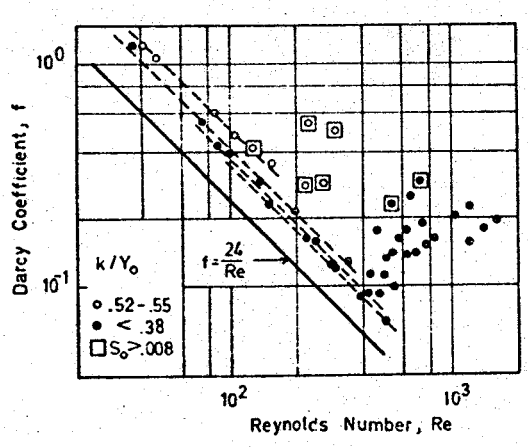

Figure 5.3.3 Flow without rain-effects of the relative roughness on the friction factor f, after Phelps (1975)

values of f were obtained and a less marked transition zone. Tests with large k/Y_o (greater than 1) are preferentially found at the lower edge of the band formed by Nittim's testpoints. For Reynolds' numbers less than 600, tests with the smallest values of k/Y_o are very close to the laminar relation ($f=24/R_e$). Thus Nittim's tests show a tendency for the friction factor to increase with decreasing relative roughness k/Y_o. It should be noted that there is a difference in chosen k/Y_o values in the two investigations. Phelps' test points all fall in the interval k/Y_o = 0.23 - 0.55 while Nittim's are considerably greater.

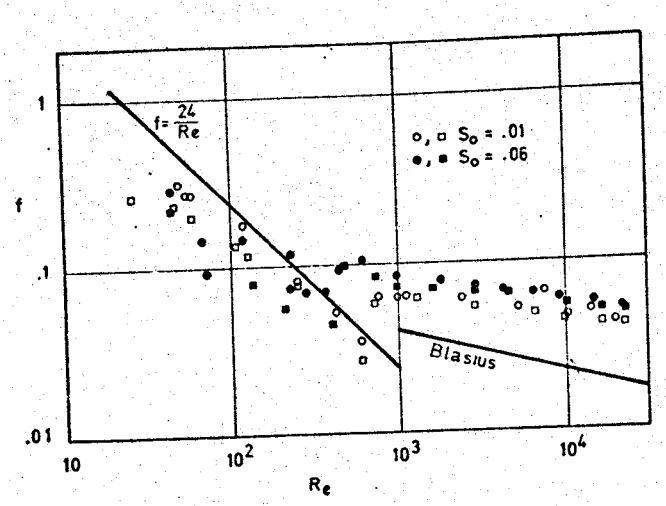

Figure 5.3.4 Friction factors at flow without rain (sphere roughness k=2.33 mm) after Nittim (1977)

Compared to Nittim's results for the smooth surface considerably greater friction factors can be observed in the region $R_e > 500$ whereas lower values were obtained at $R_e < 300$, figure 5.3.4.

Nittim's sphere covered surface was also used to study flow exposed to rain using two different intensities. At the high intensity (i = 800 l/s·ha) a great increase of

the friction factor compared to flow without rain was found. However, at the lower, more realistic, intensity (i = 180 l/s·ha) this effect is not so marked - about 20% increase at large Reynolds' numbers >800 and values smaller than $24/R_e$ for $R_e<100$.

The results presented by Kisisel shows the same great increase in f at unrealistically high rain intensities on a surface "roughened" with sand (k = 0.072 mm).

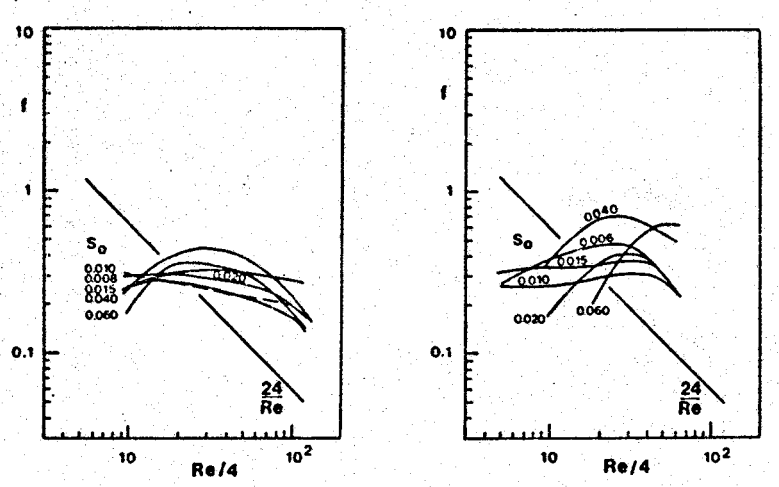

Figure 5.3.5 a-b The friction factor versus Reynold's number at i=210 l/s·ha and i=116 l/s·ha, after Woo and Brater (1962)

Woo and Brater investigated flow exposed to rain on a sandcovered surface ($k \approx 1.0$ mm). Figure 5.3.5 summarizes tests with Reynolds' numbers less than 800 and rain intensities below 210 l/s·ha. At each slope (>0.01) the friction factor reaches a maximum in the interval $80<R_e<200$ and decreases rapidly from this point with decreasing and increasing Reynolds' numbers. The moderate intensity tests (i = 116 l/s·ha) agree reasonably with those of Phelps' without rain and $k/Y_o \approx 0.5$. The high intensity tests (i = 210 l/s·ha) give slightly greater values of f than Nittim's tests (i = 180 l/s·ha). The result from Woo and Brater's

tests fits reasonably with Phelps' and Nittim's and supports the earlier results of a great effect caused by the relative roughness and a more moderate effect caused by rain.

The following conclusions can be made from the tests of flow on sand and sphere-roughened surfaces with a slope greater than 0.01:

- The friction factor differs considerably from that of a smooth surface. No laminar zone can be identified and in the turbulent zone (R_e > 1000) significantly greater friction factors are obtained (f increased by a factor 2).
- For flows having a relative roughness k/Y_o > 0.5 the traditional relation - f increasing with k/Y_o - does not apply.
- For flows without rain and a relative roughness realistic for urban surfaces, f-values less than $24/R_e$ are obtained at low Reynolds' numbers (R_e<400).
- The influence of rain on the friction factor is great at high intensities but more moderate at realistic intensities (about 20% increase at high Reynolds' numbers).
- The friction relation has characteristics resembling a transition zone at Reynolds' numbers less than 1000 with great scatter. Thus it is not possible to quantify this relation with the referred investigations as a base.

5.3.4 Flow over asphalt and concrete surface

Flow over impermeable surfaces found in urban areas, such as concrete or asphalt, has been investigated by Izzard (1944), Yu and McNown (1964), Andersson et al. (1973) and Nittim (1977). Such surfaces are characterized by having

a roughness height and shape that varies over the surface and the roughness elements form irregular patterns on the surface, all in contradiction to "artificially" roughened surfaces.

Flow without rain on a steel brushed asphalt surface has been investigated by Nittim. The surface represents a road-surface that has been worn by traffic ($k \approx 0.8$ mm). For Reynolds' numbers less than about 10^3 the obtained friction factors are quite similar to those from Nittim's "sphere" surface (k=2.33 mm), though the latter shows a greater scatter. When the Reynolds' number is greater than 10^3 the asphalt surface obtains significantly smaller values of f than the "sphere" surface. This indicates that in the fully turbulent zone, where the relative roughness is small, the traditional friction relation - f increasing with k/Y_o - holds.

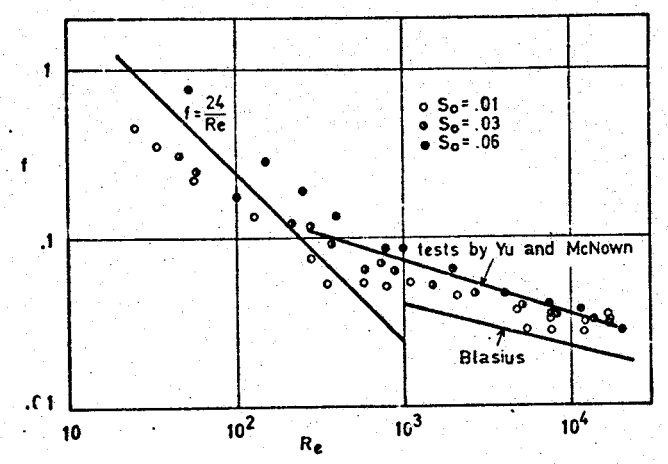

Figure 5.3.6 Flow without rain-friction factor versus Reynolds' number for an asphalt surface. After Nittim (1977)

Yu and McNown made a number of tests with flow without rain on concrete. The tests (represented in figure 5.3.6 as a line) have friction factors in the fully turbulent

zone about 80% greater than those obtained from Blasius' solution while the corresponding factor for the asphalt surface is about 50%. No information was available on the roughness height of the concrete.

Tests on an asphalt surface made by Izzard show greater friction factors than those found by Yu and McNown and Nittim but agree reasonably with Phelps' results when $R_e<600$.

Andersson et al. tested asphalt surfaces (Ab 8 t and Ab 12 ö) in the field by velocity flow measurements and found friction factors also in agreement with Phelps' results. Izzard obtained for $R_e>600$ slightly larger f-values than Nittim.

The effect of rain on Yu and McNown's and Nittim's surfaces are shown in figures 5.3.7 a,b. Nittim's data are very scattered compared to those of Yu and McNown. The greatest scatter is, however, found in the interval $R_e<200$ where Yu and McNown only have one test point. Their results, in general, agree very well with Nittim's.

Nittim's tests with rain agree reasonably with his test of the sphere surface exposed to rain, except at high Reynolds' numbers where the greater roughness height of spheres gives rise to a greater friction factor. The influence of rain can be recognized both in Yu and McNown's and Nittim's data. It should, though, be noted that in figure 5.3.7b all the filled and the half filled dots represent unrealistic rain intensitites (greater than 380 l/s·ha). If these are removed, the influence of rain becomes mainly visible as a scatter. Yu and McNown were also unable to quantify the effect of the rain intensity. In their tests, rain intensities from 180 l/s·ha to 700 l/s·ha are represented. Izzard's investigations of rain dependence show the same general trend of increasing friction factor with increasing rain intensity, but all his intensities are unrealistic (see above).

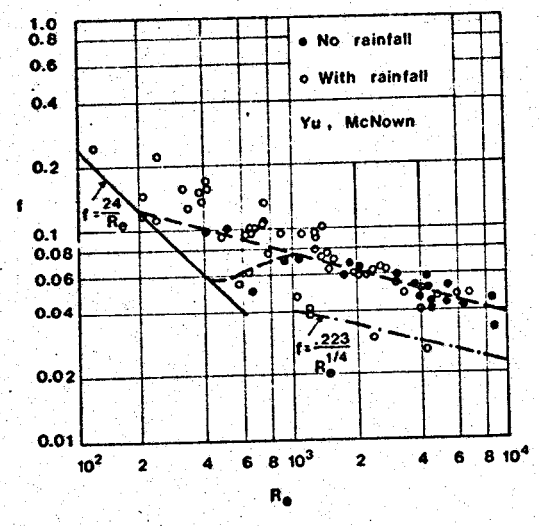

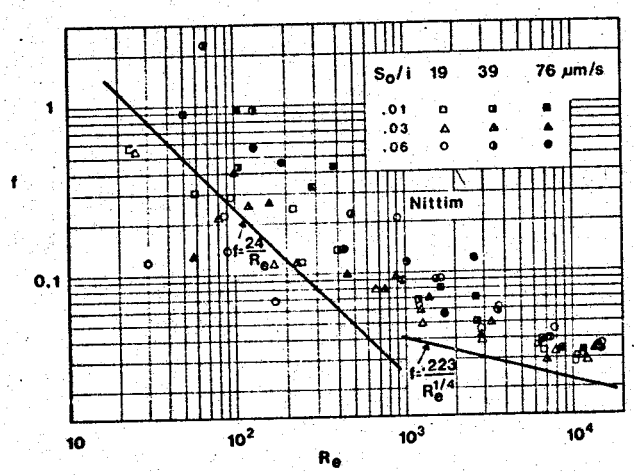

Figure 5.3.7 a,b Friction factor versus Reynolds' number for a concrete and asphalt surface after Yu and McNown (1964) and Nittim (1977), (1 µm/s = 10 l/s·ha)

The following conclusions can be drawn from the tests considered in this section, (in general agreement with those of "artificially" roughened surfaces):

- No distinction can be made between a laminar and a turbulent zone.
- At $R_e > 1000$ values of f considerably greater than those corresponding for a smooth surface are obtained.
- For $R_e > 1000$ a tendency for the friction factor to increase with increased roughness height is observed (sections 5.3.3 and 5.3.4).
- At $R_e < 300$ values of f below the "laminar values" $24/R_e$ are obtained.
- The influence of rain is clear at high intensities, but at realistic intensities only a weak trend is observed. However, the scatter becomes very great at low Reynolds' numbers.

5.4 Rollwaves

If the slope So is sufficiently steep, small disturbances (which are always present in a flow) will grow and after a certain length so called rollwaves - a form of unstable flow - will form and move downstream. The stability is judged by the Verdenikov's number V_e, defined by Chow (1959)

$$V_e = p\left(1-\frac{A}{P}\cdot\frac{dP}{dA}\right)F_o \qquad \ldots (5.4.1)$$

where p is the exponent of the hydraulic radius in the friction relation (denoted c_4 in equation (5.1.2)). P is the wetted perimeter and F_o the Froude number. Instability is assumed to occur when Vedernikov's number exceeds unity. For surface flow dP/dA is zero and for gutter-flow it is approximately zero. If the Darcy-Weissbach friction relation is used (p=0.5), then Vedernikov's number can be written

$$V_e = \sqrt{\frac{2}{f}\cdot S_o} \qquad \ldots (5.4.2)$$

Using the Chezy formula with a Chezy coefficient relevant for urban surfaces, the stability criterion becomes $S_o <$ 0.04 - 0.05. This coarse criterion agrees reasonably with data obtained by Nittim for the smooth surface and the asphalt surface. For rougher surfaces the agreement is not so good. No rollwaves seem to occur during heavy rain.

Rollwaves have a wave length and period much shorter than the waves that are the main subject of urban runoff simulation and cannot be represented by the momentum equation (3.2.1b), see Yen et al. (1977). According to Nittim's data the most realistic way of considering rollwaves in the analysis is by using an increased friction factor. For a relatively smooth surface and small Reynolds' numbers an increase of the friction factor of more than 50% may very well be obtained. At large Reynolds' numbers and surfaces with greater roughness heights, the influence is considerably less.

5.5 Wind forces

In the steady flow case, equation (5.1.1) applied to surface flow is written

$$S_o = \frac{\tau_{mp} \pm \tau_{ms}}{\rho g Y} \qquad \text{... (5.5.1)}$$

Using equation (5.2.1) the friction factor may be expressed as a function of the shear stresses

$$f = \frac{8}{V^2 \cdot \rho} \cdot (\tau_{mp} \pm \tau_{ms}) \qquad \text{... (5.5.2)}$$

where the shear stress at the surface τ_{ms} is wind generated. The wind shear stress is given by

$$\tau_w = \tau_{ms} = \rho_L \cdot C_D \cdot W^2 \qquad \text{... (5.5.3)}$$

where the density of air $\rho_L = 1.29$ kg/m^3, the resistance coefficient $C_D \approx 2.4$ (according to Engelund (1969)) and W

the wind velocity 3 m above surface. Thus

$$\tau_w \approx 3 \cdot 10^{-3} \cdot W^2 \qquad \ldots (5.5.4)$$

is obtained. The wind shear stress obtained from equation (5.5.4) at a wind velocity W = 6 m/s is 0.1 N/m^2. This can be compared with the the bottom shear stress which has values in the interval 0.01 - 1.0. The wind shear stress may evidently be of the same order as the bottom shear stress.

If the effect of wind is included in the Darcy-Weissbach' friction relation, we get (for surface flow)

$$Q_b = Y^{3/2} \sqrt{\frac{8g \cdot S_o}{f \pm 2.4 \cdot 10^{-5} \cdot \left(\frac{W}{V}\right)^2}} \qquad \ldots (5.5.5)$$

Strong wind will, in addition to the effect on the water surface friction, have an influence on the momentum of the raindrops. Surfaces in urban catchment usually have arbitrary flow directions. Wind velocities over the surfaces also have, because of houses and other obstacles, great local variation. It would therefore not be possible to calibrate, or to feed with proper input values an urban runoff model that takes the effects of wind into account. However, in studies of the validity of models using field data, wind may be treated as a source of error.

5.6 Summary and discussion

In the studies of the friction factor discussed in the previous sections, several distinct trends or relations have been specified. Examples are Shen and Li's friction factor - rain intensity relation for a smooth surface, and Phelps' observations of the influence of the relative roughness. However, even if only those tests with rain intensities, roughness heights and slopes relevant for

Swedish urban surfaces are taken into account, the variation of f appears to be very complex and difficult to interpret. The scatter in friction factor values is large for flow exposed to rain, especially at low Reynolds´ numbers. Some characteristics may, however, be noted;

- o there are no distinct laminar or turbulent zones
- o at small Reynolds´ numbers friction factors below the laminar values are obtained
- o at large Reynolds´ numbers friction factors considerably greater than those corresponding to Blasius´ solution are obtained
- o the influence of rain on the friction factor is small

The investigations give no base for establishing a relation which quantifies the influence on the friction factor, either of the relative roughness or the the rain intensity. However, the 'simple' friction relations presented in section 5.2 will be discussed and fitted to test data.

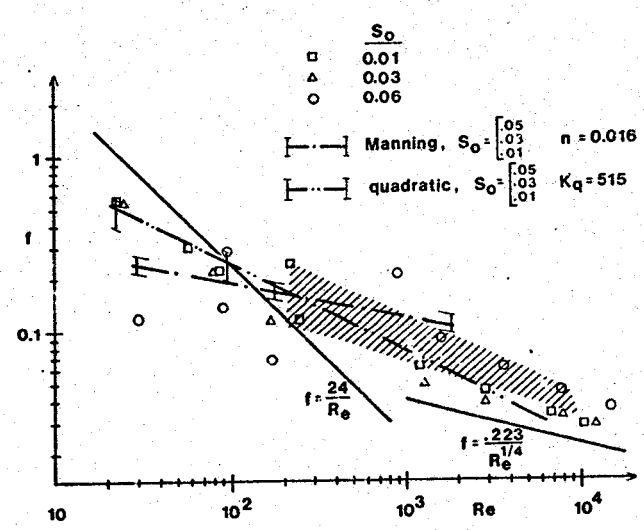

Figure 5.6.1 Comparison of the fitted friction-relation with Nittim´s (1977) and Yu and McNown´s (1963) (shaded) tests on asphalt and concrete

In figure 5.6.1 the most relevant results from section 5.3 have been put together. They are the Nittim's asphalt tests and Yu and McNown's concrete tests (shaded). All test points with unrealistically high ($i > 390$ l/s·ha) rain intensities have been removed from the plot, but this could not be done with Yu and McNown's data. Typical values of the Reynolds' number for surface flow are less than 900 while the corresponding numbers for gutter flow are greater than 900. The test points greater than 900 in the figure are therefore believed to be reasonably representative for gutter flow.

Considering the scattered results a suitable level of sophistication for a friction factor relation might be

$$f = c_1 \cdot R_e^{c_2} \qquad \ldots (5.6.1)$$

represententing a straight line in the friction factor diagram. The relation is valid for the Chezy, Manning, L- and quadratic formulas. Comparing the 'slopes' of the different friction factor relations and the test results, the L-formula generally seems to have the best overall fit. However, in the important interval $R_e < 1000$ there are no grounds for rejecting the Manning - or quadratic-formulas, provided suitable roughness coefficients are used. In figure 5.6.1 the quadratic relation ($K_q = 515$ and $S_o = 0.03$) and the Manning formula ($n = 0.016$ and $S_o = 0.03$) are shown.

The friction factor relations are also characterized by an influence from the surface slope S_o, see equations (5.2.11 - 5.2.13). This dependence could not be recognized in the series of test points. Each relation should then be represented in the diagram by a band instead of a line. The bands corresponding to the slope interval given in chapter 2 (0.01-0.05) are marked in figure 5.6.1. The quadratic friction factor relation is obviously more influenced by the surface slope. Both the relations may be manipulated to give a friction factor relation independent of S_o. This is done by using a slope exponent of

0.55 and 0.67 in the Manning and quadratic formulas, respectively (not used in this report).

The typical urban surface is not as plane and regularly shaped as the laboratory surfaces discussed in this chapter. The flow over the surface will, therefore, in some parts form rills which more closely resemble gutter flow.

By comparing model simulations and corresponding flows from field measurements more realiable friction coefficients should, in principle, be obtained. However, field measurements of surface flow are difficult to accomplish and all those known to the author contain not only surface flow but also gutter flow and sometimes, in addition, sewer flow. It is then, in practice, difficult to analyse surface flow and gutter flow separately. Simulations presented later in this report indicate, however, that the Manning formula is an appropriate friction relation using n = 0.016 in surface flow and n = 0.013 in gutter flow.

In the simulations of runoff from a small asphalt catchment (430 m^2), which are discussed in chapter 8 several friction relations were tested. It was found that the typical turbulent friction models, Chezy, Manning and Blasius formulas (b = 1.50-1.72), performed rather well. The 'intermediate' quadratic formula (b = 2) performed not so well while the laminar relation (b = 3) performed badly, even for runoff with very low Reynolds' numbers.

Falk and Niemczynowicz (1979) analysed 13 Swedish urban surfaces and developed a friction relation. This is not directly comparable with those discussed here but it should be noted that the Chezy exponent (b=3/2) was used to relate flow and water depth.

Jacobsen (1980) successfully analysed surface flow using the L-formula (b = 1.83). He reported indications of a

better fit in some cases using the quadratic relation. Jacobsen uses the same basic equations as the author but a somewhat different numerical solution method.

In an urban runoff model where the governing equations are solved by numerical methods the selection of space and time step has an influence on the simulated hydrograph, which is very similar to the effect caused by a change in roughness coefficient. It is, therefore, possible to some degree to compensate for a space step which is too long by decreasing the friction factor, Lyngfelt (1978). Thus, for different runoff models and for different uses of the models different friction coefficients may be relevant in otherwise identical applications.

A traffic load on the surface changes the characteristics of runoff. In a study of runoff from a motorway (traffic intensity 500-2000 vehicles/hour) it was found that this load increased the roughness coefficient by 100%, Bufill (1984).

6. NUMERICAL SOLUTION METHODS OF THE KINEMATIC WAVE EQUATIONS

6.1 General

The kinematic wave equations have analytical solutions only in some very special cases (c.f. chapter 4.2.3). In the general case with an arbritary rain intensity input, numerical solution methods must always be used. In these the derivatives are approximated by finite differences usually established between fixed gridpoints in the x-t plane. The finite difference solution can be expressed in many different ways, each one having its own possibilites and properties. Important properties are stability, consistency and numerical diffusivity.

The main object of the numerical algorithm is, of course to produce a solution as close as possible to the exact solution of the differential equations. If unsuitable algorithms and numerical parameters are used the deviation from the 'exact' solution can be great. A thorough knowledge of the properties of the numerical solution method is, then, just as important as the knowledge of underlying differential equations.

In this chapter numerical solution methods for the kinematic wave equations will be discussed. The analysis is mainly focused on the surface and gutter flow case (lateral inflow) but is in many parts also generally valid. The discussion is based on the weighted box scheme, which is a very general solution method.

6.2 Finite difference schemes

The structure and use of a finite difference scheme together with boundary conditions is best discussed with reference to the x-t plane. This plane is shown in figure 6.2.1 with fixed grid points, upstream and downstream boundaries.

BIBLIOGRAPHIC INFORMATION

PB86-137171

Urban Runoff Modelling: The Application of Numerical Models Based on the Kinematic Wave Theory. Volumes 1 and 2,

1985

by S. Lyngfelt.

PERFORMER: Chalmers Univ. of Technology, Goeteborg (Sweden). Institutionen foer Vattenbyggnad. SER-A-13

The study deals with modelling of the urban runoff process. The main objectives were to make recommendations for the selection of a basic model and suitable numerical solutions, and also to investigate the importance of discretization of the geometrical input data and develop usable base catchment models. The runoff process in surfaces gutters and sewers is described by one continuity and one momentum equation, the shallow water equations. A study of the influence of different terms shows that there are two approaches of interest in urban runoff modelling, the kinematic and the diffusive wave approximations. The kinematic wave approximation is defined by a very simple set of differential equations and boundary conditions. The momentum equation is reduced to an unique relation between flow and water depth.

KEYWORDS: *Runoff, *Water pollution, *Urban areas, *Foreign technology.

Available from the National Technical Information Service, SPRINGFIELD, VA. 22161

PRICE CODE: PC E11/MF E01

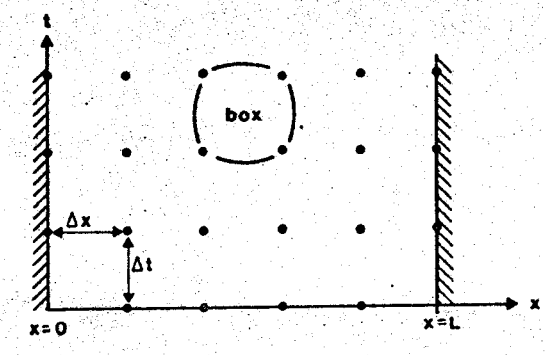

Figure 6.2.1 The x-t plane with fixed gridpoints and boundaries

Consider the problem of solving for the two unknown variables (Q,Y) at each grid point using the kinematic wave equations. The initial conditions at t=0 are assumed given along the channel reach. Because the equations have no second order derivatives it is possible to use the box-scheme where the differences are established by only one time and space step ("one step" scheme).

If the difference equations are applied to the first box-grid points (0, 0), (0, Δt), (Δx, 0), (Δx, Δt) - and Q or Y is given as upstream boundary condition, Q and Y in the first internal grid point (Δx, Δt) can be determined. Let the scheme now be successively applied in a downstream direction and water depths and flows calculated stepwise at the points (2Δx, Δt), (3Δx, Δt) and so on. When the scheme is finally applied to the last box at one time level, values of Q and Y at the downstream boundary can be determined. The given solution method is not able to take downstream conditions into account. The method is therefore valid only for supercritical flow.

In figure 6.2.1 it can be seen that the box scheme includes two points at the new time level. As the relation between Q and Y is not linear this will result in an implicit difference equation which must be solved by some iterative technique. Numerical schemes containing more than one point at the new time level are called implicit. The box scheme is a typical implicit scheme.

An explicit scheme includes only one point at the new time level and thus the unknown variable may be directly solved. In figure 6.2.2, a two-step explicit scheme (containing two successive space steps) is given as an example. Two-step schemes can be used in differentiating second order derivatives, for instance the diffusive term in the convective diffusion equation $\partial^2 Q/\partial x^2$ (section 4.3).

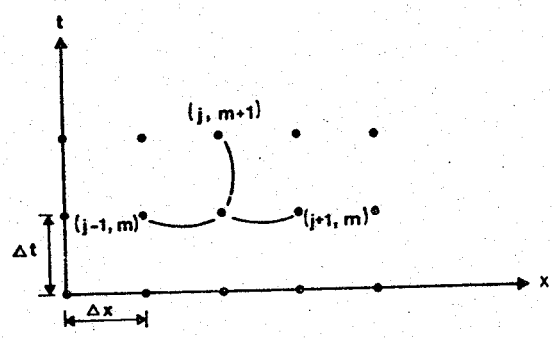

Figure 6.2.2 An example of a two step explicit scheme

Stability is an important property of the numerical scheme. With an unstable scheme a solution will be produced where the values obtained suddenly grow in an uncontrolled manner and often cause it to break down. Implicit schemes are usually regarded as unconditionally stable. Explicit schemes may become unstable for unsuitably selected time and space steps. The so called Courant condition is generally used as a stability

criterion for explicit methods, Yevjevich (1975)

$$\frac{\Delta t}{\Delta x} < \frac{1}{|V \pm \sqrt{gY}|} \qquad \ldots (6.2.1)$$

In implicit methods, mainly for stability reasons, greater time and space steps can be used and these seems then to be the most effective from a numerical point of view. The necessary iteration procedure in the non linear case reduces, however, this effectiveness and the implicit scheme is not always advantageous.

The box scheme, is for several reasons which will become apparent in this chapter, the most interesting for differentiating the kinematic wave equations. It also forms a base for analysis of and comparisons between different well known solution methods.

6.3 The weighted box scheme - general properties

6.3.1 Finite difference equations

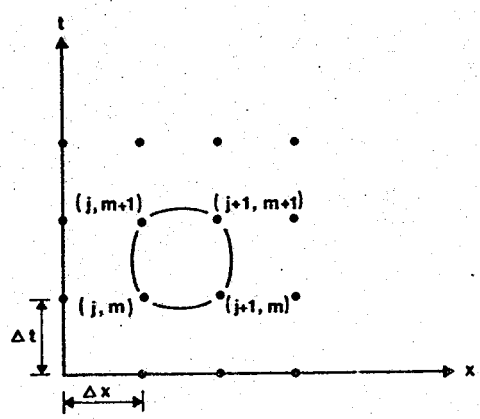

Figure 6.3.1 Grid points in an arbitrary finite box

In the kinematic wave equations only the continuity equation contains derivatives

$$\frac{\partial Q}{\partial x} + \frac{\partial A}{\partial t} = q \qquad \ldots (4.2.1)$$

Let this equation be approximated by finite differences using a box scheme, figure 6.3.1.

If all gridpoints are equally accounted for we get

$$\frac{\partial Q}{\partial x} = (Q_{j+1}^{m+1} + Q_{j+1}^{m} - Q_{j}^{m+1} - Q_{j}^{m})/2\Delta x \qquad \ldots (6.3.1a)$$

$$\frac{\partial A}{\partial t} = (A_{j+1}^{m+1} + A_{j}^{m+1} - A_{j+1}^{m} - A_{j}^{m})/2\Delta t \qquad \ldots (6.3.1b)$$

This differentiation defines a scheme which is centred on the centre of the box. By the use of weighting factors in the differentiation it is possible to consider the four gridpoints at different levels.

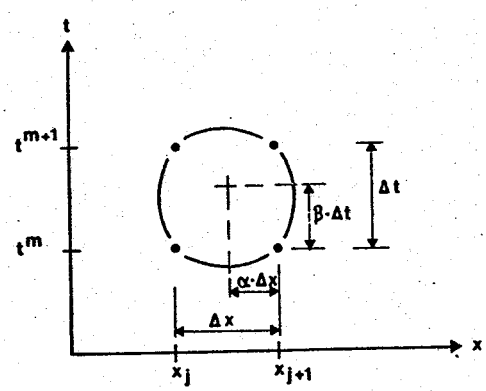

Figure 6.3.2 The relation between the centrepoint and weighting factors after Smith (1980)

$$\frac{\partial Q}{\partial x} = \left[\beta(Q_{j+1}^{m+1} - Q_{j}^{m+1}) + (1-\beta)(Q_{j+1}^{m} - Q_{j}^{m})\right]/\Delta x \qquad \ldots (6.3.2a)$$

$$\frac{\partial A}{\partial t} = \left[\alpha (A_j^{m+1} - A_j^m) + (1-\alpha)(A_{j+1}^{m+1} - A_{j+1}^m) \right] / \Delta t \qquad \ldots (6.3.2b)$$

This differentiation corresponds to a scheme which is centred on a point in the box given by α and β as shown in figure 6.3.2. The weighting factors can take values $0<\alpha<1.0$ and $0<\beta<1.0$.

6.3.2 Numerical diffusion - consistency

It can be shown by a Taylor series expansion that the weighted scheme is a better approximation of the equation,

$$\frac{\partial Q}{\partial x} + \frac{\partial A}{\partial t} + D_n \frac{\partial^2 Q}{\partial x^2} = q \qquad \ldots (6.3.4)$$

where

$$D_n = (2\alpha-1) \cdot \frac{\Delta x}{2} + (1-2\beta) c_k \frac{\Delta t}{2} \qquad \ldots (6.3.5)$$

than of the continuity equation, Smith (1980). The effect of the differentiation can thus be intepreted as an introduction of a diffusion component in the kinematic wave equations (compare equation (4.3.5)). The diffusion coefficient is a function of the numerical parameters Δx, Δt, α and β. Different combinations of these parameters together with the flow-state (represented by c_k) results in different values of the diffusion coefficient which may be both positive and negative. A negative coefficient will give an attenuating wave movement which cannot be described by the basic kinematic wave equations. A positive coefficient gives an amplifying wave movement, usually resulting in serious numerical difficulties (see below).

The second order derivative in equation (6.3.4) have factors containing both Δx and Δt. This is also true for the third order derivatives (here not included in the

equation). In the limit when Δx and $\Delta t \rightarrow 0$ the ordinary continuity equation is obtained. The numerical solution is then consistent with the underlying differential equation for any choice of α and β.

Analysis of the diffusion coefficient and its influence on the properties of weighted box models has been discussed by Smith (1980), Ponce and Theurer (1982) and Kousis (1983).

6.3.3 Classification of weighted box models

Weighted box models can be classified according to the properties of their diffusion coefficient as defined in the previous section. In this report three classes, named α-, β- and $\alpha\beta$-diffusive models, will be discussed:

The α-diffusive models are obtained for $\alpha<0.5$, $\beta=0.5$ and corresponds to a diffusivity related only to the chosen discretization in space. Of special interest is the combination $\alpha=0$, $\beta=0.5$. It will here be called the diffusive box scheme though many other combinations of α and β also result in diffusive solutions. The scheme corresponds to the differentiation

$$\partial A/\partial t = (A_{j+1}^{m+1} - A_{j+1}^{m})/\Delta t \qquad \ldots (6.3.6)$$

which is equivalent to the assumption of uniform water depth in each segment Δx. The diffusive box scheme is a frequently used solution method for the kinematic wave equations especially in sewer routing (c.f. section 6.6).

The β-diffusive models correspond to a diffusivity related to the discretization in time only and are obtained for $\alpha=0.5$, $\beta>0.5$.

In the $\alpha\beta$-diffusive models diffusivity is influenced by the discretization in both time and space. The case when

$\alpha<0.5$, $\beta>0.5$ implies a positive contribution to the diffusion by both the time and space related components. This will decrease the influence of a single discretization (in time or space). The case when $\alpha<0.5$, $\beta<0.5$ implies a negative contribution to the diffusion by the time step dependent term. Because of this term a relatively greater space dependent diffusion can be accepted. This model is then of interest in connection with the use of large space steps (reservoir models).

A special case is the fully centred scheme given in equation (6.3.1). This scheme corresponds to $\alpha = \beta = 0.5$ giving the diffusion coefficient zero, see equation (6.3.4). It is commonly called the non-diffusive scheme.

The greatest possible diffusion for given time and space steps is obtained when $\alpha = 0.0$ and $\beta = 1.0$. This scheme has been proposed by Li et al. (1975a).

In order to survey the different models and their diffusive properties, they have been put together in table 6.3.1.

Table 6.3.1 Weighted box models

Model	α	β	D_n
α-diffusive	<.5	.5	$(2\alpha-1)\Delta x/2$
β-diffusive	.5	>.5	$(1-2\beta)\Delta t\cdot c_k/2$
$\alpha\beta$-diffusive	<.5 <.5	>.5 <.5	$\frac{2\alpha-1}{2}\cdot\Delta x + \frac{1-2\beta}{2}\cdot\Delta t\cdot c_k$
Special cases			
Non-diffusive	.5	.5	0
"Diffusive box"	0	.5	$-\Delta x/2$
Li et al. (1975)	0	1	$-(\Delta x+c_k\cdot\Delta t)/2$

6.3.4 'Negative diffusion' ($D_n > 0$)

The three classes of model given in the last section all have a positive diffusion ($D_n < 0$). It is, however, possible to choose numerical parameters that give solutions with a negative diffusion ($D_n > 0$).

Theoretically, such models should produce amplifying waves. Numerical experiments show that hydrographs simulated using a negative diffusion scheme become uneven with sudden unrealistic flow peaks (shots). These disturbances do not usually make the solutions break down like disturbances can do in explicit schemes. Despite the fact that the box scheme is implicit and thus 'unconditionally stable', solutions obtaining shots will be called unstable solutions. An example of such instability is shown in figure 6.3.3 together with a hydrograph having a suitable attenuation.

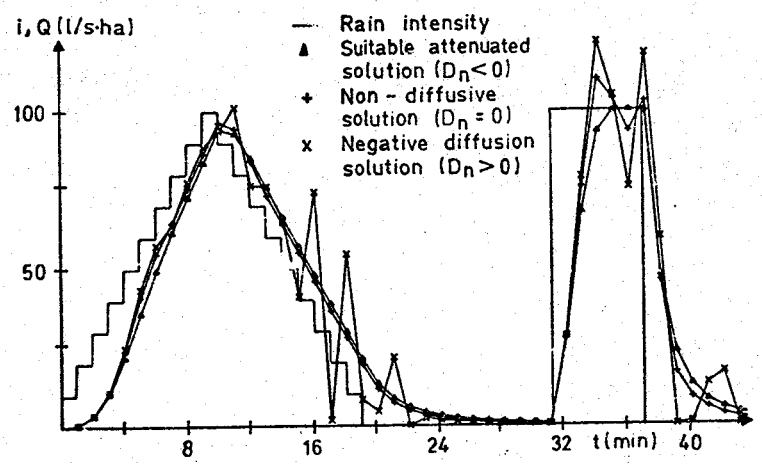

Figure 6.3.3 An example of unstable solutions (with shots) compared with one having a suitable attenuation (L_s=20 m, s_s=0.035, n=0.016)

The nondiffusive scheme has according to equation (6.3.5) no diffusion ($D_n = 0$). Despite this the hydrographs simulated by the model often become unstable in a similar way to models with negative diffusion, see figure 6.3.3. This can be explained by the neglected third order terms in D_n (equation (6.3.4)) which give a positive contribution to D_n in many flow cases. The non-diffusive scheme is therefore usually not used in kinematic wave routing. Simulations by means of this model also show that $D_n < 0$ as expressed in equation (6.3.4) cannot be taken as a totally reliable condition for stability.

6.3.5 Positive diffusion ($D_n < 0$)

Models with positive diffusion ($D_n < 0$) will produce attenuated hydrographs. The basic performance of such models is exemplified by the use of the diffusive box

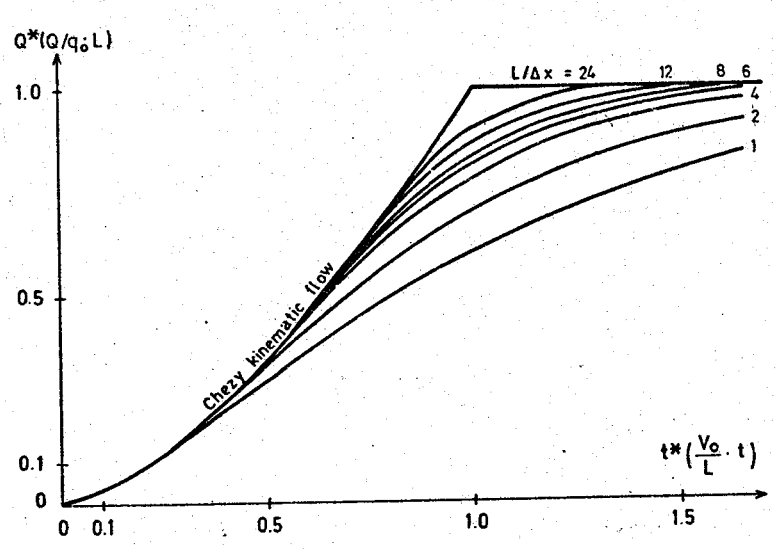

Figure 6.3.4 Dimensionless rising hydrographs obtained from the diffusive box model using various values of Δx (after Lyngfelt (1978)).

model in figure 6.3.4. Here dimensionless rising hydrographs generated using various step lengths (corresponding to different D_n) are shown, together with the analytical kinematic solution. Evidently, rather small space steps have to be used in order to obtain a solution similar to the analytical solution.

The numerical diffusion influences the solution in a way which is very similar to that caused by the acceleration and pressure force terms in the complete dynamic equation. In figure 6.3.5, dimensionless rising hydrographs generated using the complete shallow water equations are shown, Woolhiser (1967). The attenuation is a function of the kinematic wave numbers and Froude numbers.

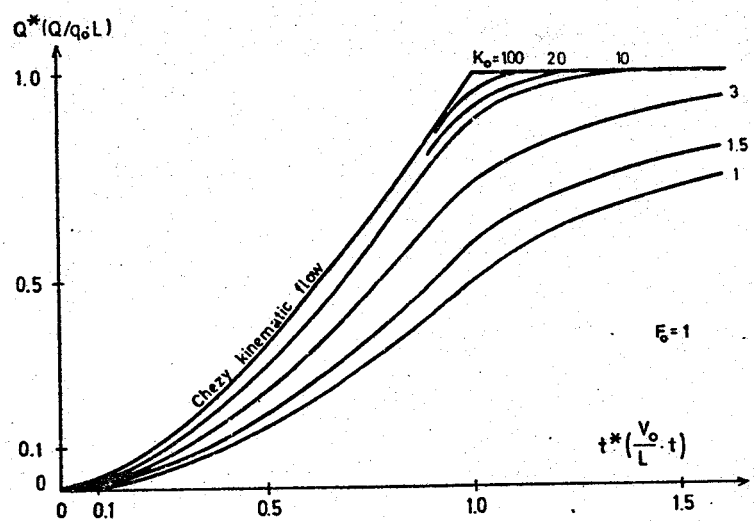

Figure 6.3.5 Dimensionless rising hydrographs obtained by the shallow water equations for various kinematic wave numbers and F_o=1 (after Woolhiser (1967)).

According to sections 3.4 and 4.3.2 the main part of the 'diffusion' in overland and sewer flow simulations is generated by the pressure force term. It should thus be

possible to estimate a suitable step length in the diffusive box model by setting the numerical diffusion coefficient D_n equal to the corresponding coefficient D in the convective-diffusion equation (section 4.3.1). This will give

$$\Delta x = \frac{Q_b}{S_o c_k} \qquad \ldots (6.3.7)$$

where Q_b = flow per unit width or, using the Manning formula

$$\Delta x = \frac{3}{5} \cdot \frac{Y}{S_o} \qquad \ldots (6.3.8)$$

which is basically valid for surface or flow in a rectangular channel. The equations show that in order to obtain the 'true' diffusion using the diffusive box model in overland flow, step lengths below 0.1 m should be used.

6.3.6 Selection of numerical parameters

In overland flow where the kinematic wave number usually exceeds 100 the optimal selection of numerical parameters is evidently one that gives a very small diffusion, like that obtained by the complete shallow water equations (see figure 6.3.5). For such a choice the numerical solution will in fact be more accurate than the underlying kinematic wave theory. In practical modelling, the numerical diffusion can not be determined with sufficient precision to follow the true value and must therefore be chosen to be greater in order to ensure that shots are avoided.

To obtain reasonably effective calculations, the greatest possible step length should be used. The diffusive box model appears from this point of view to be unsuitable and better numerical methods are found among the α-, β- and $\alpha\beta$-diffusive models (see table 6.3.1). The advantages and drawbacks of using different numerical models have to be analysed by means of numerical experiments which is done in the next section.

The selection of time step is also important and affects the diffusion. In choosing a suitable time discretization, both practical and numerical aspects have to be considered. From a practical/economical point of view the greatest possible timestep should be used. It has, however, to be small enough to preserve an appropriate reproduction of the shape of hydrographs within the system. This demands varying discretization within the system, which is not very practical. It is, furthermore, desirable to keep the time step constant between different tests in the same catchment and preferably also between different model applications.

The choice of time step has, then, to be a compromise. Referring to rain intensity/runoff measurements in catchments of different sizes made in Göteborg and Linköping (see chapters 8 and 9) Δt = 30 s seems reasonable for fast reacting catchments. In slower catchments (areas greater than 2-3000 m^2) a greater time step, Δt = 60 s, can be accepted. Greater time steps may be of interest in special cases where very great subcatchments are used or long time periods are to be simulated. In the simulations referred to in this report, the time step has been fixed at 60 s with the exception of the smallest simulated catchments, where 30 s is used. The analysis of the numerical parameters in the subsequent sections are based on these two time steps.

6.4 The weighted box scheme - numerical experiments

6.4.1 Aim and scope of the experiments

The general considerations given in the last section can not be used directly to choose suitable parameters (α, β, Δx, Δt) in the weighted box scheme. Reliable solution methods have to be based on experience from numerical experiments. In this section a series of such experiments is discussed. From this, a criterion for choices of the weighted box parameters is presented, giving

stable and suitably attenuated solutions.

As it would go too far to investigate all possible parameter combinations, the test series has been limited to cover a certain variation in flow length, rain intensity and shape of the hyetograph besides the four numerical parameters. The time step has, in accordance with the last section, been tested for 30 and 60 seconds. The tested catchment is shown in figure 6.4.1 and consists of a surface and a gutter. Four surface lengths were tested in the interval 5-40 m and three surface slopes in the interval 0.005-0.04.

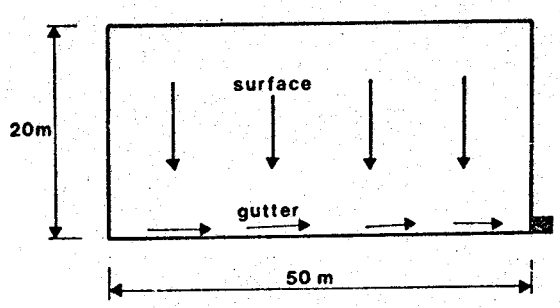

Figure 6.4.1 Test surface for numerical experiments.

Two cases of gutter length, L_g = 50, 100, and two cases of gutter slope, S_g = .005, .02, were also tested.

A standard hyetograph was used in the tests, see figure 6.4.2. It is intended to reflect one fast rising/recession part and one relatively slow one. The peak intensity was 100 l/s·ha (corresponding to a recurrence interval of 4 months at five minutes duration). For the surface length L = 20 m two alternative intensities were tested, i = 25, 50 l/s·ha.

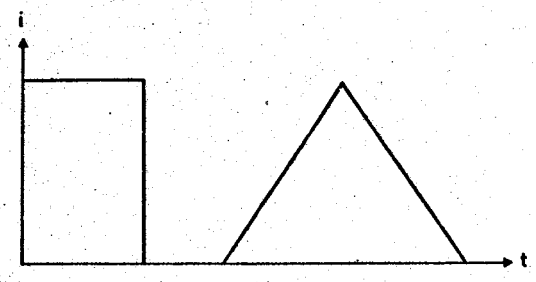

Figure 6.4.2 Hyetograph used in numerical tests

6.4.2 Numerical models and experiments

α and β were chosen in the intervals 0-0.5 and 0-1.0 respectively in order to cover the three main model cases defined in the last section; α-, β - and $\alpha\beta$ diffusive models. The tested models are given in table 6.4.1.

Table 6.4.1: Tested numerical models

β \ α	.0	.1	.2	.3	.4	.45	.48	.50
.25	$\alpha\beta^{*}$	$\alpha\beta^{*}$						
.35	$\alpha\beta^{*}$	$\alpha\beta^{*}$						
.5	α^{**}		α		α	α		ND
.52							$\alpha\beta$	
.55						$\alpha\beta$		β
.60					$\alpha\beta$			β
.65								β
.70				$\alpha\beta$				β
.75								β
.80								β
1.0								β

*) Models with a negative contribution to the diffusion from the time dependent term

**) Diffusive box scheme ND = Non-diffusive scheme

The different models are marked in the table by their prefixes α, β or $\alpha\beta$.

For each model given in table 6.4.1 a diffusive parameter was chosen and varied for different flow cases. Using small values of this parameter it was possible to stress the models to an unstable behaviour at the first intense hyetograph peak. Hydrographs generated by different values of the diffusive parameter were then compared. In each flow case a 'critical' value was chosen corresponding to the hydrograph having the smallest diffusion but still with no tendencies to instability (shots, see figure 6.3.3). These empirically obtained values represent a diffusion, which from a practical numerical point of view, is the closest possible to that of the complete equations at large values of K_o (figure 6.3.5). Below, they are called 'optimal' values.

In the numerical experiments it was found that at very large values of the discretization $\Delta x/L$, difficulties arose in properly reproducing the shapes of the hydrographs, this despite selection of 'optimal' diffusive parameters. At step lengths having a $\Delta x/L$ smaller than 1/4 this effect was negligible. The condition $\Delta x/L < 1/4$ was thus adopted as a general criterion besides the criterion for 'optimal' diffusion evaluated in the succeeding sections.

6.4.3 The α-diffusive models (α; 0.5)

In the α-diffusive models β=0.5 which reduces the diffusive term in equation (6.3.5) to

$$D_n = (2\alpha-1)\cdot\frac{\Delta x}{2} \qquad \ldots (6.4.1)$$

where $0<\alpha<0.5$. The equation shows that the space step is an important factor in discussing the performance of α-diffusive models. Δx was therefore chosen as diffusive

parameter for this class of models.

In testing various values of α and Δx it was found that provided

$0 < \alpha < 0.5$ (general condition for α-diffusive models)

$\Delta x/L < 1/4$ (general condition for all weighted box models)

$(2\alpha-1)\cdot\Delta x$ = constant

almost identical resulting hydrographs were obtained for any combination of α and Δx. All α-diffusive models may thus be transferred to the diffusive box model (0;0.5) by increasing the space step (see table 6.3.1). Discussions of the properties of the α-diffusive models will, therefore, here be entirely based on the diffusive box model.

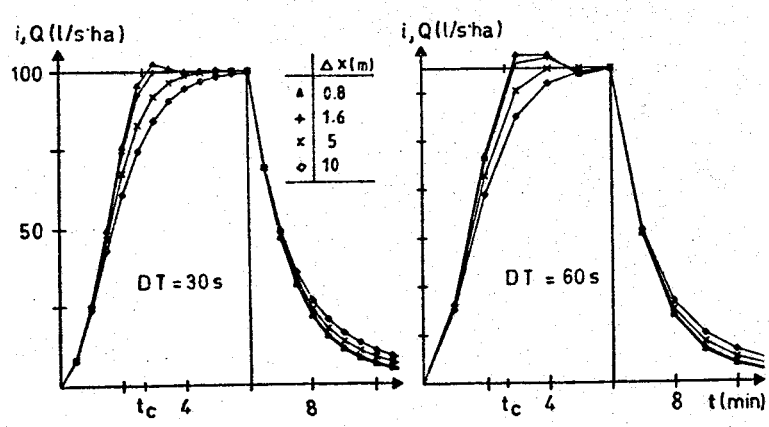

Figure 6.4.3 a,b Hydrographs simulated by the diffusive box model (L_s=20 m, S_s=.035, n=0.016 K_o=230).

In figure 6.4.3 an example from the test series is shown. The hydrographs are simulated by the diffusive box model using different values of Δx. The storm input is the first part of the standard hyetograph (figure

6.4.2). In figure a the time step Δt = 30s has been used and in b Δt=60 s. The hydrographs can be compared with the dimensionless kinematic wave solution and the dynamic wave solution at K_o=100 given in figure 6.3.5 (t_c in figure 6.4.3 corresponds to t^*=1).

From the figure some observations may be pointed out:

- For Δt=30 s an optimal value of Δx according to section 6.4.2 will be about 1.5 m. The corresponding value at Δt=60 s is about 4 m.

- The influence of the space step on the attenuation is very marked. When Δx is increased compared to the optimal value the attenuation grows and rapidly becomes too great. When Δx is decreased below the optimal value the hydrographs obtain shots despite the model having a positive diffusion (D_n < 0 according to equation (6.4.1)).

- The time step has a great influence on the attenuation and therefore influences the selection of the optimal space step. At Δt=60 s shots are obtained at space steps which were considered optimal for Δt=30 s.

The diffusive term (equation 6.4.1) includes neither the time step nor the wave velocity. The influence of these parameters on the attenuation must thus be explained by effects of the third order Taylor terms in Δt. From the expression of these terms given by Smith (1980) it is evident that they are always giving negative contributions to the diffusion (D_n > 0). This agrees, as shown above, with test observations. The diffusive term D_n as given in equation (6.4.1) can therefore not generally be used to estimate optimal step lengths.

The wave velocity c_k may be written for flows with only a lateral source,

$$c_k = k \cdot (q \cdot L)^{c_1} \cdot S_o^{c_2} \qquad \ldots (6.4.2)$$

where q=lateral inflow intensity (= i in surface flow), L=flow length, S_o=slope in flow direction, k, c_1 and c_2 are constants depending on roughness and flow section, see section 4.2.

In the tests it was found that the optimal value of Δx varied with the lateral inflow (rain intensity in surface flow) and the slope in accordance with equation (6.4.2). No variation with respect to L was observed. A modified expression $C_R^{\Delta x}$ for the Courant number was therefore tested

$$C_R^{\Delta x} = \frac{\Delta t}{\Delta x} \cdot c_k^{\Delta x} \qquad \ldots (6.4.3)$$

where $c_k^{\Delta x}$ is the wave velocity defined by equation (6.4.2) using L=Δx. Inserting the optimal step length and corresponding values of Δt and $c_k^{\Delta x}$ for all test runs gave a Courant number that was only slightly dependent on Δt;

$$C_R^{\Delta x} = 1.64 \quad \text{using } \Delta t = 30 \text{ s}$$

$$C_R^{\Delta x} = 1.76 \quad \text{using } \Delta t = 60 \text{ s}$$

The relations can be used to estimate an optimal step length which gives a suitable attenuation of hydrographs simulated by the diffusive box model. The optimal space step Δx_{opt} may be changed (preferably increased to a convenient value) with maintained attenuation if the α-diffusive model is used. Based on the relation $(2\alpha-1)\Delta x$ = constant (see previous page), the corresponding α-value α_{eq} can be determined by

$$\frac{(2\alpha_{eq} - 1) \cdot \Delta x_{eq}}{(2\alpha_{opt} - 1) \cdot \Delta x_{opt}} = 1 \qquad \ldots (6.4.4)$$

where α_{opt}=0 (diffusive box model) and Δx_{eq} is the changed space step to be used together with α_{eq}.

The general discretization condition must still be satisfied: $\Delta x < L/4$. Transferring to alternative α-diffusive models is of interest for two reasons; to reduce calculation cost and to obtain a space step which is a multiple of the actual flow length.

6.4.4 The β-diffusive models (0.5; β)

In the β-diffusive models α=0.5, which reduces the diffusive term (in equation (6.3.5)) to

$$D_n = (1-2\beta)\cdot\frac{\Delta t}{2}\cdot c_k \qquad \ldots (6.4.5)$$

where $0.5<\beta<1.0$. The equation indicates that the time step is an important factor in simulations using β-diffusive models. Since it is rather inconvenient to vary the time step, β was selected as diffusive parameter in this class of model.

In the tests it was shown that the performance of β-diffusive models is practically independent of the choice of step length ($\Delta x/L<1/4$ must still be satisfied). This is in accordance with equation (6.3.5) and indicates that the third order terms in Δx are not significant, unlike the third order terms in Δt (see α-diffusive models above).

Table 6.4.2 Optimal β-values ($\Delta x/L < 1/4$)

Δt	L	β
30	>15	.61
30	10	.66
30	5	.71
60	>15	.72
60	10	.77
60	5	.82

Optimal β-values obtained from the numerical experiments were found to be functions of the time step and flow length. In table 6.4.2 the relation between these parameters are shown.

In figure 6.4.4, hydrographs from α- and β-diffusive models using diffusive parameters according to equation 6.4.3 and table 6.4.2 are compared. The example demonstrates how the discretization Δx/L can be reduced from 1/13 to 1/4 if the β-diffusive model is used instead of the conventional diffusive box model. A similar reduction may also be obtained by using the α-diffusive model if the α-value is increased according to equation (6.4.4).

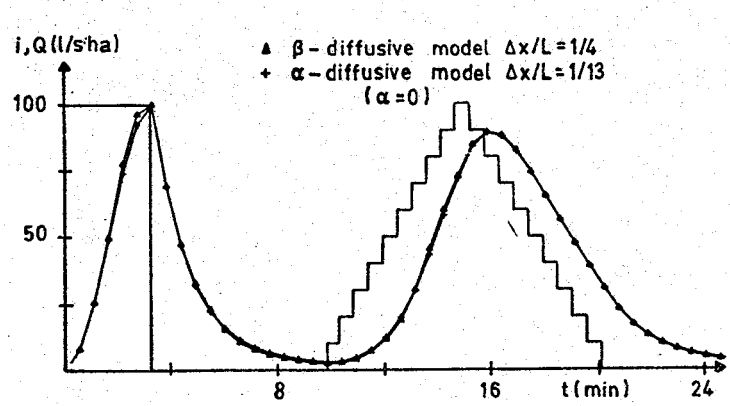

Figure 6.4.4 Comparison between α- and β-diffusive models (L_s= 20 m, S_s = 0.035, n= 0.016)

It is obviously easy to select the diffusive parameter β, as it is mainly a function of a geometric parameter. When optimal β-values are used, the β-diffusive model shows a rather impressive ability to generate suitably attenuated hydrographs, independent of the actual flow case. Compared to the α-diffusive model, which has a diffusive parameter more sensitive to changes in flow

conditions, the β-diffusive model appears to be more appropriate in the sense of both accuracy and practical application.

6.4.5 The αβ-diffusive models (α;β)

In the αβ-diffusive models the diffusion is governed by both the time and space dependent terms (equation 6.3.5). There are two types of αβ-diffusive model, each of them interesting but for different reasons.

When $\alpha<0.5$ and $\beta>0.5$, the diffusion gets a positive contribution from both the time and space dependent terms. This seems advantageous from a general point of view as the sensitivity to changes in both the flow conditions and the time step is less than the corresponding characteristic for the α-diffusive and β-diffusive models respectively. However, the sensitivity to changes in time step is not very important (usually kept constant) and the β-diffusive models appear in comparison to have the actual advantage. The αβ-diffusive model was therefore only tested in a preliminary way, see table 6.4.1. The model (0.4; 0.6) performed very well. It may be noted here that the SWMM-model in the sewer routing algorithm uses (0.45; 0.55), Price (1980b).

When $\beta<0.5$ the diffusion will be decreased by the time dependent term. This gives the opportunity to retain an appropriate diffusion when large values of Δx are used. This is of interest in the case of reservoir models where $\Delta x/L=1$. The model (0;0.25) was found to perform very well in tests at large values of Δx and appears, therefore, to be an appropriate base for a reservoir model (c.f. section 7.2.3). It becomes, however, "unstable" at small values of Δx and is therefore not suitable as solution method for the kinematic wave equations. In figure 6.3.3 such an "unstable" solution is shown (negative diffusion solution).

6.5 The Lax-Wendroff scheme

Consider a Taylor series expansion of the cross-sectional area at (j, m+1)

$$A_j^{m+1} = A_j^m + \left[\frac{\partial A}{\partial t}\Delta t + \frac{\partial^2 A}{\partial t^2}\cdot\frac{\Delta t^2}{2} + 0(\Delta t)^3\right]_j^m \quad \ldots (6.5.1)$$

Comparing with equation (6.3.6) we can see that the diffusive box scheme corresponds to neglecting second- and higher order derivatives. In this section an example of a scneme which takes also the second order derivative into account is discussed.

The continuity equation can be expressed ($Q=a\cdot A^b$)

$$\frac{\partial A}{\partial t} = -(\frac{\partial}{\partial x}\ (a\cdot A^b) - q) \quad \ldots (6.5.2)$$

which leads to, see Rovey et al. (1977)

$$\frac{\partial^2 A}{\partial t^2} = -\left[\frac{\partial}{\partial x}\left[a\cdot b\cdot A^{b-1}(\frac{\partial}{\partial x}(a(A^b)-q)\right] - \frac{\partial q}{\partial t}\right] \quad \ldots (6.5.3)$$

where $a= K\sqrt{S_o}$ and b are constants in the friction relation, equation (4.2.4). Inserting equations (6.5.2) and (6.5.3) in equation (6.5.1) will give an expression which only contains second order derivatives in Δx and which provides the basis for the so called Lax-Wendroff scheme.

In the differentiation of the equation (6.5.1) the "two step" algorithm shown in figure (6.2.2) can be used. An explicit scheme of second order accuracy is then obtained. This algorithm has been tested in surface and gutter flow by Rowey et al. (1977). Using a "two step" scheme requires special connecting equations at the boundaries x=0 and x=L. Such equations based on the characteristic equations are presented by Rowey.

The scheme is explicit and the solution may become unstable. The Courant condition can be used as a stability criterion according to Kibler and Woolhiser (1970).

Applied to the kinematic wave approximation the condition becomes

$$\frac{\Delta t}{\Delta x} < \frac{1}{c_k} \qquad \ldots (6.5.4)$$

Using equation (4.2.5), Manning's formula and $Q=i \cdot L$ we have

$$\frac{\Delta t}{\Delta x} < \frac{3 \cdot n^{0.6}}{5 \cdot (i \cdot L)^{0.4} \cdot S^{0.3}} \qquad \ldots (6.5.5)$$

Inserting $n = 0.016$ and limits of i and L according to chapter 2, $\Delta t/\Delta x$ lies in the interval 2-35. According to this criterion Δt should, in surface flow, usually be chosen below 20 seconds. There are obviously two main drawbacks using the Lax-Wendroff scheme for surface and gutter flow; the algorithm is more complex and small time steps must be used to obtain stability.

6.6 Classification of routing methods

The kinematic wave equations are the most used basic equations in models intended for the routing of water through sewers and channels. The numerical solution requires only "one step schemes" which can be related to the weighted box scheme (c.f. section 6.2). Smith (1980) analysed several well-known methods and found that they could all be regarded as weighted box solutions with different values of the parameters α and β. Below, values of α and β corresponding to different methods are given.

Models marked by SP refer to analyses by Smith (1980) or Price (1980b).

It should be noted that many algorithms in the table are basically intended for, and mainly tested in sewer and channel flows.

Model/reference	α	β	comments
Reservoir routing (SP)	0	0.5	diff.box
Muskingum-Cunge (SP)	weighting factor	0.5	
Brakensieks models (SP)	0.5	0,0.5,1.0	
SSARR (SP)	0	0.5	diff.box
SWMM (SP)	0.45	0.55	
HYMO (SP)	0.5	0.5	
RRL method (SP)	0	0.5	diff.box
Li et al. (SP)	0	1	
MIT method (SP)	0	0,	$\theta<1$
	1	1	$\theta>1$

where

$$\theta = a \cdot b \cdot \frac{\Delta t}{\Delta x} \cdot (A_{j+1}^{n} + A_{j}^{n+1})^{b-1}$$

and

$$Q = a \cdot A^{b}$$

NIVA (Lindholm 1975))	0	0.5	diff. box
ILLUDAS (Sjöberg (1979))	0	0.5	diff. box
URSULA (Jacobsen (1980))	0,0.5	0.5	mixed

6.7 Numerical solution of the diffusive wave equation - a comparison

6.7.1 The basic diffusive wave equation

In previous sections we have seen that diffusion is hardly avoided by using numerical solutions of the kinematic wave. The question arises, could the basic diffusive wave equation be used directly. However, a differentiation of these equations includes linearization and the resulting algorithm becomes a bit more complex. A diffusive wave model (DAGVL-DIFF) has been developed by Sjöberg (1981). The model is mainly intended for sewer routing but is also capable of simulating surface flow and gutter flow.

DAGVL-DIFF has been applied to the test surface and storm event which were used in the previous section. The simulated hydrographs were found to agree well with those obtained from the diffusive box model. Some simulations at very low slopes (S_o = 0.001- 0.01) were also executed and found to correspond well with the kinematic wave simulations. An example of a simulated hydrograph is shown in figure 6.7.1.

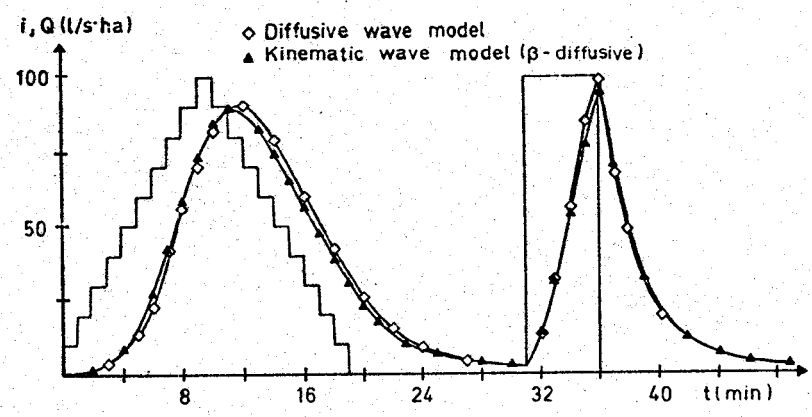

Figure 6.7.1 Comparison between the diffusive wave and weighted box solution (L_s=20 m, S_s=0.018, n=0.016)

The close agreement between the solutions indicates that the kinematic wave solutions have a sufficient precision in overland flow application. This agrees with the conclusions from theoretical considerations made in chapter 4.

6.7.2 The convective-diffusion equation

The convective-diffusion equation discussed in section 4.3.1 is a slightly simplified version of the diffusive wave equation. It has one dependent variable Q and needs a downstream boundary condition.

If the wave velocity c_k is assumed to vary slowly with respect to x the diffusive term may be written

$$\frac{\partial^2 Q}{\partial x^2} \approx - \frac{1}{c_k} \cdot \frac{\partial^2 Q}{\partial t \partial x} \qquad \ldots (6.7.1)$$

giving a modified convective-diffusive equation (see section 4.3.1)

$$\frac{\partial Q}{\partial t} + \frac{\partial Q}{\partial x} = - \frac{D}{c_k} \cdot \frac{\partial^2 Q}{\partial t \partial x} + c_k \cdot q \qquad \ldots (6.7.2)$$

With this manipulation the downstream boundary condition can be rejected and the diffusive box scheme may be used, Price (1980b). With constant values of c_k and D the equation is, according to Price, identical to the basic equation used in the fixed parameter Muskingum-Cunge method.

The equation (6.7.2) was first presented by Price (1980a,c) who also showed a suitable solution algorithm. However, according to Price, this algorithm is comparatively time consuming and the use of the equation before the basic diffusion equation is questionable in both overland and sewer routing.

6.8 Summary

This chapter has mainly focused on numerical solutions of the kinematic wave equations. These equations may be solved by a one step scheme. A very general outline of a one step scheme is given in the weighted box scheme which is defined by the numerical parameters α, β, Δt and Δx. The weighted box scheme includes most numerical solution methods for the kinematic wave equation and is therefore a suitable base for classification of and comparisons between different solution methods.

The solution algorithm gives rise to a numerical diffusion which is governed by the chosen numerical parameters. The numerical diffusion affects the solution mainly by attenuating the simulated hydrograph. Based on the way the diffusion is generated the weighted box models have been classified in three groups; the α-, β- and αβ-diffusive models. Each class is characterized by a diffusive parameter which is chosen to give a suitable diffusion.

Using an 'optimal' value of the diffusive parameter a solution is obtained which is close to the exact solution of the kinematic wave equations. In fact it is often even closer to the solution obtained by the complete shallow water equations. In practical application it is advantageous if the optimal diffusive parameter is easily estimated and does not have to be changed between different storm or design events.

In order to obtain an insight into the properties of the three classes of model, especially the variation of the optimal diffusive term, a series of numerical experiments was performed. It was found that the diffusive parameter β in the β-diffusive model was significantly dependent only on the time step and flow length. From the experiments a table relating β, Δt and L was put together from which the optimal β-value is directly obtained (table 6.4.2). As the time step is usually not varied in practical applications the diffusive parameter can be chosen once and for all for each overland flow element. The β-diffusive model was thus considered to be the most accurate and, in addition, the most easily used model. It has therefore been used as overland flow model in the simulations discussed in chapters 8 and 9.

It should be noted that the drawbacks of the α- and αβ-diffusive models which make the β-diffusive model advantageous have not been absolutely quantified. These models may, then, in many cases be sufficiently accurate

though the β-diffusive is easier to adapt and more accurate.

The most commonly used solution method for the kinematic wave equations is the so called diffusive box model. It is principally an α-diffusive model and uses impractically small space steps compared to the β-diffusive model. In the experiments it was found that these could be increased substantially by increasing the α-value.

Independent of which model and diffusive parameter was used, it was found that a minimum condition of discretization, $\Delta x/L < 1/4$ has to be satisfied in order to preserve a proper general shape of the simulated hydrograph.

7. RESERVOIR AND CASCADE MODELS

7.1 General

In the preceding chapter various numerical solution methods based on the kinematic wave equations were discussed. They all (except for $\Delta x/L=1$) work with a celerity that varies in both time and space. In this chapter, simplified solution methods based on the kinematic wave equations but with restrictions on the wave velocity are discussed. Models of this category are not classified as kinematic though the relationship is evident and the solutions sometimes show good agreement with the kinematic solutions.

A further simplification of the kinematic solution is obtained in one of two different ways; the celerity is assumed constant, either in time or in space. In the first case the nonlinear reservoir model is obtained and in the second a cascade of reservoir models. One example of the latter is the well known Time-Area Method. Both models appear, from a theoretical point of view, quite coarse. The "sophisticated" solution methods given in Chapter 6 imply sheet flow on a rectangular surface. This is usually a very coarse approximation of the real runoff. In the light of this fact a simplified solution compared to the kinematic might be appropriate in practical applications.

Assuming the celerity invariant in both time and space is the ultimate simplification of the kinematic wave solution. As a routing method this approximation is denoted the Time of entry. It is also the assumption underlying the Rational Method which is discussed in chapter 10.

The simplified models above represent well known and traditional solution methods in urban hydrological analysis. During recent years these have been subject to several studies giving new aspects of application and selection of input data, see for instance Kidd et al.

(1978), Falk et al. (1979), Lyngfelt (1981). In addition the Time-Area Method is included as overland flow model in the NIVANET and ILLUDAS models, two of our commercially most used urban runoff models, Lindholm (1975), Sjöberg (1979). It is then of interest to discuss these methods both from a more theoretical point of view which is done in this chapter and with practical simulation as a base (chapter 8).

7.2 Reservoir models

7.2.1 Linear-nonlinear reservoir models

The traditional reservoir model is based on the continuity equation and a relation between the reservoir volume and the outflow. The equations may be written

$$L \cdot \frac{\Delta A}{\Delta t} = Q_{in} - Q_{out} \qquad \text{... (7.2.1a)}$$

$$L \cdot A = c_1 \cdot (Q_{out})^{c_2} \qquad \text{... (7.2.1b)}$$

where Q_{in} and Q_{out} are inflow and outflow respectively, $L \cdot A$ is the reservoir volume and c_1 and c_2 are constants. This model is identical to the diffusive box ($\alpha=0$; $\beta=0.5$) solution of the kinematic wave equations if $\Delta x/L = 1$ is used. The reservoir model may be interpreted physically as assuming uniform flow (constant velocity) along the "reservoir length" during a time step.

The linear reservoir model ($c_2=1$) corresponds to the assumption of constant velocity in both time and space. This model will be discussed together with the Time-Area and Rational Methods.

The non-linear reservoir equations must basically be solved by an iterative technique in the same way as the diffusive box scheme (see section 6.2). Because of this little is gained in simplification of the numerical model and reducing calculation cost when the reservoir model is

used instead of a distributed model. It is then desirable to use a numerical scheme with an explicit form in connection to the nonlinear reservoir modelling. This can be done in two ways; by manipulation of either the friction relation or the box scheme parameters. The first method has been proposed by Lyngfelt (1979). An example of the second way is the so called Time-lag model which is discussed below.

The non-linear reservoir is a very common overland flow model in urban runoff simulations. It is, for instance used in the SWMM-, CTH- and MAGRÖR-models, see Huber (1977), Arnell (1980), Bengtsson (1980). It can also be used in the NIVA model, Lindholm (1975) and in the Wallingford procedure, National Water Council (1981).

7.2.2 The Time-lag model

The Time-lag model is derived from the nonlinear reservoir equations by the introduction of a time lag in the "friction" relation

$$L \cdot A_{t-\tau} = c_1 \cdot (Q_{out})^{c_2} \qquad (7.2.2)$$

By making this change, a very simple explicit solution of the nonlinear reservoir equations is obtained. The model was developed and introduced by Falk and Niemczynowicz (1979) who use a time step and time lag of one minute.

It can be shown that the Time-lag model as solution method is identical to the implicit algorithm $\alpha=0$, $\beta=0.25$ provided $\Delta x/L=1$ and $\Delta t/\tau=2$. Because of this similarity it should be possible to analyse the Time-lag model in terms of stability and diffusivity in the same way as other box scheme algorithms.

By numerical experiments it was shown that the model could be stressed to an unstable behaviour with "shots" at the recession part of the hydrograph (see figure

6.3.3). This occurs, however, only on occasions when heavy storms, steep slopes and short flow lengths are combined. Only a few tests were performed, but those indicated that the stability criterion $D_n < 0$ (see section 6.3.2) combined with the Manning formula might be used for the model. The stability of the model may according to this criterion be increased by using the time step 30 s. This will, however, also affect the numerical attenuation.

According to chapter 6 the numerical scheme which is the base of the Time-lag model has advantages with respect to the attenuation for large Δx. The Time-lag model is therefore, in addition to its practical aspects, theoretically well suited as a reservoir model. Falk and Niemczynowicz have, by an extensive measuring program, established empirical relations for the parameters in the Time-lag model for paved surfaces $< 700\ m^2$.

7.3 Cascade of linear reservoir models

7.3.1 Basic equations

In section 4.2.3 the linear friction relation (b=1) was discussed. It was found that using this relation is identical to assuming the kinematic wave velocity invariant in time and space. This is also evident looking at equation (4.2.6).

Consider the friction relation in the general form (compare equation (4.2.4))

$$Q = a(A)^b \qquad \ldots (7.3.1)$$

In the linear case the constant a appears to be the kinematic wave velocity. Applied to surface flow a very simple form of the solution is obtained according to equation (4.2.14)

$$Q(L,t) = \int_{t_o}^{t} a \cdot B \cdot i(\tau) d\tau \qquad \ldots (7.3.2)$$

with the conditions $Q(0,t)=0$ and $t_o=0$ if $t<t_c$ and where B is the width of the surface. The solution implies integration along the characteristic between t_o and t (see figure 4.2.3). If the velocity and width are assumed to be functions of the space coordinate x only we obtain

$$Q(L,t) = \int_{t_o}^{t} a(x) \cdot B(x) \cdot i(\tau) d\tau \qquad \ldots (7.3.3)$$

which implies a time invariant value of the velocity $a(x)=dx/dt$ to be specified at each point of the surface. This corresponds to characteristics having a constant shape independent of the starting point t_o, which in turn means that the integration time is constant, $t-t_o=t_c$.

Consequently, it is possible to define a time for the wave movement between any point on the surface and the downstream end, x=L. This 'relative time' is here denoted $(t-\tau)$ with $\tau=t-t_c$ for x=0 and $\tau=t$ for x=L. An arbritary surface element dA_c, for example, at $x=x_1$ may then be specified by its 'relative time' $(t-\tau_1)$ as well as its coordinate; $dA_c(x_1)=dA_c(t-\tau_1)$. If the element is approximated by a rectangle with width B(x) perpendicular to the flow direction we have

$$dA_c(t-\tau) = dx \cdot B(x) \qquad \ldots (7.3.4)$$

Equation 7.3.3 may then be written

$$Q(L,t) = \int_{t-t_c}^{t} \frac{dA_c(t-\tau)}{d\tau} \cdot i(\tau) d(\tau) \qquad \ldots (7.3.5)$$

which is a continuous expression of the so called Time-Area Method. The method is obviously analogous with the kinematic wave approach on a surface whose width may

vary in the flow direction and a wave velocity which is only a function of the distance from the downstream end, see also Newton-Painter (1974) and Lyngfelt (1981).

In order to solve equation (7.3.5), the storm intensity variation $i(t)$ and the relation $dA_c(\tau)/d\tau$, $0<\tau<t_c$, must be known. In the Time-Area Method the latter is given by the time of concentration t_c and the time-area diagram. The time-area diagram is a dimensionless relation between the cumulated area (contributing area) A_p/A_c and the time t/t_c where $A_p=A_c$ when $t=t_c$. Usually the time-area diagram is discretized in 10 segments, each one representing a part of the surface and a wave velocity. Applying the equation (7.3.5) to a catchment should then be interpreted as using a series or cascade of linear reservoirs.

The evaluation of the two 'parameters' - time of concentration and time-area diagram determines the performance of the model and will be discussed in section 7.3.2-7.3.3.

The Nash cascade model is a model based on a cascade of linear reservoirs, Sing (1977).

7.3.2 The time of concentration, t_c, in the Time-Area Method

The time of concentration was defined in section 4.2 by

$$t_c = \int_0^L \frac{1}{c_k}\,dx \qquad \ldots (7.3.7)$$

where c_k is the kinematic wave velocity. Using this definition, a constant rain intensity i and the Manning formula we obtain for surface flow

$$[t_c]_s = \frac{(n\cdot L_s)^{3/5}}{i^{2/5}\cdot S_o^{3/10}} \qquad \ldots (7.3.8)$$

and for gutter flow (V-shaped)

$$\left[t_c\right]_g = \frac{n^{3/4} \cdot (2\sqrt{1/z+z})^{1/2} \cdot L_g^{3/4}}{S_o^{3/8} \cdot (i \cdot L_s)^{1/4}} \qquad \ldots (7.3.9)$$

where L_s and L_g are flow lengths of the surface and the gutter respectively and z the slope factor of side walls.

A sewer line having many inlets along the reach may be regarded as being lateraly fed by water. It is, however, not possible to evaluate a relation corresponding the equations above for sewers because of the analytically complicated relation between flow and water depth. The relation for gutterflow (7.3.9) may, however, be used as an approximation for the sewer line if a greater value of z is used. A more suitable expression of the equation for this case is

$$\left[t_c\right]_g = \frac{n^{3/4} \cdot (2\sqrt{1/z+z})^{1/2} \cdot L_g}{(i \cdot A_c)^{1/4} \cdot S_o^{3/8}} \qquad \ldots (7.3.10)$$

where A_c is the contributing runoff area.

Equivalent or similar relations also based on the kinematic wave concept, have been presented by several investigators such as Morgali (1970), Singh (1975), Lyngfelt (1981) and Akan (1984).

When the Time-Area Method is used for simulation of runoff from a storm event with constant rain intensity, the corresponding time of concentration is easily evaluated by the relations given above. It should, however, be noted that even for this simple storm event the approach is not entirely relevant as the recession part will have a considerably lower wave velocity. It can be shown using the kinematic wave equations that the flow at the time t_c after cease of rainfall is 17% of the maximum flow (provided the duration of rainfall is greater than t_c).

Using the Time-Area Method for a storm with varying rain intensity, a representative intensity value must be selected before the time of concentration can be calculated. A suitable intensity value should be one giving a properly delayed main flow peak. Such an intensity can be expected to have values near the average intensity over a time equal to t_c during the most intense part of the storm. For a t_c evaluated in this way, the Time-Area Method would produce inaccurate flow values from less intense parts of the storm.

The kinematic wave concept is theoretically the most sound basis for evaluation of the time of concentration used in the Time-Area Method. However, the relations have to be tested by comparative simulations between the Time-Area Method and the kinematic wave model. Such simulations (discussed in the next chapter) should also give an idea of the general performance of the Time-Area Method.

7.3.3 The time-area diagram in the Time-Area Method

In the Time-Area Method the 'flow velocities' are assumed to be constant in time but to vary along the flow direction. The time area diagram reflects the relative velocities. Each diagram will then represent only one specific flow case giving a characteristic shape of the simulated hydrographs.

Consider the two hypothetical time-area curves in the figure 7.3.1.

The convex curve (b) will, if applied to a storm with constant rain intensity result in a basically correct shape of the recession of simulated runoff hydrograph. The rising part obtains, however, an incorrect shape, see figure 7.3.2.

A better resemblance to the rising part is obtained with the S-curve (a) given in figure 7.3.1. This diagram will

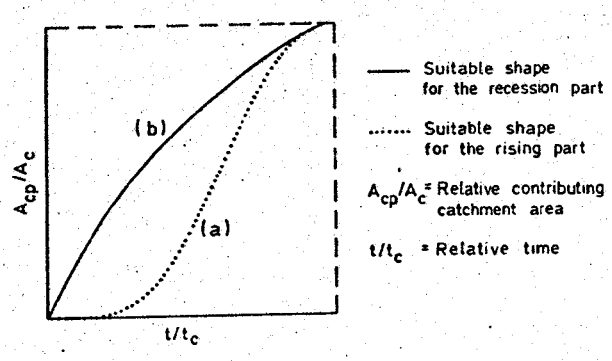

Figure 7.3.1 Hypothetical time-area diagrams

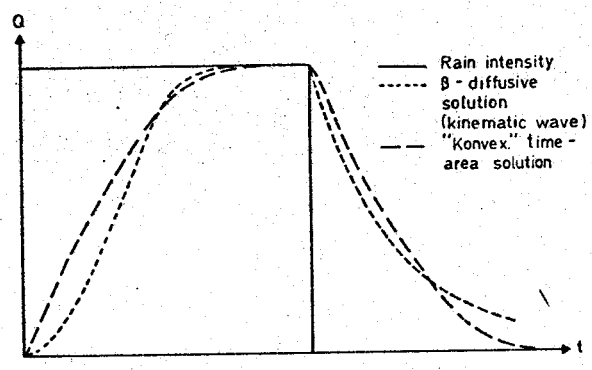

Figure 7.3.2 Principal shapes of runoff hydrographs obtained by the Time-Area Method (curve b) and the β-diffusive model (kinematic wave)

not, however, give a suitable shape of the recession which is shown in figure 7.3.3.

The rising and recession can be regarded as two extreme cases of flow state and corresponding time-area curves have, as a consequence, extreme shapes. Simulating runoff from a storm with continuously changing rain intensity a

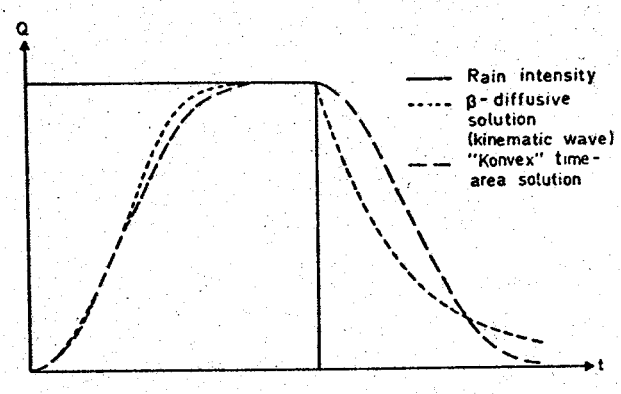

Figure 7.3.3 Principal shapes of runoff hydrographs obtained by the time area method (curve (a)) and the β-diffusive model (kinematic wave)

time-area curve which is a mean of the two extremes appears most appropriate.

A time-area curve giving the 'best fit' for the rising part in surface flow simulation was developed by comparative simulations with a numerical kinematic wave model and the Time-Area Method. Corresponding 'best fit' curve for the recession part may be obtained analytically from the kinematic wave theory. In figure 7.3.4 these curves are given together with the "mean" curve, which has been slightly modified in order to fulfill the requirement of full areal contribution at $t=t_c$.

The 'mean' curve will obviously be very near the linear time-area diagram (deviation < 5%). In runoff simulations from a single surface there is evidently no theoretical reason to use a non-linear time-area diagram.

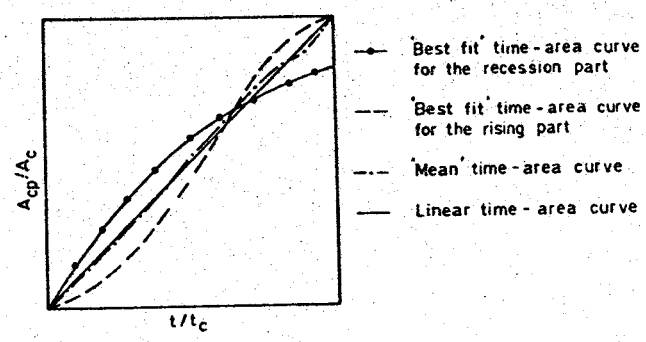

Figure 7.3.4 Time-area curves giving the 'best fit' of the rising- and recession parts of the runoff in surface flow

Time-area curves may also be developed for a catchment with one surface feeding a gutter. In this case the time area curve will be influenced by the relation between the time of concentration for the surface $[t_c]_s$ and that of the gutter $[t_c]_g$. If $[t_c]_s$ is great compared to $[t_c]_g$ or $[t_c]_g$ great compared to $[t_c]_s$, the time-area curve for the rising part will be very similar to that for surface flow. For a given catchment area A_c it can be shown that $[t_c]$ has a minimum for a certain surface length. It was found that the time-area curve for this case gave the greatest deviation from the linear one, see figure 7.3.5.

The corresponding time-area curve for the recession part was obtained by numerical simulations. It is shown in figure 7.3.5 together with the 'mean' curve between the rising- and recession curves. This mean curve evidently diverges more from the linear than the corresponding one for surface flow. The 'surface-gutter' curve is believed to apply to the ordinary 'surface-gutter' catchment while the surface runoff curve (figure 7.3.5) applies to cases where the relation $[t_c]_s/[t_c]_g$ is extensively greater or smaller than unity.

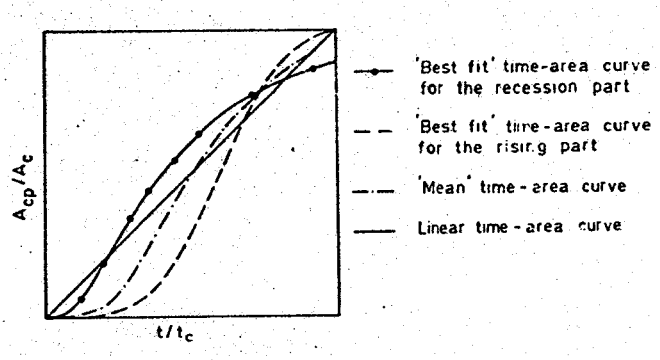

Figure 7.3.5 Time-area curves giving the 'best fit' of the rising- and recession parts of the runoff from the surface-gutter catchment at $t_c = [t_c]_s + [t_c]_g$ min

For catchments containing sewers the corresponding time area curve will principally be a function of the structure of the system. In figure 7.3.6 time area curves made

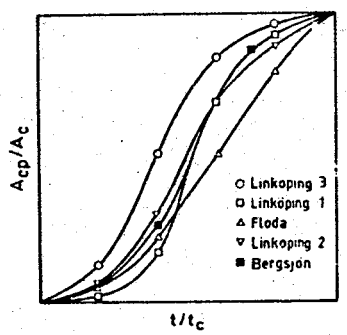

Figure 7.3.6 Time area diagrams obtained by numerical simulation of the rising part of constant rain intensity storms for four residential areas, after Lyngfelt (1981)

up from five great urban catchments are shown, Lyngfelt (1981). The diagrams have been obtained by numerical simulation (kinematic wave model) of the rising part of constant rain intensity storms.

The areas have very different flow characteristics and the curves consequently diverge a lot though the S-shape is general. No definite conclusions of the relation between the time area curves and the characteristics of the catchment can be made from the figure. The relevance of the curves for the recession part has not been studied. The recession part time-area curves can, however, be expected to have a basic shape according to that given in figure 7.3.5.

7.4 Summary

In this chapter reservoir models and models based on a cascade of linear reservoirs have been discussed. These models have a clear relationship with the kinematic wave concept but use a simplified representation of the wave velicity. The non-linear reservoir model and the Time-Area Method are the most commonly used overland flow models in commercially available urban runoff models.

The Time-lag model is a non-linear reservoir model developed by Falk, Niemczynovicz (1979). The model has been successfully tested on small urban paved surfaces. It has a simple numerical algorithm and can be used for manual calculations. As the model parameters are based on urban runoff measurements from paved surfaces < 700 m^2 the Time-lag model has not been tested as base catchment model in this study.

The Time-Area Method can be regarded as a model based on a cascade of linear reservoirs. It is a traditional method which is still much used. The method is governed by two 'parameters', the time of concentration and the time area diagram. One set of these parameters represents in fact

only one specific flow case. Applying the method to a storm with continuously varying rain intensity, the parameters should be chosen to give the best fit at the main runoff peak. The method can therefore be expected to give an unsuitable performance in other parts of the simulated hydrograph.

The class of models discussed in this chapter will simplify the calculation routines ccmpared with the kinematic wave approach. However, problems with parameter estimations arise and the numerical kinematic wave model appears to be more generally applicable in basecatchment modelling. The model tests in the following chapters will thus concentrate on the numerical kinematic wa e model. Simulations by the Time-Area Method will, however, also be performed and discussed.

8. BASE CATCHMENT MODELS

8.1 General considerations

In earlier chapters the analysis was based on surface-gutter-systems with regular geometry and constant slope. This is usually not the case for real urban catchments.

Theoretically it may be possible to use a three dimensional model and an extreme discretization in space and thereby obtain a more accurate physical description of the runoff, Chow et al. (1973), Constantinides et al. (1981). However, such a description requires a very large amount of input data and the work spent on collecting these data is unreasonably large compared with the improvements in the results.

In practice it seems reasonable to limit the description of the surface to a maximum of five or six parameters. This means that, in reality, even for a small uniform surface the physical description of a surface-gutter system becomes very approximate. Despite this several investigators have reported relatively good performance of models based on the two dimensional kinematic wave theory, Langford and Turner (1973), Woolhiser (1975), Rovey et al. (1977), Lyngfelt (1978), Jacobsen (1980).

The storm water from a surface is normally collected in collector sewers with minimum dimensions. These sewers are often long and thus significant in the runoff system. A separate surface connected to a street inlet is very seldom greater than 1000 m^2 and is normally less than 500 m^2. However, suitable sets of input data are obtained only when base units of surfaces (base catchments) greater than say 5000 m^2 are used. Then, in practice, the base catchment flow model must, in one way or another, represent both several separate surfaces with different characteristics and upstream collector sewers. The discretization of input data (size of base catchments)

has been discussed by several investigators; in most cases discussions have been based on the specific properties of the SWMM model, see for instance Proctor and Redfern (1977) and Zaghloul (1981). The use of an aggregated base catchment with a simple geometry and a time of concentration equal to that of the real catchment is a general approach, applicable to many runoff models. This approach will be used below and has earlier been discussed by Jensen (1981), Lyngfelt (1981) and Marsalek (1983).

In this chapter a number of different approaches to base catchment modelling are investigated. The discussion is based on six urban catchments where storm runoff and rain intensity have been recorded. The runoff from storms has been simulated using different models and discretizations of the geometric input data.

The main objective of the simulations is to investigate how the geometrical input describing the base catchment can, and should be, simplified. The work is focused on the numerical kinematic wave model (the β-diffusive model as described in chapter 6) but the Time-Area Method is also tested.

Below, the test catchments, measurements and models are briefly described, before the simulations are presented.

8.2 General characterization of the test catchments and measurements

The rain intensity and the runoff have been recorded in six urban catchments for a number of storm events. The catchments are all different and cover a range of conceivable base catchment characteristics. The catchments have been investigated with respect to geometric parameters such as contributing area, slope and so on.

In order to give a general impression of the catchments, the main characteristics are summarized in table 8.2.1. A more detailed description is given in appendix I.

The catchment ASPH is a part of a street feeding an inlet. It is the only catchment with no sewer system.

The catchment PCON is a parking area and consists of the top floor of a two storey car park and a collector sewer along the building.

The catchment PASP is a parking area with a uniform, small slope and three inlets to the collector system.

Table 8.2.1 Main characteristics of the catchments

Catchment	Area A_c (m^2)	Number of inlets	Slope S_s (m/m)	Number of joints	Length of sewers (m)	Slope S_m (m/m)
ASPH	430	1	.044	-	-	-
PCON	1700	7	.014	0	107	.036
PASP	3900	3	.008	1	110	.010
AASP	9700	8	.010	0	254	.0025
SASP	3000	10	.030	2	355	.007
COMP	3100	20	-	3	530	.022

The catchment AASP is part of an airport surface. It is the biggest test area with large surface flow lengths. The slope of both the surface and the sewer system is small, and consequently the characteristic time of concentration is comparatively long.

The catchment SASP is built up of three streets including pavements and a few additional surfaces (no roofs). The surfaces are connected to a sewer system which principally follows the streets.

The catchment COMP is built up of different typical urban

surfaces; roofs, parking areas, streets and pavements. The surfaces are connected to a sewer system which is longer and has more joints than the other catchments.

In table 8.2.1 the catchments have been arranged according to the complexity of the runoff system. There is obviously no relation between contributing area and this complexity. Most of the surfaces are of the bitumen type but concrete paving (PCON) and roof-felt (COMP) are also represented.

Rain intensity and runoff have been measured with the objective of obtaining a record of several separate storm events for each catchment. The measurements are briefly described together with the catchment characteristics in appendix I.

The rainfall-runoff volumes of the separate storms were plotted for each catchment. A linear regression line was fitted to each data set by the method of least squares. From the regression line the contributing runoff area was calculated as the slope of the line, and the depression storage as the intercept on the rainfall volume axis, Arnell, Lyngfelt (1975), Arnell (1980).

The contributing areas were all found to be equal to or less than the corresponding areas which had been estimated by areal measurements in the field. In five of the areas the difference was less than 10% (and for the two smallest there was no difference). In the SASP catchment a difference of 18% was found.

The obtained depression storages were found to be between 0.4 and 0.5 mm in five of the catchments. This value agrees with expected values regarding actual slope and unevenness of the surfaces, Falk, Niemczynowicz (1979). In the AASP catchment a much lower value, 0.25 mm, was obtained. This may be explained by the extremely even surface and the smooth asphalt in the catchment.

8.3 Models and criteria for comparing runoff hydrographs

All simulations in this report have been performed by the runoff model CURE, Lyngfelt (1985). The model was mainly developed in order to make it possible to compare different numerical and geometric models. In this part of the study the model was used as described below.

The surface depression storage loss is subtracted from the very first part of the rain. The surface and gutter flow is routed by the β-diffusive model (kinematic wave approach) described in chapter 6.4.4. The flow in sewers is routed by the traditional numerical solution of the kinematic wave equation (diffusive box model, section 6.3.2). The capability of the model to make simulations using the Time-Area Method is also used.

In each catchment between 3 and 8 storm events have been used in the simulations. The obtained hydrographs have been used for comparisons with recorded hydrographs and between different model approaches.

The storm water is routed through the catchment without any losses except the surface depression storage (no infiltration, no overflows). The differences in performance between models will thus appear only as differences in shape between the resulting hydrographs. The comparison between the performance of one model relative to another must then be based on these differences.

The discrepancies between two hydrographs can be described by several parameters, for instance, the integral or biased integral square error, the absolute error of peak flow values, or the time lag of peaks. Each of them show, however, only a part of the differences and none of the parameters or set of parameters can replace the survey obtained by simple visual inspection, Geiger (1984).

The discussion of the models has been based on both visual inspection, and a simple statistical analysis of the hydrographs. The statistical parameters used are

the mean and the standard deviation of the ratio between flow peaks, λ_p and σ_p, respectively

the mean absolute error in peak flow values, ε_p.

The parameters have been used in several similar studies, see for instance Arnell (1980).

8.4 Kinematic wave model simulation - comparison with recorded hydrographs

8.4.1 Detailed geometrical description of the catchments

For each of the six catchments a set of input data corresponding to a very detailed geometric representation of the runoff system was built up, the DET model. In principal each surface, gutter and sewer within the systems is represented - a discretization beyond what is usually realistic in urban runoff modelling. Values of lengths, slopes, etc, have been evaluated by field investigations. Surface roughnesses are selected according to chapter 5. For the AASP catchment, which has a very smooth and even surface (appendix I), a lower value was chosen (n=0.012).

In the PCON and SASP catchments, the basins at discharge measuring stations were found to act significantly as retention storages during low intensity storms. A retention storage model was then included in the DET-model.

8.4.2 Comparison between recorded and simulated runoff

The input data set with a high level of discretization

was used together with the kinematic wave model to simulate runoff from the six catchments. The simulated hydrographs thus obtained were compared with the corresponding recorded hydrographs.

The simulations were executed using three different versions of the detailed input data set. In version 1, a contributing area corresponding to field investigations was used. In version 2, the area was obtained by regression analysis of precipitation - runoff volumes as described in section 8.2 (fit of volumes for each catchment). Both versions include depression storages obtained from the regression analysis.

In the PCON and COMP catchments the volume fitted contributing area was found to vary significantly between storms. This causes deviations between the simulated and the recorded runoff volumes which have no connection with the discussion of the performance of the kinematic wave model.

The degree of wetness at the beginning of the individual storm is not known from the measurements. The depression storage model used is, in addition, believed to give a rather coarse description of the initial runoff process for low intensity storms.

Version 3 of the input data sets was based on depression storages, individually chosen for each storm in order to obtain a volume fit for the first part of the hydrograph. In addition, an individually volume fitted contributing area for each storm was used in the PCON and COMP catchments. Hydrographs simulated by this version of input data are plotted in appendix II.1.1 (also in figures 8.4.1 and 8.4.2).

It should be stressed that the only difference between the data sets used is in the choice of depression storage and contributing runoff area. All data describing the

catchment with regard to geometry, surface roughness and joints are all according to the DET model (section 8.4.1).

A visual inspection of the simulated and recorded hydrographs shows that they coincide fairly well with respect to general shape and delay of peaks. The main impression is, then, that the runoff process is reasonably well described by the model. Sometimes a very good performance is obtained, as for example, that shown in figure 8.4.1.

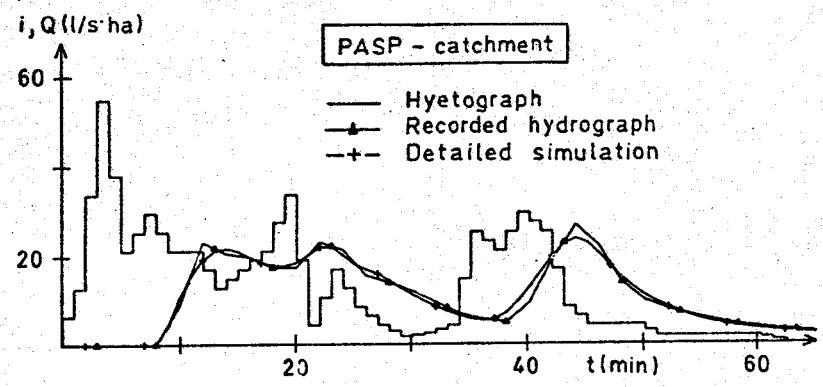

Figure 8.4.1 Recorded and simulated runoff from the PASP catchment (input data version 3)

There are, however, parts of many hydrographs with great discrepancies between simulated and recorded values, see for example figure 8.4.2. With regard to continuity and realistic flow velocities in the runoff system it can be concluded that several of the discrepancies must have causes other than the performance of the model.

A simple statistical analysis of the relation between recorded and simulated flow peaks were performed for comparative purposes. Trends such as, for example, increasing deviations with increasing catchment area or complexity were not observed. In table 8.4.1, the mean ratio λ_p, standard deviation σ_p and absolute error ε_p

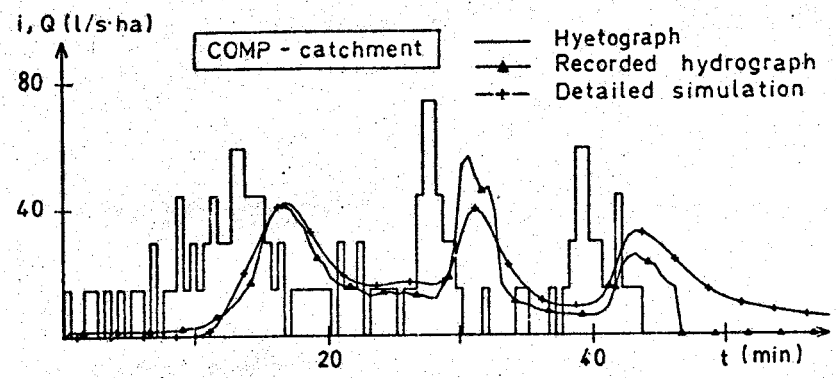

Figure 8.4.2 Recorded and simulated runoff from the COMP-catchment (input data version 3)

defined in section 8.3 are given for the two sets of input data, one using not volume fitted data and the other using volume fitted data for each catchment. The flow peaks shown in appendix II:1.1 were used with the exception of those in three low intensity storms where the performance of the retention storage model was not acceptable (the characteristic retention storage area varied between different storms). Five recorded flow peaks with great deviations from the corresponding simulated hydrographs were also excluded (as recording errors were suspected).

Table 8.4.1 Mean ratio λ_p standard deviation σ_p and absolute error ε_p for not volume fitted data and volume fitted data for each catchment.

Input data	Number of peaks	Mean ratio λ_p	Standard dev. σ_p	Abs.error ε_p %
No volume fit (Version 1)	30	1.08	0.21	15
Volume fit for each catchment (Version 2)	30	1.00	0.15	11

If the five "error peaks" are included in the fitted data set, the standard deviation and absolute error are increased to 0.26 and 18% respectively.

From the table it can be seen that the deviation between recorded and simulated flow peaks is reduced by the use of volume fitted contributing areas. Typical is the general over estimation of flow peaks ($\lambda_p = 1.08$) using not volume fitted data. Although the verison 3 hydrographs give a general impression of better performance than the version 2 hydrographs, corresponding statistical parameters are the same for the two versions.

The differences between recorded and simulated hydrographs shown in appendix II.1.1 and table 8.4.1 may be explained by

- error in measured rain intensity - runoff values
- error in or insufficient description of the runoff system input data
- insufficient accuracy in the model description of the runoff process.

The two first points include sources of errors such as bad representation of the real rain intensities over the catchment, increased/decreased contributing area during parts of the storm event or water leaking into or out of the sewer system.

The errors in rain intensity and runoff values are difficult to evaluate. A general level of the total error in the interval ± (10-20%) can, however, be assumed for both rain intensity and runoff values. These errors have been discussed by Arnell (1980) who used measuring devices similar to those used in this study. He estimates a total error of about ± 15% for rain intensity values and corresponding error for runoff values of ± (10-15%).

In a study of the performance of 12 different models, Colyer (1977) found the 'best' models to have a mean ratio λ_p in the range of 0.95 to 1.05, a standard deviation σ_p of 0.15 - 0.20 and an absolute error ε_p between 10 and 20%. The model used here obviously has a performance at a level similar to Colyer's 'best' models.

As discussed above, there are many sources of "errors" which are not connected with the performance of the model. It is thus probable that a large proportion of the deviations indicated by the table 8.4.1 and those found by Colyer are caused by errors in measurements and insufficient knowledge of the properties of the real catchment. Because of this, defined judgement of the performance of models and also comparisons between models based on recorded runoff appear difficult.

In summary, the discussion in this section illustrates the difficulties in performing representative field measurements and also the difficulties in judging the performance of models. The comparisons indicate, however, that the kinematic wave model, using detailed geometrical input data, describes the runoff process well, provided that proper estimates of the contributing area and the depression storage are used.

It is believed that the influence of the choice of depression storage values and depression storage model is much less marked in the case of design storms than in the analysis above.

8.5 Simulations using simplified geometric input data

8.5.1 General

To use a very detailed description of the catchment in the input data such as the DET model input is usually not

realistic in practical applications of runoff models. The geometric representation of a catchment has to be more generalized to reduce the effort of generating input data. It is characteristic of the kinematic wave model that it can simulate the velocity variations along the runoff system (a spatially distributed model). These variations are partly governed by the geometry (runoff system structure and successive cross-sections of flow). Simulations made with the kinematic wave model using a simplified representation of the runoff system geometry appear to be meaningful only when this geometry is chosen in such a way that the real spatial velocity distribution becomes represented in a reasonably appropriate way.

In the preceding two sections, different simplified geometrical representations of the base catchment are discussed. A number of geometrical models are defined which are characterized by the number of free parameters used such as surface flow length, slope and so on. It is basic for all simplified models that the catchment area and the time of concentration are maintained from the real catchment.

There is no real basis for selecting roughness values individually for each type of impermeable surface. Another parameter which is mostly is difficult to choose individually is the side wall slope of the gutter cross section. These parameters are thus not regarded as free in the geometrical models.

8.5.2 Representation of catchments with no sewer net - the KW3, KW4G and KW6G models

The simplest possible geometrical description of a catchment is given by figure 8.5.1a, where the runoff is modelled by sheet flow over a single surface without change of flow section. The catchment is represented by three parameters - catchment area A_c, surface flow length L_s and slope S_s - and the model is here denoted KW3.

Including a gutter along the surface with the standard section gives an essential improvement to the catchment model while the catchment parameters are only increased by the gutter slope S_g. The model is here denoted the KW4G model, see figure 8.5.1b.

Gutters are often fed by lateral inflow from two sides and manholes sometimes collect water from two gutters. Neither of the geometric models above is suitable in these cases. A representation according to figure 8.5.2 covers these cases including the KW4G model, and will generally be more flexible. However, the number of geometric parameters is increased to six, and the model is called the KW6G model.

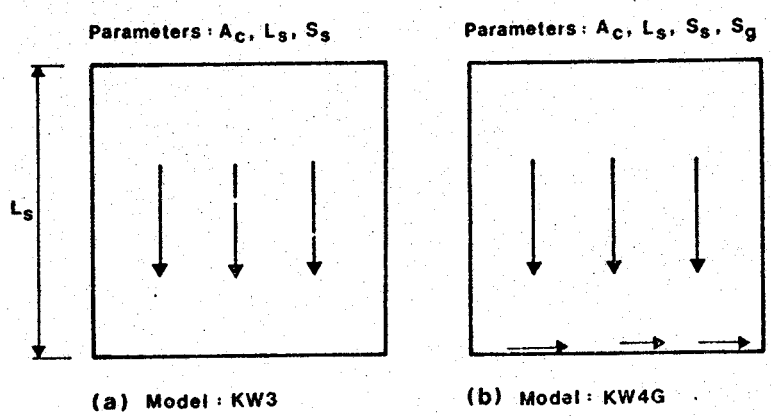

Figure 8.5.1 Representation of base catchments by three and four parameters in the kinematic wave model.

The KW6G model is usually directly adaptable to a given single surface while the KW3 and KW4G models require adjustment of the parameters length, slope and/or roughness to maintain the characteristic time of concentration. For instance, if the gutterflow is replaced by an

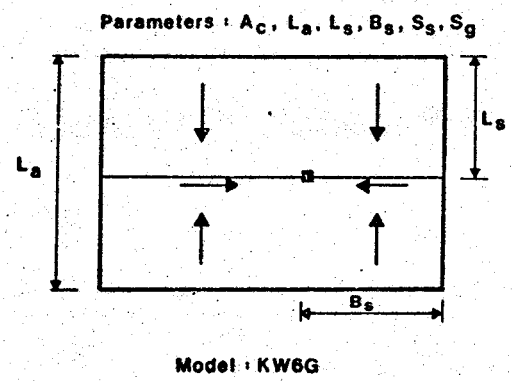

Figure 8.5.2 Representation of a base catchment by six parameters in the kinematic wave model

increased surface flow length, this equivalent length $[L_s]_{eq}$ is (derived from equation 7.3.8 and 7.3.9)

$$[L_s]_{eq} = (L_s^{3/5} + c_1 \cdot L_g^{3/4})^{5/3} \qquad \ldots (8.5.1)$$

where c_1 is a parameter containing rain intensity, roughness, slope and shape factor of gutter flow section. The relation implies maintained surface slope and roughness for the equivalent surface (KW3 surface).

Increasing the surface flow length will result in an increase not only of t_c but also of the water volume stored on the surface. This increase of volume is directly proportional to the time of concentration. Therefore, maintaining t_c by adjusting the length, slope or roughness will have the same effect on water volume stored. The two conditions, maintained time of concentration and maintained stored water volume, may not be satisfied at the same time. Any of the three parameters, or combinations of them, may then be used to satisfy the first condition.

Whether the increased storage volume on the surface corresponds to the 'loss' of volume in the system caused by neglecting the gutter, depends on its shape and slope. A test of a few representative surface-gutter catchments indicated a reasonably maintained storage volume for the equivalent surface.

8.5.3 Representation of catchments with a sewer net - the KW6S, KW6S-S and KW4G-I models

In normal application the base catchment includes several single surfaces and a connecting sewer system. There are, of course, numerous approaches to obtaining a simplified geometrical representation of such a catchment. Below, some geometrical models are described which have been used in the simulations. They include some of the main principles on which a simplified geometric model may be built, for example, lateral inflow along the sewer lines, standard values of surface-gutter system (the KW4G-model) or a standardized network system.

A very simple geometric description of a base catchment containing a sewer is according to the KW4 model with the gutter section replaced by a sewer, figure 8.5.3. The

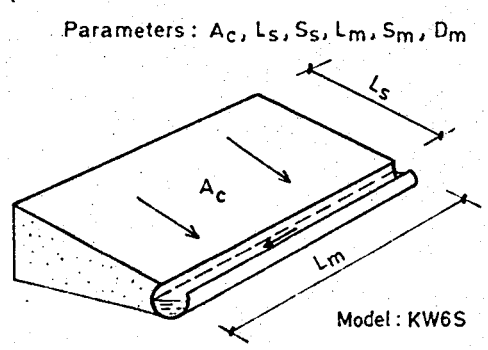

Figure 8.5.3 Representation of the catchment by the KW6S model

sewer represents the main sewer line of the system and is characterized by its length L_m, slope $S_m = \Delta H/L_m$ and diameter D_m. The surface flow in the model represents the surface-gutter and sewer branch flows in the real catchment.

If the surface flow length L_s and slope S_s are regarded as free parameters, they may be evaluated in the same way as for the KW3 model. In this case, the delay caused by flow in sewer branches may be added according to section 7.3.2. As the width of the surface (A_c/L_s) will deviate from the main sewer line length, the geometric model assumes the lateral inflow to the sewer to be evenly distributed along its length. The model, here called KW6S is governed by six free parameters,

catchment area A_c
equivalent surface length L_s
equivalent surface slope S_s
length of main sewer line L_m
mean slope of main sewer line S_m
diameter of main sewer line D_m

The discretization level of the geometrical model of the catchment is increased if a number of KW6S units are applied to the catchment, see figure 8.5.4.

Let one representative value for each of the parameters surface length L_s, surface slope S_s, sewer line slope S_m and sewer line diameter D_p be used for all units. The number of free parameters then becomes $4 + 2 \cdot n$ where n is the number of applied units. The two parameters which are varied between the units are the contributing area and the sewer length.

If, in addition, the sewer slope and surface length are considered individually for each unit, the number of free parameters will be $2 + 4 \cdot n$. This geometrical model is here called KW6S-S. Its level of discretization is mostly governed by the number of KW6S units applied.

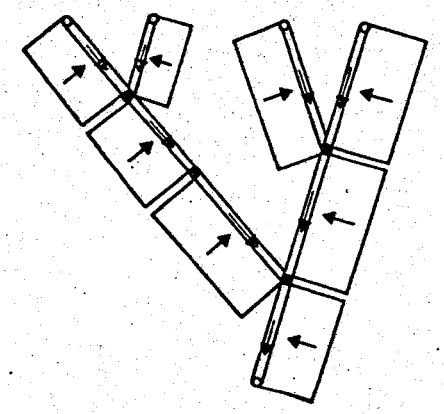

Figure 8.5.4 Example of a model structure containing only KW6S units, the KW6S-S model

An alternative way of using only a few free parameters and still having a discretized sewer net is to define permanent sewer structures. Examples are shown in figure 8.5.5 with a fixed number of inlets and distances between them. To each of the inlets identical KW4G models with characteristic values are connected (contributing area is (total area)/(number of inlets)).

The system is defined by 10 parameters

sewer structure according to figure 8.5.5
total catchment area A_c
length of the surface L_s
slope of the surface S_s
gutter flow slope S_g
length of main line L_m
mean slope of main sewer line S_m
length of downstream sewer L_d
diameter of sewer D_m
length of sewer branch L_b

and is here called the KW4G-I model.

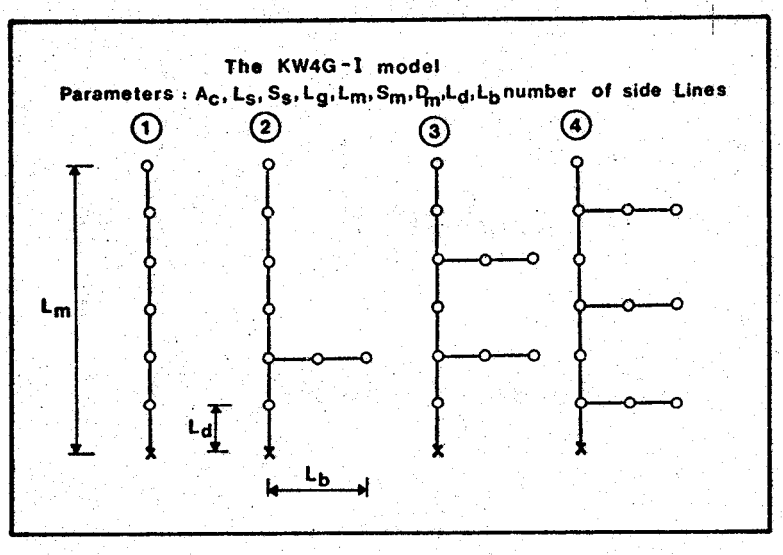

Figure 8.5.5 Four alternative sewer structures. To each of the inlets identical KW4G models are connected.

8.5.4 Application of simplified geometric models

For each of the six catchments, sets of input data have been built up according to the simplified geometric models discussed above. The main characteristics of the simplifications are;

- o simplified representation of the sewer net geometry (the KW4G-I and KW6S models)
- o use of mean slopes of the sewer net (the KW4G-I and KW6S models)
- o replacement of gutter and sewer flow by surface flow (the KW6S-S, KW6S and KW3 models)
- o use of representative surface/gutter/sewer reaches (the KW4G-I model)

The free parameters of overland flow in the simplified models have been adjusted to maintain the representative time of concentration from the real base catchment. For example, corresponding time used to evaluate L_s or S_s in the KW3 model is

$$[t_c]_{eq} = [t_c]_s + [t_c]_g/2 + [t_c]_p/2 \qquad \ldots (8.5.2)$$

where $[t_c]_s$ is obtained from a representative surface, $[t_c]_g$ from corresponding gutter and $[t_c]_p$ from the main sewer line of the base catchment. The choice of $[t_c]_g/2$ is a compromise considering the fact that the upstream part of the surface is drained through the full length of the gutter while the downstream part is not drained by the gutter at all. If the main sewer line of the base catchment is considered as being mainly laterally fed, the same principle is applied, $[t_c]_p/2$.

The calculations are based on the t_c relations given in section 7.3. In the simulations it was found that appropriate values of the side wall slope are z = 0.02 (gutter flow) and z = 0.27 (approximation of sewer flow). Roughness parameters were chosen according to the DET model in section 8.4. A mean of the maximum intensities from the storms used in the simulations in each catchment was used as a representative rain intensity (one value for each catchment).

In order to show how the different geometric simplifications affect the volumes of input data and calculations the numbers of routing units and free parameters used are given in tables 8.5.1 and 8.5.2 respectively. Corresponding information for the Time-Area Method (TAM) has been added for comparison.

A routing unit means any separate surface, gutter or sewer reach to which the routing model has been applied. The number of routing units is then a relative measure of the calculation volumes of the geometric models.

The tables show the great difference between the detailed and the simplified geometric models both regarding calculation volumes and volumes of input data sets. It can also be seen that the use of the KW4G-I model is only justified

compared to the KW6S-S model, in catchments with more complex sewer nets.

Table 8.5.1 Number of routing units for different test area and geometric models

Catchment \ Model	DET	KW6S-S	KW4G-I	KW6S	TAM
ASPH	3	-	-	-	1
PCON	13	2	-	2	1
PASP	18	4	9	2	1
AASP	37	4	6	2	1
SASP	90	8	11	2	1
COMP	36	10	11	2	1

Table 8.5.2 Number of free parameters used in different test areas with different geometric models

Catchment \ Model	DET	KW6S-S	KW4G-I	KW6S	TAM
ASPH	6	-	-	-	3
PCON	52	6	-	6	3
PASP	72	18	10	6	3
AASP	148	18	10	6	3
SASP	360	36	10	6	3
COMP	144	42	10	6	3

8.5.5 Simulations by simplified geometric models

The geometric models above can all be regarded as simplified versions of the detailed model DET. Nothing is added to the description of the runoff process and it is thus natural to compare the performances of the simplified models and the detailed. Comparisons with DET model hydrographs instead of recorded ones also improves the making of comparisons between the simplified models.

Simulated hydrographs are shown in appendix II 1.2. In the small street catchment (ASPH), only the overland flow models KW4G and KW3 have been tested; in the small very regularly shaped parking area catchment (PCON), only the KW6S and KW3 models. All models used in the two catchments show very good performance, generally better than in the larger and more complex catchments.

In the four largest catchments, the KW6S-S, KW4G-I, KW6S and KW3 models have been used. The main impression from visual inspection is that they perform well, with hydrograph shapes very similar to those of the detailed model. The simplest model KW3 and to some extent also the KW6S model, tend to have hydrographs with deviations in shape in some cases. Generally, all model simulations made for the AASP and SASP catchments show not quite as good performance as for other catchments. It should be noted that storms with comparatively low intensities have been used for these catchments.

The five highest flow peaks simulated in each of the four largest catchments have been used to estimate the statistical parameters λ_p, σ_p and ε_p. In table 8.5.3 the parameters are given for each of the models used.

Table 8.5.3 Statistical parameters for the simplified geometrical models compared with the DET-model (five peaks in each of the four greatest catchments)

Model	λ_p	σ_p	ε_p(%)	Number of peaks
KW6S-S	1.02	.07	5.7	20
KW4G-I	1.02	.10	8.1	20
KW6S	1.01	.09	6.9	20
KW3	0.96	.13	11.5	20

Characteristic of the models' performance is the variation in the attenuation of the hydrographs. While some

are too little attenuated giving flow peaks which are too high and too fast, some are too attenuated with too low, delayed peaks. The ratio between flow peaks λ_p is a good measure of the attenuation. For all catchments together this attenuation appears balanced according tc table 8.5.3 (the KW3-model gives a mean underestimation of peaks by about 4%). The variation of the attenuation between the catchments and models represented by λ_p is shown in table 8.5.4.

The difference in λ_p is obviously smallest for the most detailed model (KW6S-S) and greatest for the simplest geometric model.

Table 8.5.4 Variation intervals for λ_p for the simplified geometric models (five peaks in each of the four greatest catchments)

Model	smallest λ_p	greatest λ_p	Difference
KW6S-S	0.94	1.06	0.10
KW4G-I	0.87	1.06	0.19
KW6S	0.90	1.11	0.21
KW3	0.82	1.12	0.30

Looking at each catchment separately, it is clear that all models can give both too small and too great attenuation. This is an indication that the estimated times of concentration on which the selection of all input data which influences the attenuation is based, are not representative for all storms. A more precise evaluation of these times would probably increase the accuracy of the models (or decrease the differences in table 8.5.4). However, a more sophisticated way of estimating the time of concentration is rather pointless when the basic idea is to simplify the creation of input data for the kinematic wave model.

The influence of the selected times of concentration on the attenuation was tested in one of the catchments (the COMP-catchment). The parameters in the models were shifted to correspond to a 30% less and a 30% greater time of concentration compared to the basic value. In table 8.5.5 λ_p values from the test have been put together for the different models.

The effect of the parameter variations on the attenuation depends not only on the properties of the model but also the properties of the catchment and hyetograph. The figures in table 8.5.5, should therefore be regarded only as examples of a variation.

In the table it is seen that, with the exception of the KW6S-S-model, the interval between maximum and minimum flow values increases as the geometrical discretization becomes coarser.

Table 8.5.5 The effects on the attenuation of varying the parameters in the models (corresponding to a variation in (t_c)

Model	λ_p(0.70 t_c)	λ_p (1.30 t_c)	Difference
KW6S-S	1.13	0.92	.21
KW4G-I	1.05	0.99	.07
KW6S	1.09	0.95	.14
KW3	1.19	0.87	.31

The time of concentration for the sewer net is included in the parameter variation for the KW3 model but not for the others. These can thus be expected to be less sensitive to errors in the estimation of the time of concentration. As shown in the table, the KW3 model has consequently the greatest difference between the peakflows from the two sets of parameters.

A sensitivity test using parameters corresponding to $0.5t_c$ and $1.5t_c$ increased the difference to about 0.27 in

mean for the KW6S-S, KW4G-I, KW6S models and to 0.5 for the KW3 model.

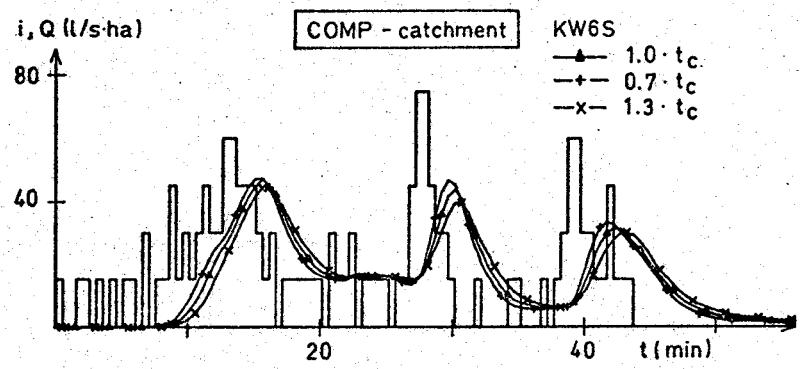

Figure 8.5.6 Sensitivity of the KW6S-model corresponding to $0.7t_c$ and $1.3t_c$

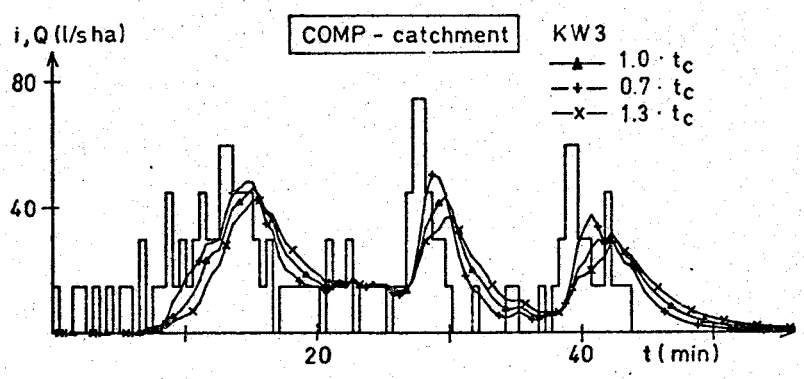

Figure 8.5.7 Sensitivity of the KW3-model corresponding to $0.7t_c$ and $1.3t_c$

In figures 8.5.6 and 8.5.7 the sensitivity to a change in parameters corresponding to $0.7t_c$ and $1.3t_c$ are shown for the KW6S and KW3 models (the corresponding DET simulation is shown in appendix II:1.3).

The standard deviation σ_p and the absolute error ε_p in table 8.5.3 reflects the ability of the models to reproduce the flow peaks of the detailed model. The parameters may thus be used for comparisons between the simplified models. It is clear from the table that the standard deviation and the absolute error increase as the used geometric input data becomes more simplified. However, the differences are not very marked and no drastic changes in the performances are obtained by making the simplifications. In particular the KW6S model appears to have a good performance considering its relative simplicity.

According to the study, the performance of the detailed kinematic wave model is reasonably well maintained

- assuming lateral inflow to the main sewer line
- using the mean slope of the main sewer line
- excluding minor branches from the sewer system

8.6 Simulations by the Time-Area Method

The performance of the Time-Area Method has been examined in much the same way as the simplified kinematic wave models in section 8.5.5, that is by making comparisons with the detailed model (DET). The time of concentration was chosen as the time from the most distant surface to the downstream end using the relations given in section 7.3.

Several time-area curves were investigated. Attempts to select a non-linear time-area diagram to get a "best fit" for each simulated hydrograph were not successful, though parts of the hydrographs (for example the rising part) could be improved in comparison with the linear-diagram hydrographs. This result is consistent with that of section 7.3 where the theory of the Time-Area Method was discussed. In figure 8.6.1, an example of the effects of using different time-area curves is shown .

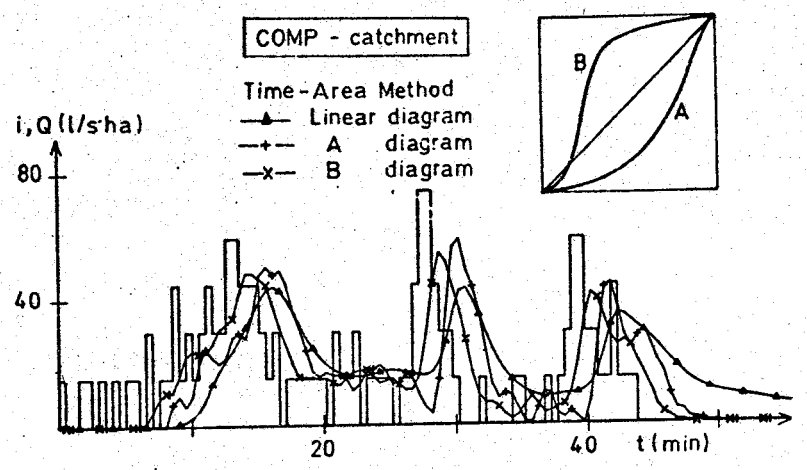

Figure 8.6.1 Example of effects of using different time-area curves

We can see how the shapes of the hydrographs are changed by the time-area curve. It is also evident that the delay and level of the peaks is influenced by the curve. A general method for estimating the time of concentration must then be based on one selected time-area curve. As the best general performance was obtained using the linear time-area diagram together with the way of estimating of the time of concentration given above, this method was used throughout the study.

In appendix II:1.4, hydrographs simulated by the Time-Area Method are shown. A statistical analysis of corresponding flow peaks was made in the same way as in section 8.5.5 and is summarized in table 8.6.1.

According to the table the peaks are on average underestimated by about 7%. Regarding the standard deviation and absolute error the method appears to be as good as the kinematic wave models with an acceptable ability to reproduce a balanced attenuation of single peaks. However, looking at both the general shape and delay of the

hydrographs, the deviation from the DET- model is more marked than for any of the kinematic wave models.

Table 8.6.1 Statistical parameters for the Time-Area Method compared with the DET-model (five peaks in each of the four greatest catchments)

λ_p	σ_p	ε_p (%)	Number of peaks
.93	.10	9.2	20

The Time-Area Method was also found to be more sensitive to variations in the general level of rain intensity. This is indicated in the catchment which has the greatest variations in maximum rain intensities between different storms (29 l/s·ha to 108 l/s·ha). In this catchment (the PASP-catchment) the Time-Area Method has a standard deviation about three times greater than the kinematic wave models.

The influence of reducing and increasing the time of concentration by 30% was also investigated as in section 8.5.5. Corresponding values for the Time-Area Method are given in table 8.6.2.

As we can see, the effects are at the same level as for the KW3-model. In the figure 8.6.2 an example is given of the effects of the variations on the hydrograph shape.

Table 8.6.2 The effects of varying the time of concentration in the Time-Area Method

λ_p (0.70 t_c)	λ_p (1.30 t_c)	Difference
1.13	0.86	0.27

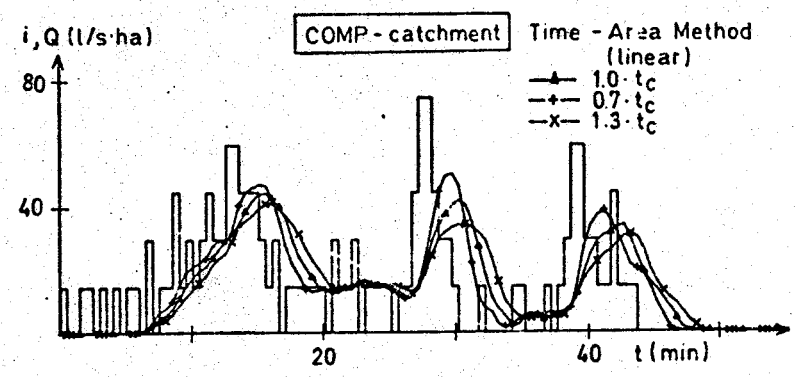

Figure 8.6.2 Example of variations in hydrograph shape caused by variations in time of concentration

8.7 Summary

The kinematic wave model has been applied to six catchments, using different simplified geometric models. In addition, the Time-Area Method has been investigated. The geometric models have all been compared with a kinematic wave model using a very detailed geometric description of the catchment. This detailed approach has been compared with recorded runoff from a number of storms. The comparison with recorded runoff indicated uncertainties in the measurements and model performance of some catchments. However, it was concluded that the detailed model reflected the runoff process reasonably well. The validity of the kinematic wave model has been documented by several investigators, for example Jacobsen (1980).

The effects of using simplified geometric descriptions of the catchments for the kinematic wave model were investigated by making comparisons with the detailed kinematic wave model. It was found that the performance of the kinematic wave model is still very good, even for great simplifications of the catchment geometries such as

- replacement of gutters by increased surface lengths
- assuming only lateral surface inflow to the main sewer line
- using the mean slope of the main sewer line
- excluding minor branches in the sewer system.

The simulations by the Time-Area Method showed that reasonably accurate values of single flow peaks may be obtained. However, the general shape and delay of the simulated hydrographs were not as good as those of the kinematic wave models.

In runoff simulations from catchments built up of several base catchments, the general performance (shape and delay of hydrographs) of the base catchment models is as important as the ability to reproduce flow peaks. The kinematic wave models should then generally be preferred as base catchment models. These models are also specially favourable in cases when input data can be calibrated by runoff measurements.

Independent of the model used, the main difficulty is to choose representative input data which give suitably attenuated hydrographs. In this study the choice has been based on an evaluation of representative times of concentration by the relations based on kinematic wave models given in section 7.3. As the evaluation is approximate, the probability of an unsuitable attenuation is introduced. The probability of large errors is greatest for the simplest models (the KW3 model and the Time-Area Method). A more precise evaluation of the time of concentration would possibly increase the accuracy of the models. This, however, requires a more sophisticated way of estimating this time which is pointless as the basic idea was to develop a simplified method of creating input data for the kinematic wave model.

The most suitable geometric simplification for the kinematic wave model, regarding both the demand for simplicity in inputdata and accuracy is the KW6S model. The model is composed of a sewer with the length and mean slope of the main sewer line in the catchment. The sewer is laterally fed by a surface with length and slope corresponding to an estimated time of concentration which is representative for runoff to the main sewer line.

9. BASE CATCHMENT MODELS APPLIED

9.1 General

In the last chapter the discussion concerned mainly three catchment models, the KW6S and the KW4G-I models and the Time-Area Method. These have been applied to two urban catchments, Bergsjön and Linköping 2, which are considerably greater than the catchments used in chapter 8. The catchments and measurements are described in appendix I.

The Bergsjön catchment is a mainly steep residential area with a flat central part. The runoff area is about 15 hectares, 5 of which contribute directly to the runoff in the storm water system. A characteristic time of concentration for ordinary storms is about 6 minutes. The sewer system has a tree shape with four main branches.

The Linköping 2 catchment is a residential area with small slopes. It is about 18 hectares in size with 5.7 hectares contributing directly to runoff. A characteristic time of concentration for ordinary storms is about 12 minutes. The sewer system is built-up of two major branches.

Three levels of subdivision into base catchments have been used. The finest division corresponds to base catchment areas of about 0.5 hectares (directly contributing area).

The discussion of the performance of the models are here based on comparison between hydrographs in the same way as in the previous chapter: The recorded flow is compared with hydrographs simulated by a detailed kinematic wave model (DET), and hydrographs simulated by simplified models are also compared with those from this detailed model.

9.2 Kinematic wave model simulation - comparisons with recorded hydrographs

The recorded runoff hydrographs were compared with hydrographs simulated by the detailed kinematic wave model (DET-model). In this model, in principle every surface, gutter and sewer within the system is represented. However, the available information of the runoff system in Bergsjön and Linköping 2 was not quite as detailed as in the six catchments in last chapter. The application of the models to Bergsjön and Linköping 2 is therefore more like a realistic case.

In appendix II:2.1, simulations of five storms from Bergsjön and four storms from Linköping 2 are presented. The contributing areas used in each catchment were obtained from regression analysis of storm volumes recorded over 22 months (Bergsjön) and 12 months (Linköping 2, two summer - autumn reasons). They were found to be 75% and 90% of the impermeable surfaces in Bergsjön and Linköping 2 respectively, Arnell (1980).

A visual inspection of the hydrographs shows that the simulated and recorded hydrographs coincide reasonably well with respect to general shape and delay of peaks. There are, however, parts of several hydrographs with marked deviations. There are also, for some storms, deviations between recorded and simulated runoff volumes. Probable explanations for the deviations have been discussed in section 8.4.2 and are not repeated here.

A statistical analysis of the relation between recorded and simulated flow peaks was performed for the hydrographs presented. No marked differences in the statistical parameters were found between the catchments. The result is then summarized for both catchments in table 9.2.1.

As shown in the table, the model gives on average flow peaks which are slightly too attenuated for both catch-

Table 9.2.1 Mean ratio λ_p, standard deviation σ_p and absolute error ε_p for recorded and simulated flow peaks in Bergsjön and Linköping 2.

Number of peaks	Mean ratio λ_p	Standard dev. σ_p	Abs. error ε_p %
18	0.96	0.13	11

ments. This can be compared with the analysis of the six "small" catchments in the last chapter where the DET model gave peaks which were too little attenuated. The standard deviation and absolute error are smaller compared with the six catchments. Compared with Colyer's conclusions previously mentioned (section 8.4.2), the model performs well.

The same two catchments have previously been used by Arnell (1980) to test a runoff model (the CTH model) of about the same level of sophistication as the DET model. Comparing the two models the standard deviation and absolute error are smaller for the DET model than the CTH model. This may be explained by the fact that the CTH model does not take gutterflow into account. It should, however, be noted that the statistical measures are partly based on different flow peaks which may have an influence on the deviations.

9.3 Simulations using different base catchment sizes

Three levels of subdivision into base catchments have been investigated

- nine base catchments (L1)
- one base catchment for each main sewer branch (four in Bergsjön and two in Linköping) (L2)
- the entire catchment as one base catchment (L3)

The KW6S-S model has been applied to each catchment and each discretization level. They will be denoted here as

the KW6S-L1, KW6S-L2 and KW6S-L3 models for the three levels respectively. The first level corresponds to base catchments of about the same size as those investigated in the last chapter, 0.3-1 ha (contributing area). The second level means four base catchments in Bergsjön and two in Linköping 2. The KW4G-I model was applied to the third level (L3). The input data sets have been based on representative times of concentration and the different models compared with the DET model. The different steps have been performed in the same way as in last chapter.

The simulated hydrographs are shown in appendix II:2.1. The main impression from a visual inspection is that the models perform well with hydrograph shapes very similar to those of the DET-model. The best simulations are obtained from the KW6S-L1 model, but those from the KW4G-I and KW6S-L2 models are also very good. The simulations by using the KW6S-L3 model are also good in the Linköping 2 catchment, but become too little attenuated in the Bergsjön catchment (λ_p = 1.09), see also appendix II:2.3.

From the statistical analysis of the flow peaks it can be concluded that the models generally perform better in Bergsjön than in the flatter Linköping 2 area. In table 9.3.1 the statistical parameters are summarized for both catchments.

Table 9.3.1 Statistical parameters for simulated flow peaks in the Linköping 2 and Bergsjön areas

Model	λ_p	σ_p	ε_p(%)	Number of peaks
KW6S-L1	1.01	0.05	3.2	18
KW6S-L2	0.98	0.07	5.5	18
KW6S-L3	1.04	0.13	9.9	18
KW4G-I	0.99	0.07	4.3	18

The table shows that a balanced attenuation is obtained for the models. The standard deviation and absolute error have low values in general. These parameters increase

with a decreasing level of discretization, indicating that more discretized models perform better.

The most marked difference is between the KW6S-L2 and KW6S-L3 models. This deviation is most probably caused by the approximating of the sewer system to only one main sewer line, which in both Bergsjön and Linköping 2 appears to be a coarse approximation. It should also be noted that the KW4G-I model performs almost as well as the KW6S-L1 model despite the fact that it is based on a very standardized network system.

The influence on the attenuation of the selected representative times of concentration on the attenuation was investigated in Bergsjön. The parameters in the models were shifted to correspond to 30% less and 30% greater time of concentration compared to the basic chosen value. In table 9.3.2, λ_p values from this test are put together.

Table 9.3.2 λ_p values for different times of concentration in Bergsjön

Model	λ_p (0.7 t_c)	λ_p (1.3 t_c)	Difference
KW6S-L1	1.05	0.96	0.09
KW6S-L2	1.11	0.94	0.17
KW6S-L3	1.17	0.92	0.25
KW4G-I	1.08	0.96	0.12

As shown in the table the interval between the mean peak flows for the two choices of parameter increases with decreasing discretization of the catchment. The effect of an improperly estimated representative time of concentration is obviously greater for more simplified catchment descriptions.

9.4 Simulation by the Time-Area Method

The Time-Area Method used as base catchment model was examined at the two levels of discretization L1 and L3,

as defined in section 9.3 (9 and 1 base catchments). The simulated hydrographs were compared with the detailed kinematic wave model DET and the times of concentration were evaluated in the same way as in chapter 8. Only linear time-area diagrams were used.

In appendix II:2.4 hydrographs simulated by the Time-Area Method are shown. These show generally a more marked deviation from the DET-model than those simulated by the kinematic wave model. The hydrographs are too little attenuated and delayed. Compared with the Time-Area Method hydrographs analysed in last chapter, they show a better performance with regard to general shape. It should be noted that the former are, on average, too attenuated.

In table 9.4.1 the statistical analysis of flow peaks from the two catchments are summarized. The models corresponding to levels L1 and L3 are denoted TAL1 and TAL3, respectively.

Table 9.4.1 Statistical parameters for the Time Area Method compared with the DET-model

Model	λ_p	σ_p	ε_p(%)	Number of peaks
TAL1	1.07	0.15	10.4	18
TAL2	1.06	0.13	9.9	18

The standard deviation and absolute error are generally greater than the corresponding values for the kinematic wave models. There is very little difference between the two discretization levels and the TAL1 model has obviously a worse performance than corresponding kinematic wave model at this base catchment level, the KW6S-L1 model. This is probably due to the fact that the sewer lines of the branches are represented in the KW6S-L1 model by routing units, which is not the case in the TAL1 model.

The influence of reducing and increasing the time of concentration by 30% was also investigated in the Bergsjön area. Corresponding values for the Time-Area Method are given in table 9.4.2.

Table 9.4.2 Variation of the time of concentration using the Time-Area Method in Bergsjön

Model	λ_p (0.7 t_c)	λ_p (1.3 t_c)	Difference
TAL1	1.16	0.98	0.18
TAL3	1.18	0.97	0.21

The interval between mean peak flows for the two choices of parameters are, as shown in the table, about the same for the two base catchment levels. Compared with the kinematic wave models the sensitivity at the first level (L1) is considerably greater. At the third level (L3) the sensitivity is of about the same order for the two categories of model. This is most probably caused by the difference in representation of sewer lines mentioned above.

9.5 Summary

The runoff models presented in last chapter have been applied as base catchment models in two urban catchments with total areas of 15 and 19 hectares, respectively. Three levels of subdivision into base catchments have been used where the finest division corresponds to sizes around 0.5 ha.

The general impression of the performance of the models applied to these areas is much the same as in chapter 8. The models based on the kinematic wave appear to perform well, better than those based on the time-area relationship at comparable discretization levels.

A simple geometric model (one sewer laterally fed by a rectangular surface - the KW6S model) has been applied as

base catchment model at the three different levels of subdivision. Using greater base catchment sizes the performance is not quite as good. However, there are no drastic changes and it is obviously possible to obtain a very good performance using quite great base catchments, provided the catchment characteristics (for instance the time of concentration) are properly evaluated. It should be stressed here that as the base catchment increases the effects of making misjudgements in these evaluations increases. It was also found that when the main sewer system contains several long branches they must be represented in the input data system and should not be replaced by one main sewer line.

The Time-Area Method does not perform quite as well as the kinematic wave model despite the fact that the same amount of catchment data is required. Though the model properly used has a performance which is acceptable in many applications there is no obvious argument for its use.

It can finally be concluded that:

- Independent of the model used and base catchment size, the choice of input parameters in the base catchment model (overland flow parameters) has a significant effect on the result.

- The kinematic wave model (KW6S model) is both possible to use and effective as base catchment model.

- With this model relatively great simplifications of the input data geometry can be used with a reasonably well maintained performance, this provided the catchment characteristics are properly evaluated. That may be done using relations derived from the kinematic wave equations, assuming constant rain intensity.

10. EVALUATION OF STATISTICAL MAXIMUM FLOWS

10.1 General

In many cases it is of interest to make only a fast and simple evaluation of maximum flows in a couple of key points in the sewer system. This may be done by the so called Rational Method. The method was formerly the only available design tool and then much criticized for being too approximate. It is easily applied but may, as all strongly simplified models, give very misleading results if it is improperly used.

The Rational Method is commonly regarded as an empirical model. There is, however, a clear relation between the model and the basic equations used in this report, as has been pointed out by Newton-Painter (1974). Despite the relationship to the Time-Area Method the Rational Method is basically quite different from all the previous discussed models by being a statistical method for maximum flows rather than a routing method.

In the following sections some theoretical and practical aspects of the method will be discussed in order to discuss the relevance of the underlying model. An alternative method for evaluating design flow rates based on the traditional Rational Method is also proposed.

10.2 Basic deterministic relations

Using the Time-Area Method corresponds, as shown in section 7.3, to applying the kinematic wave equations with a wave velocity that is fixed in time but not in space. The discretization of the time area diagram defines the space step in the equations used. Fixing the wave velocity in space as well corresponds to a straight line in the time area diagram. This approximation requires no spatial discretization and may be regarded as a reservoir model (linear). The solution takes the form

$$Q(t) = a \cdot B \cdot \int_{t_o}^{t} i(\sigma)\, d\sigma \qquad \ldots (10.2.1)$$

(see equation 7.3.2)).The wave velocity may be written $a=L/t_c$ where L is the length of the surface and t_c the time for the wave movement over the surface. According to section 4.2.2, $t-t_o= t_c$ giving

$$Q(t) = L \cdot B \frac{1}{t_c} \cdot \int_{t-t_c}^{t} i(\sigma)\, d\sigma \qquad \ldots (10.2.2)$$

This relation corresponds to an averaging of the intensities over the time t_c. For each storm event a maximum value of the average intensity can be found

$$i_{max} = \left[\frac{1}{t_c} \cdot \int_{t-t_c}^{t} i(\sigma) d\sigma\right]_{max} \qquad \ldots (10.2.3)$$

The maximum flow is obtained as

$$Q_{max} = L \cdot B \cdot i_{max} \qquad \ldots (10.2.4)$$

The model (equation (10.2.4)) expresses the deterministic relation underlaying the Rational Method. The relevance of maximum flow values obtained by this model depends mainly on

- how well the time t_c is estimated
- the divergence in "real" rain intensities from the maximum average intensity i

Hager (1985) has shown that the variation of rain intensities in an interval equal to the time of concentration has little influence on the peak flow value for a rectangular surface (effects of delay were not negligible).

The results from this theoretical study can not be generalized to an arbritary urban catchment but gives an indication of the possibilites of the basic model.

10.3 The Rational Method

The design of a network system is basically a statistical problem. In principle, one possible way to balance pipe size against risk is to design the system for each storm in a long series of rainfall events (perhaps 30 years). The return period for the different flows is calculated and a choice between risk levels with corresponding pipe sizes can be made. Design methods based on statistical analyses of simulated discharges have been proposed by Johansen (1979) and Arnell (1982).

A more practical but also more approximate approach is based on storms generated by statistical parameters, design storms. By using such a storm a design flow is evaluated which is assumed to have the same return period as the storm.

The traditionally used statistical storm is the Maximum Average Intensity storm (MAI-storm) which is defined by its average intensity i_{max} and corresponding averaging time (duration time t_d), compare equation (10.2.3).

Each historical storm can be described by a series of MAI-storms with different durations. From a series of historical storms, frequencies of MAI-storms can be evaluated. For each duration a distribution function for the intensities can be plotted. Examples of such functions obtained from a two year series are given in figure 10.3.1 (after Arnell, Lyngfelt (1975)). The three rain distributions correspond to the durations t_d = 6, 9 and 12 minutes. The frequency is here given as the return period in years (T). The distribution of maximum discharges from a residential area (15 hectares) during the same period is also shown in the figure.

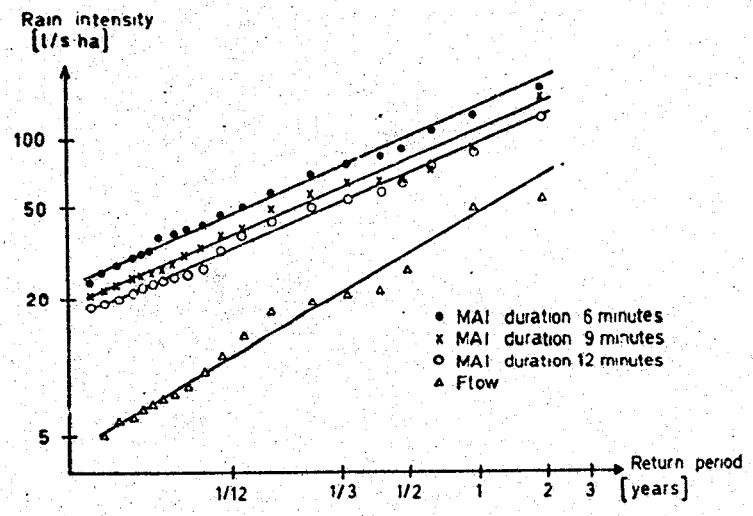

Figure 10.3.1 Distribution functions for MAI-storms and maximum discharge (after Arnell, Lyngfelt 1975)

Assuming parallel intensity and discharge distributions we obtain

$$Q_{max}(T) = c_1 \cdot i(T, t_d) \qquad \ldots (10.3.1)$$

where $Q_{max}(T)$ and $i(T, t_d)$ are flow and MAI-storm distributions, T the return period, t_d the duration time and c_1 a constant. As we can see, all the chosen MAI-storm distributions diverge slightly from this assumption. The storm distributions get closer to the flow distribution with increasing return period. The same tendency can be found in other catchments analysed in a similar way, see Shaake et al. (1967) and Arnell et al. (1980).

If the time of concentration is used as the duration of the MAI-storm, the corresponding intensity distribution

will have a 'steeper' slope. In a study of five catchments it was found that the distribution $i(T,t_c)$ was always in better accordance with the flow distribution than any distribution $i(T,t_d)$ using constant duration. It was also found that the constant c_1 (equation 10.3.1) was close to the estimated contributing area A_c, Lyngfelt (1981). The relation becomes

$$Q_{max}(T) = A_c \cdot i(T, t_c) \qquad \ldots (10.3.2)$$

where t_c is a function of i.

10.4 The time of concentration

The traditional way of presenting MAI-storm distributions for a series of historical storms is the intensity duration frequency diagram (IDF-diagram). In Sweden IDF-curves have been established at six locations. In figure 2.2.2 the IDF-diagram used in Göteborg is shown.

The curves are characterized by having steep gradients for the durations of interest in urban drainage design (5-20 minutes). Overestimating the time of concentration by, for example, five minutes may very well result in an underestimation of the discharge by more than 20%. The time of concentration is thus a significant parameter and the estimation of the parameter is of great importance in the application of the method.

Relations for estimating of the time of concentration based on the kinematic wave concept are given in section 7.3. In chapters 8 and 9 they were used in model analysis and found to give appropriate values for the Time-Area Method using a linear time-area diagram. The expressions for surface-gutter and sewer flow may be summarized by

$$t_c = K_1/i^{0.25} + K_2/i^{0.4} \qquad \ldots (10.4.1)$$

where K_1 and K_2 includes catchment parameters such as slopes, lengths and roughnesses. The parameters may be evaluated from equation (7.3.8) - (7.3.10).

Lyngfelt (1981) evaluated by regression analysis an empirical relation which gives values of t_c close to those obtained by the relation (10.4.1). The regression is based on catchments having contributing areas greater than 1.6 ha.

10.5 Evaluation of the maximum flow

The IDF-curves may be expressed by the relation

$$i = \frac{a}{t_d+b} + c \qquad \text{... (10.5.1)}$$

where a, b and c are parameters which vary with location and return period. Using the Rational Method we are looking for the rain intensity corresponding to the time of concentration estimated by equation (10.4.1) which is a function of the rain intensity. The intensity is obtained, together with the time of concentration, by solving the equation system

$$i(T,t_c) = a/(t_c+b)+c \qquad \text{...(10.5.2a)}$$

$$t_c = K_1/(i(T,\ t_c))^{0.25}+K_2/(i(T,\ t_c))^{0.4} \qquad \text{...(10.5.2b)}$$

This may be done by using the regression equation

$$(t_c)_{n+1} = K_1/\left[\frac{a}{(t_c)_n} + c\right]^{0.25} + K_2/\left[\frac{a}{(t_c)_n} + c\right]^{0.4} \qquad \text{...(10.5.3)}$$

The intensity $i(T, t_c)$ is obtained from equation 10.5.2a for a given t_c and the maximum flow by equation 10.3.2.

10.6 Tests - discussion

The Rational Method relates the distribution functions of rain intensity and flow in a catchment. It is therefore only possible to investigate the relevance of the model in catchments where such functions have been established.

Arnell (1982) used a detailed runoff model and a series of historical storms to evaluate distribution functions for discharge and rain intensity in 30 catchments with different characteristics. All of them are subcatchments in the areas Linköping 1, Linköping 2 or Bergsjön, see Arnell et al. (1980). The evaluation was done in order to compare different design storms used in design of sewer nets by detailed runoff models. In figure 10.6.1 the sewer network of Bergsjön is shown with calculation points.

Flow rates evaluated by the Rational Method, as described in the last two sections, were compared with Arnell's distribution functions. The method was found to perform with about the same accuracy as the detailed model using a design storm. Three examples are given in figures 10.6.2 - 10.6.4.

When a detailed runoff model is used in design, the flow is repeatedly simulated for different durations of the design storm until a maximum flow is obtained. With this procedure there is not a "perfect" fit between rain intensity and response time of the catchment, as there is the case in the Rational Method as described above. This fact is believed to compensate for the coarse deterministic runoff model included in the Rational Method. It also emphasizes the importance of including the rain intensity in the estimation of the time of concentration.

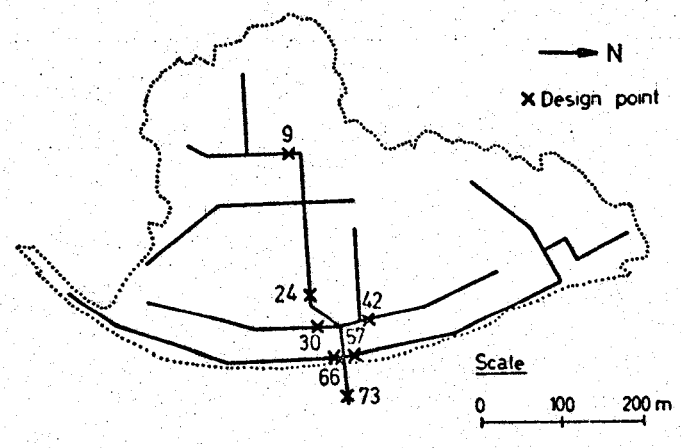

Figure 10.6.1 The sewer network of Bergsjön (after Arnell (1982))

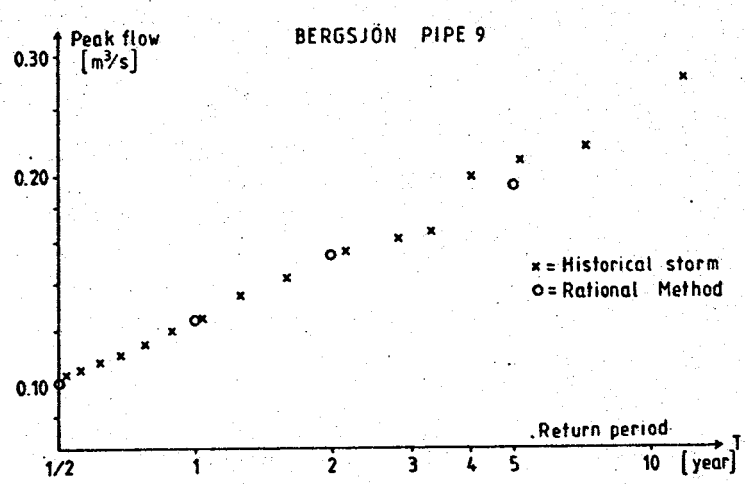

Figure 10.6.2 The distribution function for the discharge in point 9 in Bergsjön (see appendix II) after Arnell (1982) with the Rational Method points included

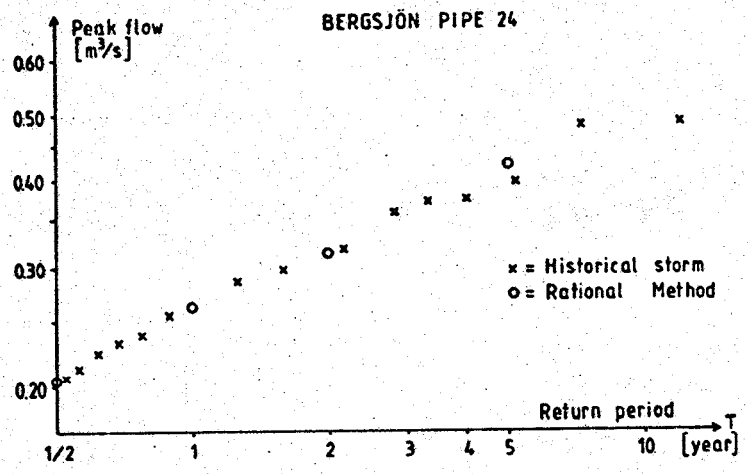

Figure 10.6.3 The distribution function for the discharge in point 24 in Bergsjön (see appendix II) after Arnell (1982) with the Rational Method points included

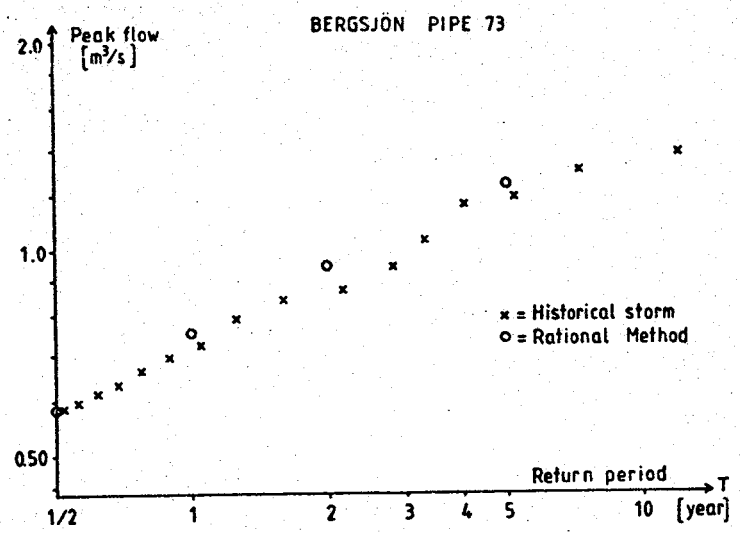

Figure 10.6.4 The distribution function for the discharge in point 73 in Bergsjön (see appendix II) after Arnell (1982) with the Rational Method points included

The Rational Method appears surprisingly capable of estimating statistical design flows. It should, however, be stressed that the method as it is used here requires much the same amount of input data as the kinematic wave models. In addition it is usually advantageous to have the entire hydrograph and not only the design flow as a basis in the design situation. Runoff systems with retention storages or overflows are examples where routing methods must be used. The Rational Method is a very suitable method for calculating flow rates in the preliminary design stage of a network system, in small or simple systems and also for checking the input data to more complex models. When this method is used, the time of concentration should be evaluated by relations based on the kinematic wave theory (see section 7.3). Particular care should be taken in estimating t_c when this time is short (< 10 minutes).

LIST OF SYMBOLS

SI-units are generally used. If not the unit is specified in the text.

A	cross-section of flow
A^*	dimensionless cross-section of flow A/A_o
A_o	cross-section at stationary flow
A_c	contributing catchment area
A_p	part of contributing catchment area
a	parameter in the non-linear friction relation or parameter in the IDF relation (section 10.5)
a_1 a_2	amplitudes at section 1 and 2 (section 3.5)
B	width of channel
B_s	one of the gutter flow lengths in the kW6G geometrical model
b	exponent in the non-linear friction relation or parameter in the IDF relation (section 10.5)
C1,C2	characteristic number 1 and 2 (section 4.2.5)
C_D	resistance coefficient
C_R	Courant number
$C_R^{\Delta x}$	modified Courant number (section 6.4.3)
c	wave velocity or parameter in the IDF-curve relation
c^*	dimensionless celerity (c/V_o)
c_k	kinematic wave velocity
D	diffusion coefficient
D^*	dimensionless time at which the lateral inflow ceases (section 4.3.1)
D_m	diameter of the main sewer line
D_n	numerical diffusion coefficient
D_p	diameter of sewer
F_o	Froude number
f	Darcy-Weissbach friction factor

Preceding page blank

g	acceleration due to gravity or index for gutter flow variables
i	rain intensity
i_{max}	maximum average rain intensity (section 10.2)
$i(T,t_c)$	maximum average rain intensity distribution
$j,j+1$	space step j and j+1
K	friction and shape parameter in the non-linear friction relation
K_o	kinematic wave number
K_L	friction parameter in the L-formula
K_q	friction parameter in the quadratic formula
k	effective absolute roughness
L	length in flow direction
L_a	catchment length in the KW6G geometric model
L_b	length of branches in the KW4G-I model (chapter 8)
L_d	length of downstream sewer in the KW4G-I model
L_g	length of gutter in flow direction
L_p	length of sewer
L_s	length of surface in flow direction
L_m	length of main sewer line
$m,m+1$	time step m and m+1
n	Manning's coefficient of roughness
P	wetted perimeter
p	exponent of the hydraulic radius in the friction relation (section 5.4) or index for sewer flow variables
Q	flow rate
Q^*	dimensionless flow rate Q/Q_o
$Q_{max}(T)$	maximum flow distribution
Q_o	stationary flow rate

Q_{max}	maximum flow rate obtained by the Rational Method
Q_b	surface flow per unit width
Q_{in} Q_{out}	inflow and outflow rates to a reservoir (section 7.2.1)
q	lateral inflow
q^*	dimensionless lateral inflow (q/q_o)
q_o	stationary lateral inflow
q_k	constant lateral inflow
R	hydraulic radius
R_e	Reynolds' number
S_o	slope in flow direction
S_f	friction slope
S_g	gutter slope in flow direction
S_p	slope of sewer in flow direction
S_m	mean slope of main sewer line ($L_m/\Delta H$)
S_s	surface slope in flow direction
s	index for surface flow variables
T	return period (chapter 10)
t	time
t_o	starting time for a characteristic at upstream boundary (section 4.2.2)
t^*	dimensionless time ($t\ V_o/L$)
t_c	time of concentration
t_k	time constant in lateral inflow
U	velocity of lateral inflow, cross-sectional mean
U^*	dimensionless velocity of lateral inflow U/U_o
U_o	velocity of lateral inflow at stationary flow
U_i	velocity of rain
U_g	velocity in gutter, cross-sectional mean

U_p	velocity in sewer, cross-sectional mean
U_s	velocity in surface flow, cross-sectional mean
V	velocity of flow, cross-sectional mean
V^*	dimensionless velocity of flow V/V_o
V_e	Vedernikov's number
V_o	stationary velocity of flow
W	velocity of wind
x	space coordinate
Y	cross-sectional water depth
Y^*	dimensionless waterdepth Y/Y_o
Y_o	stationary cross-sectional water depth
Y_g	water depth in gutter flow section
Y_p	water depth in sewer flow section
Z1, Z2	zones in the x-t plane (figure 4.2.3)
z	slope factor of side walls ($\tan\alpha = z$)
α	numerical parameter (weighted box scheme) slope angle of channel
α_{eq}	equivalent numerical parameter (α-diffusive model)
β	correction factor for the cross-sectional velocity distributions or numerical parameter (weighted box scheme)
ΔH	elevation between two points in the sewer system
Δt	time step
Δx	space step
δ	logarithmic decrement = $\ln(a_2/a_1)$
ε_p	mean absolute error in compared peak flow values
θ	parameter in the MIT model (section 6.6)
λ	length of sinusoidal wave
λ_p	mean of the ratio between flow peaks
ν	kinematic viscosity of water

ρ	density of water
ρ_L	density of air
σ	integration variable
σ_o	wave number
σ_p	standard deviation of the ratio between compared flow peaks
τ	integration variable or time-lag in the Time-lag model (chapter 7)
τ_{mp}	mean shear stress along the wetted perimeter
τ_{ms}	mean shear stress along the surface
τ_w	shear stress of wind
ϕ	angle between main and lateral flow vectors
Ψ	angle between rain velocity vector and surface flow velocity vector

REFERENCES

Akan, A.O. and Yen, B.C. (1981). Diffusion-Wave Flood Routing in Channel Networks. Journal of Hydraulics Division, ASCE, HY6, June.

Akan, A.O. (1984). A Physics-Based Approach to Determine Inlet Concentration Times. Proc. 3rd International Conference on Urban Storm Drainage, Vol.1, Göteborg.

Andersson, S., Svensson, J. (1973). Surface Runoff. Basic Theories and Field Studies. Chalmers University of Technology, Department of Hydraulics, Master of Science Thesis Work, 1973:5. Göteborg. (In Swedish).

Arnell, V. and Lyngfelt, S. (1975). Rainfall-Runoff Measurements in Bergsjön 1973-1974. Chalmers University of Technology, Urban Geohydrological Research Group, No. 13, Göteborg (in Swedish).

Arnell, V. (1980). Description and Validation of the CTH-Urban Runoff Model. Chalmers University of Technology, Department of Hydraulics, Report Series A:5, Göteborg.

Arnell, V., Strander, H. and Svensson, G. (1980). Storm-Water Runoff, Quantity and Quality, at Ryd, Linköping 1976-1977. Chalmers University of Technology, Urban Geohydrology Research Group, Report No 48, Göteborg (in Swedish).

Arnell, V. (1982). Rainfall Data for the Design of Sewer Pipe Systems. Chalmers University of Technology, Department of Hydraulics, Report Series A:8, Göteborg.

Preceding page blank

Bengtsson, L. (1980). MAGRÖR. Manual for a Storm Water Computer Program. University of Luleå. Department of Water Resources Engineering. Report TULEA 1980:34. Luleå. (In Swedish).

Berg, A. (1983). Flushing of Sewers with Self-Cleansing Problems. Vassdrags- og Havnelaboratoriet. Norges Hydrodynamiske Laboratorier. Report SFT 60 A83027. ISBN 82-595-3114-3. Trondheim. (In Norwegian).

Borah, K., Prasad, S.N. and Alonso, C.V. (1980). Kinematic Wave Routing Incorporating Shock Fitting. Water Recources Research, Vol. 16, No. 3, June 1980.

Brakensiek, D.L. (1965). Hydrodynamics of Overland Flow and Nonprismatic Channels. Transactions of the ASAE, 1966.

Brakensiek, D.L. (1967). Kinematic Flood Routing. Transactions of the ASAE, 1967.

Brutsaert, W. (1971). De Saint-Venant Equations Experimentally Verified. Journal of Hydraulics Division, ASCE, HY9, September 1971.

Bufill, M.C. (1984). Hydrological Aspects of the Study of Non-Point Pollution on a Motorway Catchment. Proc. 3rd International Conference on Urban Storm Drainage, Vol 1, Göteborg.

Carslaw, H.S. and Jaeger, J.C. (1959). Conduction of Heat in Solids. Second Edition. Clarendon Press, Oxford.

Chen, C.L. (1981). Generalized Manning Formula for Urban Storm Runoff Routing. Proc. 2nd Int. Conference on Urban Storm Drainage, Urbana, Illinois.

Chow, V.T. (1959). Open Channel Hydraulics. Mc Graw-Hill Book Co. New York.

Chow, V.T. (1964). Handbook of Applied Hydrology. Mc Graw-Hill Book Co. New York.

Chow, V.T. and Ben-Zvi, A. (1973). Hydrodynamic Modelling of Two-Dimensional Watershed Flow. Journal of Hydraulics Division, ASCE, HY 11, November 1973.

Constantinides, A.C. and Stephenson, D. (1981). Two-Dimensional Kinematic Overland Flow Modelling. Proc. 2nd Int. Conf. on Urban Storm Drainage, Urbana Illinois.

Crank, J. (1975). The Mathematics of Diffusion, Sec. Edition, Clarendon Press, Oxford, England.

Colyer, P. (1977). Performance of Storm Drainage Simulation Models. Proc. Inst. Civ. Engineers, Part 2, 63, June 1977, pp 293-309.

Daily, J.W. and Harleman, B.R. (1966). Fluid Dynamics. Addison-Wesley Publishing Company, Inc., Reading, Massachusetts.

Eagleson, P.S. (1970). Dynamic Hydrology. McGraw-Hill Book Co., New York.

Engelund, F.A. and Cristensen (1969). The Hydraulics of Stratified and Inhomogeneous Fluids. Polyteknisk Forlag, Copenhagen, Denmark (In Danish)

Ericsson, M., Cedergårdh, P., Svensson, P. (1978). Percolation Pond in Halmstad. Chalmers University of Technology, Department of Hydraulics, Master of Science Thesis Work 1976:2. Göteborg. (In Swedish).

Eskenazi, E. (1984). Laboratory Study of Absorbed Runoff Flow by Different Gully Grating Systems. Proc. 3rd International Conference on Urban Storm Drainage, Vol. 1, Göteborg.

Falk, J. and Niemczynowicz, J. (1979). Modelling of Runoff from Impermeable Surfaces. Lund Institute of Technology, Department of Water Resources Engineering, Report No 3024, Lund.

Falk, J. and Niemczynowicz (1978). Characteristics of the Above-Ground Runoff in Sewered Catchments. Proc. 1st Int. Conference on Urban Drainage, University of Southampton, Editor P.R. Helliwell, Pentech Press, London, U.K.

Fawkes, P.E. (1972). Roughness in a Model of Overland Flow. M.S. Thesis, Colorado State University, Fort Collins, Colorado.

Geiger, W. (1984). Goodness and Limits in Urban Runoff Modelling. Proc. 3rd Int. Conf. on Urban Storm Drainage, Vol. 2, Göteborg.

Grace, R.A. and Eagleson, P.S. (1966). The Modeling of Overland Flow. Water Resources Research, Vol. 2, No. 3, third quarter 1966.

Hager, W. (1985). Effects of Excess Rainfall Time Distribution on Catchment Area Hydrograph. (To be published in Nordic Hydrology).

Haegerström, J., Melin, H., Ryberg, M. (1978). Urban Runoff Modelling in Two Housing Areas in Linköping. Chalmers University of Technology, Department of Hydraulics, Master of Science Thesis Work 1976:1.

Henderson, F.M. (1963). Flood Waves in Prismatic Channels. Journal of the Hydraulics Division, ASCE, HY 4, July 1963.

Horton, R.E. and Leach, H. R., van Vliet, R. (1934). Laminar Sheet-Flow. Transactions, American Geophysical Union. Hydrology Reports and Papers, 1934.

Huber, W.C. (1977). Interim Documentation. Release of EPA SWMM. Draft Report. National Environmental Research Center, Office of Research and Development, U S Environmental Protection Agency, Cincinnati, Ohio.

Izzard, C.F. (1944). The Surface-Profile of Overland Flow. Transactions, American Geophysical Union, Part VI, 1944.

Jacobsen, P. (1980). Urban Surface Runoff Simulation. Technical University of Denmark, Department of Sanitary Engineering, Rep. 80-51, Lyngby.

Jensen, M. (1981). Urban Catchment Simplification Based on Rational Method Design and Kinematic Wave Analysis. Technical University of Denmark. Department of Environmental Engineering. Report No 81-54, Lyngby.

Jensen, M. (1984). A Method for Simplified Urban Catchment Description. Proc. 3rd International Conference on Urban Storm Drainage, Vol. 1, Göteborg.

Johannisson, T., Lindblad T. (1978). Calibration of Weirs for Flow Measurements in Manholes. Chalmers University of Technology, Department of Hydraulics, Master of Science Thesis Work 1977:3.

Johansen, L. (1979). Design Rainfalls for Sewer Systems. Report 79-2. Department of Sanitary Engineering, Technical University of Denmark, Köpenhamn (In Danish).

Johansson, H., Bernhardsson, P-A. (1981). Urban Runoff Measurements in an Asphalt Catchment. Chalmers University of Technology, Department of Hydraulics, Master of Science Thesis work 1980:2. Göteborg. (In Swedish).

Kibler, D.F. and Woolhiser, D.F. (1970). The Kinematic Cascade as a Hydrologic Model. Colorado State University, Hydrology Papers, No. 39, Fort Collins, Colorado.

Kibler, D.F. and Woolhiser, D.A. (1972). Mathematical Properties of the Kinematic Cascade. Journal of Hydrology, No. 15.

Kidd, C.H.R. (1978). Rainfall - Runoff Process over Urban Surfaces. Proc. of an International Work held at IH, April 1978. Institute of Hydrology, Wallingford, Oxon, U.K.

Kisisel, I.T. and Rao, A.O. (1973). Turbulence in Shallow Water Flow under Rainfall. Journal of Engineering Mechanics Division, ASCE, EM1, Feb. 1973.

Kousis, A.D. (1983). Unified Theory for Flood and Pollution Routing. Journal of Hydraulics Division, ASCE, HY 12, December 1983.

Langford, K.J. and Turner, A.K. (1972). An Experimental Study of the Application of Kinematic-Wave Theory to Overland Flow. Journal of Hydrology, No. 18.

Laws, O.J. and Parsons, D.A. (1943). The Relation of Raindrop-Size to Intensity. American Geophysical Union, Transactions Part 2, Twenty-Fourth Annual Meeting, April 23-24, 1943.

Li, R-M, Simons, D.B. and Stevens, M.A. (1975a). Nonlinear Kinematic Wave Approximation for Water Routing. Water Resources Research, Vol. 11, No. 2, April 1975.

Li, R-M, Simons, D.B. and Stevens, M.A. (1975b). On Overland Flow Water Routing. National Symposium on Urban Hydrology and Sediment Control, University of Kentucky, Lexington, KY, July 28-31, 1975.

Lighthill, M.J. and Whitham, G.B. (1955). On kinematic waves: 1. Flood movement in long rivers. Proc. Royal Soc. of London, Ser. A, Vol. 229.

Ligget, J.A. and Woolhiser, D.A. (1967). Different Solutions of the Shallow-Water Equation. Journal of the Engineering Mechanics Division, EM 2, April 1967.

Ligget, J.A. (1975). Basic Equation of Unsteady Flow. Unsteady Flow in Open Channels, Vol. I, Water Resources Publ. Fort Collins, Colorado.

Lindholm, O. (1975). System Analysis of Sewage Systems, Prosjektkomitéen for rensning av avlöpsvann, Pra 1, Oslo.

Linsley, R.K., Kohler, M.A. and Paulhus, J.L.H. (1975). Hydrology for engineers. McGraw-Hill Book Company, Second ed. New York (ISBN 0-07-037967-3).

Lyngfelt, S. (1975). Rainfall - Runoff Studies in Bergsjön, Göteborg. Chalmers University of Technology, Urban Geohydrological Research Group, No 15, Göteborg. (In Swedish).

Lyngfelt, S. (1978). An Analysis of Parameters in a Kinematic Wave Model of Overland Flow in Urban Areas. Chalmers University of Technology, Department of Hydraulics, Series B, No. 13, Göteborg.

Lyngfelt, S. (1979). On Numerical Solutions of the Kinematic Wave Equations Used in Overland Flow. Lecture at Nordic Seminar on Overland Flow, Lund.

Lyngfelt, S. (1981). Design of Storm Sewer Systems. The Rational Method. Chalmers University of Technology, Urban Geohydrological Reserach Group, No 56, Göteborg. (In Swedish).

Lyngfelt, S. and Svensson, G. (1983). Storm Water Runoff from Large Urban Catchments. Methodology of Simulation Tested in Göteborg. Chalmers University of Technology, Urban Geohydrological Research Group, No. 68, Göteborg. (In Swedish).

Lyngfelt, S. (1985). Manual for the Urban Runoff Model CURE. Chalmers University of Technology, Department of Hydraulics, Report Series B:47, Göteborg. (In Swedish).

Marsalek, J. (1983). SWMM Model and Level of Discretization. Journal of Hydraulics Division, ASCE, Vol. 109, December 1983.

Mitchell, J.K. and Jones, Jr, B.A. (1976). Micro-Relief Surface Depression Storage: Analysis of Models to Describe the Depth-Storage Function. Water Resources Bulletin. Vol. 12, No. 6, December 1976.

Morgali, J.R. (1970). Laminar and Turbulent Overland Flow Hydrographs. Journal of the Hydraulics Division, ASCE HY 2, February 1970.

Morris, E.M. (1979). The Effect of the Small-Slope Approximation and Lower Boundary Conditions on Solutions of the Saint-Venant Equations. Journal of Hydrology, No. 40 (1979).

Morris, E.M. and Woolhiser, D.A. (1980). Unsteady One-Dimensional Flow Over a Plane: Partial Equilibrium and Recession Hydrographs. Water Resources Research, Vol. 16, No. 2, April.

National Water Council (1981). Design and Analysis of Urban Storm Drainage. The Wallingford Procedure - in five volumes. NWC London.

Newton, S.G. and Painter R.B. (1974). A Mathematical Examination of Urban Runoff Prediction. Proceedings of the Institution of Civil Engineers, Vol. 57, U.K.

Niemczynowicz,J. (1984). An Investigation of the Areal and Dynamic Properties of Rainfall and its Influence on Runoff Generating Processes. Lund Institute of Technology, Department of Water Resources Engineering, Report No 1005, Lund.

Nittim, R. (1977). Overland Flow on Impervious Surface. Water Research Laboratory. University of New South Wales. Report No 151. NSW Monly Vale N.S.W. Australia.

Nordqvist, H., Karlsson, B. (1982). Urban Runoff from a Great Asphalt Surface. Chalmers University of Technology, Department of Hydraulics, Master of Science Thesis Work 1981:3.

Parlange, J.Y., Rose, C.W. and Sander, G. (1981). Kinematic Flow Approximation of Runoff on a Plane: An Exact Analytical Solution. Journal of Hydrology, No. 52.

Papadakis, C. and Preul, H.C. (1972). University of Cincinnatti Urban Runoff Model. Journal of Hydraulics Division, ASCE, Vol. 98, HY10, October 1972

Pecher, R. (1970). Die zeitliche Abhängigkeit des Abflussbeiwertes von der Regendauer und der Regenintensität. g.w.f. - Wasser/Abwasser, 111 (1970) H8.

Pecher, R. (1969). Der Abflussbeiwert und seine Abhängigkeit von der Regendauer. Berichte aus dem Institut für Wasserwirthschaft und Gesundheitsingenieurwesen, Technische Hochschule München, No. 2, München.

Pethick, R.W. (1982). Kinematic Wave Calculations of Peak Flow Reductions in Urban Storm Runoff. Hydraulics Researcn Station, Wallingford, Oxon, U.K.

Phelps, H.O. (1975). Shallow Laminar Flows over Rough Granular Surfaces. Journal of the Hydraulics Division, HY 3, March 1975.

Ponce, V.M. and Simons, D.B. (1977). Shallow Wave Propagation in Open Channel Flow. Journal of Hydraulics Division, ASCE, HY12, December.

Ponce, V.M. and Simons, D.B. (1978). Applicability of Kinematic and Diffusion Models. Journal of Hydraulics Division, ASCE, H3, March.

Ponce, V.M. and Theurer, F.D. (1982). "Accuracy in Diffusion Routing". Journal of the Hydraulics Division, ASCE, Hy 6, December.

Price, R.K. (1980a). Flout - A River Catchment Flood Model. Hydraulics Research Station, Report IT 168, Wallingford, Oxon, U.K.

Price, R. K (1980b). Numerical Solutions of the Kinematic Wave Equation. Nordic Seminar on Calculation of Unsteady Flow in Storm Sewer Networks, October 7-8, Chalmers University of Technology, Göteborg.

Price, R.K. (1980c). Flow Routing for River Regulation. "Engineering Problems in the Management of Gravel-Bed Rivers". International Workshop, Newton, June 1980.

Proctor and Redfern Ltd and James F. McLaren Ltd (1976). Storm Water Management Model Study, Vol. 1. Research Program for the Abatement of the Municipal Pollution under Provision of the Canada-Ontario Agreement on Great Lakes Water Quality. Research Report No. 47, Toronto.

Rovey, E.D. and Woolhiser, D.A. (1977). A Distributed Kinematic Model of Upland Watersheds. Colorado State University, Hydrology Paper No 93, Fort Collins, Colorado.

Shaake, J.C., Geyer, J.C. and Knapp, J.W. (1967). Experimental Examination of the Rational Method. Journal of Hydraulics Division, ASCE, HY6, November 1967.

Shen, H.W. and Li, R-M (1973). Rainfall Effect on Sheet Flow Over Smooth Surfaces. Journal of the Hydraulics Division, HY 5, May 1973.

Shilling, W. (1984). A Quantitative Asessment of Uncertainties in Stormwater Modelling. Proc. 3rd Int. Conf. on Urban Storm Drainage, Volume 2, Göteborg.

Singh, V.P. (1976). A Distribution Converging Overland Flow Model. 3. Application to Natural Watersheds. Water Resources Research, Vol. 12, No. 5, October 1976.

Singh, V.P. (1975): Derivation of Surface Water Lag Time for Converging Overland Flow. Water Resources Bulletin, AWRS, Vol. 11, No. 3, June 1975.

Singh, V.P. (1977). Estimation of Parameters of a Uniformly Nonlinear Surface Runoff Model. Nordic Hydrology, No. 8, 1977.

Sjöberg, A. (1976). Calculation of Unsteady Flows in Regulated Rivers and Storm Sewer Systems. Chalmers University of Technology, Department of Hydraulics, Report Series A:6, Göteborg (In Swedish).

Sjöberg, S. et al. (1979). Manual for ILLUDAS (Version S2). A Computer Program for Design and Analysis of Storm Water Systems. Chalmers University of Technology, Department of Hydraulics, Report Series B, No 14, Göteborg. (In Swedish).

Sjöberg, A. (1981). The Sewer Network Models DAGVL-A and DAGVL-DIFF. Chalmers University of Technology, Department of Hydraulics, Report Series B, No 28, Göteborg.

Smith, A.A. (1980). A Generalized Approach to Kinematic Flood Routing. Journal of Hydrology, No 45.

Strömvall, L., Andersson, M. (1976). Urban Runoff Modelling in Two Urban Catchments in Göteborg and Oslo. Chalmers University of Technology, Department of Hydraulics, Master of Science Thesis Work 1975:7. Göteborg (In Swedish).

Svensson, G. and Ören, K. (1976). Planning models for Storm Water. Chalmers University of Technology, Urban Geohydrological Research Group, No. 41, Göteborg.

VAV, Swedish Water and Wastwater Works Association (1976). Manual for Design of Sewer Systems. VAV Publ. P28, Stockholm (in Swedish).

Woo, D-C and Brater, E.F. (1962). Spatially Varied Flow from Controlled Rainfall. Journal of the Hydraulics Division, HY 6, November 1962.

Wooding, R.A. (1965). A Hydraulic Model for the Catchment-Stream Problem. I. Kinematic-wave theory. Journal of Hydrology. No. 3, 1965.

Woolhiser, D.A. and Liggett, J.A. (1967). Unsteady, One-Dimensional Flow over a Plan - the Rising Hydrograph. Water Resources Research, Vol. 3, No. 3.

Woolhiser, D.A. (1975). Simulation of Unsteady Overland Flow in Open Channels, Vol. II, Water Resources Publ. Fort Collins, Colorado.

Yen, B.C., Wenzel, H.G. Jr. and Yoon, Y.N. (1972). Resistance Coefficients for Steady Spatially Varied Flow. Journal of the Hydraulics Division, HY 8, August 1972.

Yen, B.C., Chow, W.T. and Akan, A.O. (1977). Storm Water Runoff on Urban Areas of Steep Slope. Environmental Protection Agency, Municipal Environmental Research Laboratory, Environmental Protection Technology Series, EPA-600/2-77-168, Cincinnati, Ohio.

Yevjevich, V. (1975). Unsteady Flow in Open Channels. Vol. I, Water Resources Publ., Fort Collins, Colorado.

Yoon, Y.N. and Wenzel, H.G. Jr. (1971). Mechanics of Sheet Flow under Simulated Rainfall. Journal of the Hydraulics Division, HY 9, September 1971.

Yu, Y.S. and McNown, J.S. (1964). Runoff from Impervious Surfaces. Journal of Hydraulic Research, Vol. 2, No. 1.

Zaghloul, N. (1981). SWMM Model and Level of Discretization. Journal of Hydraulics Division, ASCE, HY11, June.

LIST OF FIGURES

		Page
Figure 2.2.1	Typical intensity variations for a storm event	6
Figure 2.2.2	IDF-diagrams used in Göteborg, after VAV (1976)	6
Figure 2.2.3	Water surface at constant rain-intensity and rain velocity vectors	7
Figure 2.3.1	Water surface profiles when the rain intensity is constant and the time $t < t_c$. (The scaling of water depths is not realistic).	8
Figure 2.3.2	Water profiles when $i=0$ and $t>t_c$ (The scaling of water depths is not realistic)	9
Figure 2.3.3	A part of a street with gutter, pavement and inlet	10
Figure 2.4.1	Gutter flow with lateral inflow	12
Figure 2.5.1	Network system of the band- and the tree type	13
Figure 3.3.1	Characteristic directions in sub- and supercritical flow	19
Figure 3.5.1	The relation between the celerity c^*, the wave number σ_o and the Froude number F_o (after Ponce and Simons (1977)).	24
Figure 3.5.2	The relation between the logarithmic decrement $-\delta = \ln(a_1/a_2)$, the wave number σ_o and the Froude number F_o. (After Ponce and Simons (1977)).	25
Figure 4.2.1	Kinematic characteristics in the case of lateral and upstream inflow	30
Figure 4.2.2	Converging surface (after Singh (1976))	31
Figure 4.2.3	A system of kinematic characteristics in the case of lateral inflow only	33
Figure 4.2.4	The lateral inflow	36
Figure 4.2.5	Outflow hydrographs from an asphalt surface derived by the kinematic equations	37
Figure 4.2.6	Comparison between rising hydrographs calculated with and without lateral momentum	39

Figure 4.2.7 Two characteristics emanating from the upstream boundary 40

Figure 4.2.8 The kinematic solution in a case of intersecting characteristics (physically unrealistic). 42

Figure 4.2.9a,b Dimensionless partial equilibrium hydrographs. D* is the dimensionless time at which the lateral inflow ceases (after Morris and Woolhiser (1980)). 43

Figure 4.3.1 Dimensionless partial equilibrium hydrograph. D* is the dimensionless time at which the lateral inflow ceases (after Morris and Woolhiser (1980)) 49

Figure 5.2.1 "Slopes" of the friction factor relation used in different friction formulas 57

Figure 5.3.1 Values of the friction factor f measured for flow without rain over glass after Nittim (1977) 59

Figure 5.3.2 a,b Tests on the impact of rain on flow over a smooth surface (U_i=raindrop velocity) After Shen and Li (1973) (1 μm/s = 10 l/s·ha) 60

Figure 5.3.2 c,d Tests on the impact of rain on flow over a smooth surface (U_i=raindrop velocity) after Nittim (1977). (1 μm/s = 10 l/s·ha) 61

Figure 5.3.3 Flow without rain-effects of the relative roughness on the friction factor f, after Phelps (1975) 63

Figure 5.3.4 Friction factors at flow without rain (sphere roughness k=2.33 mm) after Nittim (1977) 64

Figure 5.3.5 a-b The friction factor versus Reynolds' number at i=210 l/s·ha and i=116 l/s·ha, after Woo and Brater (1962) 65

Figure 5.3.6 Flow without rain-friction factor versus Reynolds' number for an asphalt surface. After Nittim (1977) 67

Figure 5.3.7 a,b Friction factor versus Reynolds' number for a concrete and asphalt surface after Yu and McNown (1964) and Nittim (1977), (1 μm/s = 10 l/s·ha) 69

Figure 5.6.1 Comparison of the fitted friction-relation with Nittim's (1977) and Yu and McNown's (1963) (shaded) tests on asphalt and concrete 73

Figure 6.2.1 The x-t plane with fixed gridpoints and boundaries 78

Figure 6.2.2 An example of a two step explicit scheme 79

Figure 6.3.1 Grid points in an arbitrary finite box 80

Figure 6.3.2 The relation between the centrepoint and weighting factors after Smith (1980) 81

Figure 6.3.3 An example of unstable solutions (with shots) compared with one having a suitable attenuation (L_s=20 m, s_s=0.035, n=0.016) 85

Figure 6.3.4 Dimensionless rising hydrographs obtained from the diffusive box model using various values of Δx (after Lyngfelt (1978)). 86

Figure 6.3.5 Dimensionless rising hydrographs obtained by the shallow water equations for various kinematic wave numbers and F_o=1 (after Woolhiser (1967)). 87

Figure 6.4.1 Test surface for numerical experiments. 90

Figure 6.4.2 Hyetograph used in numerical tests 91

Figure 6.4.3 a,b Hydrographs simulated by the diffusive box model (L_s=20 m, S_s=.035, n=0.016 K_o=230). 93

Figure 6.4.4 Comparison between α- and β-diffusive models (L_s= 20 m, S_s = 0.035, n= 0.016) 97

Figure 6.7.1 Comparison between the diffusive wave and weighted box solution (L_s=20 m, S_s=0.018, n=0.016) 102

Figure 7.3.1 Hypothetical time-area diagrams 114

Figure 7.3.2 Principal shapes of runoff hydrographs obtained by the Time-Area Method (curve b) and the β-diffusive model (kinematic wave) 114

Figure 7.3.3 Principal shapes of runoff hydrographs obtained by the time area method (curve (a)) and the β-diffusive model (kinematic wave) 115

Figure 7.3.4 Time-area curves giving the 'best fit' of the rising- and recession parts of the runoff in surface flow 116

Figure 7.3.5 Time-area curves giving the 'best fit' of the rising- and recession parts of the runoff from the surface-gutter catchment at $t_c = \left[\left[t_c\right]_s + \left[t_c\right]_g\right]_{min}$ 117

Figure 7.3.6 Time area diagrams obtained by numerical simulation of the rising part of constant rain intensity storms for four residential areas, after Lyngfelt (1981) 117

Figure 8.4.1 Recorded and simulated runoff from the PASP catchment (input data version 3) 127

Figure 8.4.2 Recorded and simulated runoff from the COMP-catchment (input data version 3) 128

Figure 8.5.1 Representation of base catchments by three and four parameters in the kinematic wave model. 132

Figure 8.5.2 Representation of a base catchment by six parameters in the kinematic wave model 133

Figure 8.5.3 Representation of the catchment by the KW6S model 134

Figure 8.5.4 Example of a model structure containing only KW6S units, the KW6S-S model 135

Figure 8.5.5 Four alternative sewer structures. To each of the inlets identical KW4G models are connected. 137

Figure 8.5.6 Sensitivity of the KW6S-model corresponding to $0.7t_c$ and $1.3t_c$ 143

Figure 8.5.7 Sensitivity of the KW3-model corresponding to $0.7t_c$ and $1.3t_c$ 143

Figure 8.6.1 Example of effects of using different time-area curves 145

Figure 8.6.2 Example of variations in hydrograph shape caused by variations in time of concentration 147

Figure 10.3.1 Distribution functions for MAI-storms and maximum discharge (after Arnell, Lyngfelt 1975) 161

Figure 10.6.1 The sewer network of Bergsjön (after Arnell (1982)) 165

Figure 10.6.2 The distribution function for the discharge in point 9 in Bergsjön (see appendix II) after Arnell (1982) with the Rational Method points included. 165

Figure 10.6.3 The distribution function for the discharge in point 24 in Bergsjön (see appendix II) after Arnell (1982) with the Rational Method points included. 166

Figure 10.6.4 The distribution function for the discharge in point 73 in Bergsjön (see appendix II) after Arnell (1982) with the Rational Method points included. 166

LIST OF TABLES

		Page
Table 6.3.1	Weighted box models	84
Table 6.4.1	Tested numerical models	91
Table 6.4.2	Optimal β-values ($\Delta x/L < 1/4$)	96
Table 8.2.1	Main characteristics of the catchments	122
Table 8.4.1	Mean ratio λ_p, standard deviation σ_p and absolute error ε_p for not volume fitted data and volume fitted data for each catchment.	138
Table 8.5.1	Number of routing units for different test area and geometric models	139
Table 8.5.2	Number of free parameters used in different test areas with different geometric models	139
Table 8.5.3	Statistical parameters for the simplified geometrical models compared with the DET-model (five peaks in each of the four greatest catchments)	140
Table 8.5.4	Variation intervals for λ_p for the simplified geometric models (five peaks in each of the four greatest catchments)	141
Table 8.5.5	The effects on the attenuation of varying the parameters in the models (corresponding to a variation in (t_c)	142
Table 8.6.1	Statistical parameters for the Time-Area Method compared with the DET-model (five peaks in each of the four greatest catchments)	146
Table 8.6.2	The effects of varying the time of concentration in the Time-Area Method	146
Table 9.2.1	Mean ratio λ_p, standard deviation σ_p and absolute error ε_p for recorded and simulated flow peaks in Bergsjön and Linköping 2.	152
Table 9.3.1	Statistical parameters for simulated flow peaks in the Linköping 2 and Bergsjön areas	153
Table 9.3.2	λ_p values for different times of concentration in Bergsjön	154
Table 9.4.1	Statistical parameters for the Time Area Method compared with the DET-model	155
Table 9.4.2	Variation of the time of concentration using the Time-Area Method in Bergsjön	156

Preceding page blank

Department of Hydraulics
Chalmers University of Technology

Report Series A

A:1 Bergdahl, L.: Physics of ice and snow as affects thermal pressure. 1977.

A:2 Bergdahl, L.: Thermal ice pressure in lake ice covers. 1978.

A:3 Häggström, S.: Surface Discharge of Cooling Water. Effects of Distortion in Model Investigations.1978

A:4 Sällgren, A.: Slurry Transportation of Ores and Industrial Minerals in a Vertical Pipe by Centrifugal Pumps. 1978.

A:5 Arnell, V.: Description and Validation of the CTH-Urban Runoff Model. 1980.

A:6 Sjöberg, A.: Calculation of Unsteady Flows in Regulated Rivers and Storm Sewer Systems. (in Swedish). 1976.

A:7 Svensson, T.: Water Exchange and Mixing in Fjords. Mathematical Models and Field Studies in the Byfjord. 1980.

A:8 Arnell, V.: Rainfall Data for the Design of Sewer Pipe Systems. 1982.

A:9 Lindahl, J. och Sjöberg, A.: Dynamic Analysis of Mooring Cables. 1983.

A:10 Nilsdal, J-A.: Optimeringsmodellen ILSD. Beräkning av topografins inverkan på ett dagvattensystems kapacitet och anläggningskostnad. 1983.

A:11 Lindahl, J.: Implicit numerisk lösning av rörelseekvationerna för en förankringskabel. 1984.

A:12 Lindahl, J.: Modellförsök med en förankringskabel. 1985.

A:13 Lyngfelt, S.: On Urban Runoff Modelling. Application of Numerical Models based on Kinematic Wave Theory. 1985.

Report Series B

B:1 Bergdahl, L.: Beräkning av vågkrafter. 1977. (Ersatts med 1979:07).

B:2 Arnell, V.: Studier av amerikansk dagvattenteknik. 1977.

B:3 Sellgren, A.: Hydraulic Hoisting of Crushed Ores. A feasibility study and pilot-plant investigation on coarse iron ore transportation by centrifugal pumps. 1977.

B:4 Ringesten, B.: Energi ur havsströmmar. 1977.

B:5 Sjöberg, A. och Asp, T.: Brukar-anvisning för ROUTE-S. En matematisk modell för beräkning av icke-stationära flöden i floder och kanaler vid strömmande tillstånd. 1977.

B:6 Annual Report 1976/77.

B:7 Bergdahl, L. and Wernersson, L.: Calculated and Expected Thermal Ice Pressures in Five Swedish Lakes. 1977.

B:8 Göransson, C-G and Svensson, T.: Drogue Tracking - Measuring Principles and Data Handling.

B:9 Göransson, C-G.: Mathematical Model of Sewage Discharge into confined, stratified Basins - Especially Fjords.

B:10 Arnell, V. och Lyngfelt, S.: Beräkning av dagvattenavrinning från urbana områden. 1978.

B:11 Arnell, V.: Analysis of Rainfall Data for Use in Design of Storm Sewer Systems. 1978.

B:12 Sjöberg, A.: On Models to be used in Sweden for Detailed Design and Analysis of Storm Drainage Systems. 1978.

B:13 Lyngfelt, S.: An Analysis of Parameters in a Kinematic Wave Model of Overland Flow in Urban Areas. 1978.

B:14 Sjöberg, A. and Lundgren, J.: Manual for ILLUDAS (Version S2). Ett datorprogram för dimensionering och analys av dagvattensystem.

B:15 Annual Report 1978/79.

B:16 Nilsdal, J-A. och Sjöberg, A.: Dimensionerande regn vid höga vattenstånd i Göta älv.

B:17 Stöllman, L-E.: Närkes Svartå. Hydrologisk inventering.1979.

B:18 Svensson, T.: Tracer Measurements of Mixing in the Deep Water of a Small, Stratified Sill Fjord.

B:19 Svensson, T., Degerman, E., Jansson, B. och Westerlund,S.: Energiutvinning ur sjö- och havssediment. En förstudie. R76:1980.

Report Series B

B:20 Annual Report 1979

B:21 Stöllman, L-E.: Närkes Svartå. Inventering av vattentillgång och vattenanvändning. 1980.

B:22 Häggström, S. och Sjöberg, A.: Effects of Distortion in Physical Models of Cooling Water Discharge. 1979.

B:23 Sellgren, A.: A Model for Calculating the Pumping Cost of Industrial Slurries. 1981.

B:24 Lindahl, J.: Rörelseekvationen för en kabel. 1981.

B:25 Bergdahl, L. och Olsson, G.: Konstruktioner i havet. Vågkrafter-rörelser. En inventering av datorprogram.

B:26 Annual Report 1980.

B:27 Nilsdal, J-A.: Teknisk-ekonomisk dimensionering av avloppsledningar. En litteraturstudie om datormodeller. 1981.

B:28 Sjöberg, A.: The Sewer Network Models DAGVL-A and DAGVL-DIFF. 1981.

B:29 Moberg, G.: Anläggningar för oljeutvinning till havs. Konstruktionstyper, dimensioneringskriterier och positioneringssystem. 1981.

B:30 Sjöberg, A. och Bergdahl, L.: Förankringar och förankringskrafter. 1981.

B:31 Häggström, S. och Melin, H.: Användning av simuleringsmodellen MITSIM vid vattenresursplanering för Svartån.

B:32 Bydén, S. och Nielsen, B.: Närkes Svartå. Vattenöversikt för Laxå kommun. 1982.

B:33 Sjöberg, A.: On the stability of gradually varied flow in sewers. 1982.

B:34 Bydén, S. och Nyberg, E.: Närkes Svartå. Undersökning av grundvattenkvalitet i Laxå kommun.

B:35 Sjöberg, A. och Mårtensson, N.: Regnenveloppmetoden. En analys av metodens tillämplighet för dimensionering av ett 2-års perkolationsmagasin.

B:36 Svensson, T. och Sörman, L-O.: Värmeupptagning med bottenförlagda kylslangar i stillastående vatten. Laboratorieförsök

B:37 Mattsson, A,: Koltransporter och kolhantering. Lagring i terminaler och hos storförbrukare. (Delrapport).

B:38 Strandner, H.: ILL-DIFF. Ett datorprogram för sammankoppling av ILLUDAS och DAGVL-DIFF, 1983.

Report Series B

B:39 Svensson,T. och Sörman,L-O.: Värmeupptagning med bottenförlagda slangar i rinnande vatten. Laboratorieförsök.

B:40 Mattsson,A.: Koltransporter och kolhantering. Lagring i terminaler och hos storförbrukare. Kostnader. Delrapport 2.

B:41 Häggström,S. och Melin,H.: Närkes Svartå. Simuleringsmodellen MITSIM för kvantitativ analys i vattenresursplanering. Inst.f.Vattenbyggnad, CTH. Göteborg 1983.

B:42 BFR - R60:1984. Hård,S.: Seminarium om miljöeffekter vid naturvärmesystem. Dokumentation sammanställd av S.Hård, VIAK AB.

B:43 Lindahl,J.: Manual för MODEX-MODIM. Ett datorprogram för simulering av dynamiska förlopp i förankringskablar. Göteborg 1983.

B:44 Activity Report. Göteborg 1984.

B:45 Sjöberg, A: DAGVL-DIFF. Beräkning av icke-stationära flödesförlopp i helt eller delvis fyllda avloppssystem, tunnlar och kanaler.

B:46 Bergdahl,L. och Melin, H.: WAVE FIELD. Manual till ett program för beräkning av ytvattenvågor.

B:47 Manual för dagvattenmodellen CURE av Sven Lyngfelt. 1985.

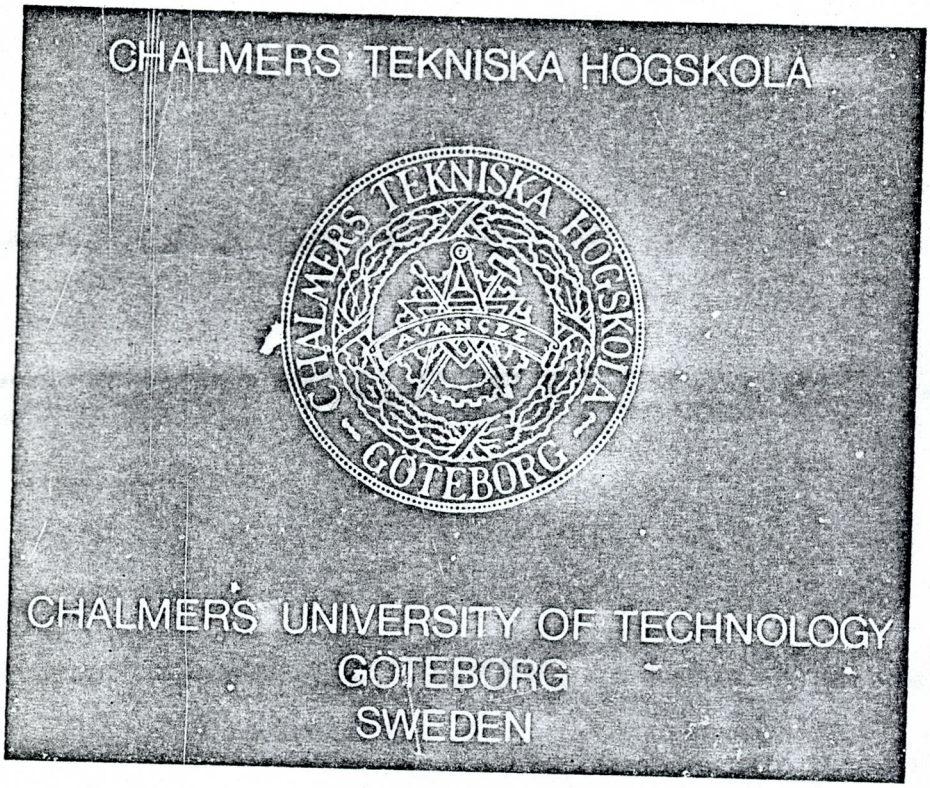

On Urban Runoff Modelling

The Application of Numerical Models Based on the Kinematic Wave Theory

Volume II

by

Sven Lyngfelt

Report Series A:13
Department of Hydraulics
Chalmers University of Technology
1985

CHALMERS TEKNISKA HÖGSKOLA

CHALMERS UNIVERSITY OF TECHNOLOGY
GÖTEBORG
SWEDEN

On Urban Runoff Modelling

The Application of Numerical Models Based on the Kinematic Wave Theory

Volume II

by

Sven Lyngfelt

Report Series A:13
Department of Hydraulics
Chalmers University of Technology
1985

Institutionen för Vattenbyggnad
Chalmers Tekniska Högskola

Department of Hydraulics
Chalmers University of Technology

On Urban Runoff Modelling

The Application of Numerical Models Based on the Kinematic Wave Theory Volume II

Sven Lyngfelt

Report
Series A:13
ISSN 0348-1050

Göteborg 1985

Address: Department of Hydraulics
Chalmers University of Technology
S-412 96 Göteborg, Sweden

Telephone: 031/81 01 00

2-1.a.

PREFACE

This part, Volume II, of the report contains two appendices. In the first, catchments and rain intensity runoff measurements used in the simulations are described. In appendix II, simulated hydrographs are presented. The documentation in this volume gives an important background for the discussion in the chapters 8 to 10 in Volume I. Regarding appendix II it was considered suitable to gather all hydrographs into one place in the report.

LIST OF CONTENTS

PREFACE I

CONTENTS III

APPENDIX I - TEST AREAS AND MEASUREMENTS

I:1	Introduction	1
I:2	Test areas larger than 1 hectar	1
I:2.1	General	1
I:2.2	The Bergsjön catchment	2
I:2.3	The Linköping 2 catchment	3
I:2.4	Rain intensity - runoff measurements	4
I:3	The small test catchments	5
I:3.1	General	5
I:3.2	The air port surface AASP	6
I:3.3	The parking place PASP	7
I:3.4	The street surface SASP	8
I:3.5	Rain intensity - runoff measurements	9
I:4	The small test catchments in Bergsjön	10
I:4.1	General	10
I:4.2	The street catchment ASPH	11
I:4.3	The parking place PCON	12
I:4.4	The composite catchment COMP	13
I:4.5	Rain intensity - runoff measurements	13

APPENDIX II - SIMULATED AND RECORDED RUNOFF HYDROGRAPHS

II:1	Hydrographs from the small catchments (< 1 ha)	18
II:1.1	Comparison between the recorded and simulated runoff	18
II:1.2	Comparison; the detailed kinematic wave - KW6S-S and KW4G-I models	22
II:1.3	Comparison; the detailed kinematic wave - KW6S and KW3 models	34
II:1.4	Comparison; the detailed kinematic wave model and the Time-Area Method	44
II:2	Hydrographs from Bergsjön and Linköping 2	54
II:2.1	Comparison between the recorded and simulated runoff	54
II:2.2	Comparison; the detailed kinematic wave - KW6S-L1 and KW4G-I model	58
II:2.3	Comparison; the detailed kinematic wave -, KW6S-L2 and KW6S-L3 models	62
II:2.4	Comparison; the detailed kinematic wave model and the Time-Area Method	66

I TEST AREAS AND FIELD MEASUREMENTS

I:1 Introduction

Measurements of rain intensity and runoff in urban catchments have been performed over a number of years by the Department of Hydraulics in cooperation with the Department of Sanitary Engineering. The circumstances and objectives have varied between different locations causing differences in measuring techniques, sampling periods, evaluations, etc. In this appendix, catchments and measurements which have been used in chapters 8, 9 and 10 (Volume I) are described. The catchments which have had similar measuring techniques applied are described together.

In section I:2 the largest catchments used in the analysis are described. These have been used in earlier analyses for instance Arnell & Lyngfelt (1975), Arnell (1980), Lyngfelt (1981) and Arnell et al (1980).

In section I:3 the smaller catchments are described. The measurements have been published as Master of Science Theses; Ericsson et al (1978), Johansson et al (1981) and Nordqvist et al (1982).

In section I:4 the three smallest catchments are described. The measurements in these catchments have been performed using a central sampling unit, Lyngfelt (1975).

I:2 Test areas larger than 1 ha

I:2.1 General

Two large runoff catchments have been used in the report. These are mainly residential areas with some central buildings. With respect to building structure, topography structure of sewer net, etc., the areas are very different. For instance, the slopes of the main sewer systems

are 12 and 45°/oo, respectively, in the two areas.

The areas chosen may be regarded as typical for Sweden in all respects except for the available information and quality of the sewer system. In these respects the areas are probably better than the average.

I:2.2 The Bergsjön catchment

Bergsjön (15 ha) is a housing area NE of central Göteborg. It is situated about 90 m above sea level and is quite steep, although it has a flat central part. The runoff catchment is well delimited by a road and a mountain ridge. The suburb was built during the 60's and contains buildings with three and six storeys. In the area there are also two parking decks and a business location.

BERGSJÖN

Surface material	Area 10^4 m^2	Part of the total area %	Average slope ‰
Aspahlt, concrete	4.2	27	29
Roofs	1.6	11	30
Rocky areas	0.6	4	-
Lawns	3.4	22	65
Forest areas	4.3	28	100
Remaining areas	1.3	8	-
Total	15.4	100	

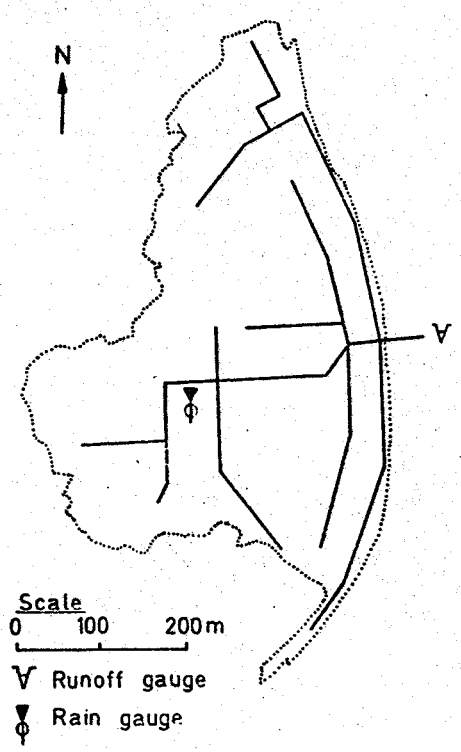

Figure I:2.1 The Bergsjön catchment, after Arnell (1980).

The catchment is drained by a separate urban stormwater system. The structure of the sewer net, measuring points and the sizes of different types of surfaces are illustrated in figure I:2.1 (see also Strömvall et al (1976)).

I:2.3 The Linköping 2 catchment

Linköping 2 (18.5 ha) is a part of a larger catchment, Linköping 1, Arnell (1980). The area is flat and contains link houses, villas and school premises. The catchment is

Surface material	Area 10^4 m^2	Part of the total area %	Average slope ‰
Streets/ sidewalks asphalt	3.3	18	5 - 50
Roofs	3.0	16	50 - 1000
Lawns	8.9	48	10 - 30
Bushes and forests	3.3	18	-
Total	18.5	100	

LINKÖPING 2

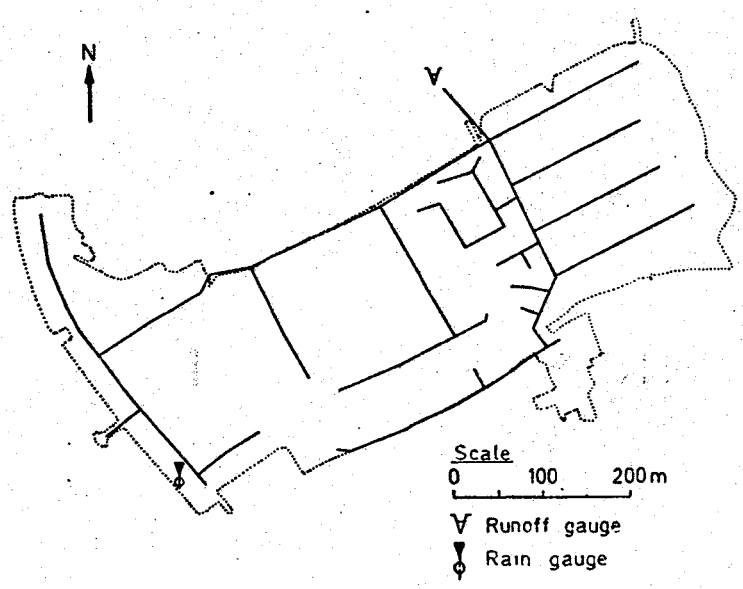

Figure I:2.2 The Linköping 2 catchment, after Arnell (1980).

drained by a separate urban stormwater system. The structure of the sewer net, measuring points and the distribution of different types of surfaces are illustrated in figure I:2.4.

I:2.4 Rain intensity - runoff measurements

Measurements in both areas are basically made in the same way with a rain gauge at one point in the catchment and a discharge measuring weir at the outlet. In Linköping 1 two precipitation recorders were installed and the flow was recorded in two points inside the catchment area.

The precipitation was measured by an instrument of the siphon type, which gives an accumulated precipitation curve on a chart recorder. The resolution in time is 1-2 minutes and in volume 0.05 mm.

The runoff was measured with different types of sharp-crested weirs. In Bergsjön, a pond was constructed at the outlet of the sewer system and in Linköping 2 the weir was installed in a manhole. The manhole arrangement was calibrated by model tests in the laboratory (Johanison et

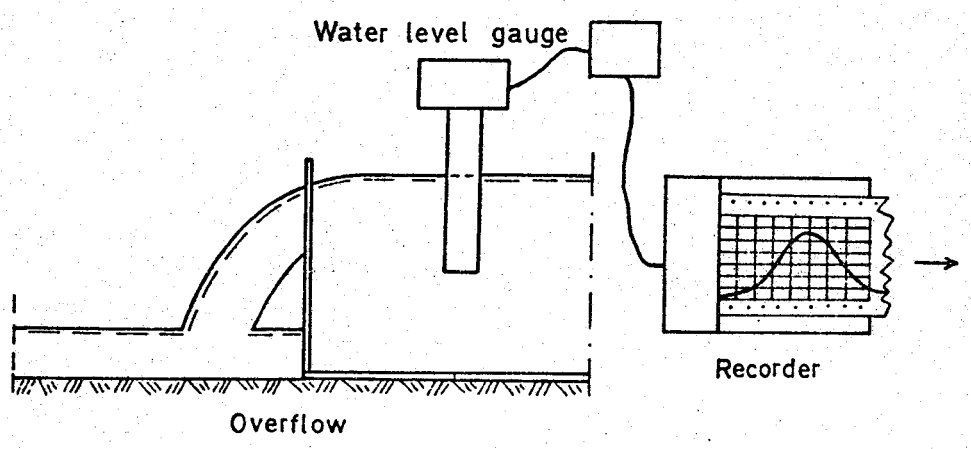

Figure I:2.3 Recorder and equipment for water level measurements.

al, 1981). Water level measurements were made by ultrasonic water level gauges (in Bergsjön a floating gauge) and were recorded on a chart recorder (resolution 1-2 minutes), see figure I:2.3.

As the rain intensity and runoff were recorded separately it was not possible to get perfect time coordination. Most of the obtained records were digitized and stored for computer evaluation (Arnell & Lyngfelt, 1975; Arnell et al, 1980). From these records, values of rain intensity and flow (in 1 minute intervals) for separate storms were evaluated and used in the model simulations.

Arnell (1980) analysed the sources of error in the measurements and found a total error of about ±15% for the rain intensity measurements and ±10-15% for the runoff measurements. This estimation can be regarded as an upper limit for errors in volume for separate storms. The error in single (or some) precipitation intensities and flow values might, however, be more than 15%.

From the rain intensity and runoff records it was possible to estimate the contributing runoff area and the average surface depression storage. Those parameters were calculated by regression analysis of rainfall and runoff volumes for all separate storms, see Arnell & Lyngfelt (1975) and Arnell (1980).

I:3 Small test areas

I:3.1 General

When discussing different approaches to base catchment modelling, it is of interest to compare simulated runoff with the corresponding measurements in small areas. A series of measurements has been made in such catchments. In this section three of them, where measurements and evaluations have been made in a similar way, are described.

The measurements were concentrated in a short period of the summer in order to obtain 5-10 separate, intensive storm events.

I:3.2 The airport surface AASP

The runoff area is one part of the so called freight apron at Landvetter airport (20 km E of Göteborg). The surface is situated at the side of the runway and is surrounded on two sides by permeable surfaces (grass and crushed stone respectively). The other sides are ridges that delimit the surface from other parts of the freight apron. From the ridges the surface slopes towards a low point line and the collecting sewer. The water is collected in 8 inlets 30 m apart, see figure I:3.1. The greatest flow-length of the surface is about 65 m and the average slope is $10^{o}/oo$. The collecting sewer has a diameter of Ø300 mm and the slope $2.5^{o}/oo$. The total catchment area is 10 130 m^2.

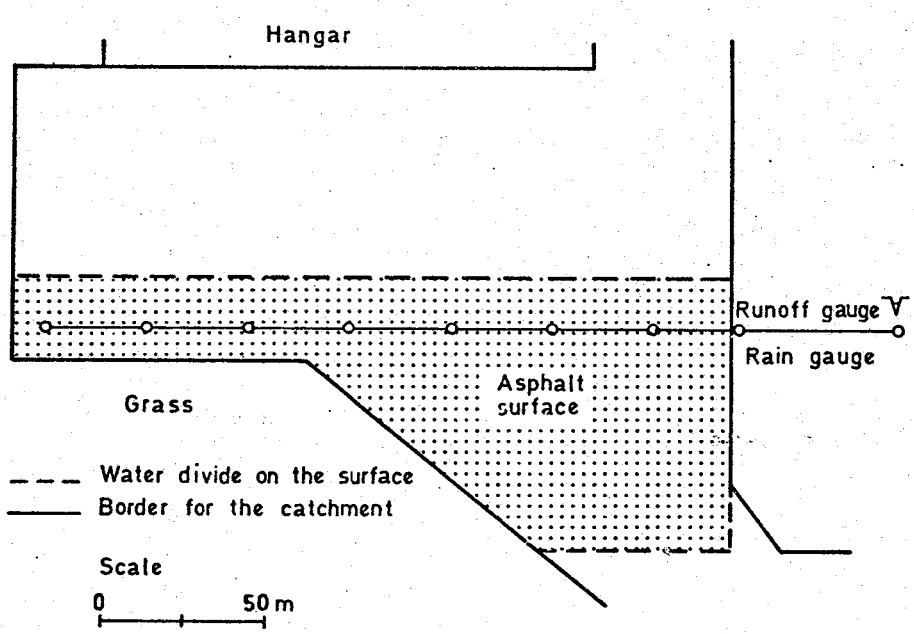

Figure I:3.1. The airport area AASP.

The area consists of even and easily defined asphalt surfaces. The location is advantageous as the area has low traffic load. The runoff area with measurements are also described by Nordqvist et al (1982).

I:3.3 The parking place PASP

The parking lot PASP is situated at Landvetter airport between two administration buildings. The area is delimited by these buildings and the kerbstone towards a grass area. At the entrance and exit the area is limited by ridges, see figure I:3.2. From the ridges the area slopes towards a low point line and the collecting sewer. At the upstream end of the sewer net there are three inlets, 30 m apart. The runoff area is quite evenly sloping with the greatest slope measured being 11°/oo. The greatest flow length is about 30 m. The diameter of the sewers is Ø300 mm, and the slope is 10°/oo. The runoff area is 4 260 m^2.

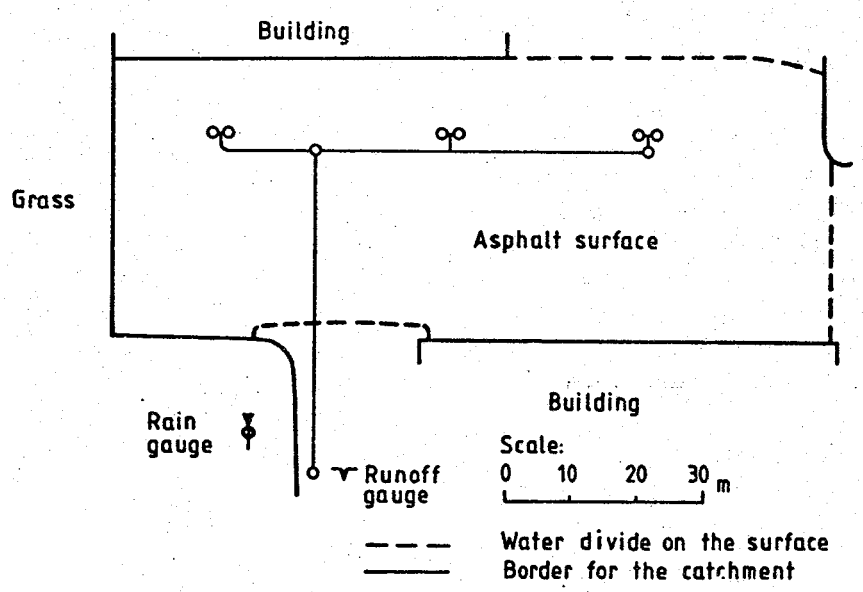

Figure I:3.2 The parking lot PASP.

The traffic load on the surface is low, and the area was not used as a car park during the measuring period. The runoff area, with measurements, is also described by Johansson et al (1981).

I:3.4 The street surface SASP

The runoff area is situated in a housing area in central Halmstad. The runoff surfaces consist of street surfaces, drained separately to a percolation pond. The streets are traditional with pavement and roadway (slope around 3%). The surfaces are in general well delimited by kerbstones and houses. The collecting sewers have the diameter Ø225 mm. The average slope in the network system is around 7°/oo. The sewer system was reconstructed when the percolation pond was built. The structure of the system is shown in figure I:3.3. The runoff area is 3 670 m^2.

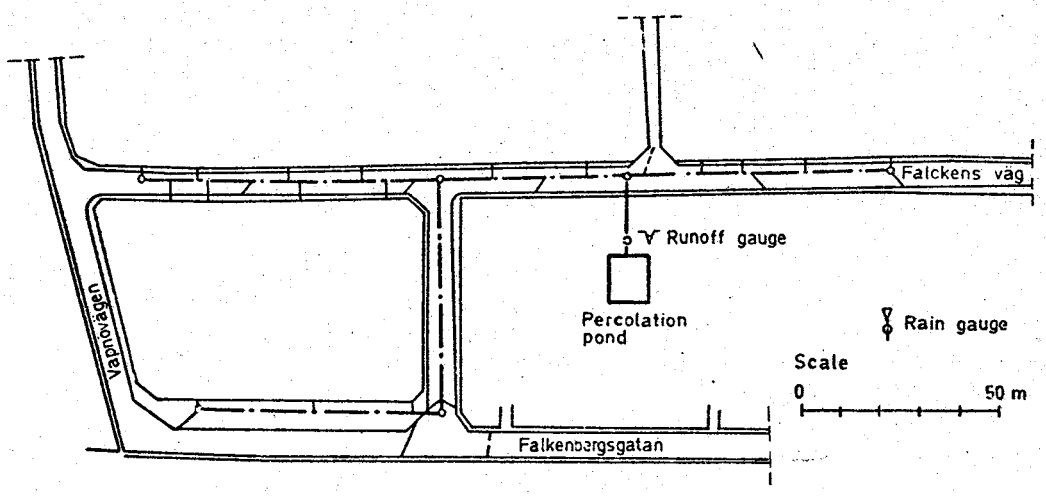

Figure I:3.3 The street surface SASP.

Mapping and precipitation-runoff measurements were made as a part of the analysis of the function of the percolation pond (Ericsson et al, 1978).

I:3.5 Rain intensity - runoff measurements

Measurement of rain intensity and discharge in the three areas were made in almost the same way as the measurements described in section II:2 and the same equipment was used as well. Although the catchments are small the characteristic times of concentration are long, for two of them longer than corresponding time in Bergsjön. For these areas the resolution in time can be regarded as acceptable. In the smallest catchment this resolution is too small. However, in this case the measuring pond showed significant influence on the attenuation of runoff. In view of this attenuation the resolution in this area can also be regarded as acceptable.

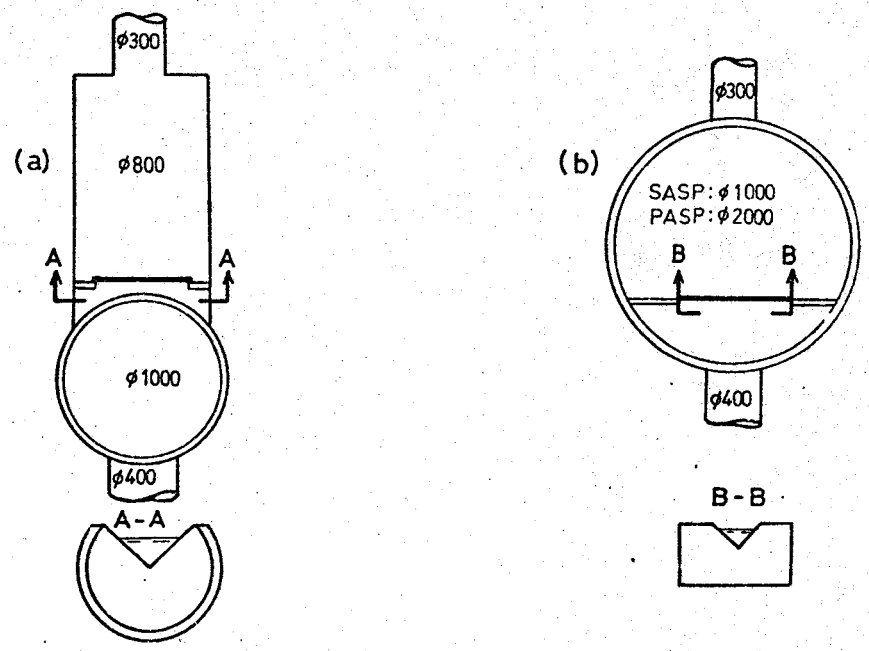

Figure I:3.4 a The measuring point at the AASP catchment.

b The measuring point at the PASP and SASP catchment.

The discharge measuring weirs have in all cases been located in manholes in the sewer system. The two measuring points at the airport were prepared for

measurement by increasing the manhole diameter in one case and, in the other, by enlarging the incoming pipe. The measuring points are shown in figure I:3.4.

None of the weirs have good inflow conditions. All measuring points were calibrated by using fire-hydrant water and fire-fighting water from a fire engine. Thus calibration flow corresponding to at least 80% of the highest runoff measured were obtained. The accuracy of flow values should therefore be at least as good as the one for large area measurements.

In each catchment the participating impermeable surface and depression storage was determined by linear regression analysis.

I:4 Small test catchments in Bergsjön

I:4.1 General

In Bergsjön initially five small areas were chosen for a close study:

* A small asphalt surface (street area)
* A roof surface (one half of an apartment house)
* A parking deck of concrete
* A grass surface
* A part of the catchment consisting of several roof and asphalt surfaces

The main objective was to get a basis for testing different runoff models. During the first measuring season there was no runoff from the grass surface although it was very large and had a steep slope (more than $100^{o}/oo$). The study of this surface was then suspended.

The "roof surface" catchment consists of half the roof surface of a roughly 100 m long block of flats (area about 800 m^2) with a collecting sewer at the side and the measuring point at one gable. A closer analysis of the runoff conditions showed that this system was heavily influenced by the collecting sewer. There was a depression about 10 m upstream of the measurement point, from which significant backwater effects were obtained. The test catchment was therefore not used in the final model simulations.

Analysing the runoff from small surfaces requires a higher resolution in time compared with the measurements described previously. Therefore a special data collecting system was built with a central unit where all data were registered on tape, see below, Lyngfelt (1975).

I:4.2 The street catchment ASPH

The area consists of a part of a road surface and a pavement that is drained through a gutter towards a gully. The gutter length is about 50 m. The runoff area is 430 m^2, see figure I:4.1.

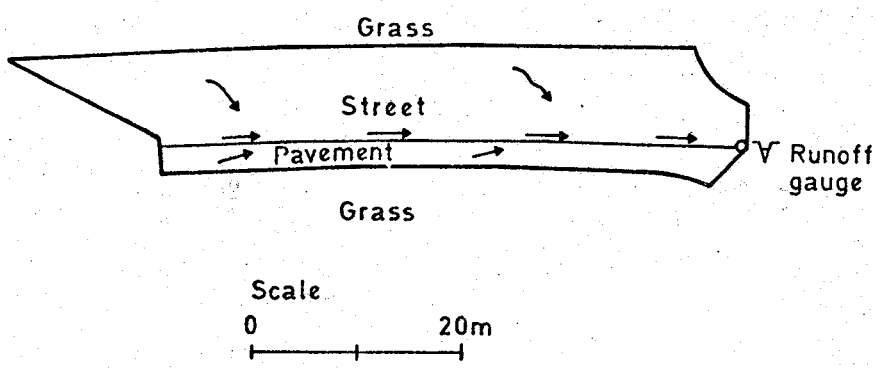

Figure I:4.1 The street catchment ASPH.

The water divide at the upstream end might be expected to vary a little with the flow during a rainfall. Therefore a dividing asphalt line was laid along this divide. This also continued over the gutter to prevent inflow from the upstream gutter.

The catchment consists of a coarser asphalt material than in the ones described in the preceding chapter and is also considerably more "uneven". The slope is also greater - around 44°/oo.

I:4.3 The parking place PCON

The catchment consists of the upper floor of a two storey car park and the area is thus well defined. The deck is drained by six inlets at one side of the rectangular deck. The surface material is rough concrete, the flow length 14 m and the slope 14°/oo. The collecting sewer goes along the long side of the deck to the measuring point and is thus relatively long, just more than 100 m, see figure I:4.2. The sewer diameter is Ø225 mm and has the average slope 36°/oo. The runoff area is 1700 m^2.

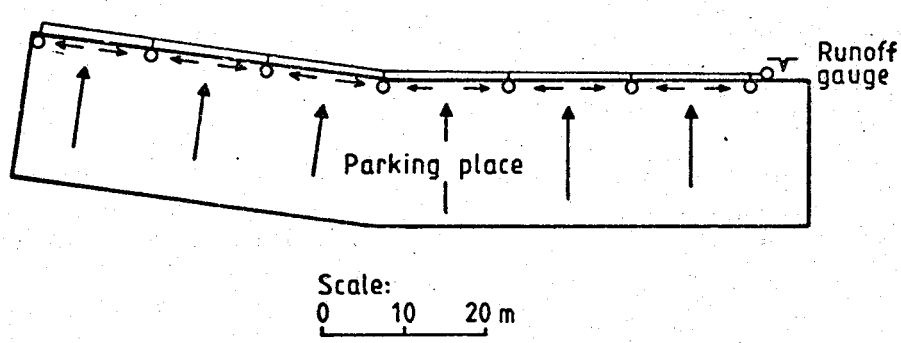

Figure I:4.2 The parking place PCON.

I:4.4 The composite catchment COMP

The catchment is a part of Bergsjön (see I:2.2) and can be regarded as representative for Bergsjön itself as well as a small urban catchment in general. The composite catchment has several quite large surfaces, a roof area of about 1400 m^2 and a parking area of 700 m^2. The other areas attached are mainly road surfaces, pavements and foot paths. The sewer system has the diameters Ø225 mm and 300 mm. The average slope in the system is $22^o/oo$. The structure of the system is shown in figure I:4.3. The total area of the catchment is 3490 m^2.

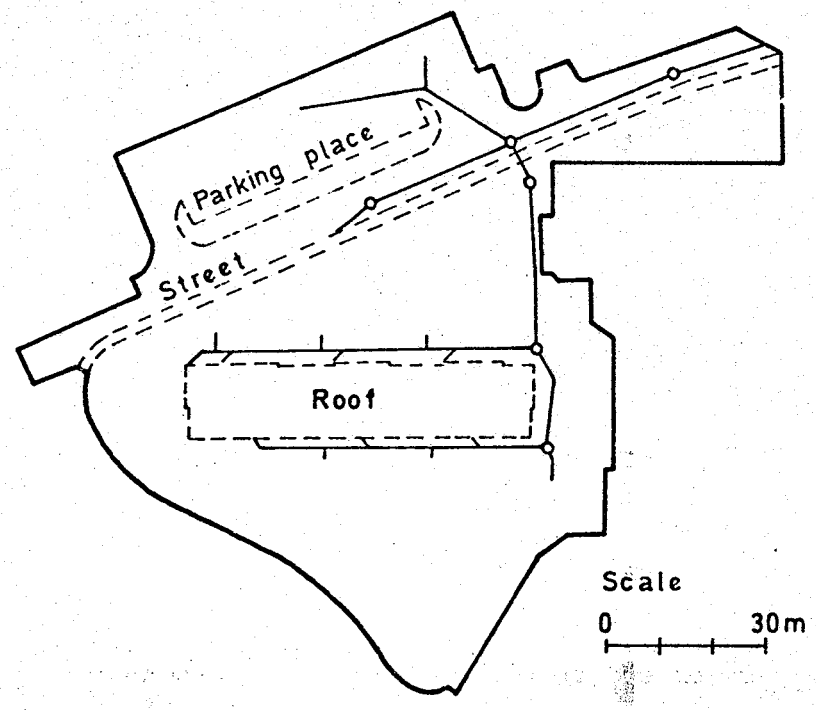

Figure I:4.3 The sewer system and runoff areas in the composite catchment COMP.

I:4.5 Rain intensity - runoff measurements

<u>Characteristics of the measuring points</u>

The choice of runoff catchments is to a great extent

governed by the possibility of finding suitable places for discharge measurements. It has not been possible to create any ideal measurement conditions in Bergsjön, but since the catchments are quite small, it has been possible to calibrate the discharge weirs with the aid of fire-hydrant water.

The sharp crested measuring weirs were made of metal, V-shaped in three cases and rectangular in one. The angle of the V-shaped weirs were adjusted so that the two year rainfall, calculated according to the Rational Method, could be registered for an overflow height of 25 cm.

The measurement weirs in the PCON and COMP catchments were installed in existing manholes, Ø900 mm, see figure I:4.4. The weir was placed at such a level that discharge mappe was aired, and the influenced area upstream of the weir was small. The lowering of the magazines during dry weather was small due to careful jointing and the low evaporation in closed systems.

The measuring weir of the ASPH catchment was placed in a gully. A metal box was constructed to get as slow an inflow as possible towards the overflow. A perforated metal sheet with holes was placed in the middle of the box to distribute the water over the cross section, see figure I:4.4.

Measuring equipment

The measurement system consists of point level gauges placed in the measuring stations and a central, registering unit. The point gauge is motor-driven and connected to a potentiometer, see figure I:4.5.

The central unit consists of a data logger (Epsylon) recording the data on magnetic tape and a clock unit, see figure I:4.5. Each measuring sequence is started by the clock unit which gives a pulse to the gauge motor to lift

a weight (for 7 seconds) and then lower it to the water surface. When the weight reaches the water surface the motor power is cut off. The measuring sequence is ended with a pulse from the clock to the data logger, to record the potentiometer values.

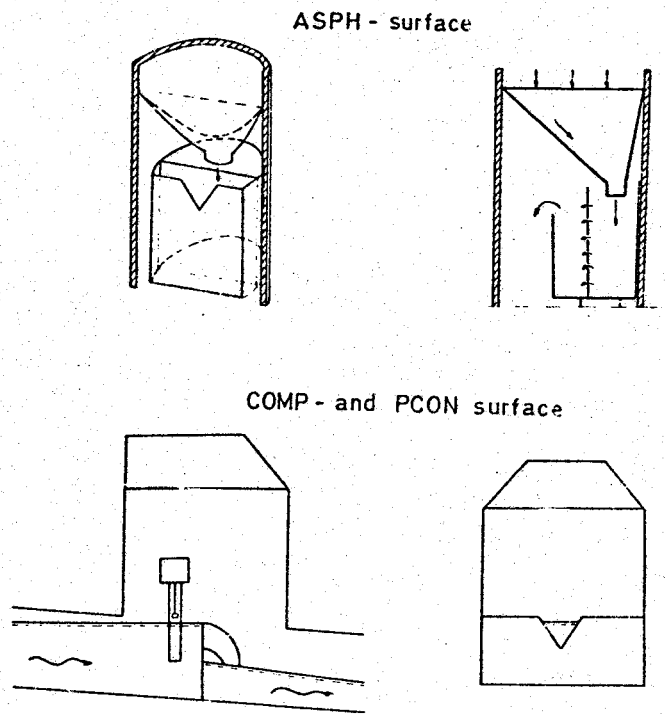

Figure I:4.4 The discharge measuring stations at Bergsjön.

The demand for high resolution in time for the records results in large amounts of data. To reduce the amount of data a special level gauge was placed at the measuring point of the asphalt surface. When the water level at this point exceeded a fixed value, a sampling interval of 30 seconds was used. Below this level the interval was 10 minutes.

The central unit was placed in a manhole at the centre of the catchment and signal cables were drawn from the

gauges in the sewer net. In this way the sampling system could be placed beneath the ground which is an advantage when the risk for damage is considered.

Calibration of overflows

The measuring weirs were calibrated by fire-hydrant water. The flow was measured by flow meters connected to the fire-hydrant heads. At each measuring point the response was registered by the data logger for five different flows. Thus a direct correlation between the digital unit of the data logger and the flow was achieved. As the calibration was made also for the greatest flows, the calibration curve was used directly at the evaluation and no analytical relation between water level and flow was evaluated.

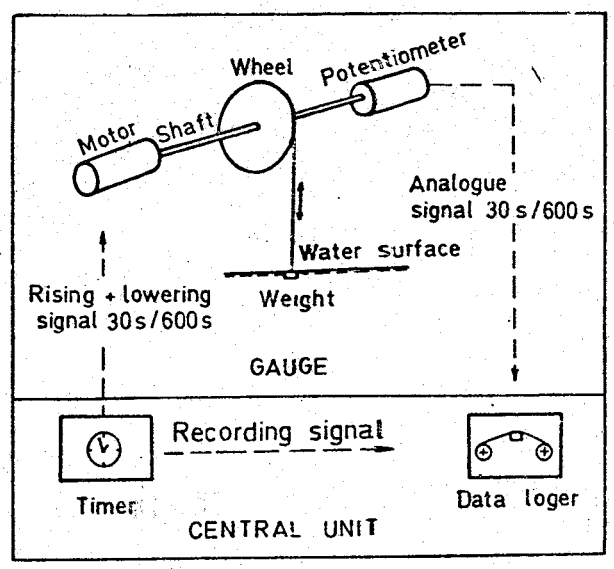

Figure I:4.5 Measuring system for the small catchments in Bergsjön.

II SIMULATED AND RECORDED RUNOFF HYDROGRAPHS

In order to facilitate comparisons all hydrographs have been gathered in this appendix. The plots are divided into two main groups, II:1 and II:2, corresponding to the simulations in chapters 8 and 9, respectively.

Within each group hydrographs simulated by a specific model have been put together for all catchments and storms.

As the rain intensities and storm durations vary considerably between storms it was necessary to use different scalings. The runoff rates are expressed in the same unit as the rain intensity [l/s·ha].

II:1 Hydrographs from the small catchments (< 1 ha)

In this section the hydrographs from the six catchments discussed in chapter 8 are presented.

II:1.1 Comparison between the recorded and simulated runoff

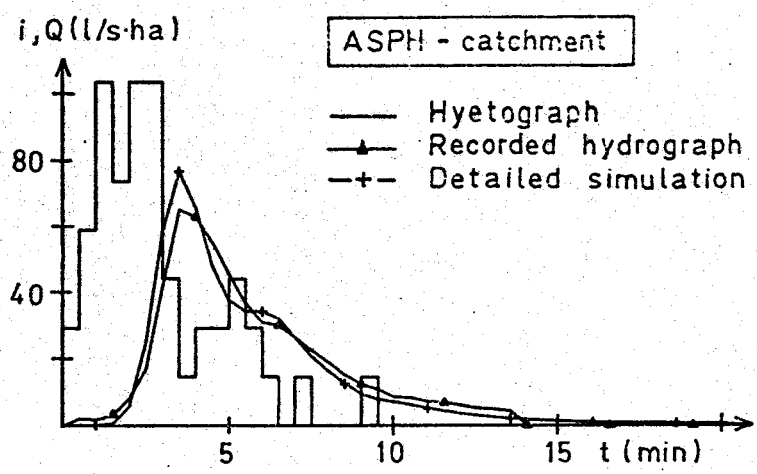

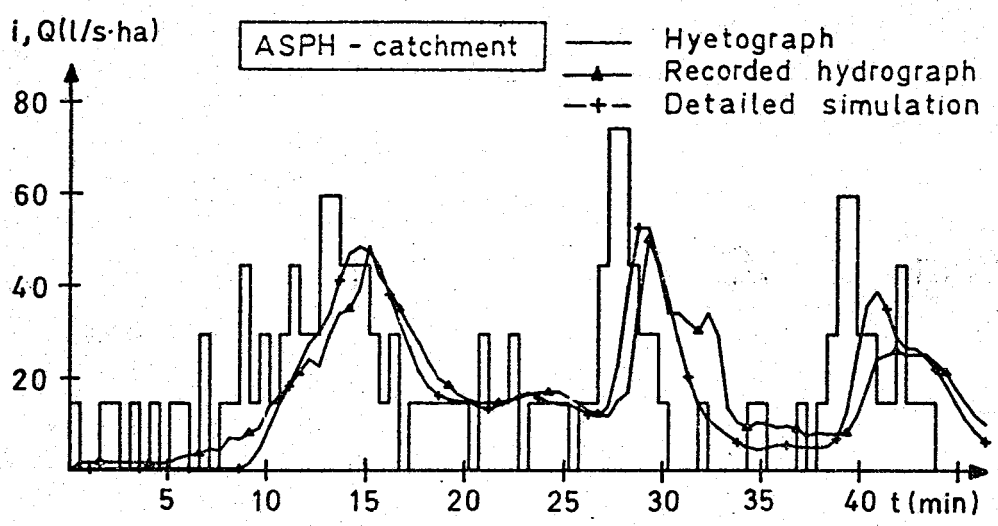

recorded-simulated hydrographs, continued

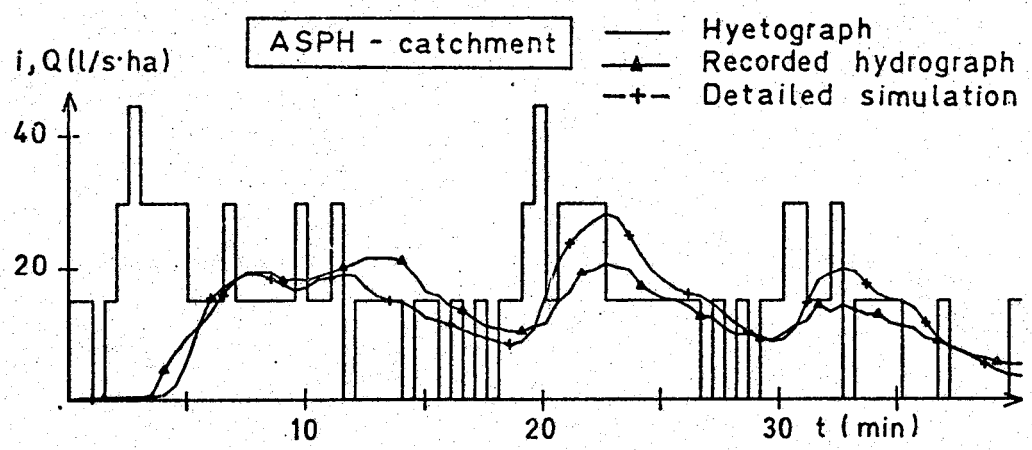

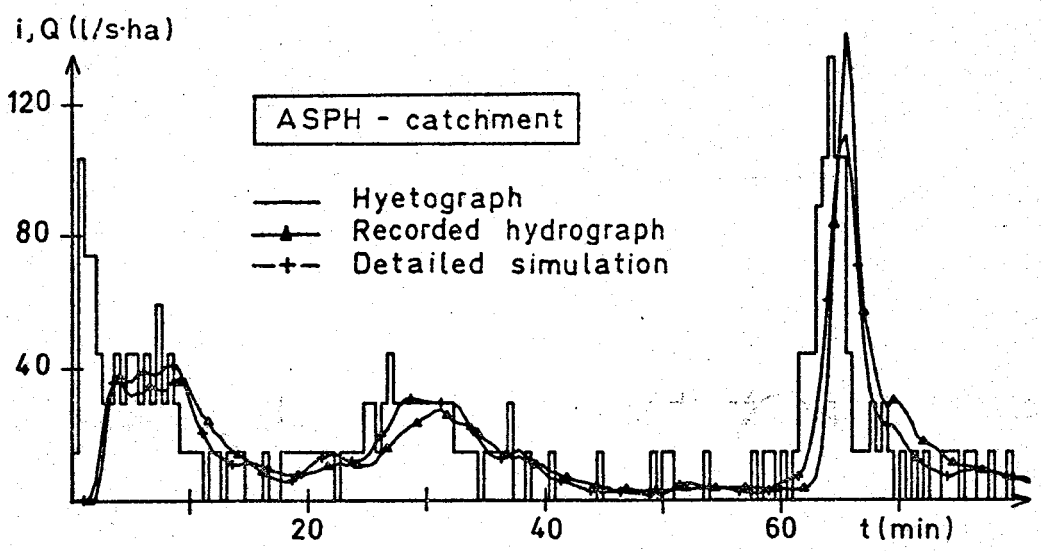

recorded-simulated hydrographs, continued

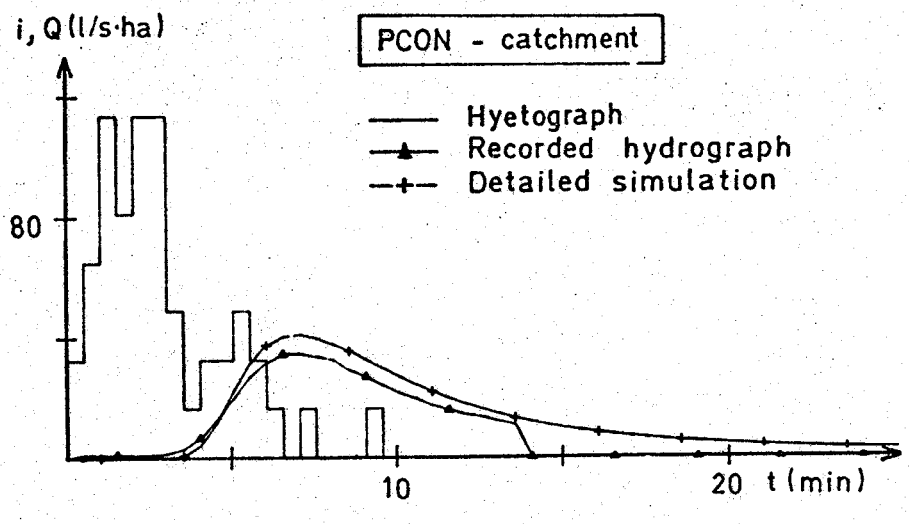

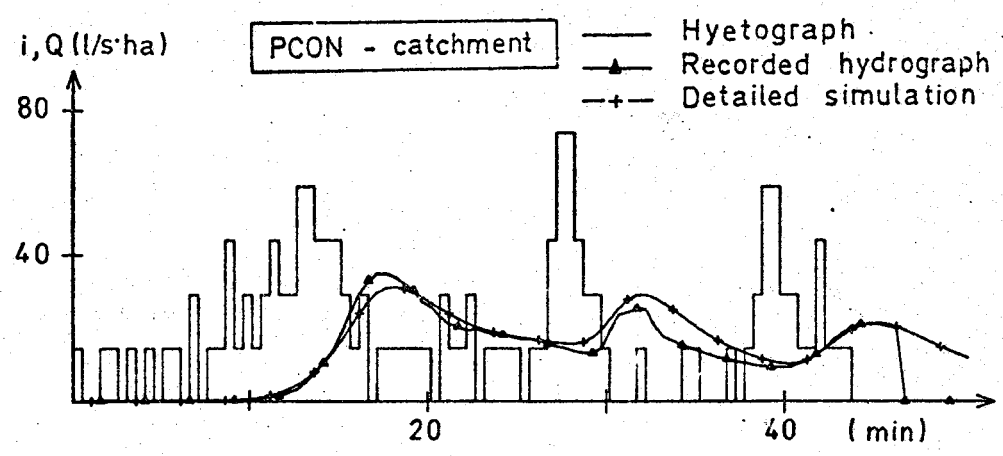

recorded-simulated hydrographs, continued

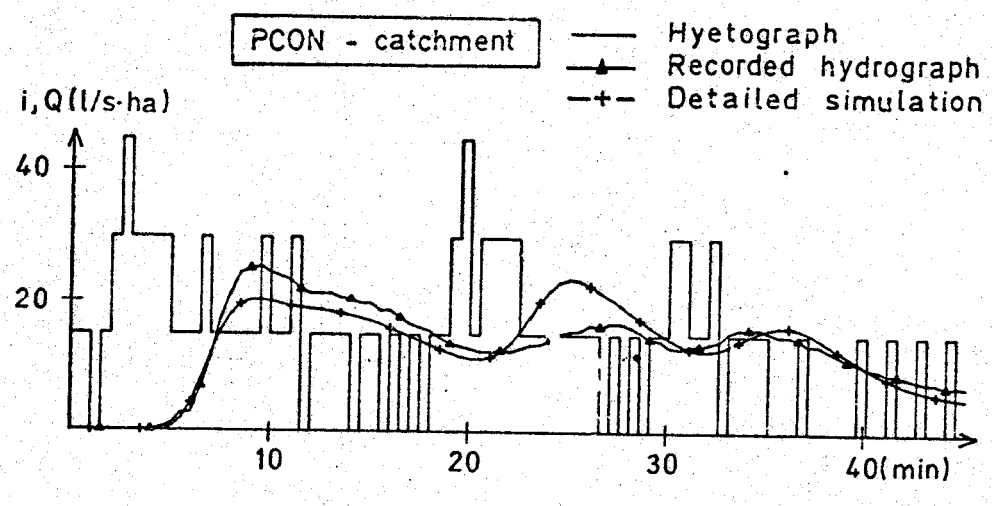

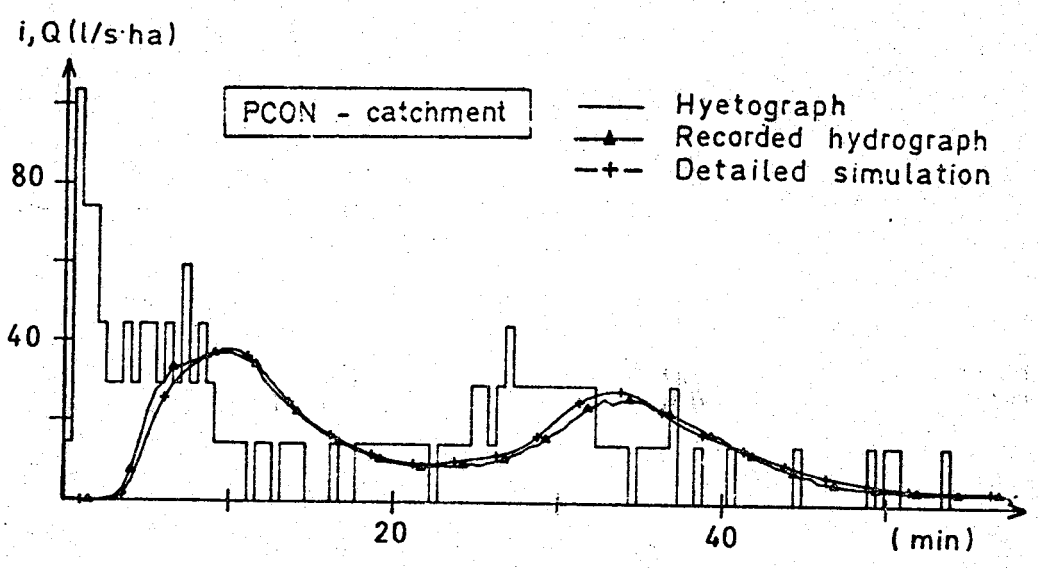

recorded-simulated hydrographs, continued

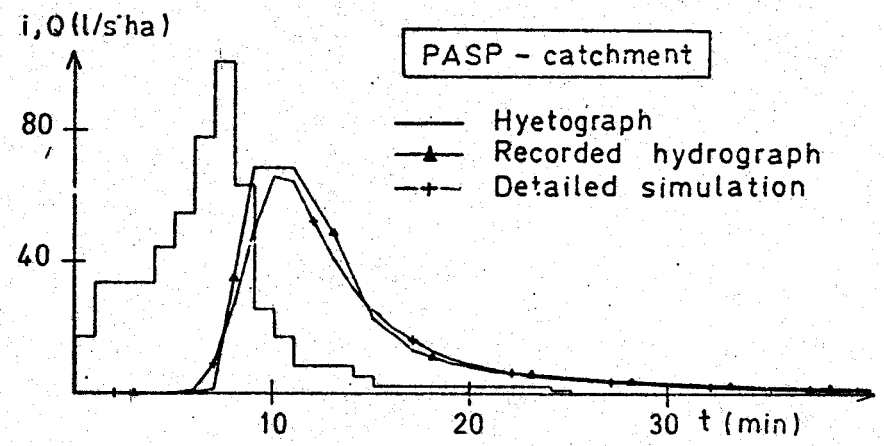

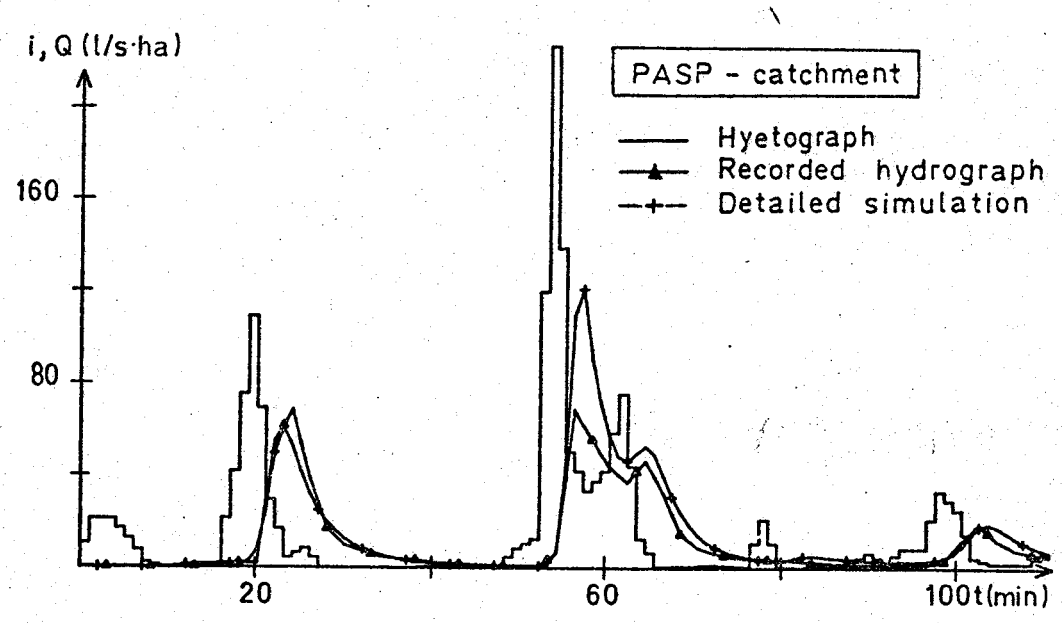

recorded-simulated hydrographs, continued

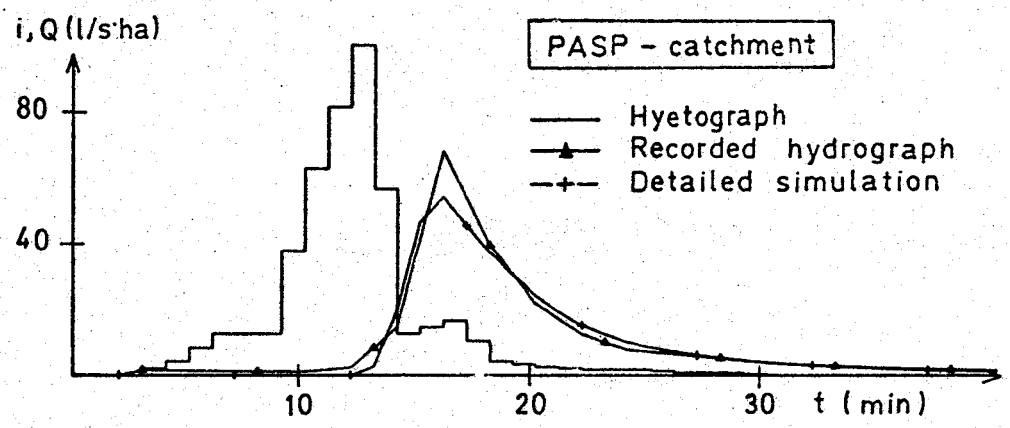

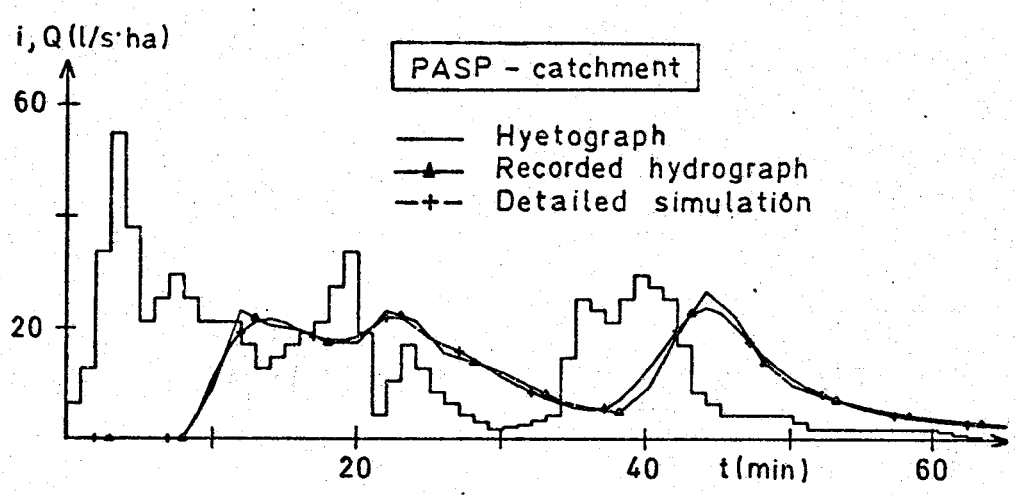

recorded-simulated hydrographs, continued

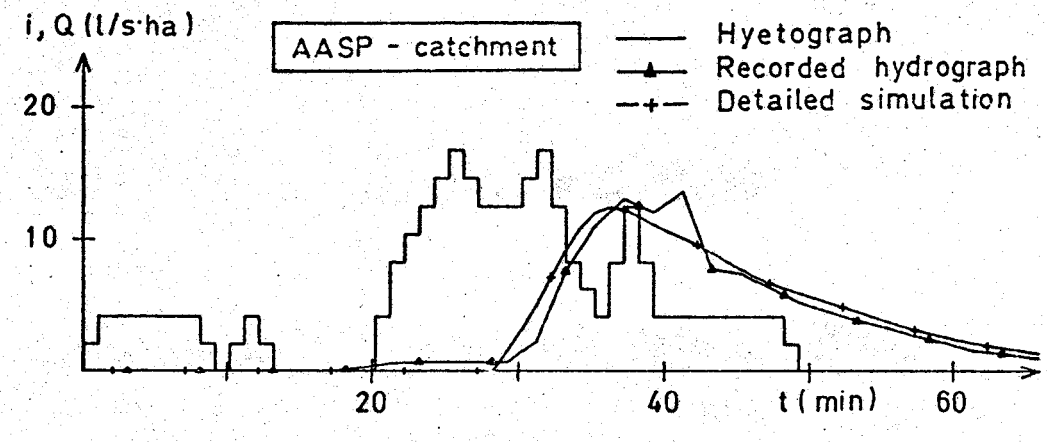

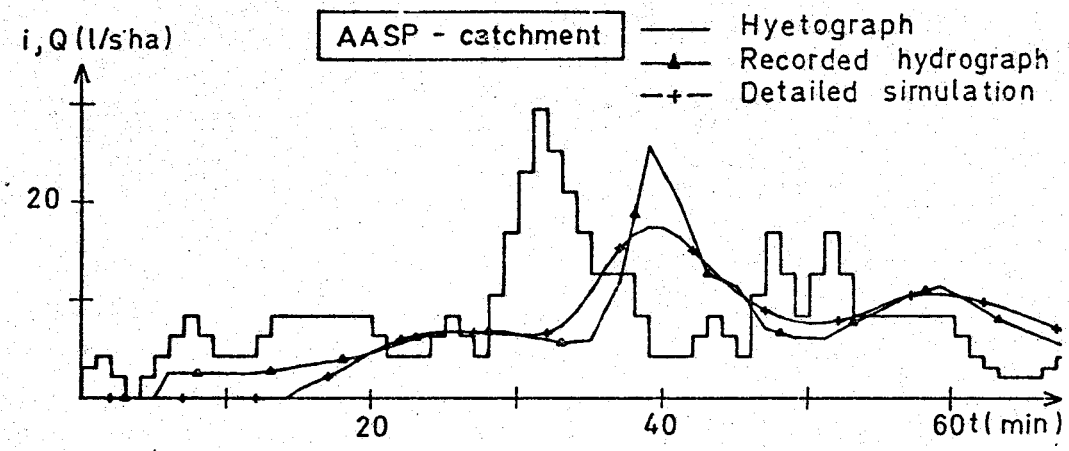

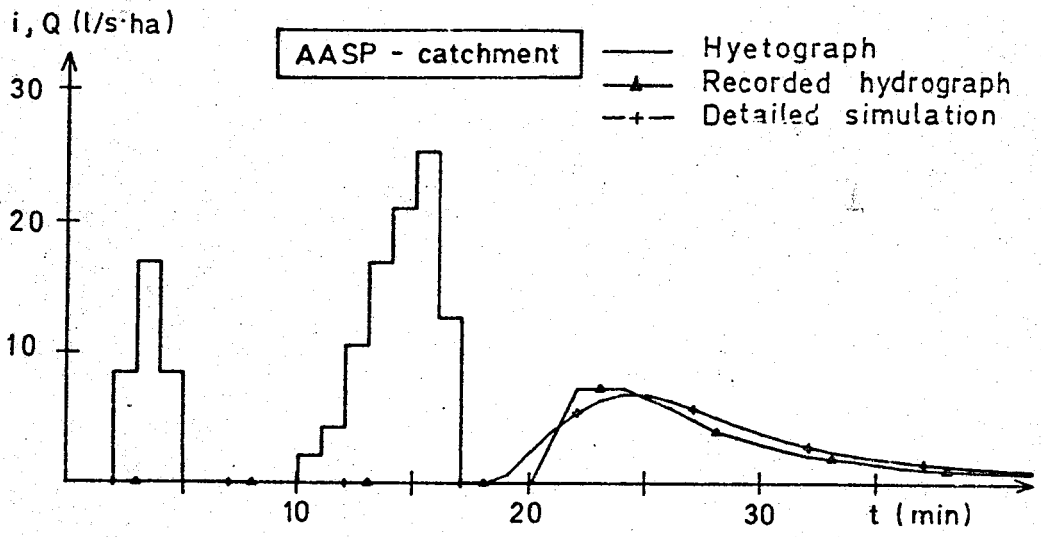

recorded-simulated hydrographs, continued

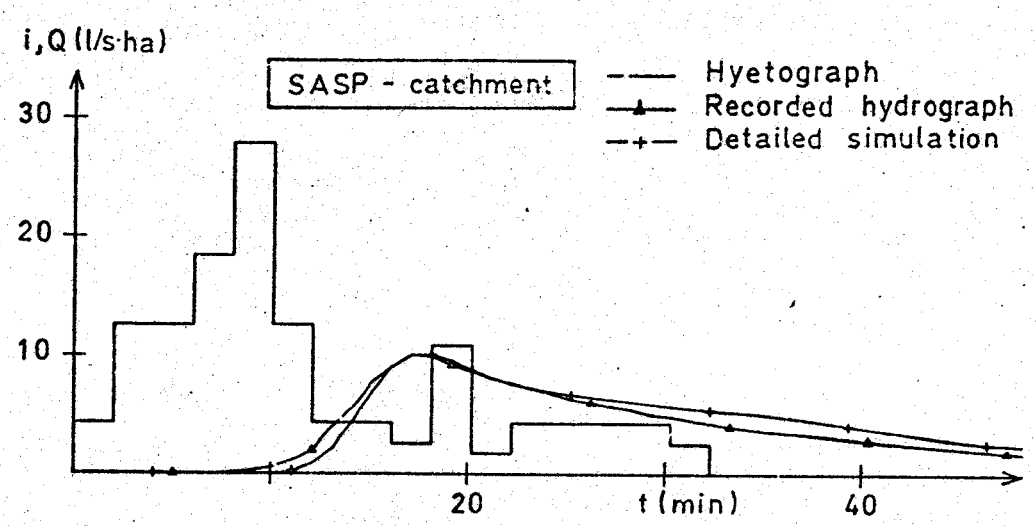

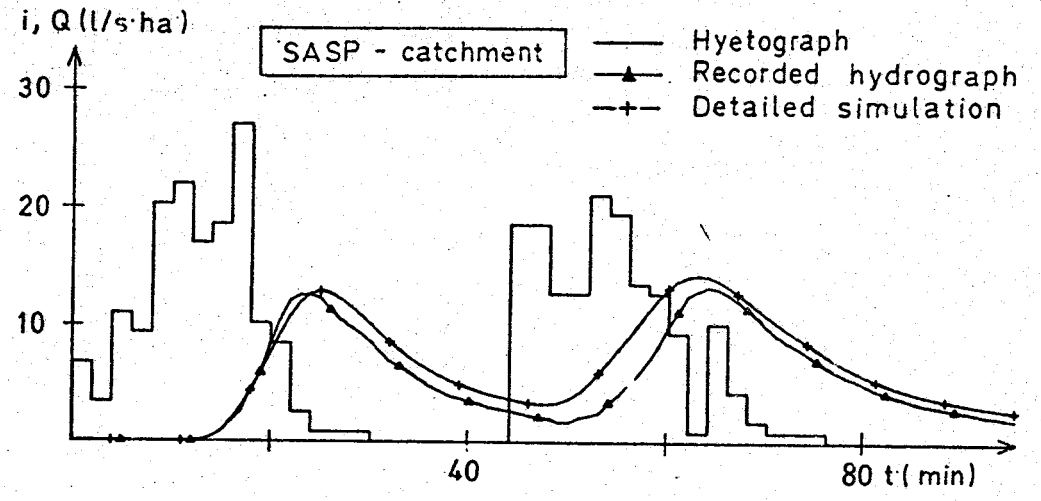

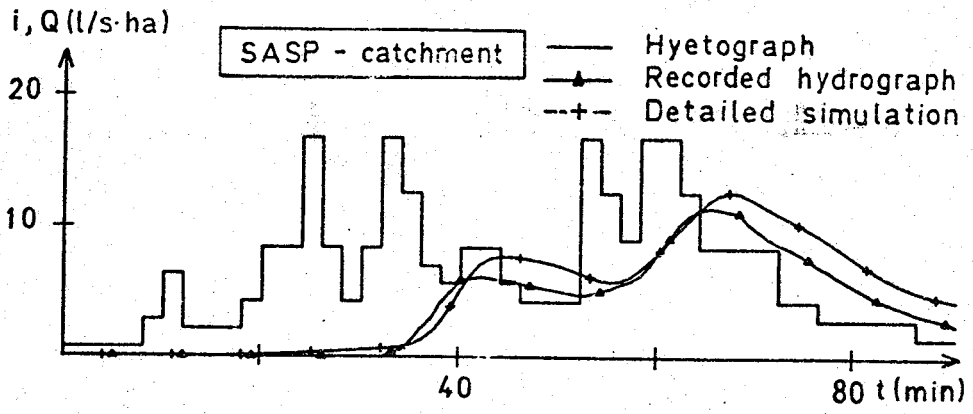

recorded-simulated hydrographs, continued

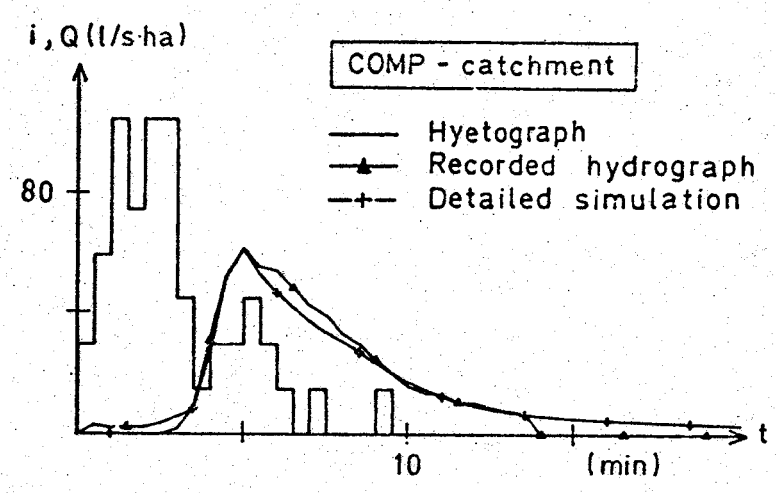

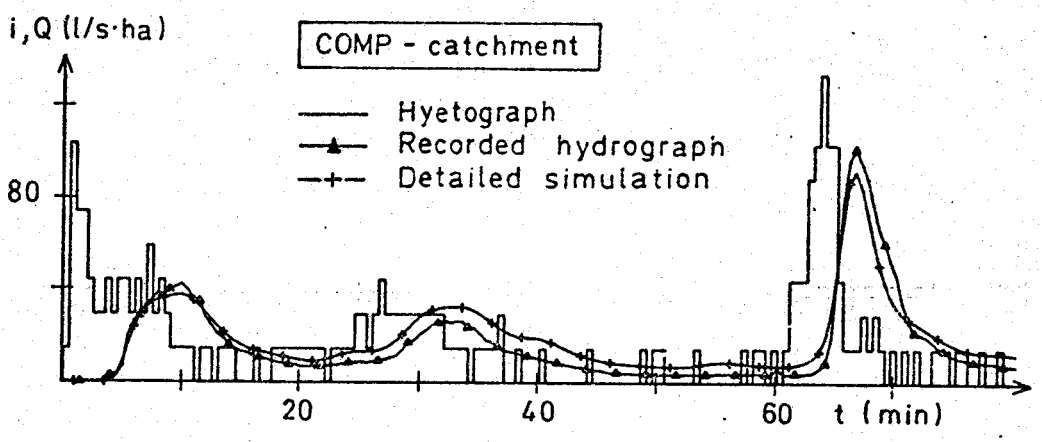

recorded-simulated hydrographs, continued

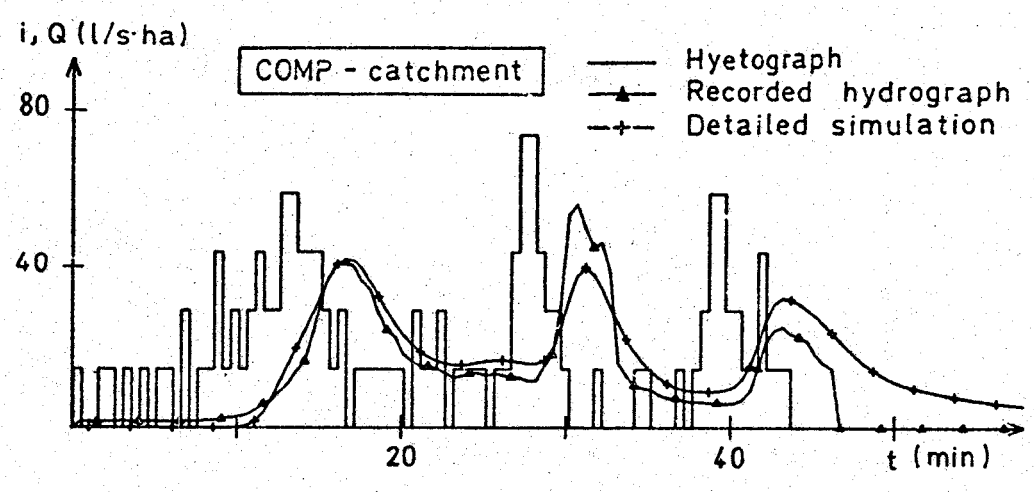

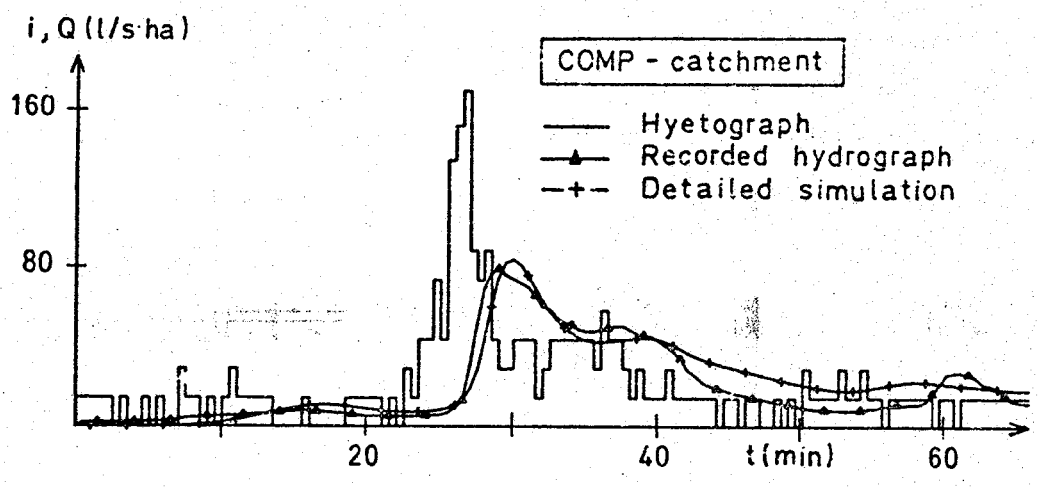

II:1.2 Comparison; the detailed kinematic wave model, KW6S-S model, and KW4G-I model

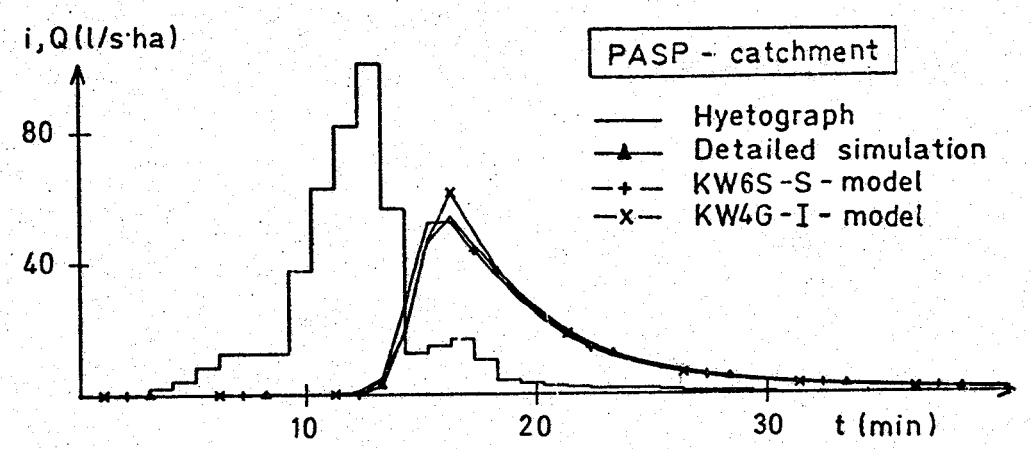

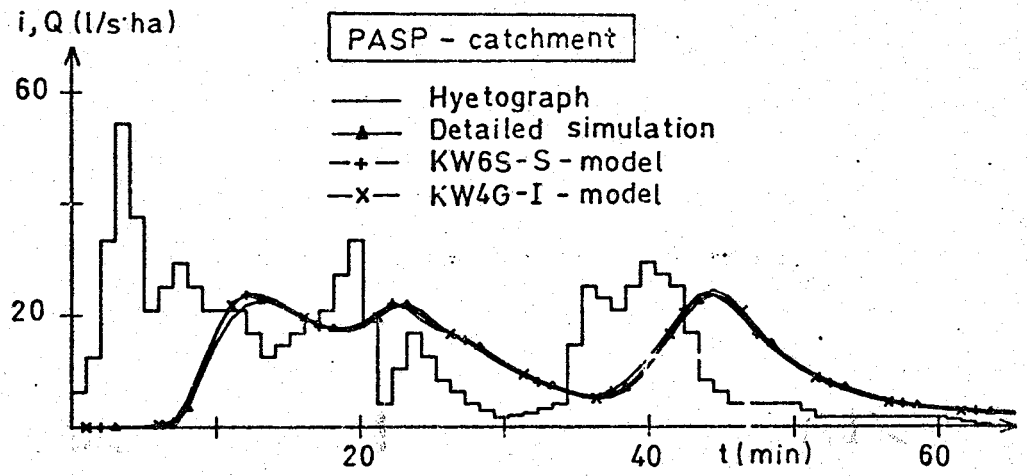

KW6S-S and KW4G-I model hydrographs, continued

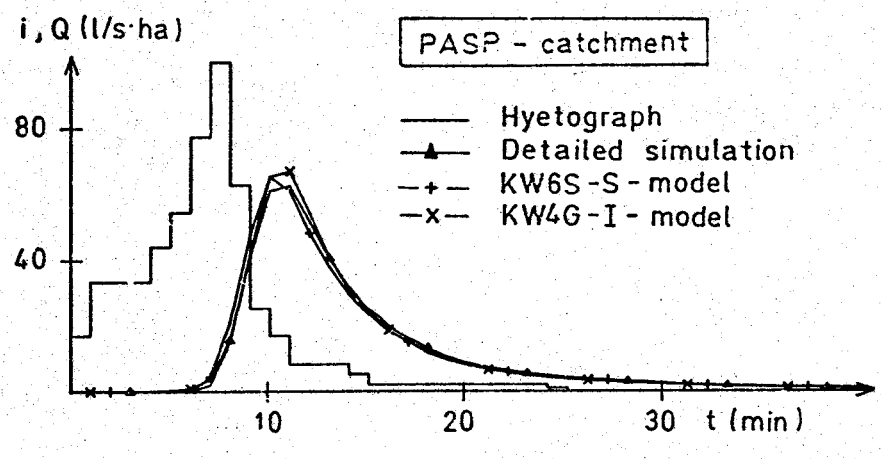

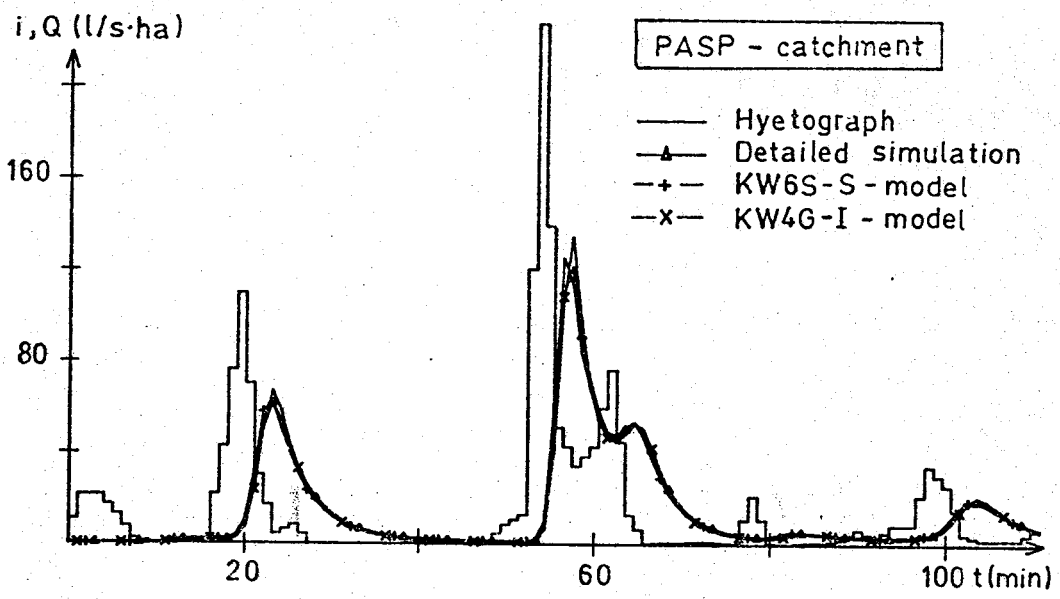

KW6S-S and KW4G-I model hydrographs, continued

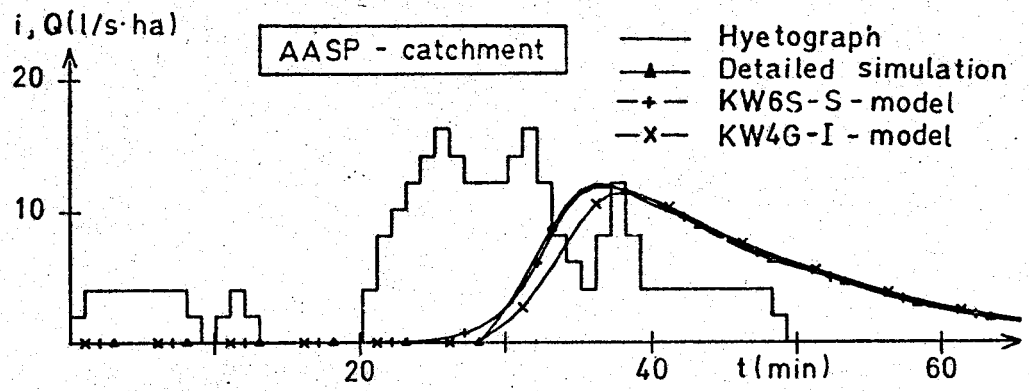

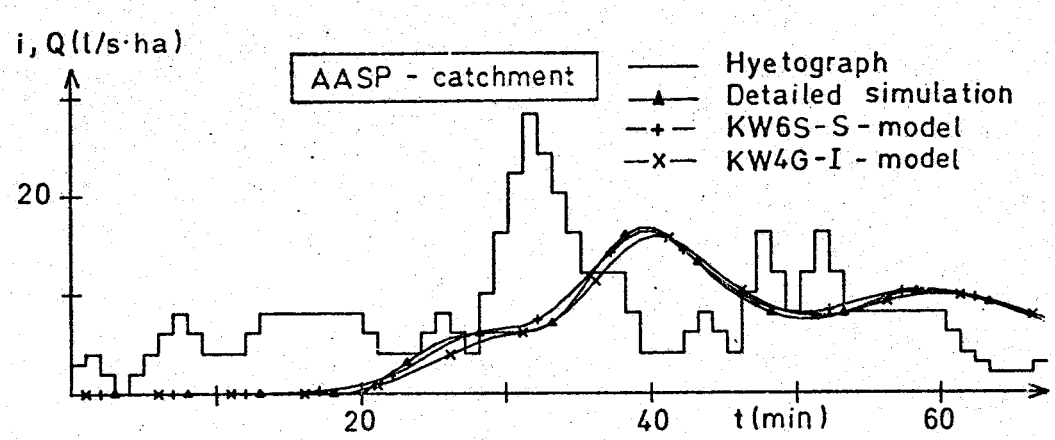

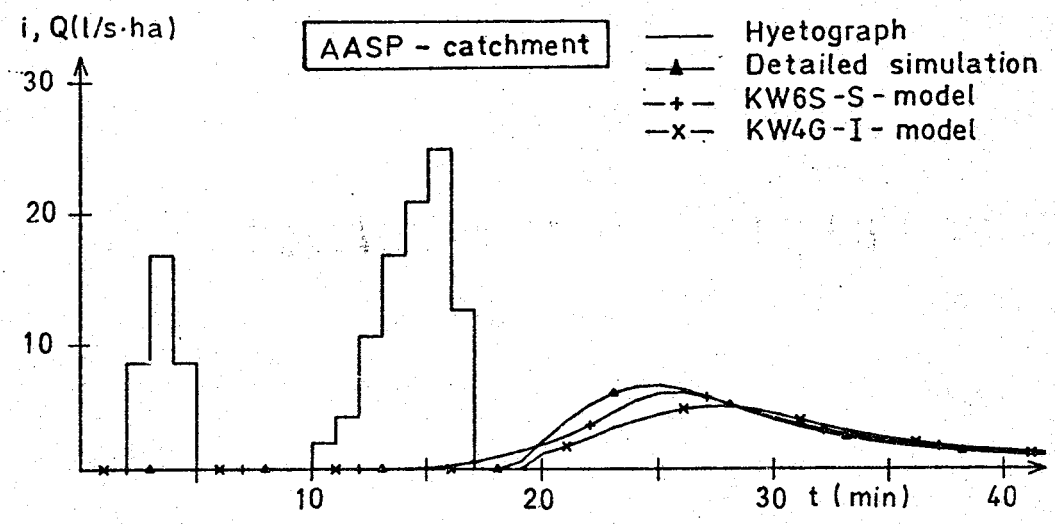

KW6S-S and KW4G-I model hydrographs, continued

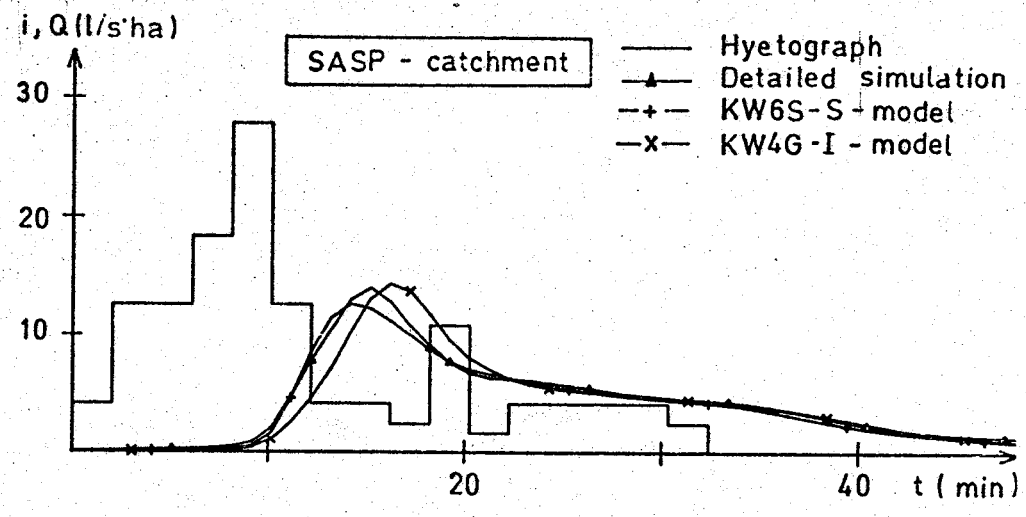

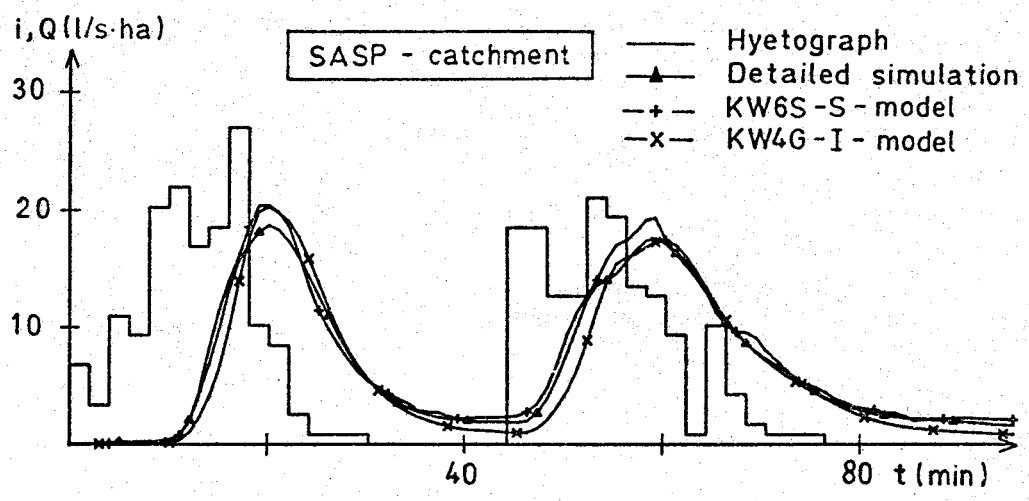

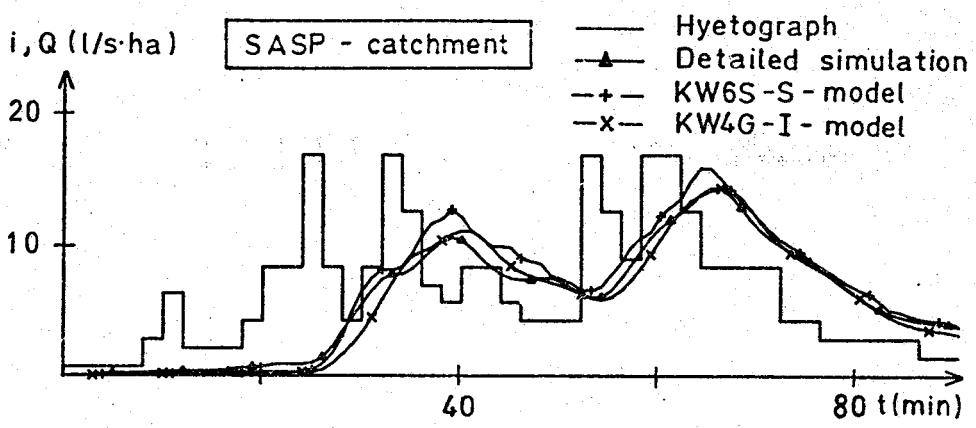

KW6S-S and KW4G-I model hydrographs, continued

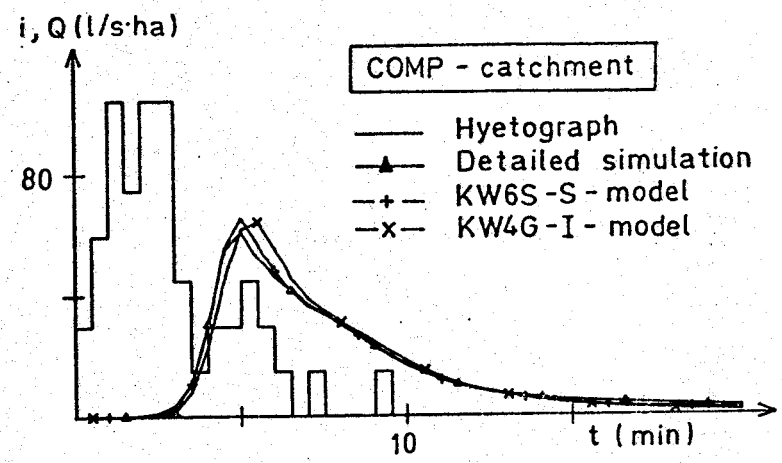

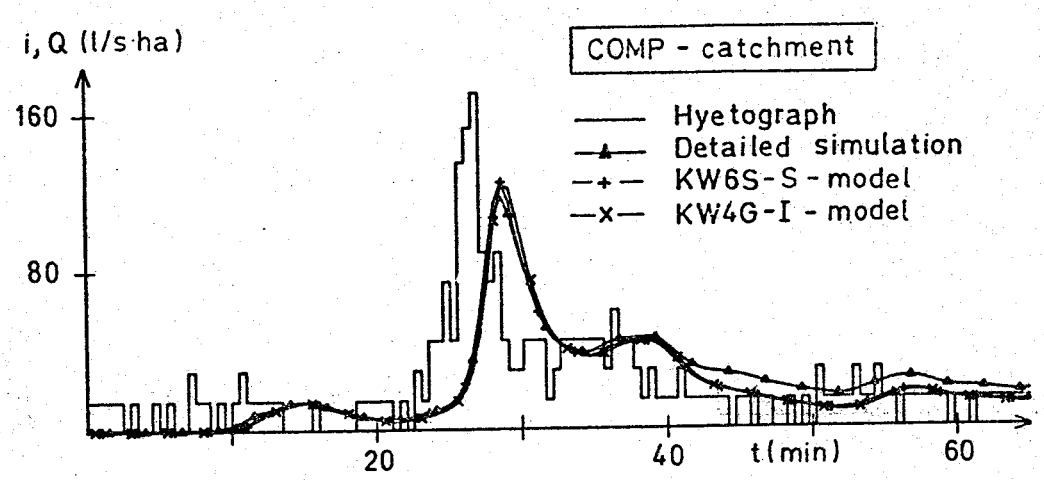

KW6S-S and KW4G-I model hydrographs, continued

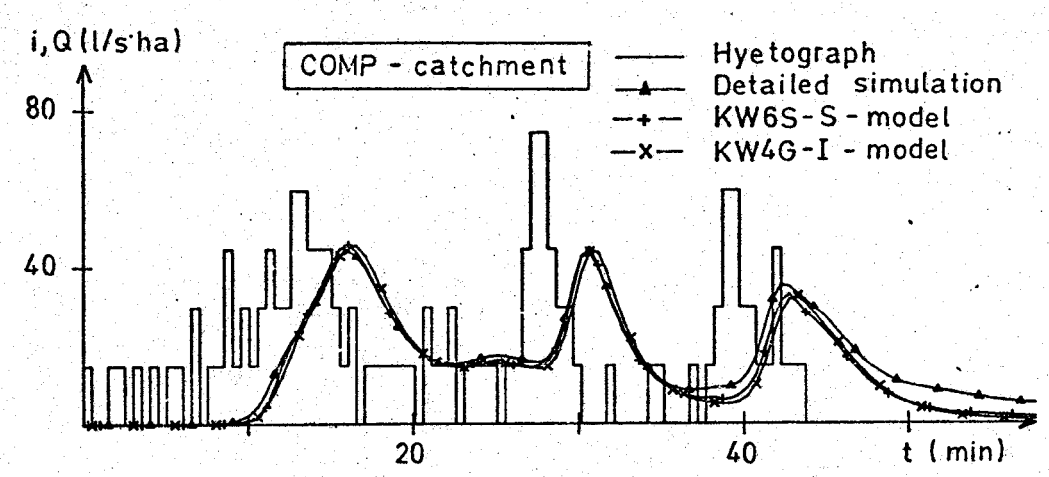

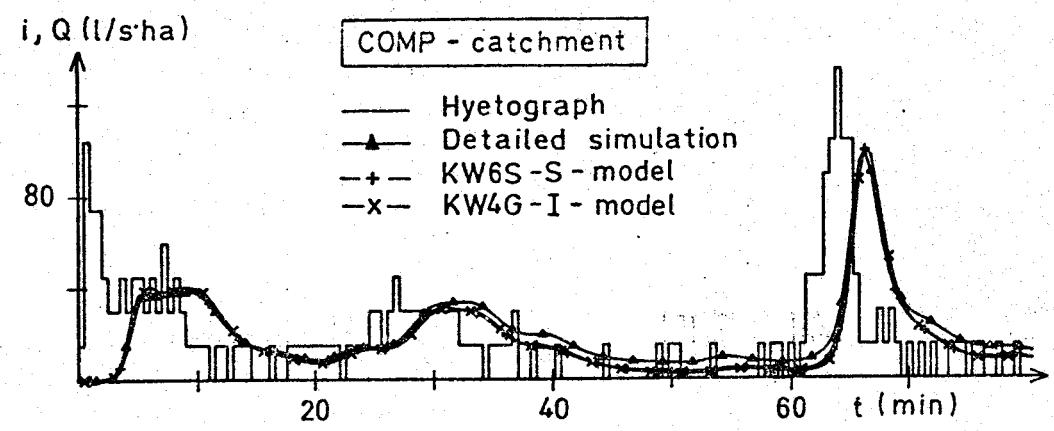

II:1.3 Comparison: the detailed kinematic wave model, KW6S model and KW3-model (KW4G used in the ASPH catchment)

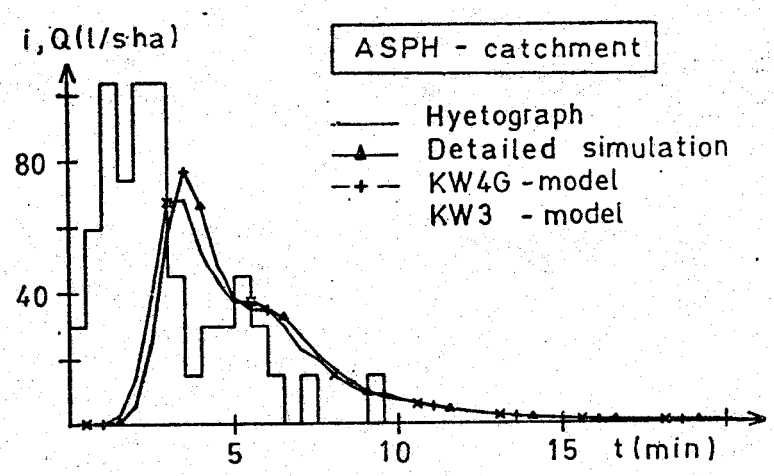

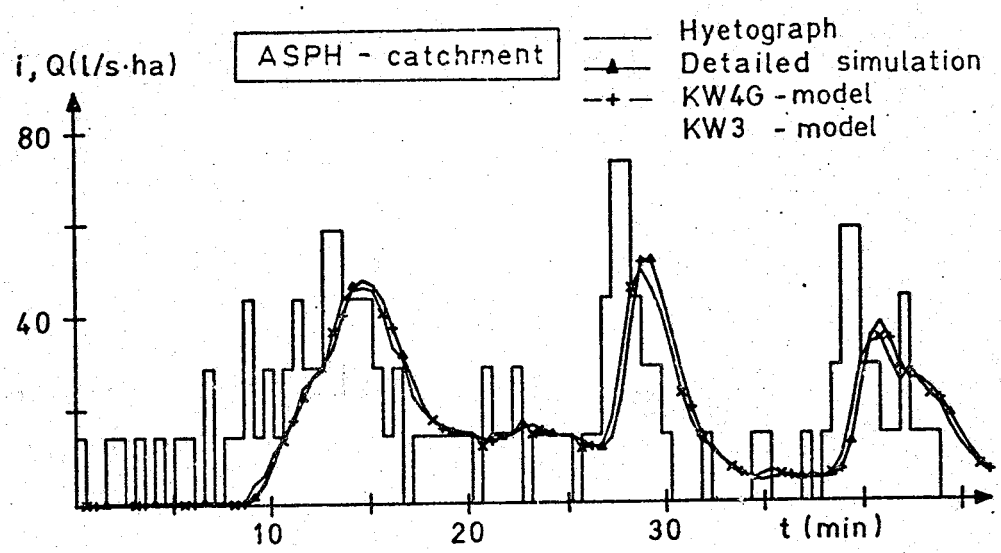

KW4G and KW3 model hydrographs, continued

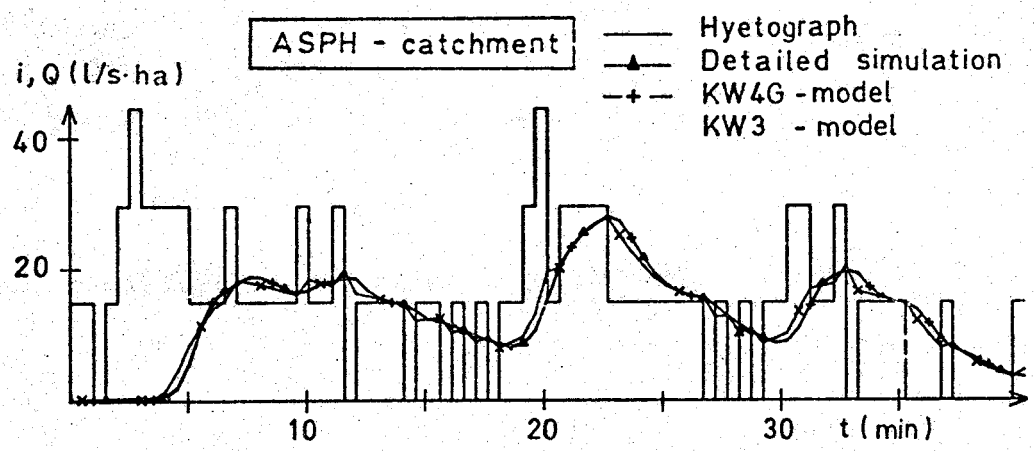

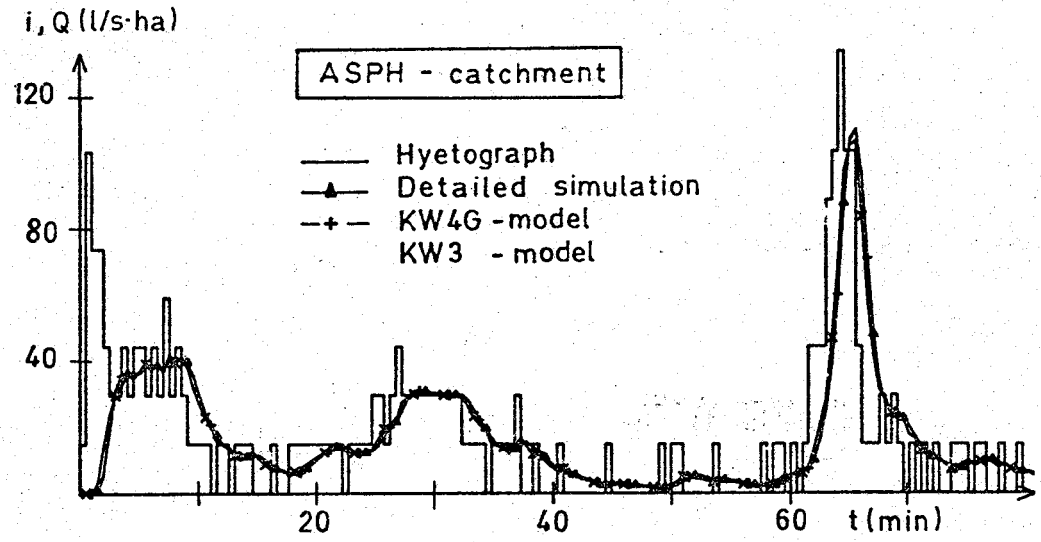

KW6S and KW3 model hydrographs, continued

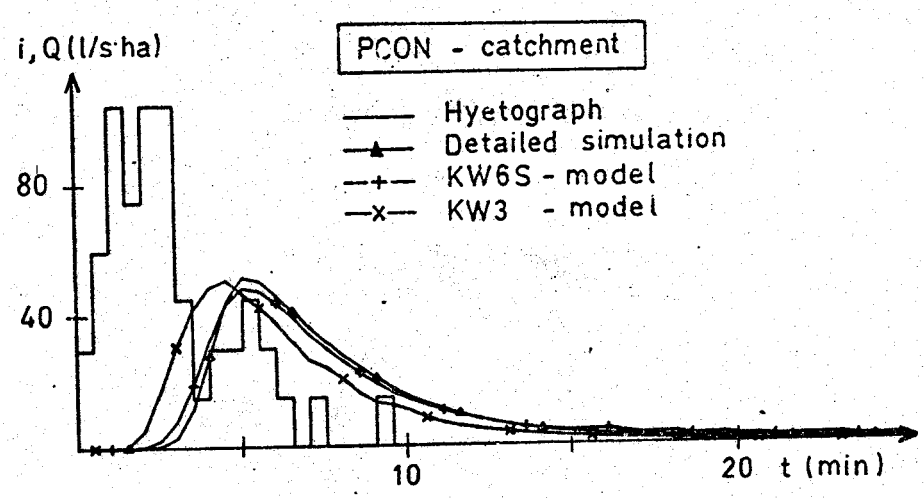

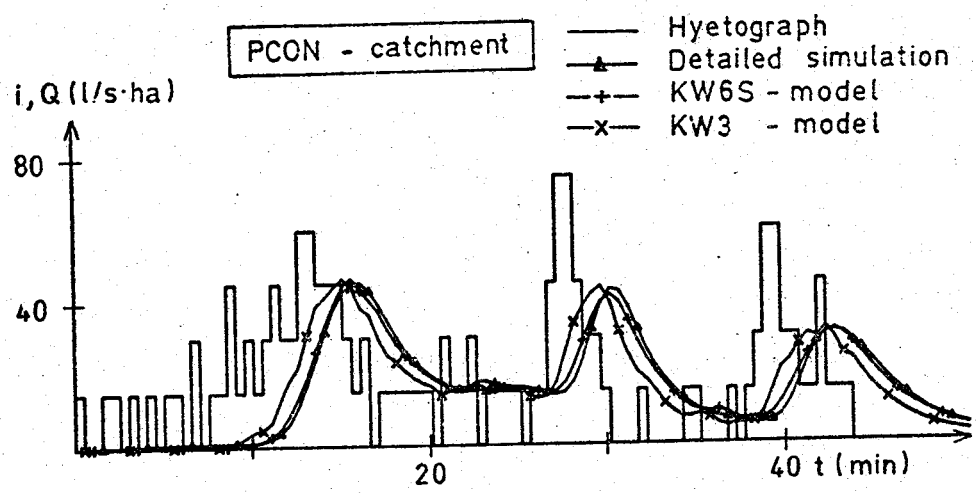

KW6S and KW3 model hydrographs, continued

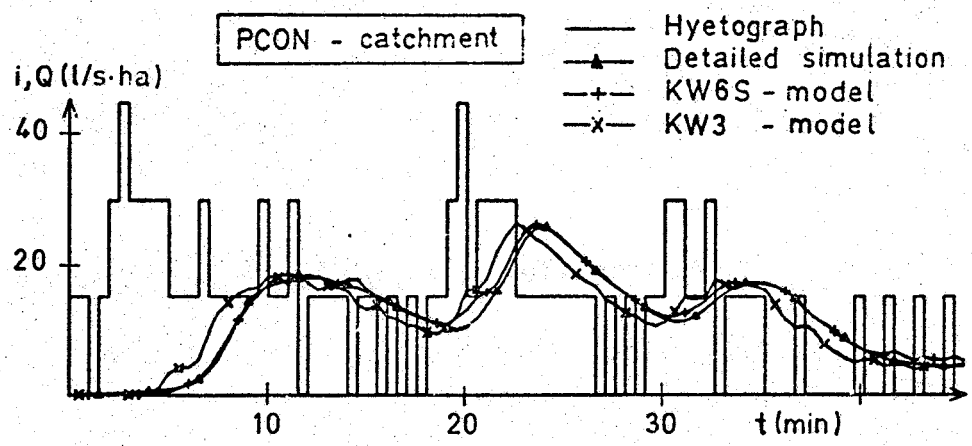

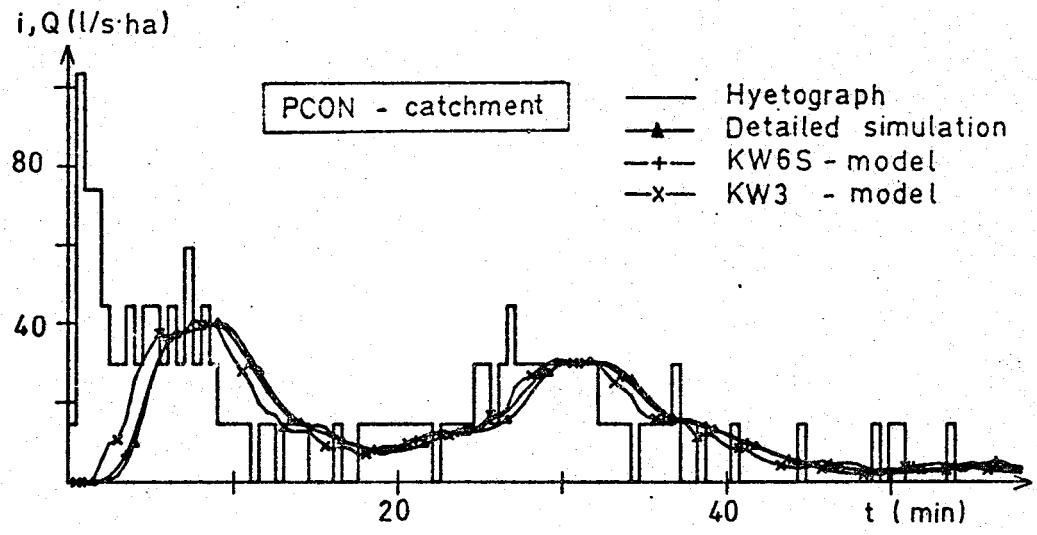

KW6S and KW3 model hydrographs, continued

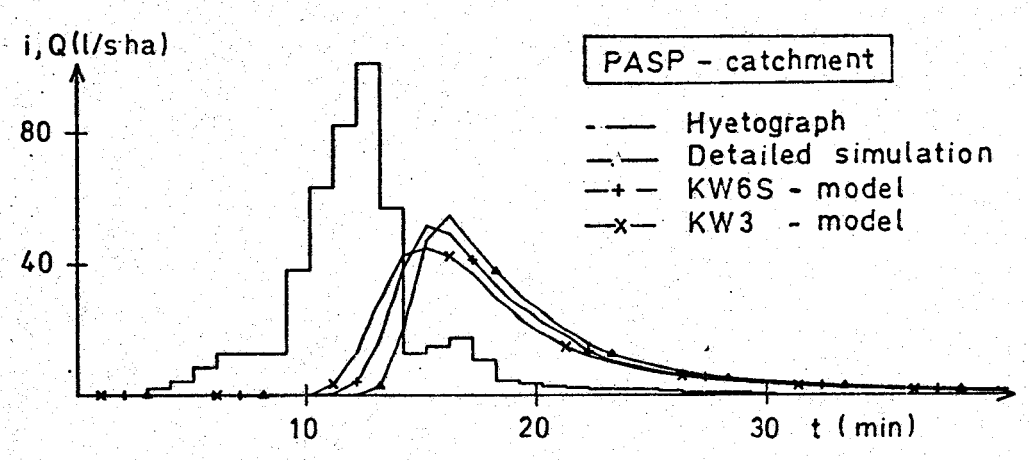

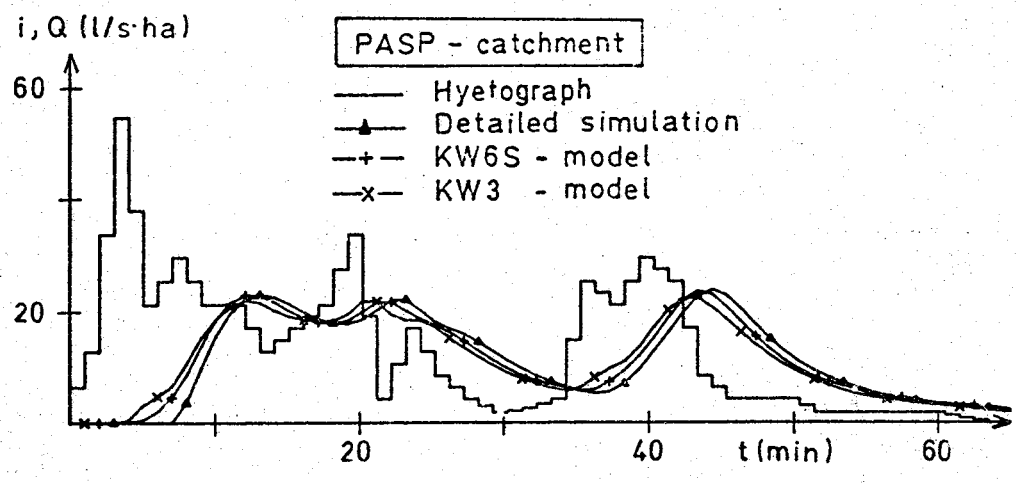

KW6S and KW3 model hydrographs, continued

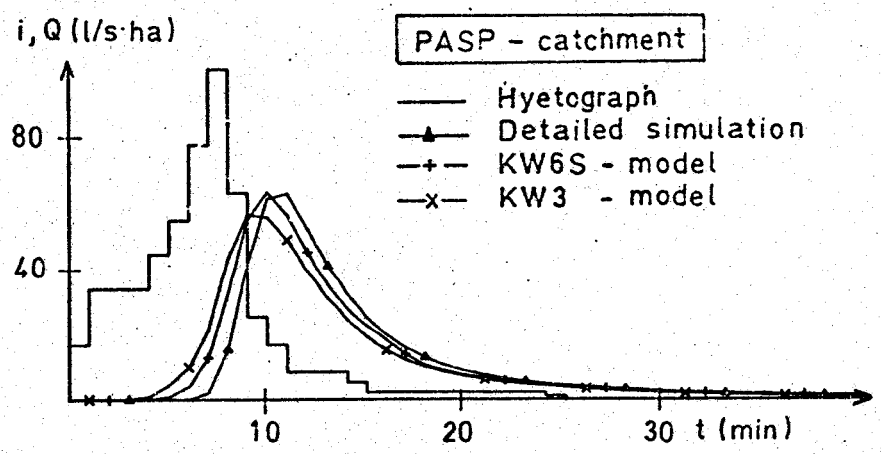

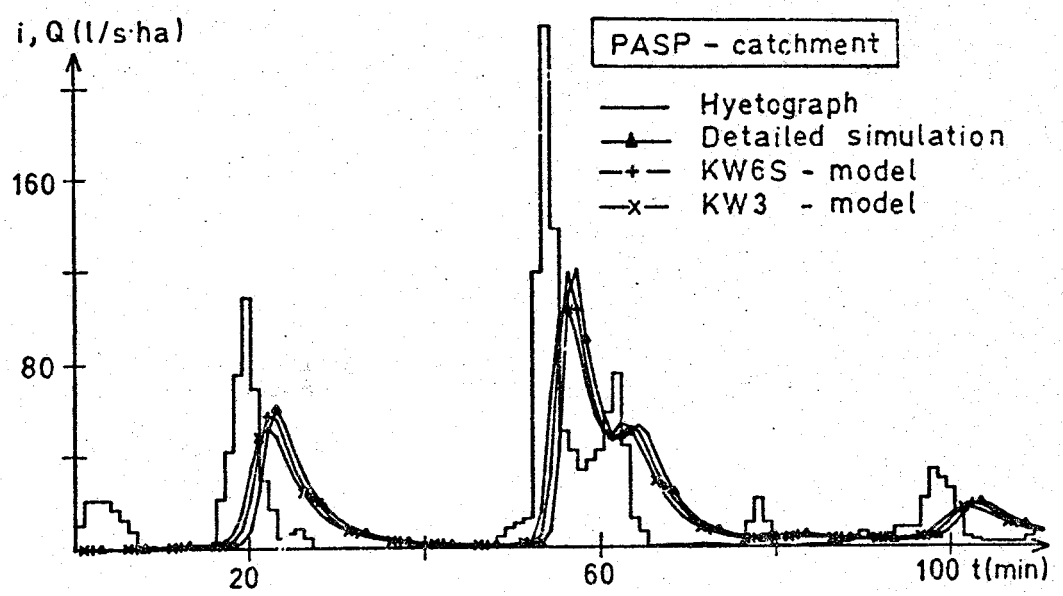

KW6S and KW3 model hydrographs, continued

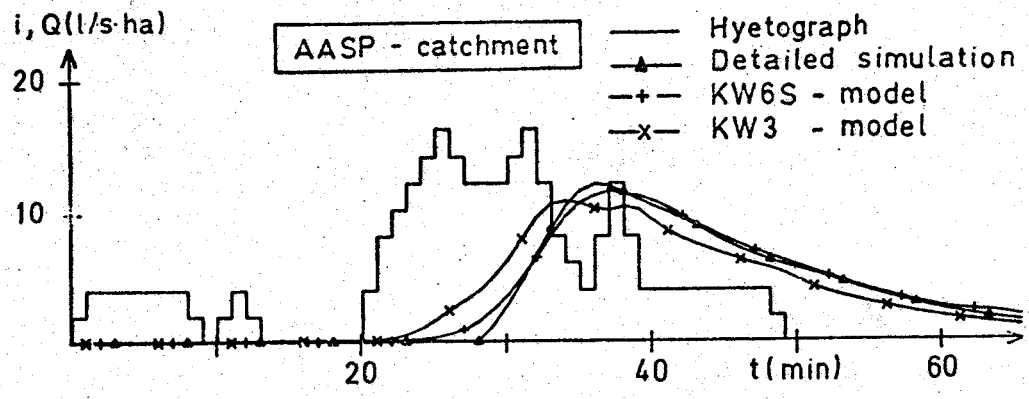

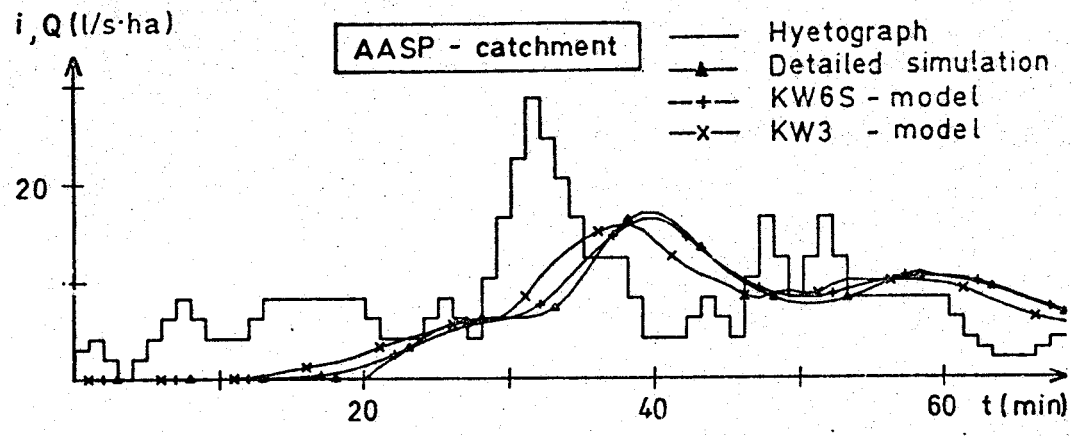

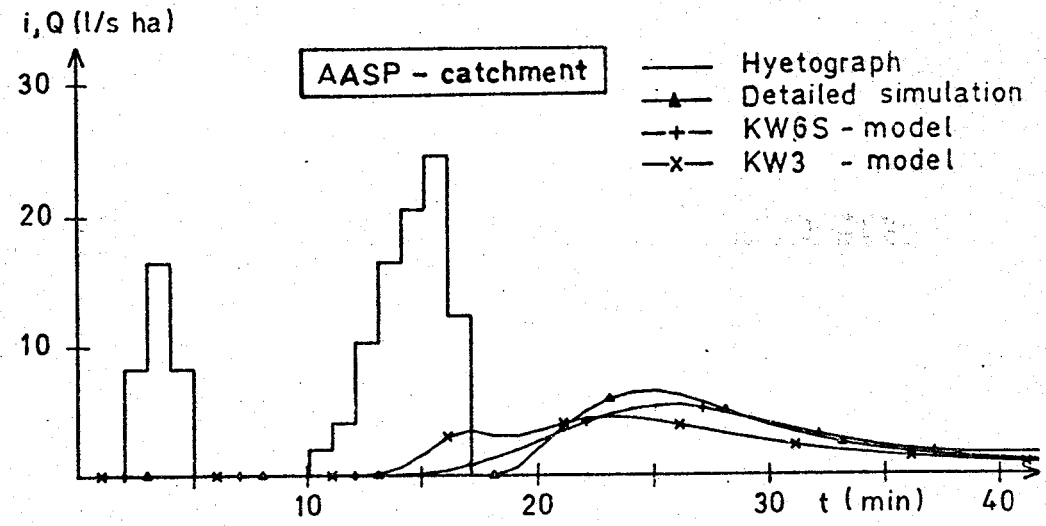

KW6S and KW3 model hydrographs, continued

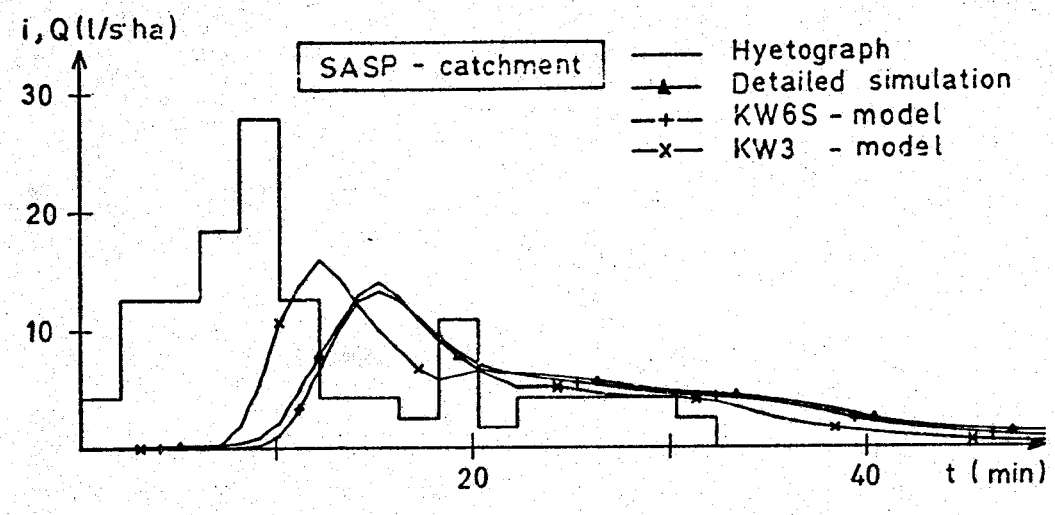

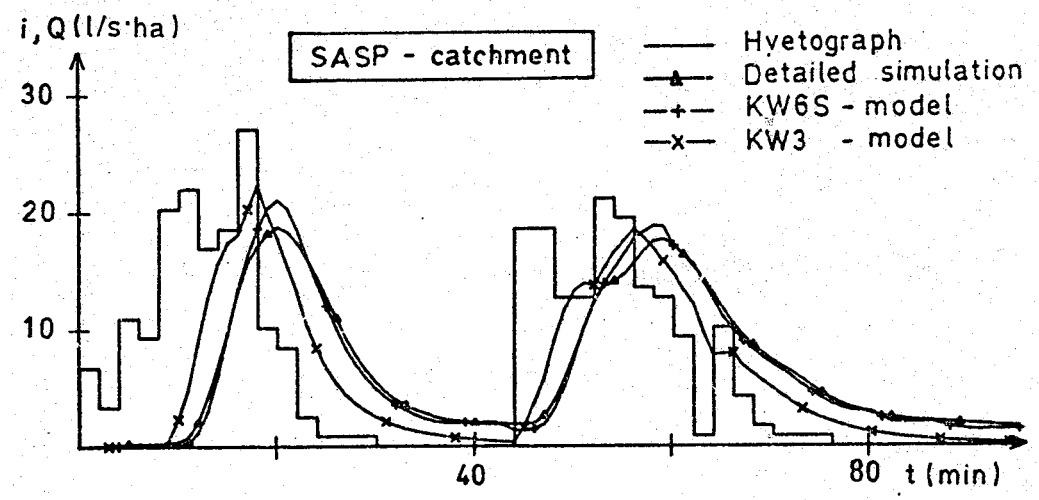

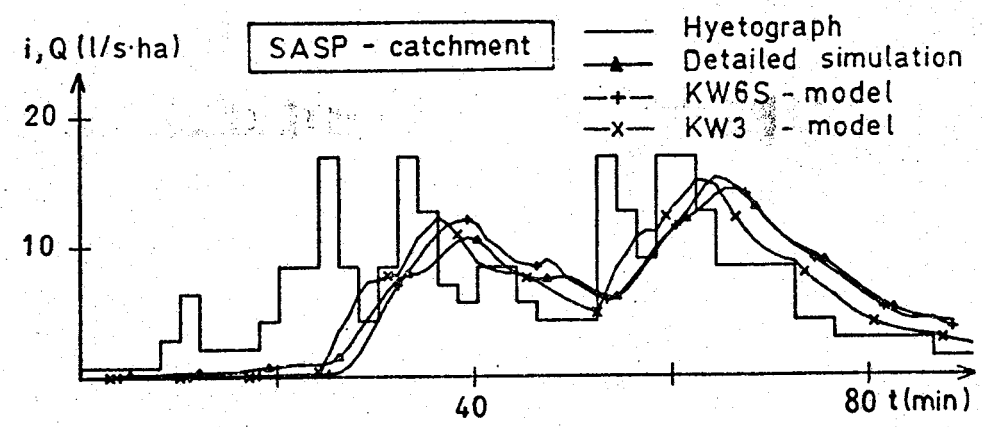

KW6S and KW3 model hydrographs, continued

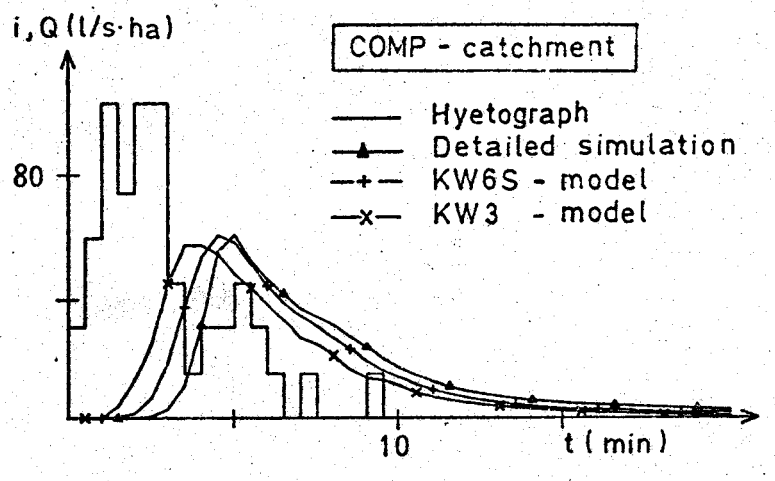

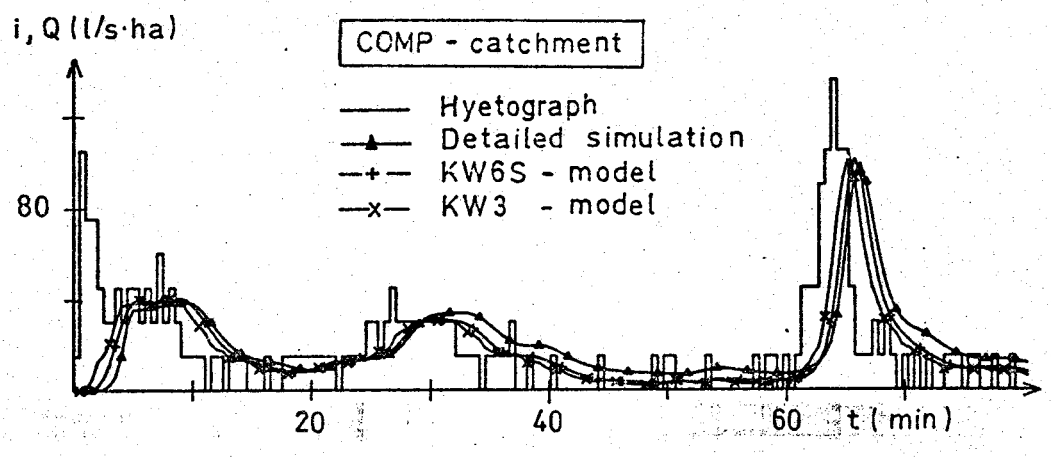

KW6S and KW3 model hydrographs, continued

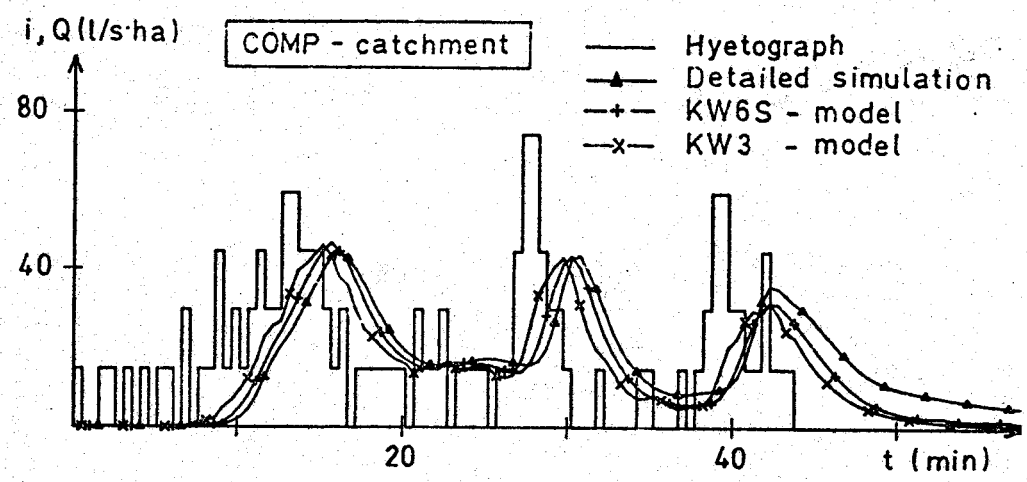

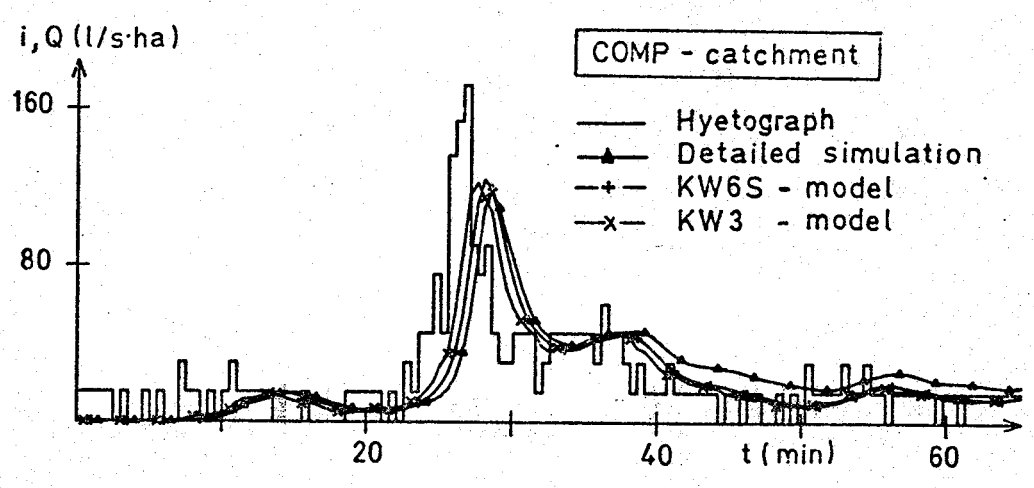

II:1.4 Comparison: the detailed kinematic wave model and the Time-Area Method

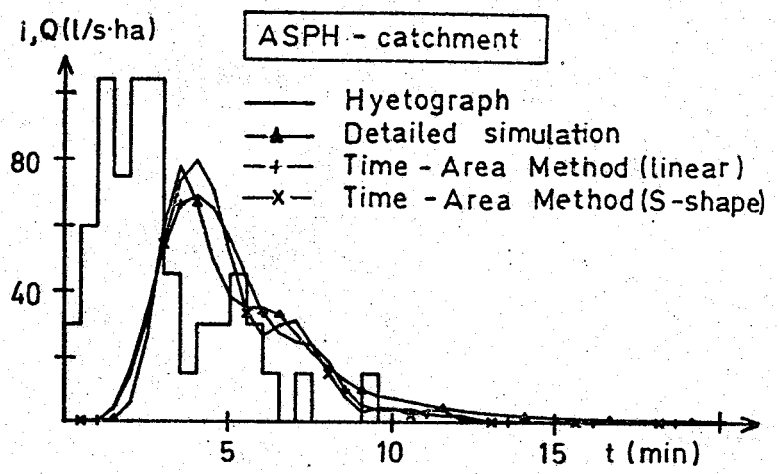

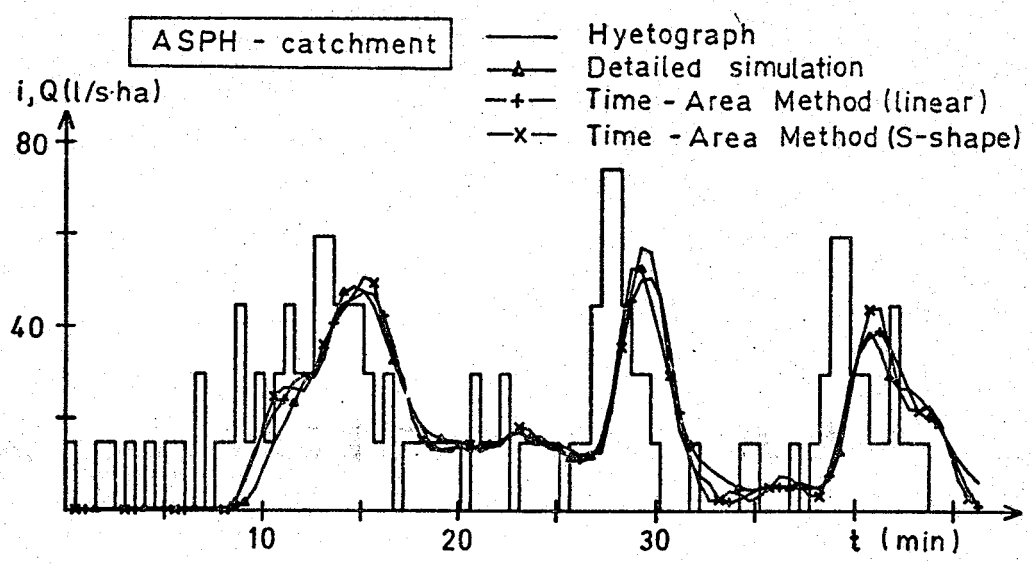

Time-Area Method, continued

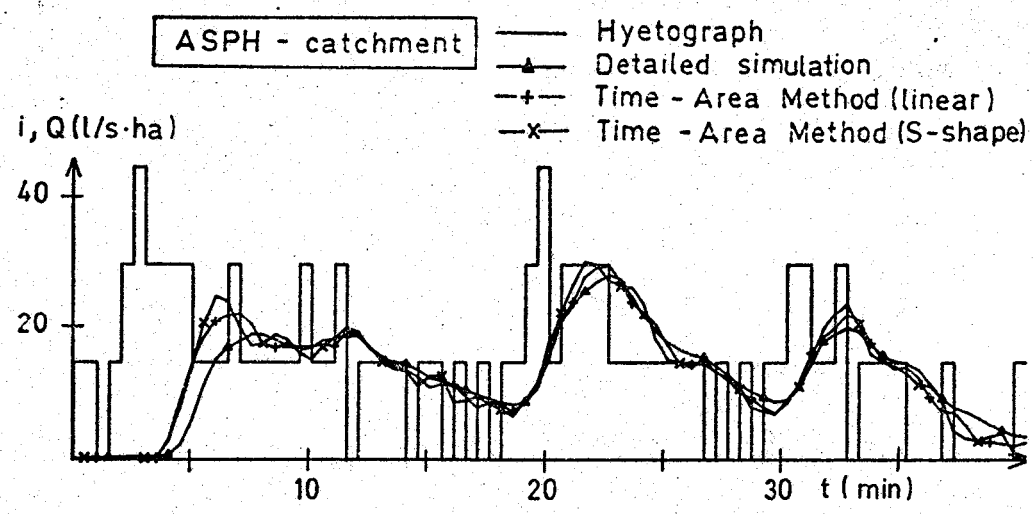

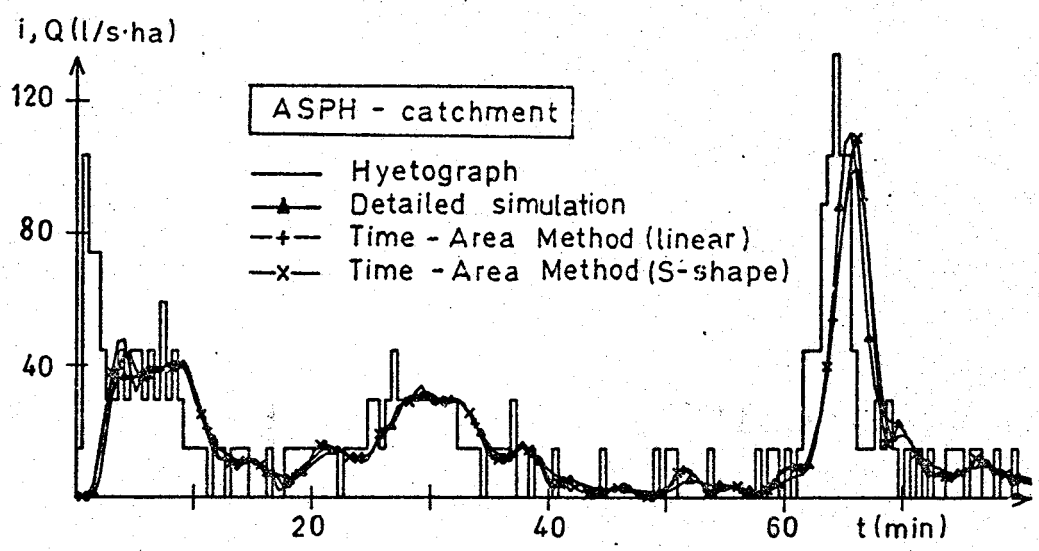

Time-Area Method, continued

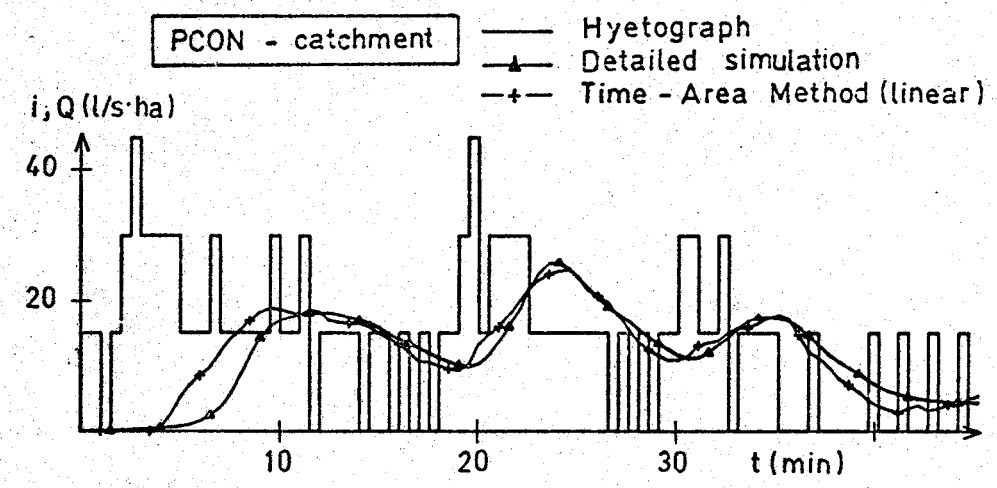

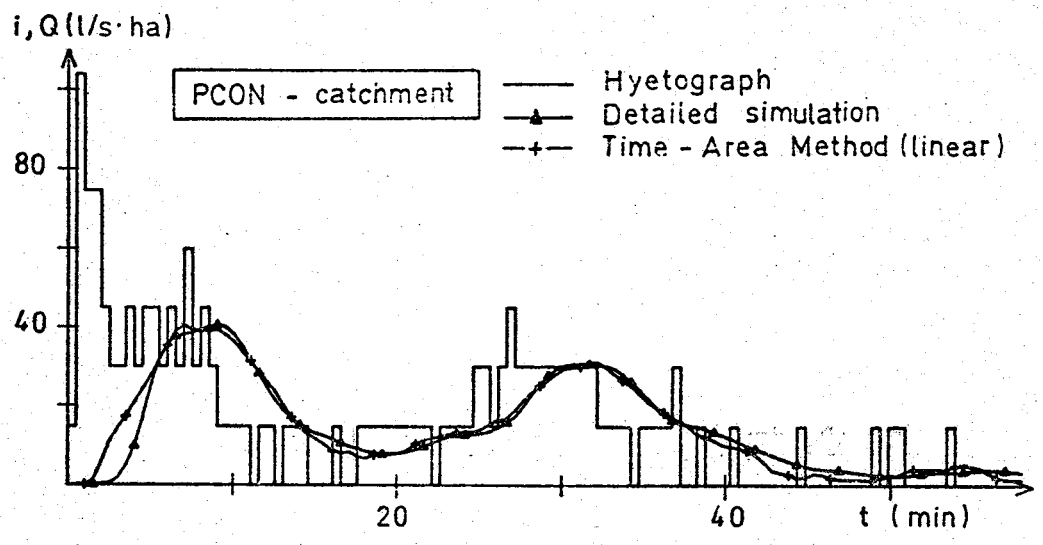

Time-Area Method, continued

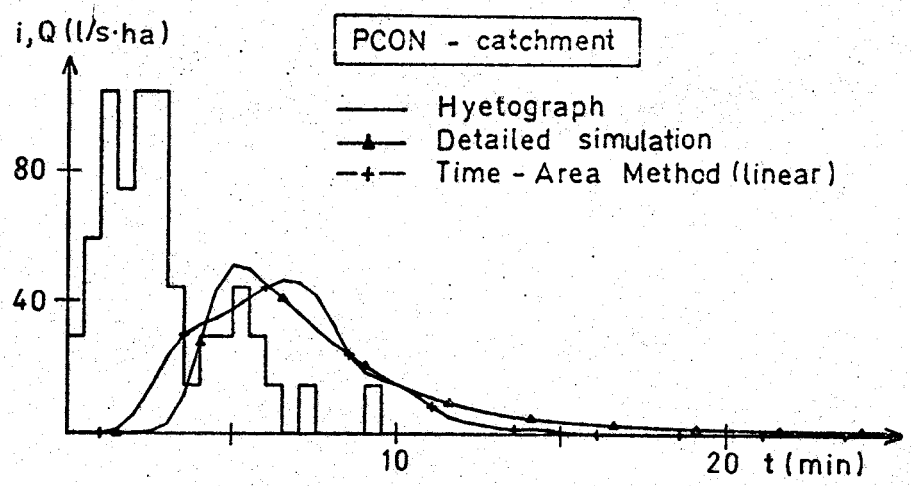

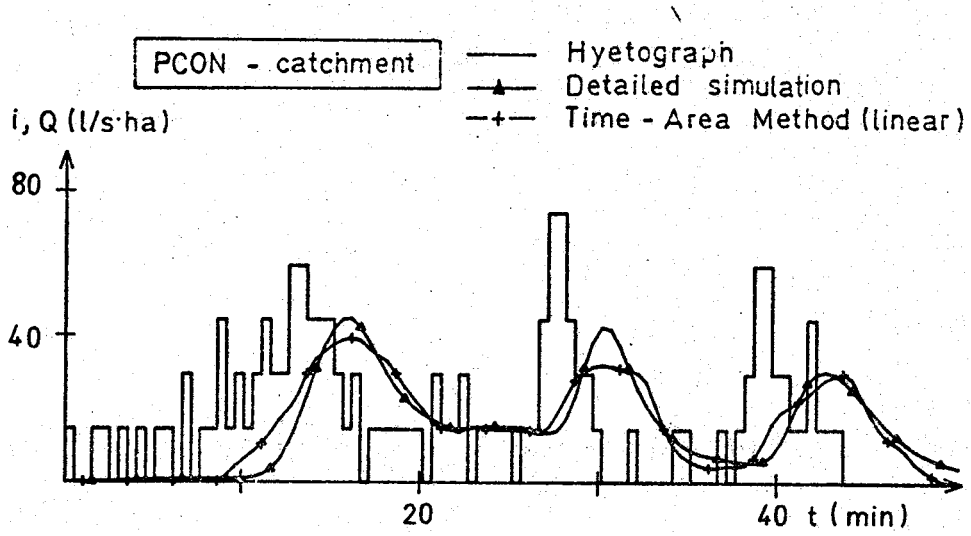

Time-Area Method, continued

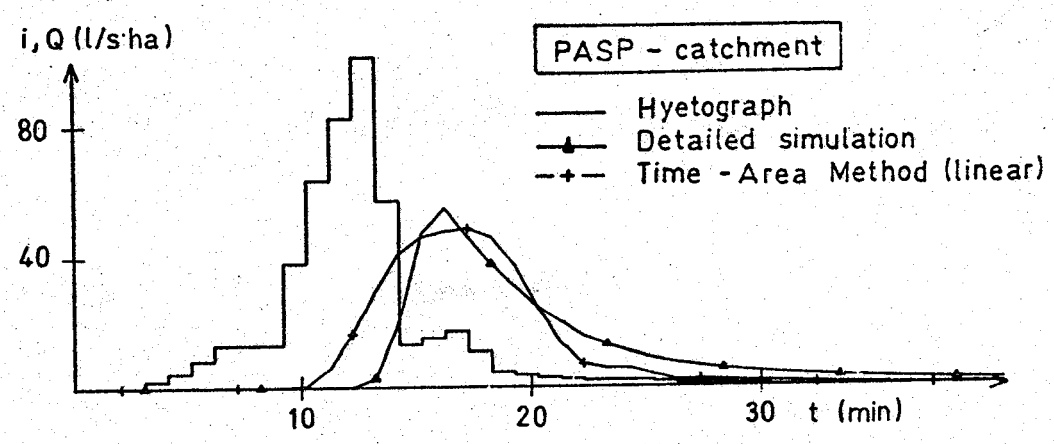

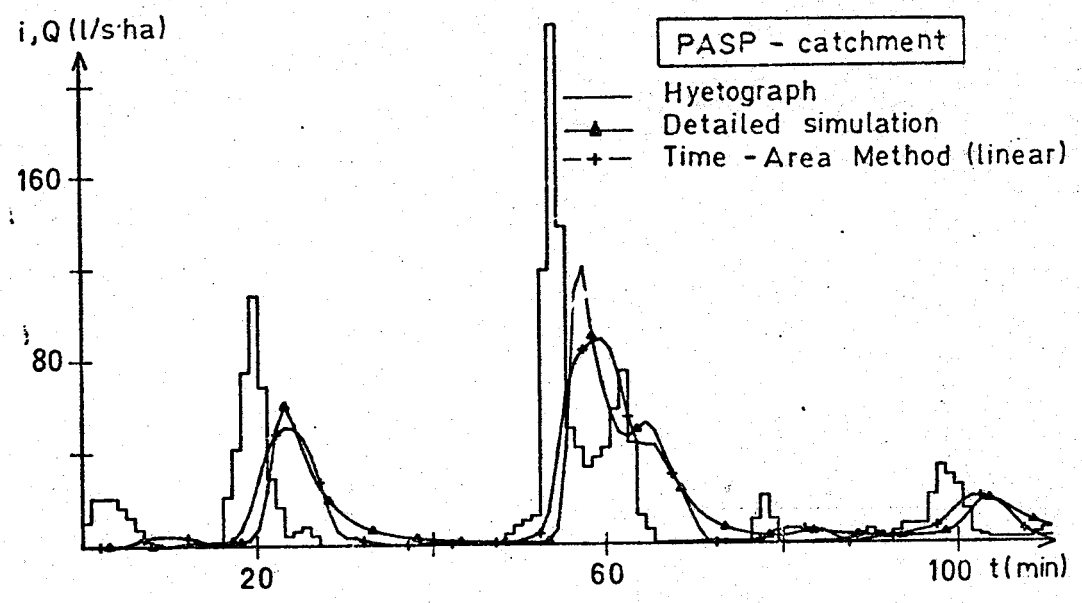

Time-Area Method, continued

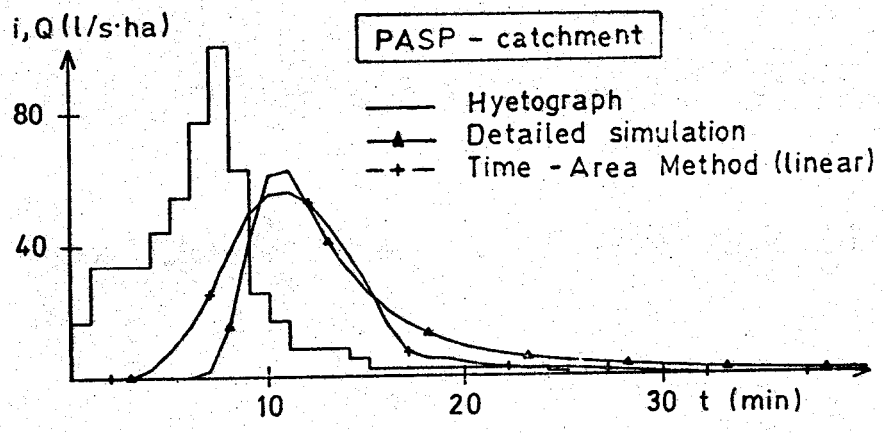

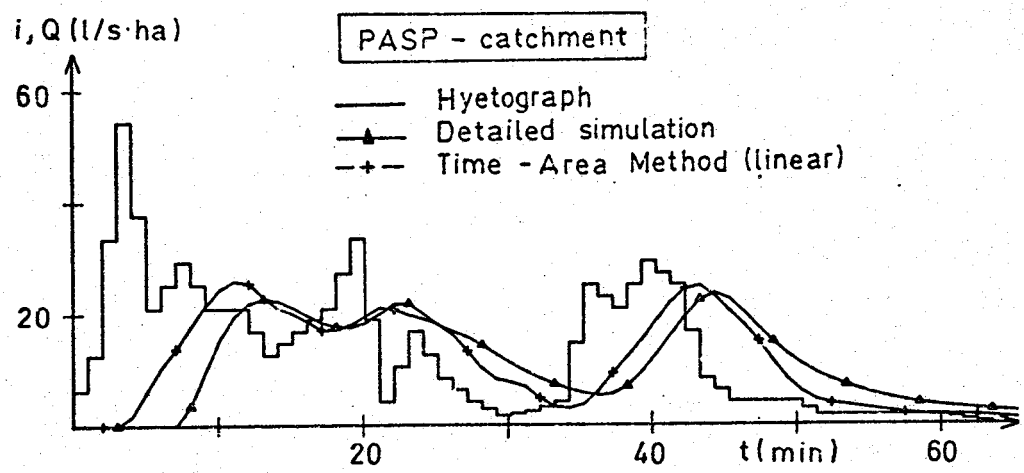

"ime-Area Method, continued

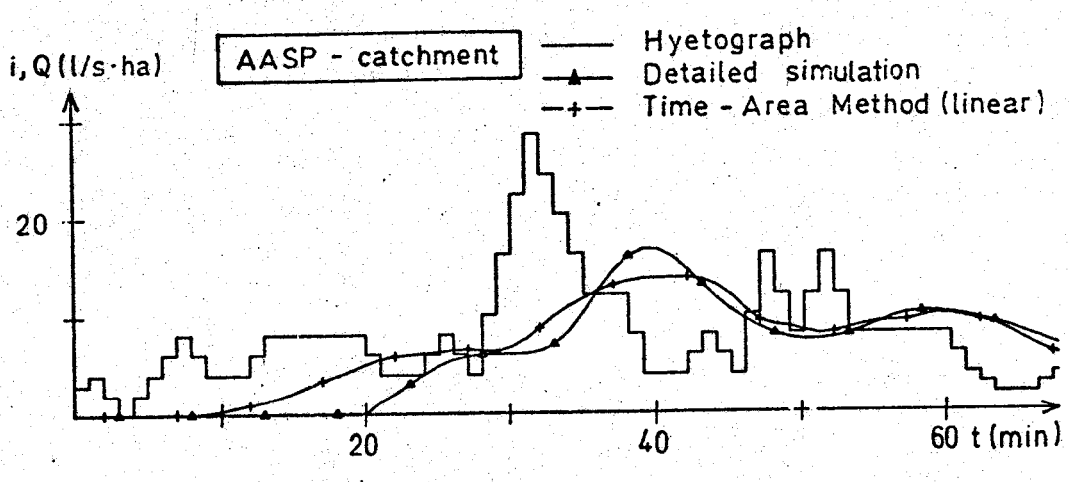

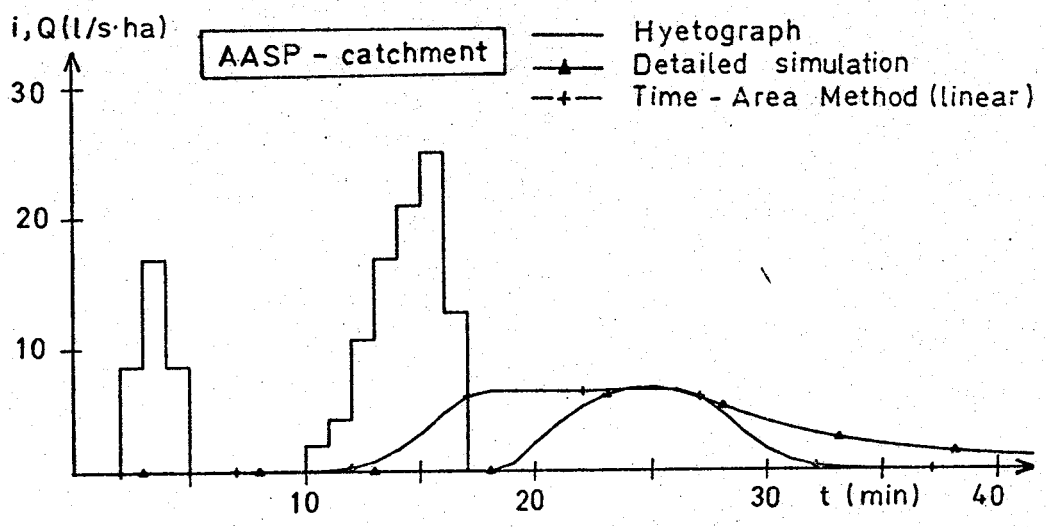

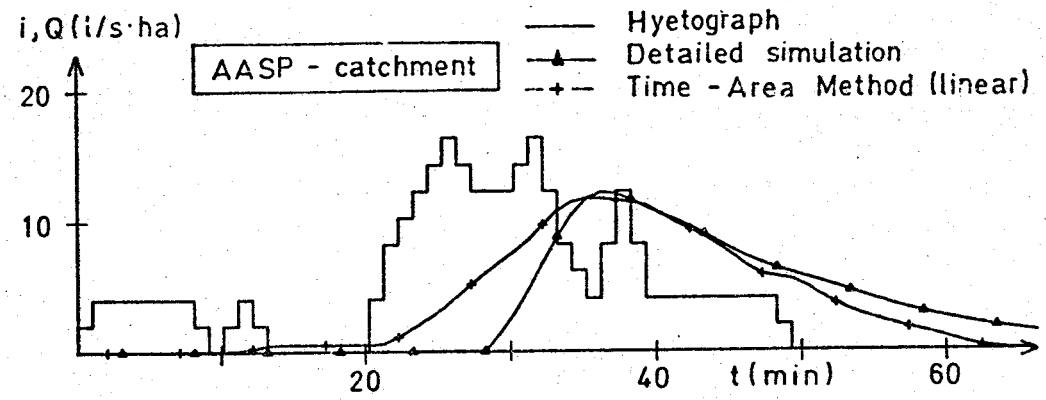

Time-Area Method, continued

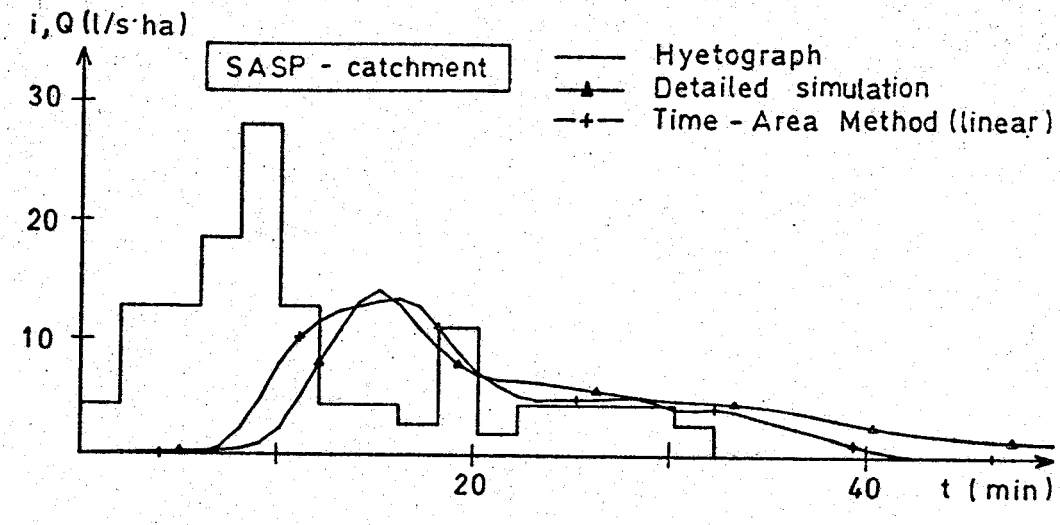

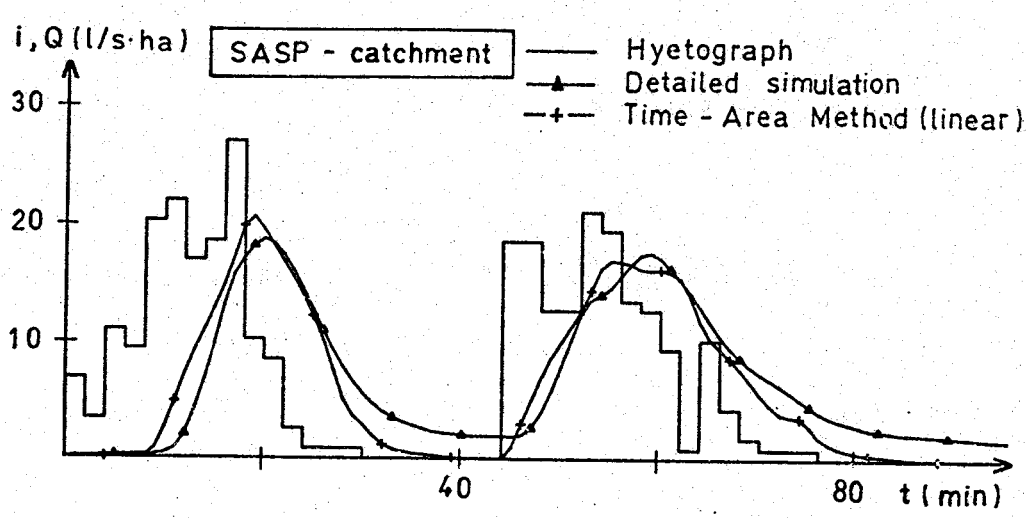

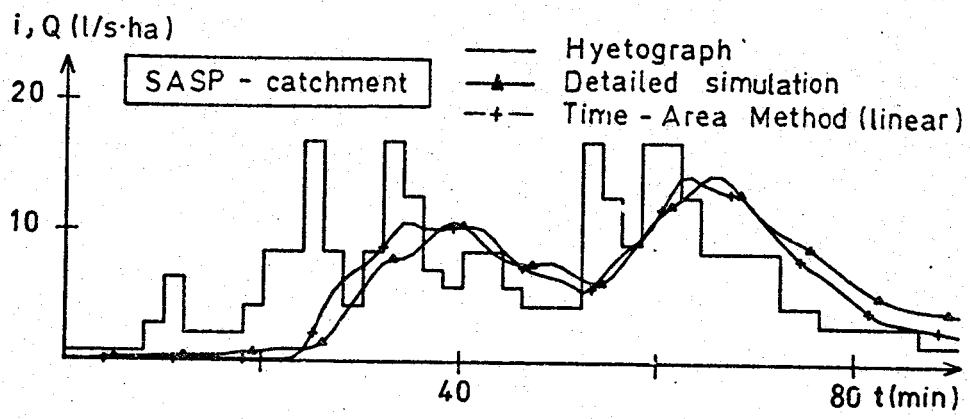

Time-Area Method, continued

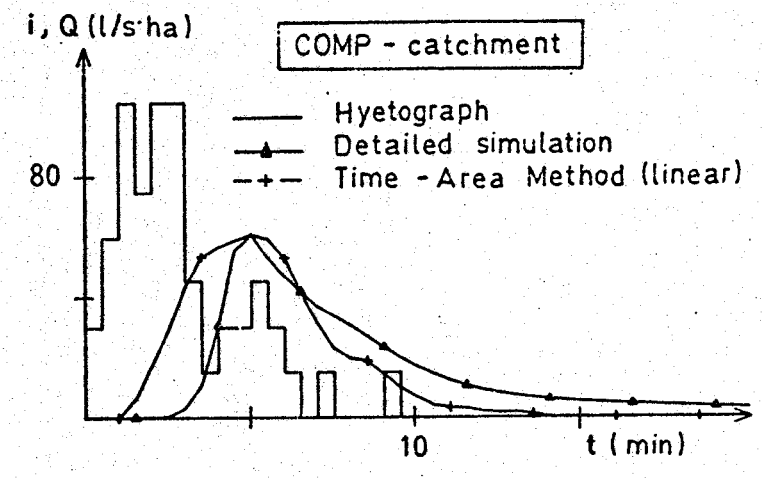

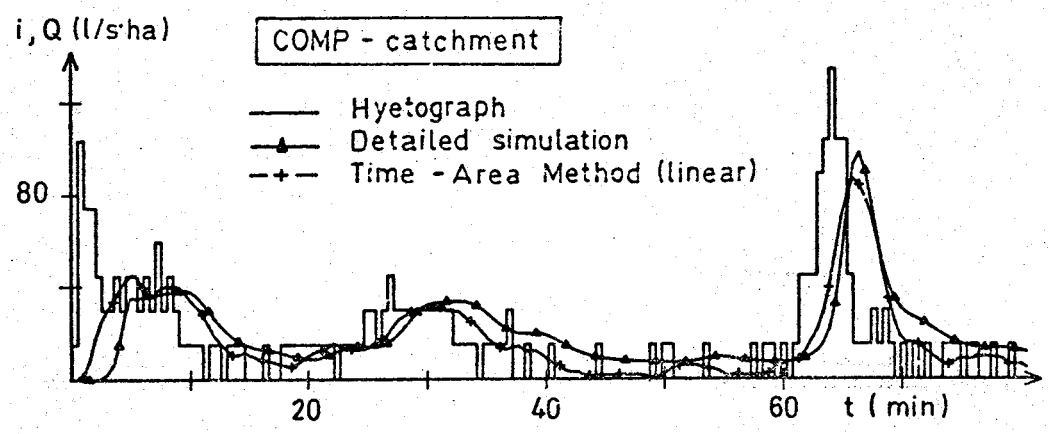

Time-Area Method, continued

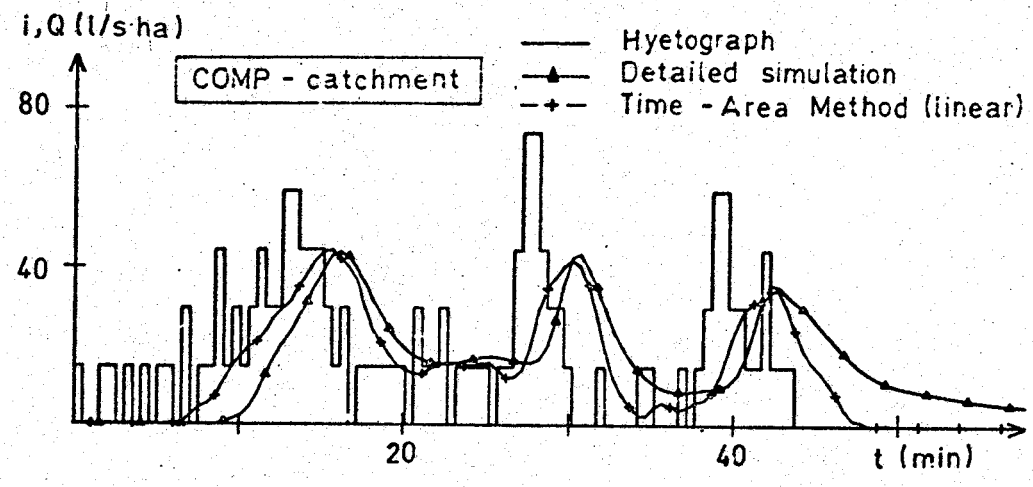

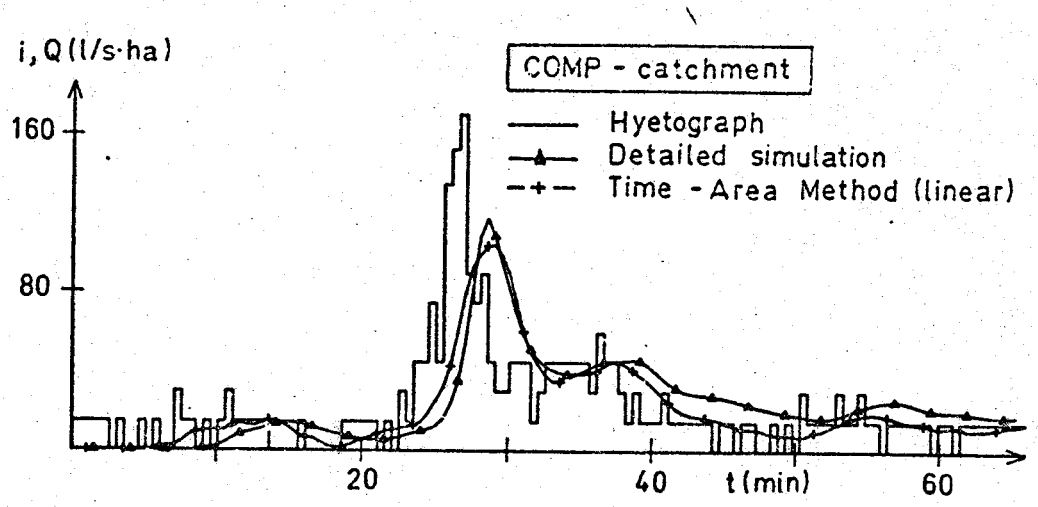

II:2 Hydrographs from Bergsjön and Linköping

In this section the hydrographs from the two catchments Bergsjön and Linköping 2, discussed in chapters 9 and 10, are presented.

II:2.1 Comparison between the recorded and simulated runoff

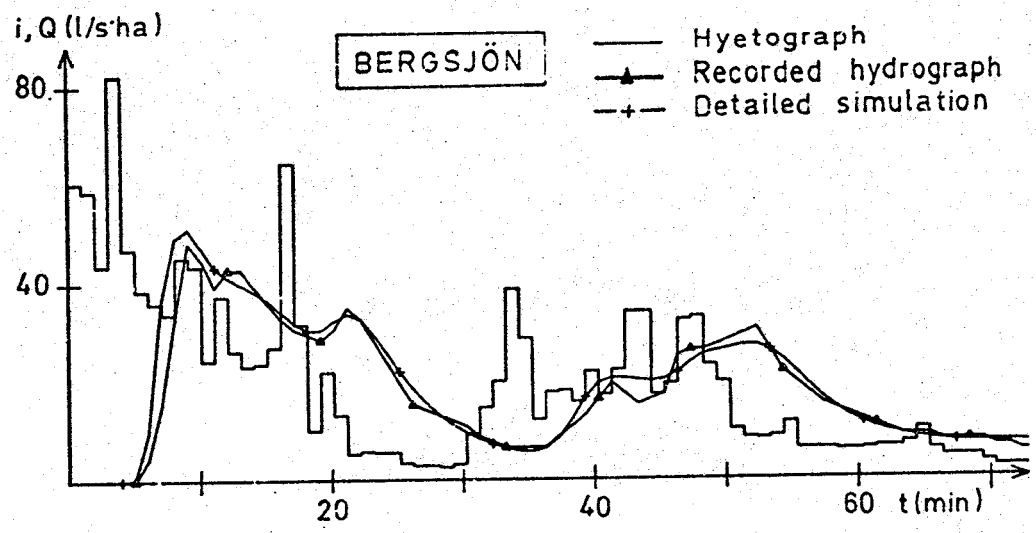

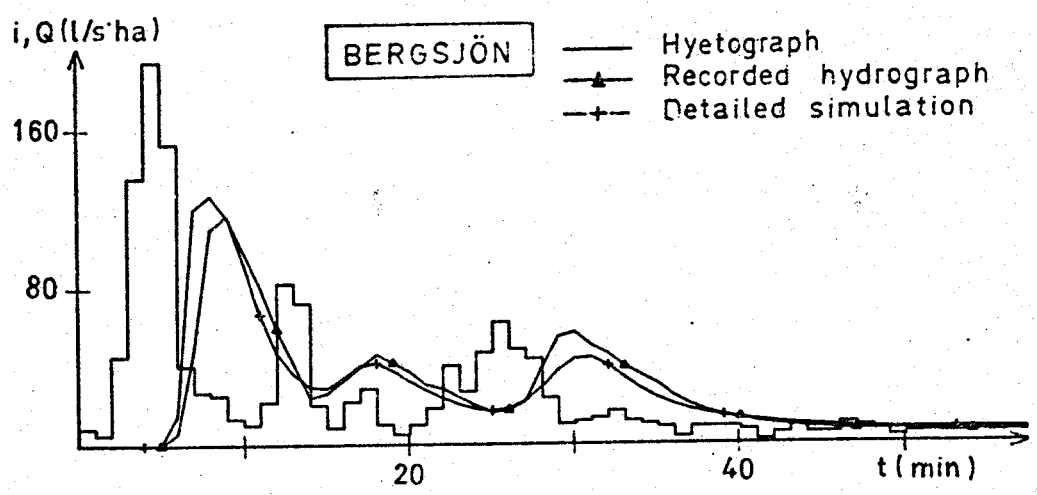

recorded-simulated hydrographs, continued

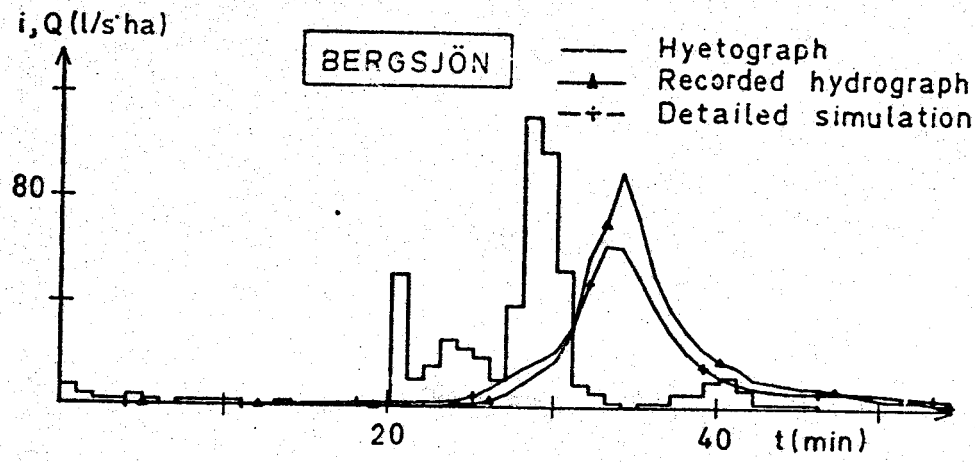

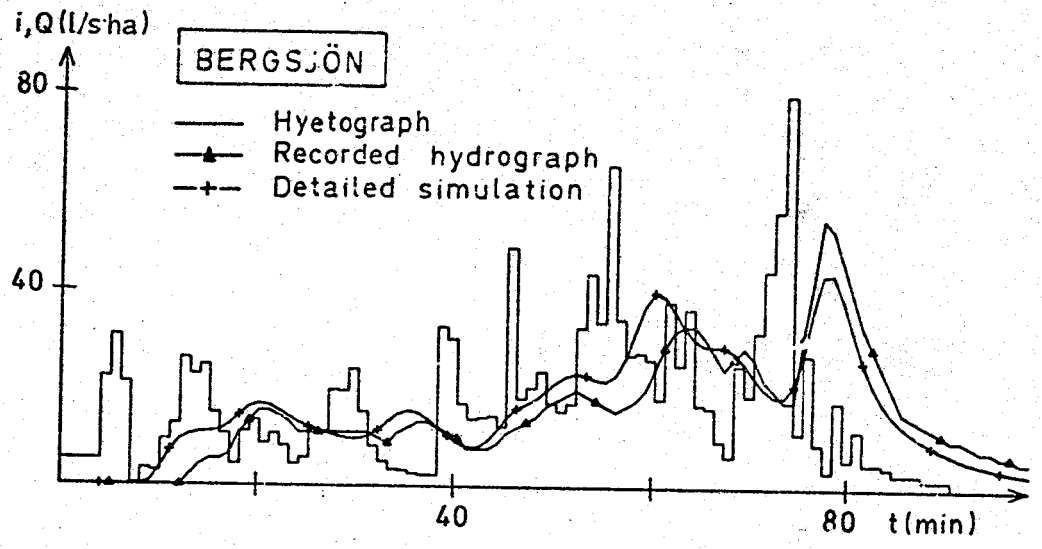

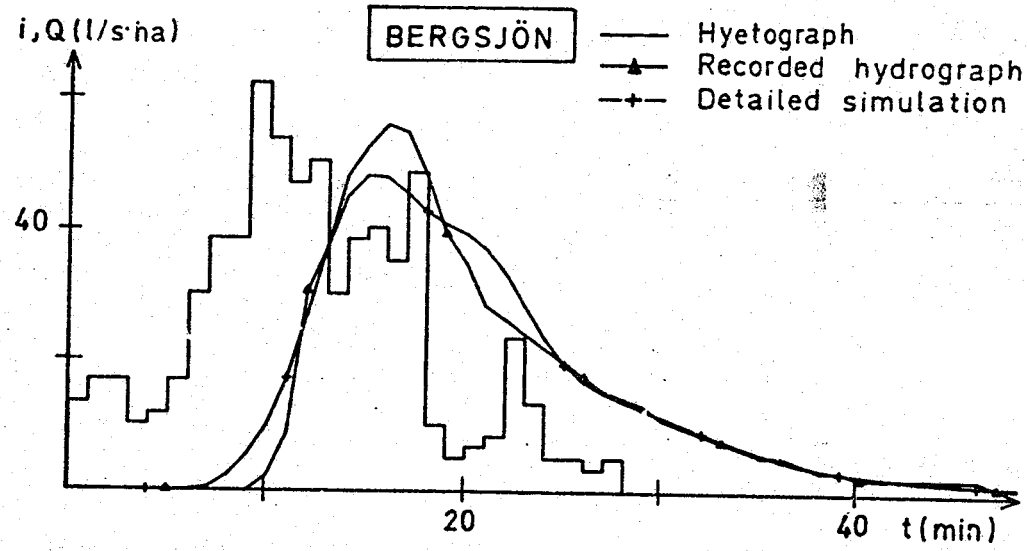

recorded-simulated hydrographs, continued

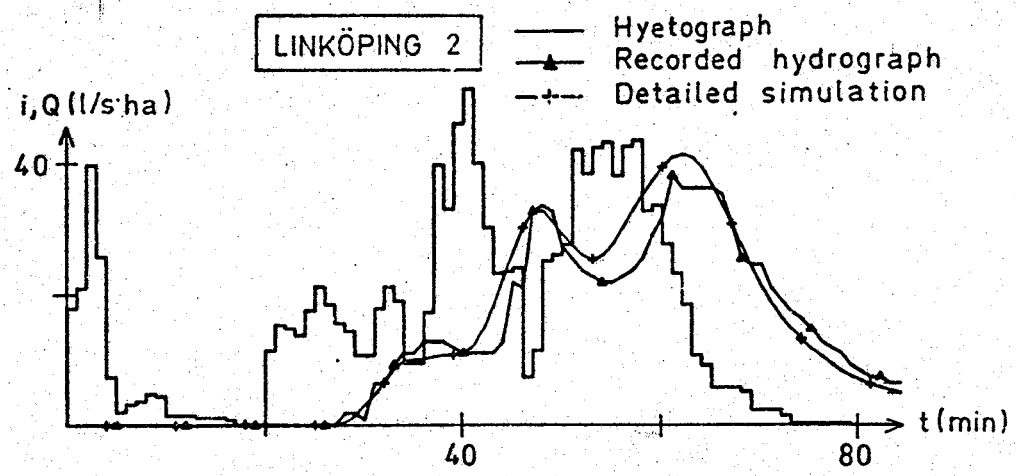

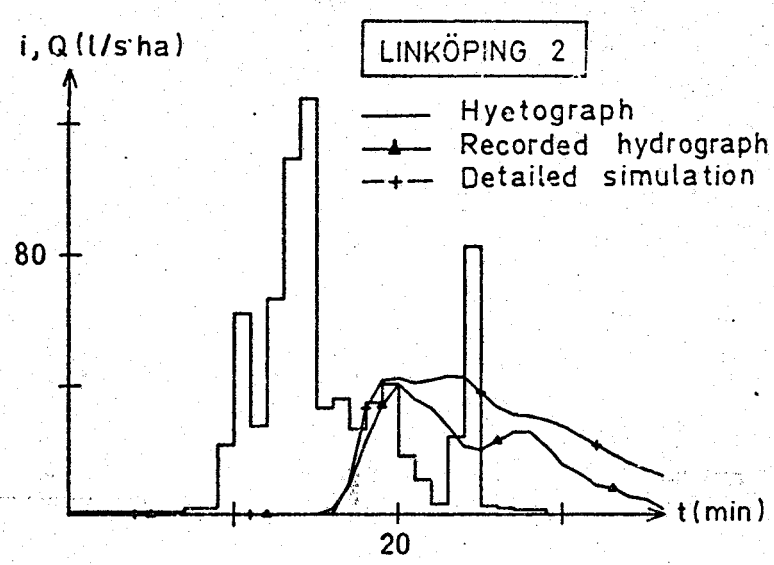

recorded-simulated hydrographs, continued

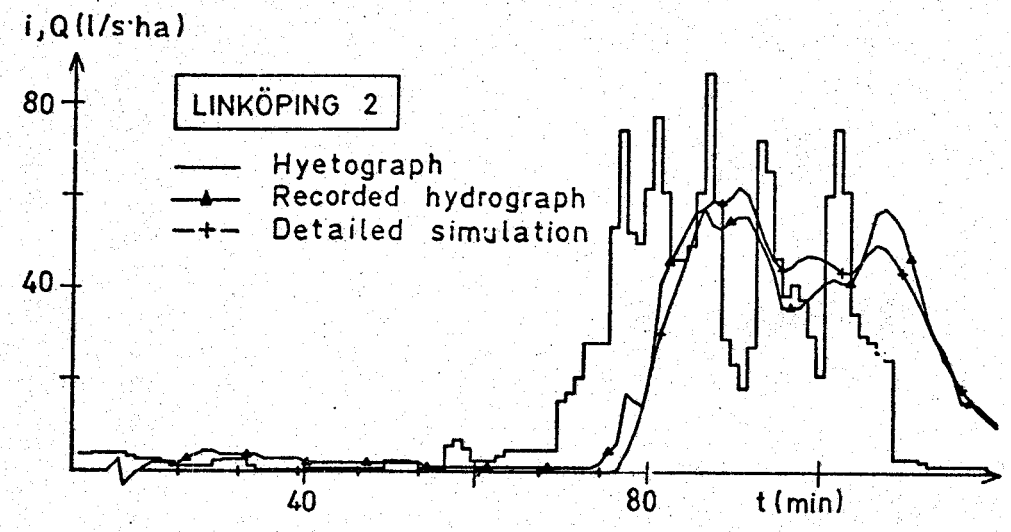

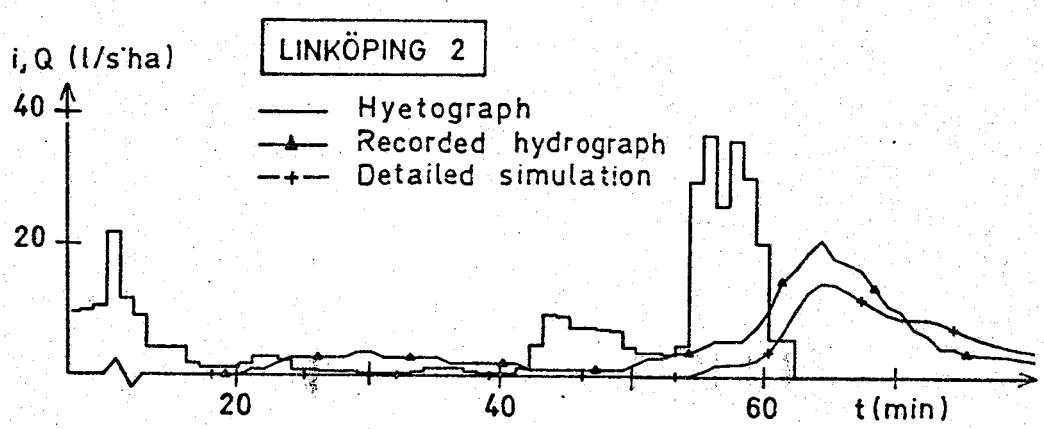

II:2.2 Comparison; the detailed kinematic wave KW6S-L1 and KW4G-I models

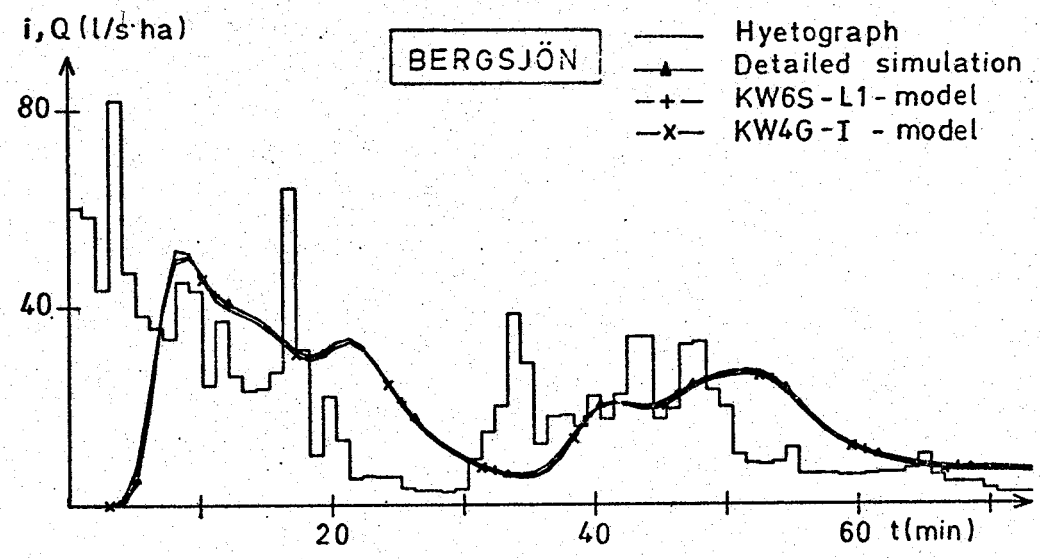

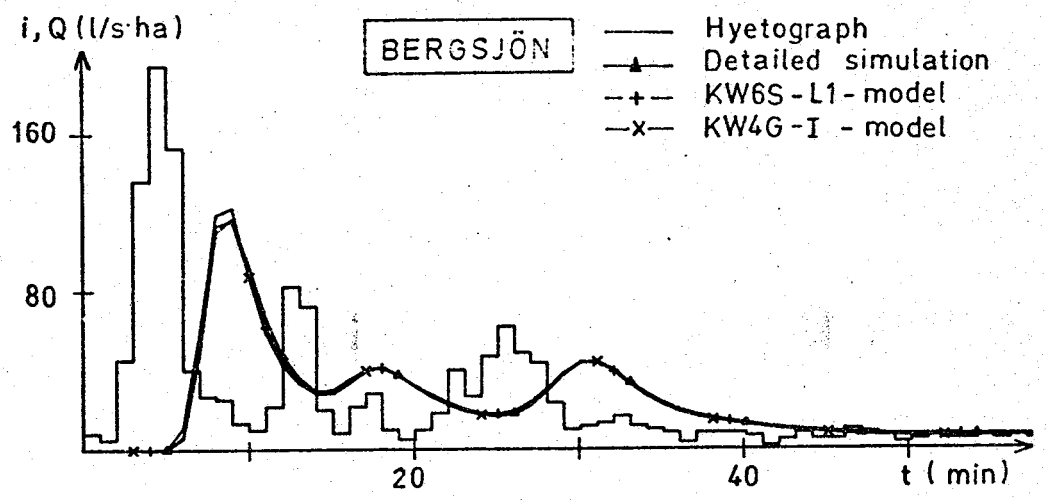

KW6S-L1 and KW4G-I model hydrographs, continued

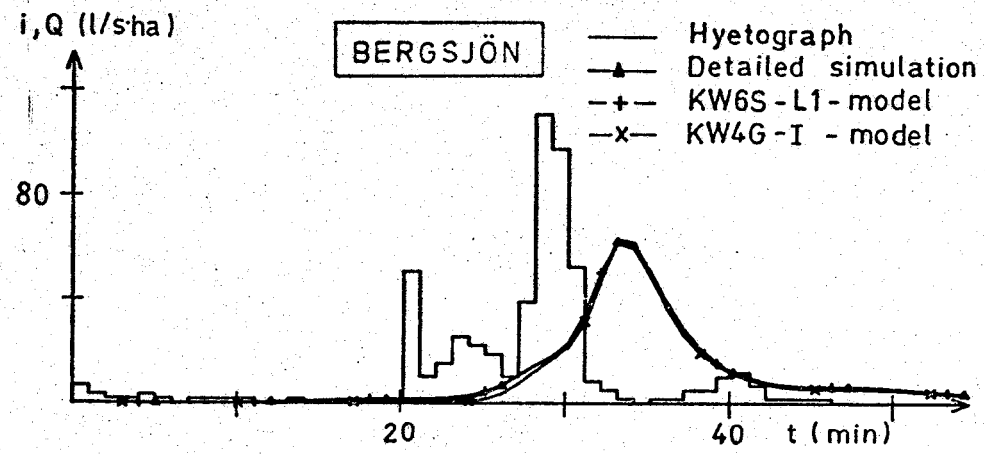

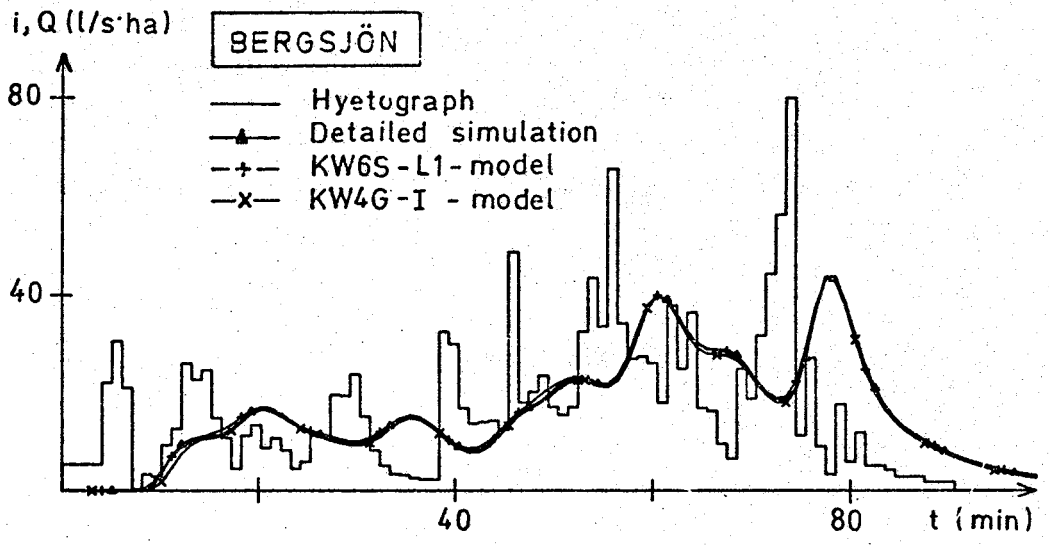

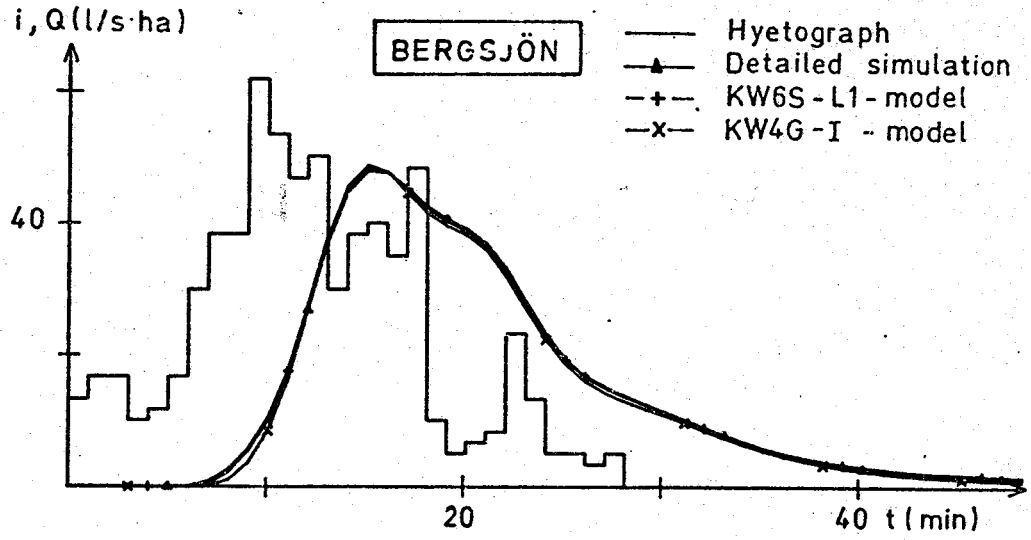

KW6S-L1 and KW4G-I model hydrographs, continued

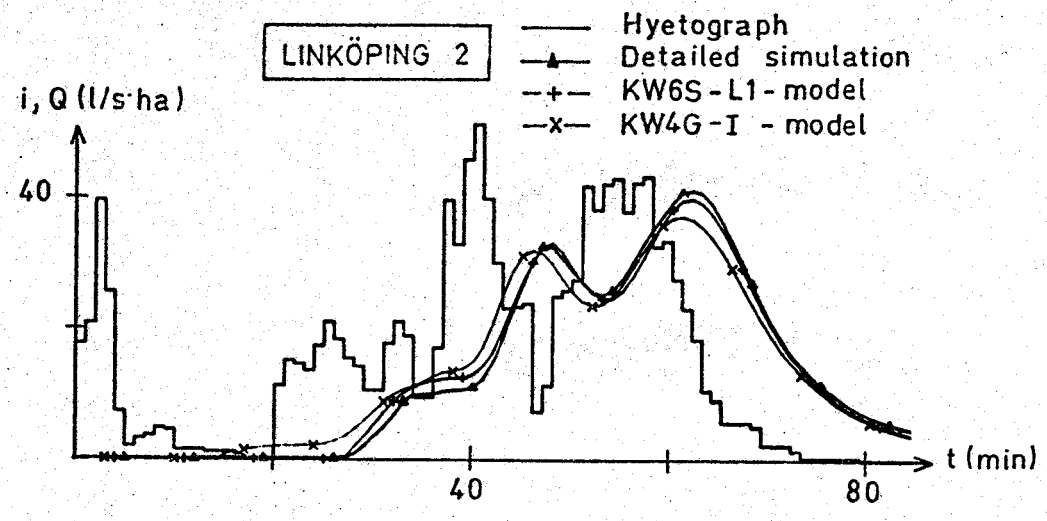

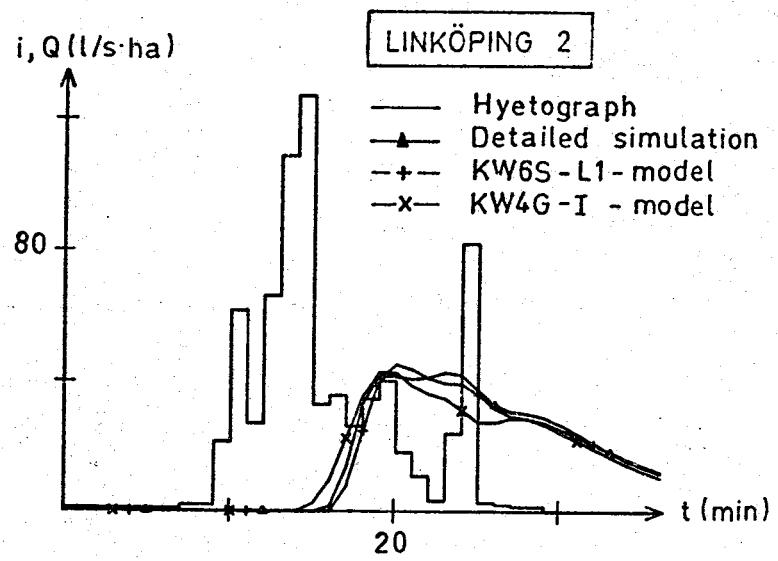

KW6S-L1 and KW4G-I model hydrographs, continued

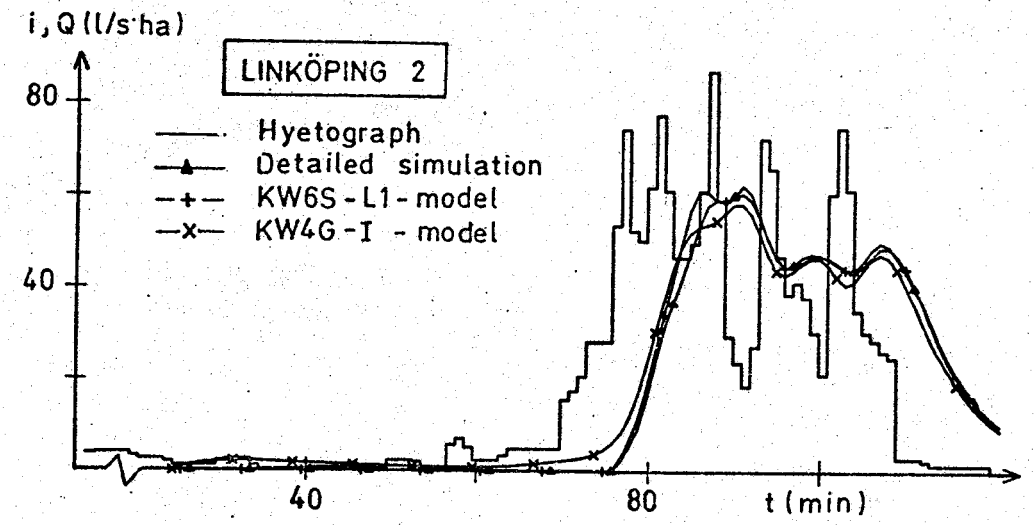

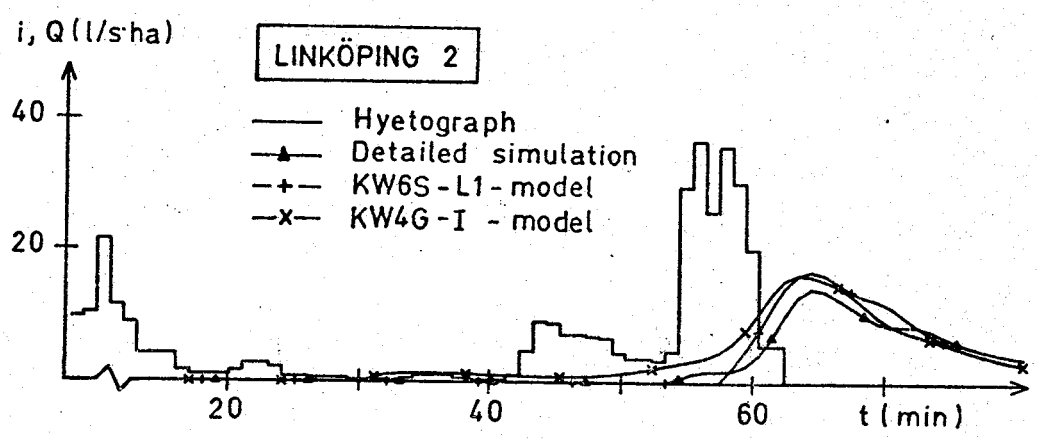

II:2.3 Comparison; the detailed kinematic wave model, KW6S-L2 model and KW6S-L3 model

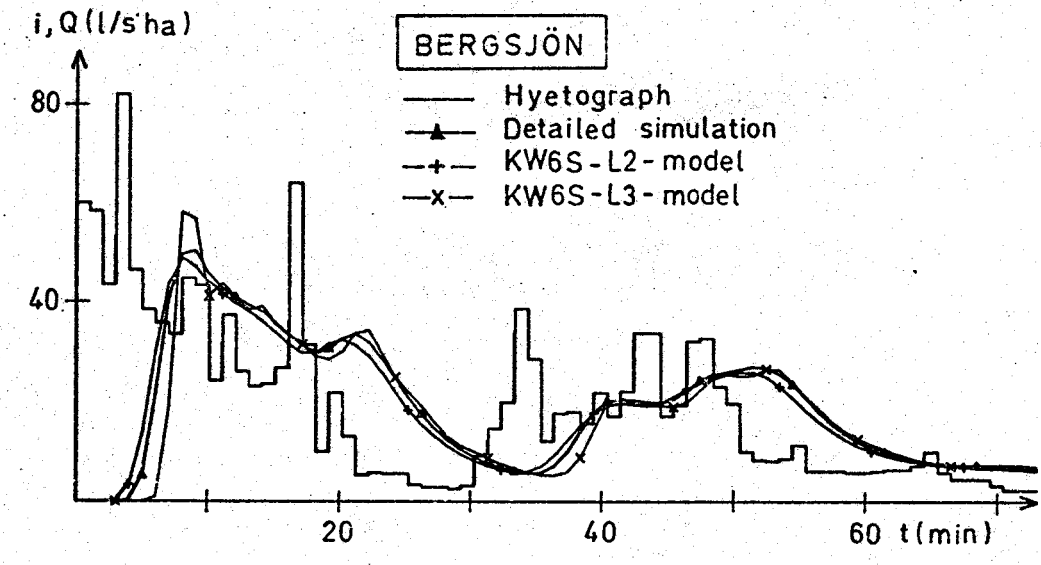

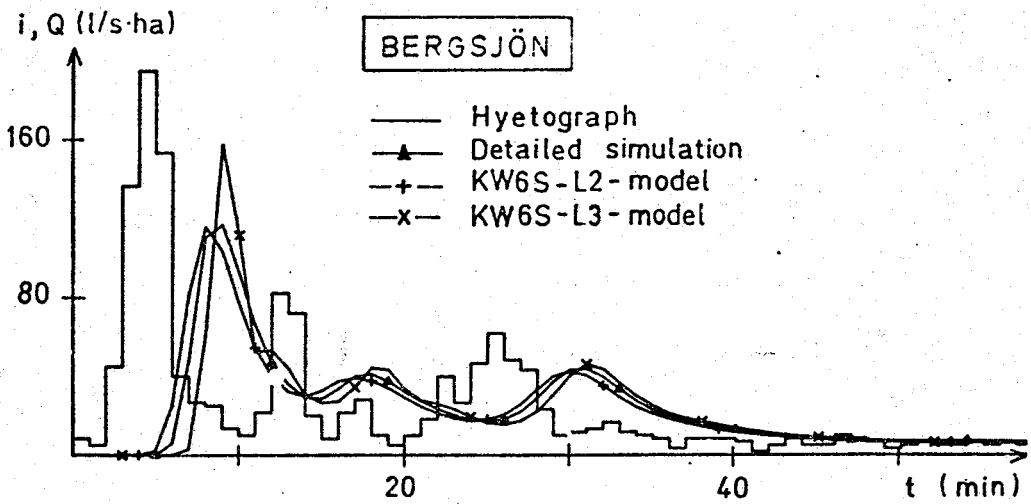

KW6S-L2 and KW6S-L3 model hydrographs, continued

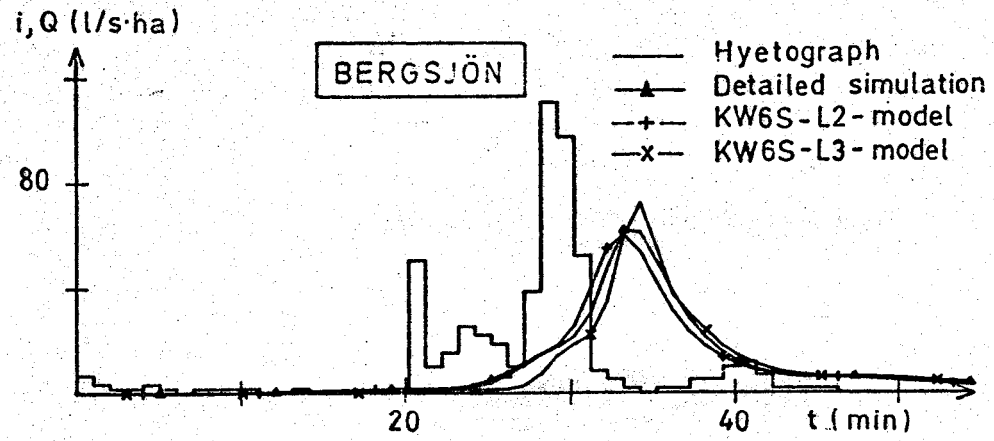

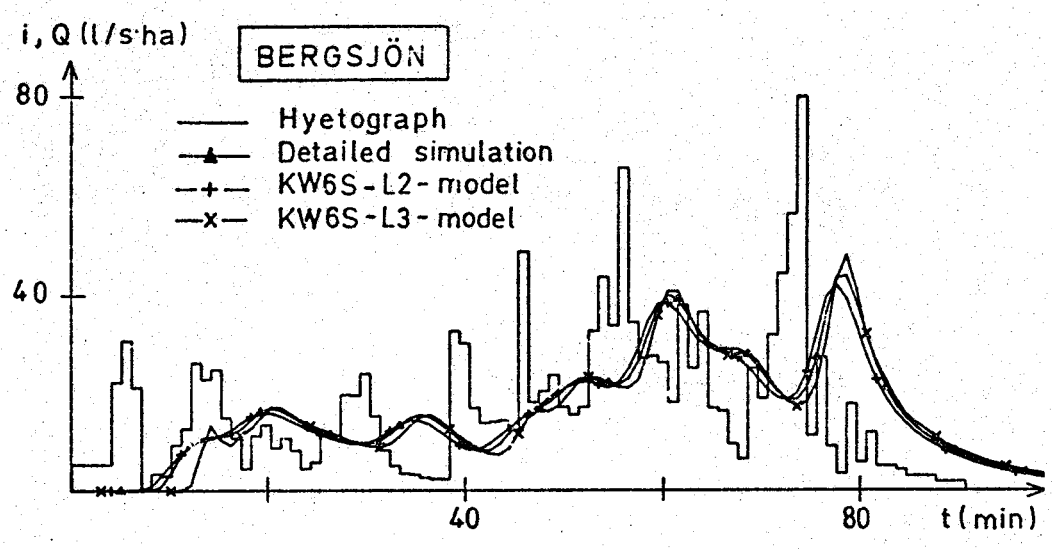

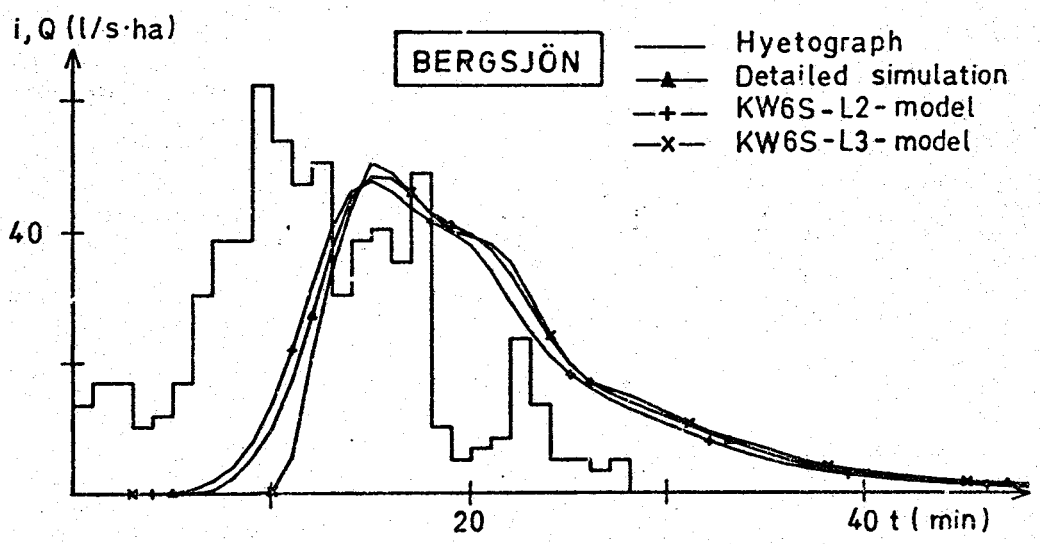

KW6S-L2 and KW6S-L3 model hydrographs, continued

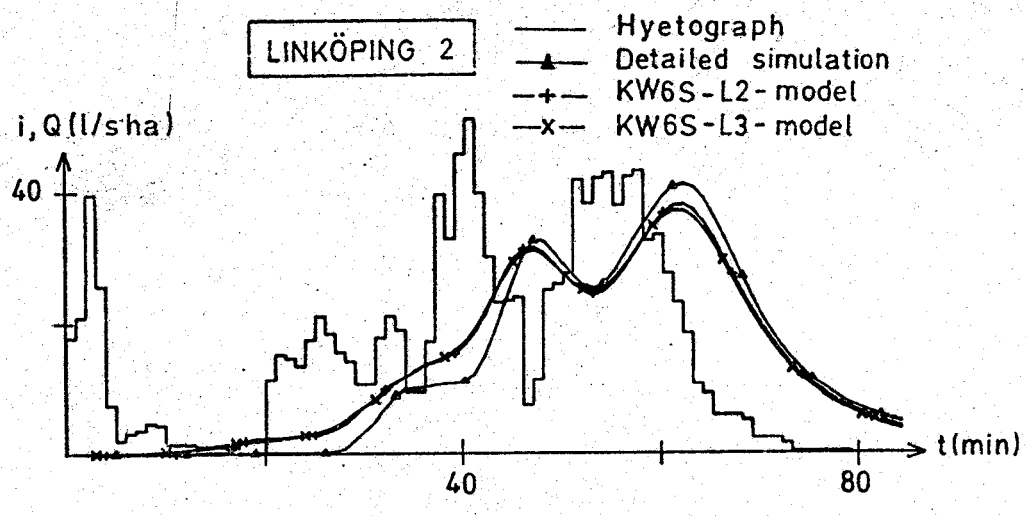

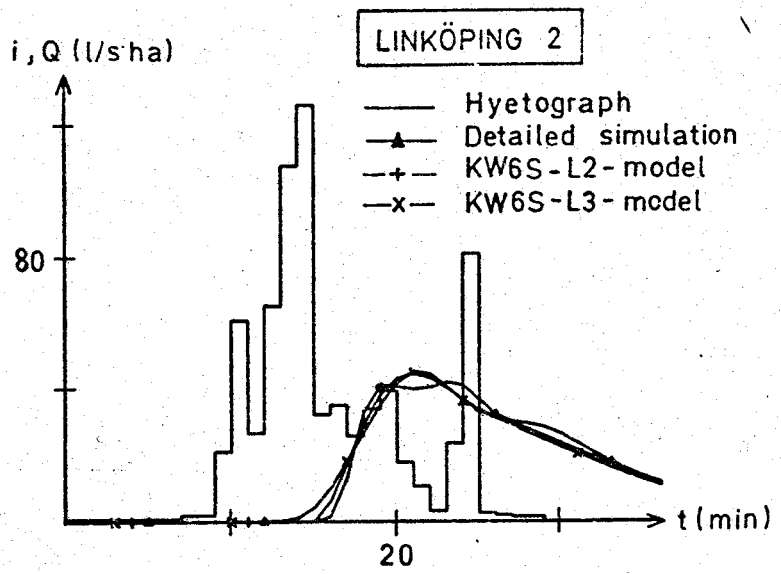

KW6S-L2 and KW6S-L3 model hydrographs, continued

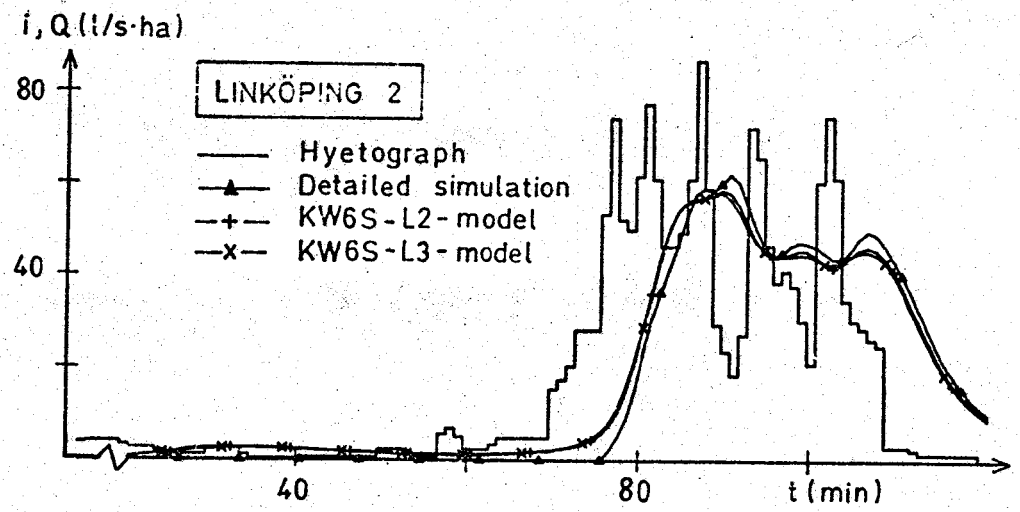

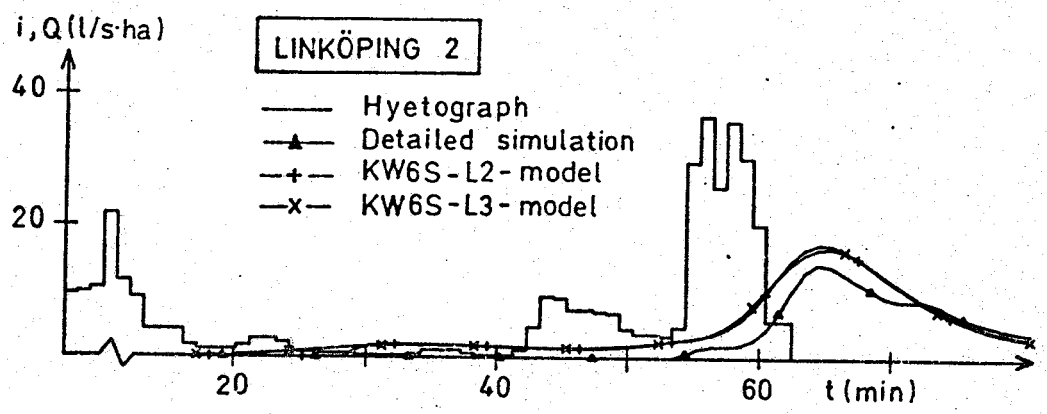

II:2.4 Comparison; the detailed kinematic wave model and the Time-Area Method (TAL1 and TAL2)

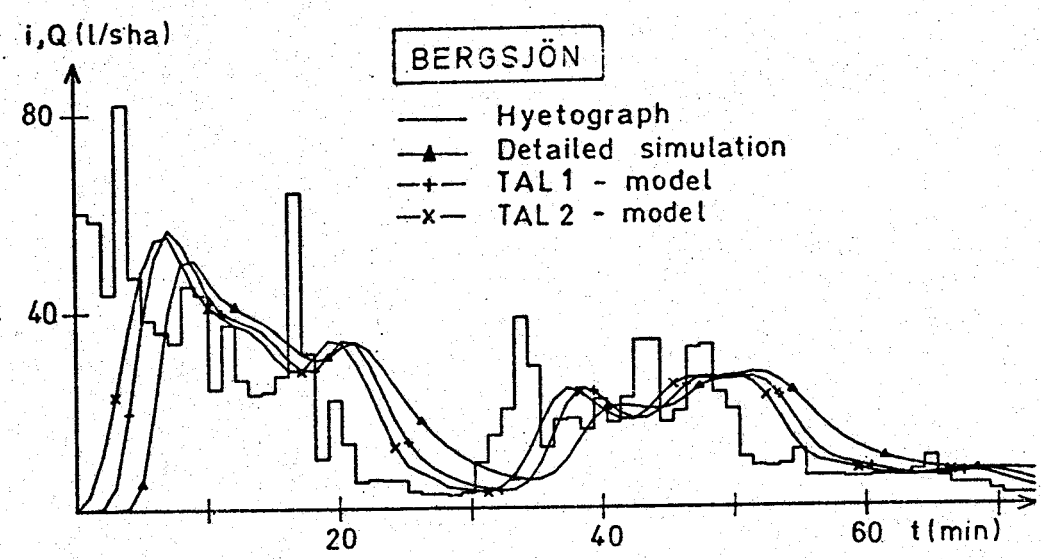

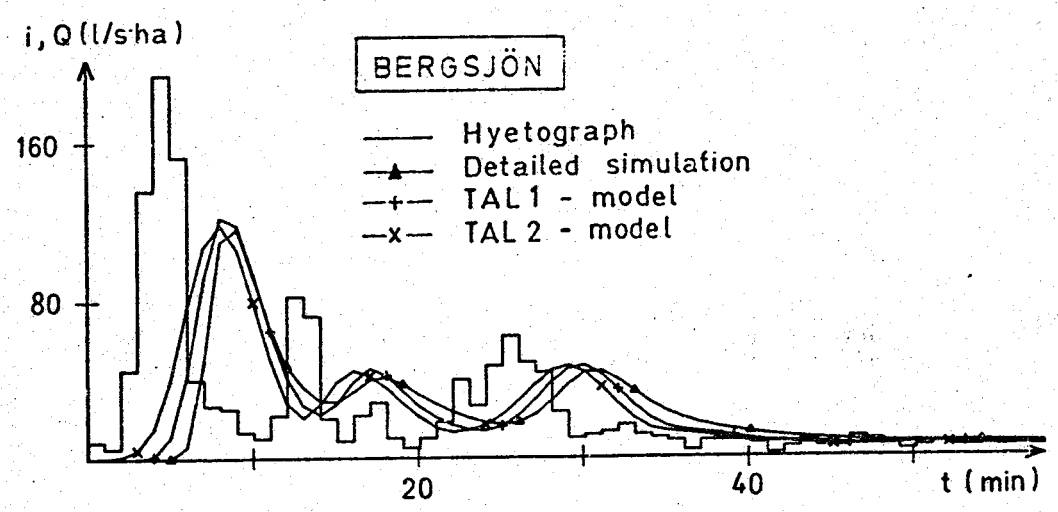

TAL1 and TAL2 model hydrographs, continued

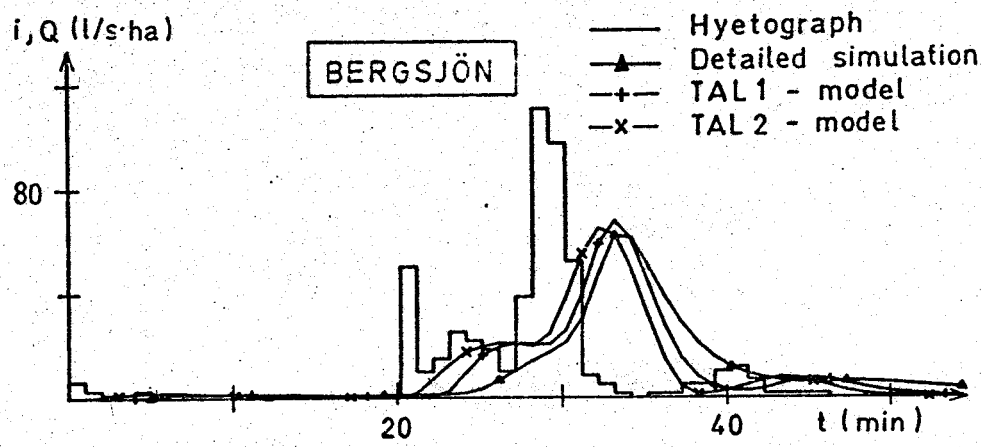

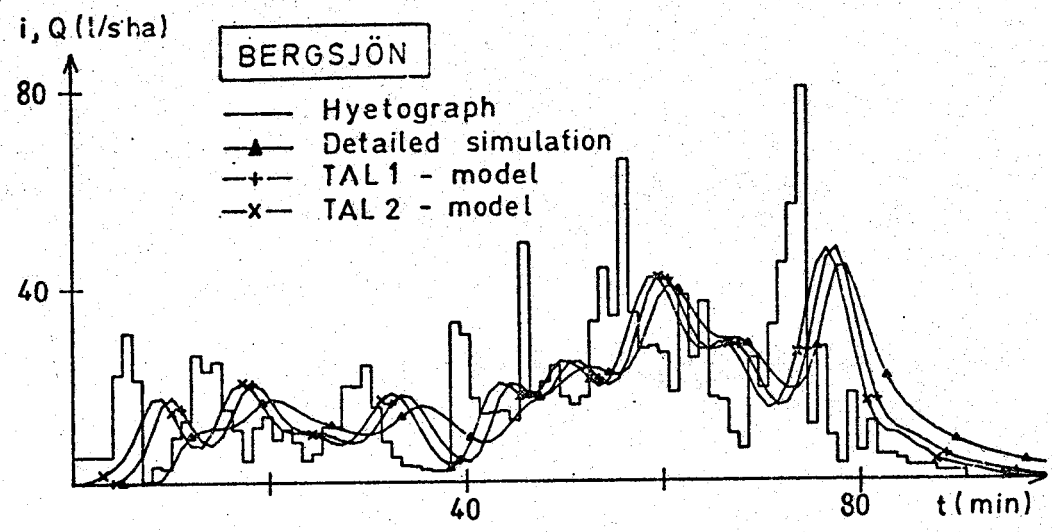

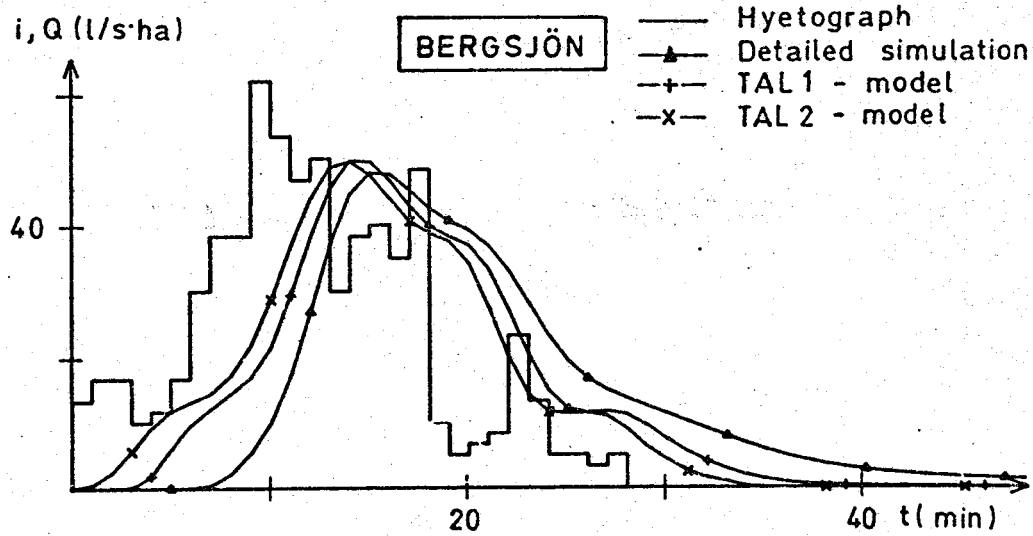

TAL1 and TAL2 model hydrographs, continued

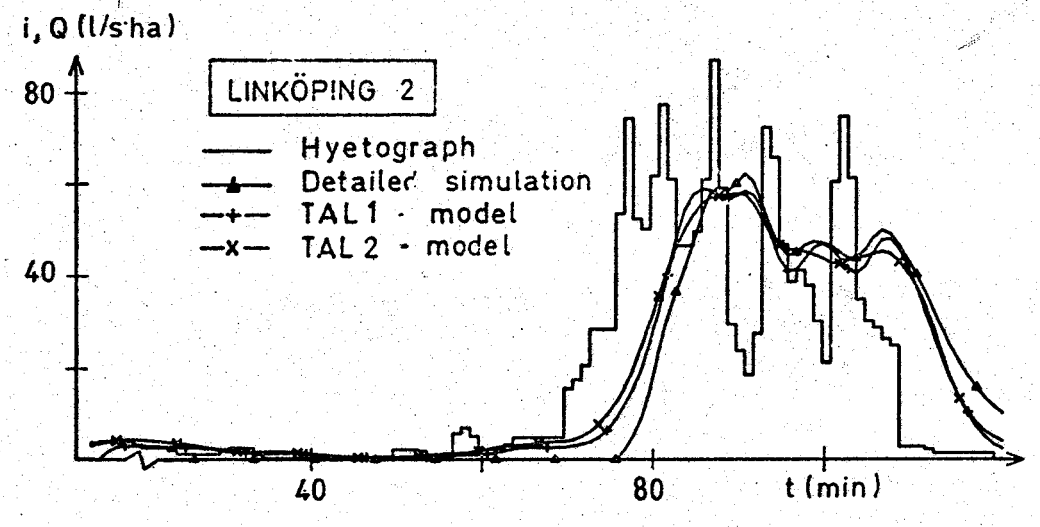

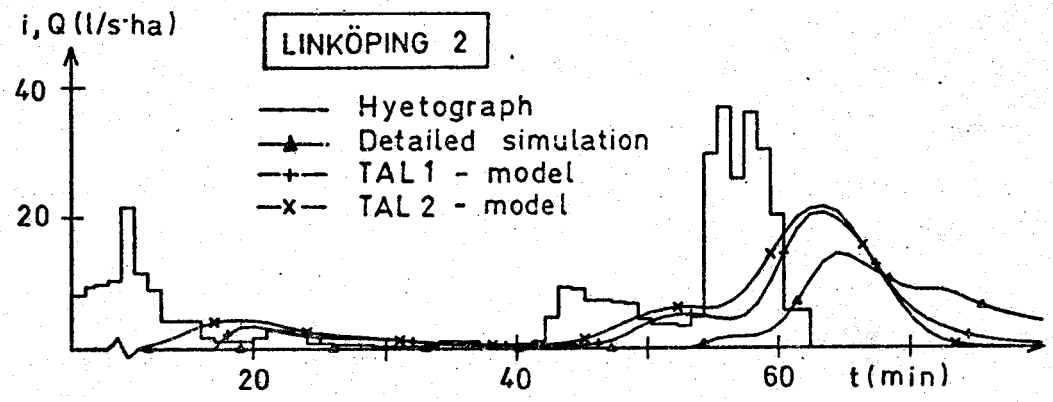

TAL1 and TAL2 model hydrographs, continued

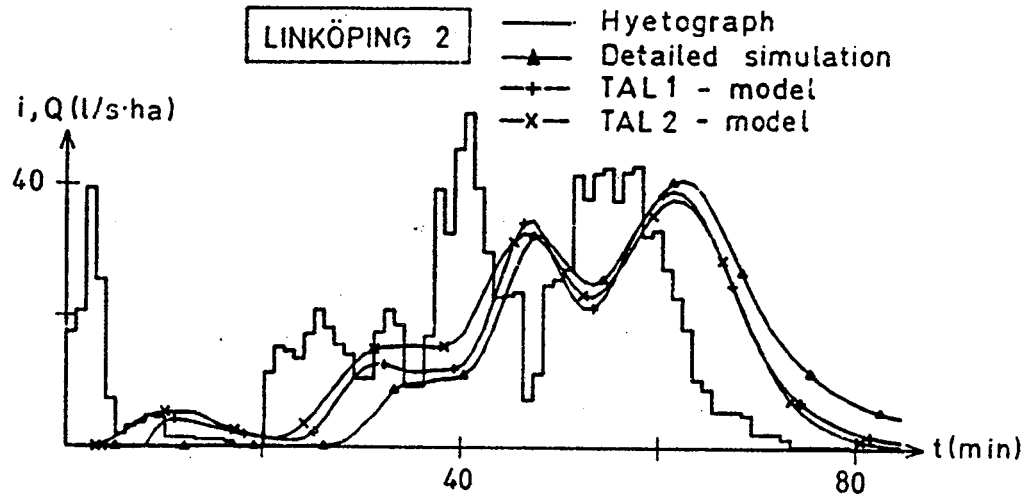

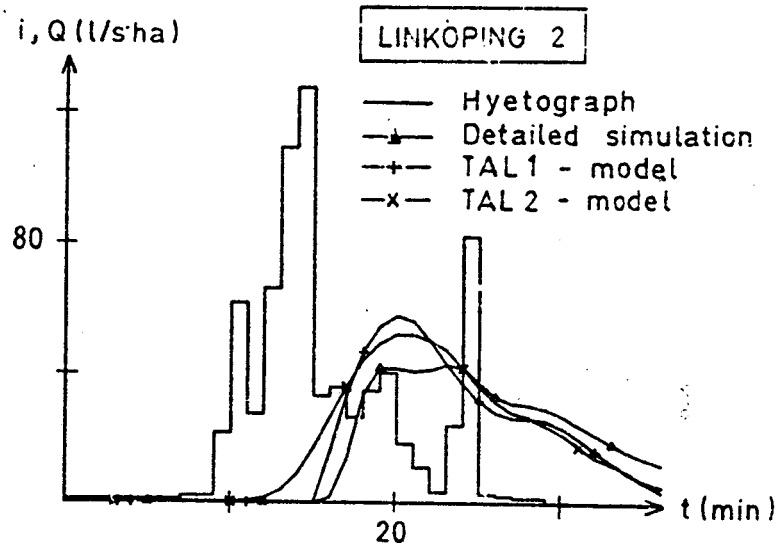
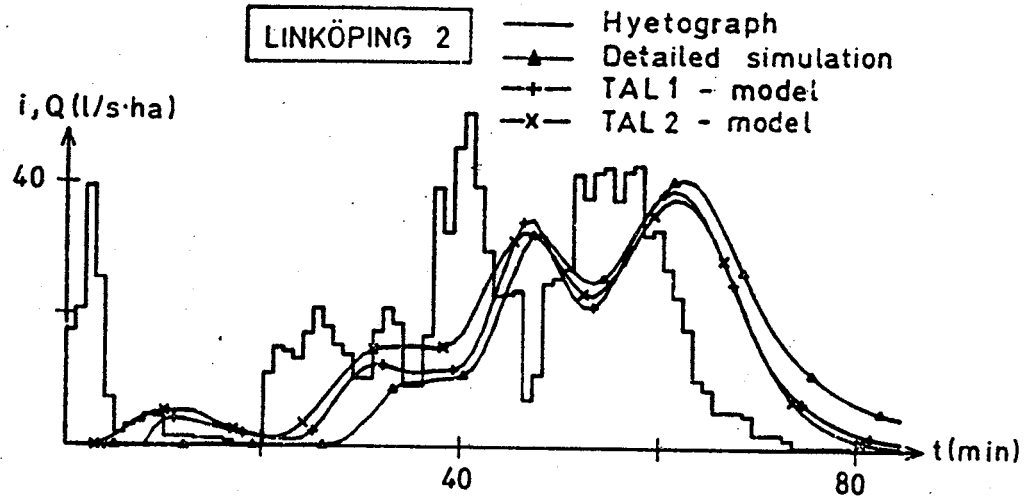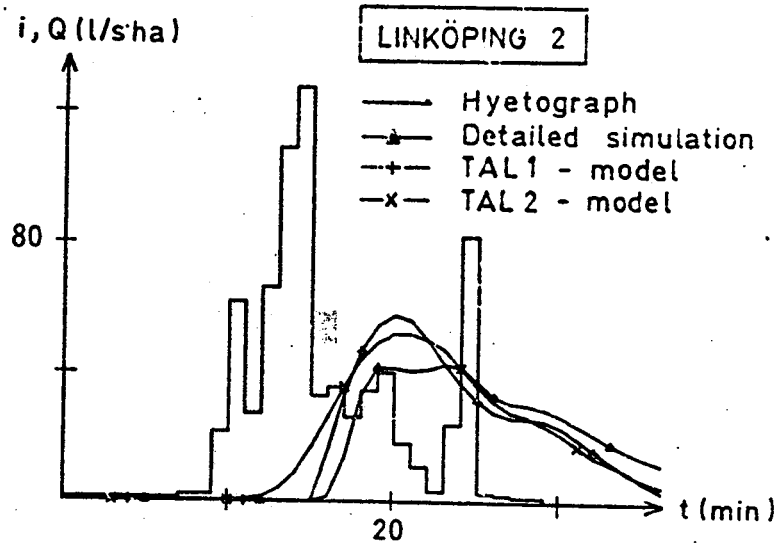
TAL1 and TAL2 model hydrographs, continued